Keele UNIVERSITY

Developing a 3D tissue-engineered model to study the biology and treatment of atherosclerosis

Jassim Hanoon Jassim Echrish
School of Medicine, Keele University

Thesis submitted for the degree of
Doctor of Philosophy

December 2021

Acknowledgments

Initially I would like to express my deep appreciation and gratefulness to Allah (SWT) for the immense help and support. My deep gratitude and thanks to my lead supervisor Dr Alan Harper for his huge, unremitting efforts for this reason I was incredibly lucky to be supervised by him. My great thanks for my second supervisor Professor Ying Yang for her support and help. I am grateful to my funder (Iraqi Ministry of Health) and my sponsor (Iraqi Ministry of Higher Education & Scientific Research) for the financial, administrative, and psychological sport. Thank you so much for my colleague, Dr David Cabrera for his helps in cryosectioning, Jacob Ranjbar for his help in the 3D printing and Wanjiku Njoroge for her help and cooperation. I am very grateful to my wife Dr Suhad for her help, support, and encouragement during the whole period of my PhD study.

Contents

Figure List

List of Abbreviations

ABCA1	ATP binding cassette transporter 1
ACS	Acute coronary syndrome
APO-E	Apolipoprotein E
CAD	Coronary artery disease
CVD	Cardiovascular disease
ECG	Electrocardiography
ECs	Endothelial cells
HDL	High density lipoproteins
HLA	Human leukocyte antigen
ICAM-1	Intercellular adhesion molecule1
IDL	Intermediate density lipoprotein
IFN-ɣ	Interferon-gamma
IHD	Ischemic heart disease
IL	Interleukin
iPSCs	Induced pluripotent stem cells
IMTC	Intima media thickness of carotid artery
LDL	Low density lipoproteins
MI	Myocardial infarction
MMP	Matrix metalloproteinase
MPO	Myeloperoxidase
NO	Nitric oxide
NF-κβ	Nuclear factor kappa B
Ox LDL	Oxidized low density lipoprotein
OCT	Optimal cutting temperature

PDGF	Platelet derived growth factor
PE	Plaque érosion
PF	Plaque fissuring
PG	Prostaglandin
PLA	Poly-L, D-lactic acid (96% l/4% d)
PMA	Phorbol 12- myristate 13- acetate
PGA	Polyglycolic Acid
PR	Plaque rupture
PLA	Polylactic acid
PAR1	Protease activated receptor 1
PAR4	Protease activated receptor 4
PECAM-1	Platelet endothelial cell adhesion molecule-1
PPP	Platelet poor plasma
PRP	Platelet rich plasma
SMCs	Smooth muscle cells
VLDL	Very low-density lipoprotein
VCAM-1	Vascular cell adhesion molecule-1
VTE	Vascular tissue engineering
TF	Tissue factor
Th1	T-helper lymphocyte 1
TIA	Transient ischemic attack
TNF	Tumor necrosis factor
vWF	Von Willebrand factor

UA	Unstable angina

Abstract

Coronary heart disease is the primary global cause of morbidity and mortality, accounting for about 33% of global deaths in 2013. Atherosclerosis is the principal cause of coronary heart disease and is caused by inflammation of the arterial wall. This begins with the accumulation of foam cells in the subendothelial space of an inflamed segment of the endothelium to create the fatty streak. The accumulation of these cells, and their apoptosis creates a proinflammatory necrotic core. This triggers smooth muscle cells migration into the subendothelial space, where these cells form a fibrous cap that mechanically strengthens the plaque. The ongoing inflammatory condition infit smooth muscle cell apoptosis which leads to cap thinning and eventual rupture of the plaque, triggering thrombus formation. Recreating this complex multi-step pathogenesis has principally relied on animal studies. However, key differences have been observed between the human and animal plaques. This has triggered attempts to develop a humanised *in vitro* models, however none of these have been demonstrated to reach later stages of plaque development, where plaque rupture trigger atherothrombosis. Previously our lab has used a layer-by-layer fabrication method to create a healthy tissue-engineered arterial construct. In this project, the aim was to develop and validate a simple 3D cell cultured neointimal model that can be inserted into this arterial construct to provide a novel tissue-engineered atherosclerotic plaque model. A protocol was developed to generate a 3D neointimal culture model in which the THP-1 monocytic cell line can be differentiated into THP-1-derived foam cells within a compressed collagen hydrogel. The cells were demonstrated to remain viable and secrete greater quantities of pro-inflammatory cytokines (such as TNF-α and IL-6) than macrophages.

The neointimal construct was found to possess significant tissue factor activity and could be observed to induce a slow platelet aggregation. These prothrombotic effects were reduced when the 3D neointimal model was treated with atorvastatin during the ox LDL loading period of the culture. These results provided the first demonstration that a tissue-engineered atherosclerotic plaque model could replicate the prothrombotic properties of the native neointima. A co-culturing method was successfully developed that allowed reversible attachment of the neointimal model to the previously developed tissue-engineered medial layer using a fibrin hydrogel. Through treatment with plasmin containing solutions, the different layers of the co-culture could be shown to detach from one another, providing a basis for creating the first plaque rupture model in an *in vitro* atherosclerosis model. Additionally, it was possible to observe the migration of human coronary artery smooth muscle cells from the medial layer into the neointima. This provides the first evidence that tissue-engineered atherosclerosis models can elicit this key event in the development of the advanced stage of fibroatheroma. Overall, this thesis demonstrates the power of using a layer-by-layer fabrication method to develop a 3D human neointimal model that can replicate the early events in fibroatheroma. This ability to replicate both early and more advanced stage events highlight the potential for this construct to be further developed into an effective model of atherosclerotic plaque rupture to allow us to study human atherothrombosis more effectively in an *ex vivo* environment, and as a replacement to current *in vivo* animal models.

Chapter 1: Introduction

1.1 The clinical importance of atherosclerotic plaques formation and rupture

In 2013, Coronary artery disease (CAD) caused 17.3 million deaths globally, accounting for 31.5% of the general mortality rate (Timmis *et al.*, 2018). It is the principal cause of all mortality in developed countries (Islam *et al.*, 2016). In the UK, and despite a significant decrease in the mortality and morbidity rates of CAD during the previous decade, it is still a significant health problem. As till April 2021, there were 7.6 million patients who have CAD with an average of 100,000 new hospital admissions because of CAD each year (BHF, 2021). Atherosclerosis is the main cause of CAD. It is a chronic inflammation of the blood vessel, characterized by progressive, focal, or diffuse thickening of the tunica intima (the interior layer of the blood vessel; Otsuka *et al*., 2016). The natural history of this disease involves stages of formation, progression, and rupture of the atherosclerotic plaque. However, the acceleration or regression of atherosclerosis also depends on the presence or absence of other risk factors, such as hypertension diabetes mellitus, hypercholesterolemia and genetic susceptibility (Bentzon *et al.*, 2014). There are two groups of risk factors for atherosclerosis, modifiable and non-modifiable risk factors. Modifiable risk factors include high blood pressure, high plasma levels of LDL, hypertriglyceridemia, homocysteinemia, high C-reactive protein, smoking, obesity, sedentary lifestyles, impaired glucose tolerance, psychological stress, and diabetes mellitus. Non-modifiable risk factors include genetic susceptibility, male gender, age and race (Fruchart *et al.*, 2004)

1.2 The pathological consequences of atherosclerosis in the coronary circulation

The signs, symptoms and outcomes of atherosclerotic plaque rupture are dependent on which artery becomes affected by displaced plaque or resulting thrombus. The coronary circulation is a network of arteries that supply heart muscles with blood. As the heart is a vital organ, any ischaemic damage caused by loss of blood supply may lead to a fatal heart attack. Thromboembolic phenomena related to disruption of atherosclerotic plaques may also affect other blood vessels, such as cerebral blood vessels, leading to a transient ischaemic attack (TIA) or ischaemic stroke (Timmis *et al.*, 2018). In this project, we will be modelling a coronary artery to focus on the consequence of atherosclerosis in the coronary circulation. As atherosclerosis is a chronic progressive disease, it will gradually cause narrowing to the cross-sectional area of the coronary artery as the atherosclerotic plaque extends into the lumen of the affected artery, even though the patient may remain asymptomatic for an extended period owing to the neovascularization and collateral circulation that can be created at the site of arterial narrowing. Once the narrowing of the lumen approaches 50% and above of the arterial lumen, the patient will start to suffer from symptoms of cardiac ischaemia such as exertional chest pain and shortness of breath, as the oxygen demand of the myocardium will exceed the rate of oxygen supply. These symptoms and signs are usually short-term and mild in severity and usually disappear after the patient rest or after the disappearance of the other provocative factors. This clinical syndrome is called stable angina pectoris (Valgimigli and Biscaglia, 2014). If the atherosclerotic inflammation progresses in severity, there will be more narrowing of the arterial lumen. The retrosternal chest pain will become more severe, and the attack may happen suddenly, even during rest. This clinical syndrome is called unstable angina pectoris (UA, Cavallari *et al.*, 2018). Several post-mortem studies of people who had a

fatal heart attack caused by UA reported that the atherosclerotic lesions were diffuse, and the arterial narrowing exceeded 75% of the total cross-sectional area of the coronary artery (Khandkar *et al.*, 2021). Furthermore, arterial thrombosis may also be seen in UA. However, these are called mural thrombi, as they do not obstruct the arterial lumen. Other scientists reported that coronary thrombi in UA might wax and wane in size, so they might only temporarily occlude the arterial lumen. This might explain the rhythm of the ECG records seen during the attack, as there will be a temporary ST-segment elevation, which will return to normal after a period, even without any additional medical intervention (Braunwald *et al.*, 2002). The advanced atherosclerotic plaque is characterized by the thin fibrous cap, a necrotic core filled with collagen, tissue factor, calcification and multiple spots of haemorrhage or neovascularization (Virmani *et al.*, 2003). This structure can be structurally unsound and, therefore, can fissure or rupture. This can lead to the highly thrombogenic contents of the plaque (such as collagen and tissue factor) being released into direct contact with the blood. This can trigger uncontrolled platelet aggregation and blood coagulation around the dislodged plaque (Asada *et al.*, 2020; Davis *et al.*, 2014). This abnormal thrombus can be carried in the blood to downstream vessels. If it is a small micro embolus, the clot may not block any of the coronary arteries and create clinical symptoms, being filtered out in the pulmonary circulation. However, if it is large enough to block these vessels without sufficient collateral circulation at the site of obstruction, this will cause myocardial infarction (MI). The myocardium downstream of thrombotic obstruction will become ischemic and undergo necrosis – leading to a loss of cardiac function. If the coronary obstruction is complete, there will be severe infarction, and the necrotic area will extend across the whole thickness of the myocardium (from the endocardium to epicardium); this situation is called a full-thickness MI. Clinically, severe, prolonged, retrosternal chest pain may be associated with diaphoresis,

shortness of breath, hypotension, or hypertension. If the arterial occlusion is not complete (for example, >90% occlusion), this is known as a partial thickness MI. The clinical features of this disease will be like the full thickness MI although it will be moderate in severity (Van de Werf *et al*., 2003; Cavallari *et al*., 2018).

1.3 The biological basis for the development of atherosclerotic plaques

1.3.1 Normal arterial structure and function

The normal structure of the artery consists of three primary layers - the tunica intima, the tunica media, and the tunica adventitia (Figure 1.1). The tunica intima covers the interior surface of the blood vessels. This layer comprises a monolayer of endothelial cells (ECs) (Islam *et al.*, 2016). Under normal physiological conditions, the endothelium plays an essential role as a barrier that prevents particles from passing from the plasma to the tunica media. The endothelial barrier is selective, such that water and small molecules in plasma can pass freely between ECs via spaces in intercellular junctions to the subendothelial area. Three types of endothelial cell junctions have been recognized, tight, adherence, and gap junctions. Occludin, a transmembrane protein, is the main constituent of the tight junction. The primary function of tight junctions is to prevent the diffusion of small particles across the endothelial cells. On the other hand, the transmembrane proteins vascular endothelial (VE-cadherin) are the main constituent of the adhesion junctions, which mainly regulate the movement of red blood cells across the endothelial cells. However, larger proteins and cells are prevented from passing. Low-Density Lipoproteins (LDL) carrying cholesterol and albumin particles are usually prevented from leaving the bloodstream by the EC barrier under normal physiological conditions. The permeability of these junctions is principally regulated by junctional proteins

VE-cadherin. Inhibiting the function of VE-cadherin may lead to an increase in endothelial membrane permeability (Dejana, Orsenigo and Lampugnani, 2008). On the other hand, the integral membrane protein connexins (Cx) is the main constituent of gap junction which mainly work to regulate ions and small molecules movement across endothelial membrane (Goodenough &Paul,2009). In addition to their barrier function, ECs play an essential role in maintaining the normal haemostatic state of blood by preventing blood clotting in undamaged blood vessels. This is achieved by producing endogenous inhibitors of platelet activation such as nitric oxide (NO), prostacyclin, and inhibitors of the coagulation cascade such as anti-thrombin III, tissue factor pathway inhibitor and endothelial protein C receptors. However, upon vascular injury, ECs assist in recruiting platelets to the site of damage and formation of a blood clot to block the wound and prevent more bleeding by producing von Willebrand factor (vWF) and plasminogen activator inhibitor 1 (PAI-1). A thin layer called the internal elastic lamina (IEL) separates the tunica intima from the tunica media, containing elastin and basement membrane proteins (Aird, 2005). The middle layer of the blood vessel is the tunica media. This layer consists of smooth muscle cells (SMCs) and extracellular matrix (ECM). In contrast, the tunica media of veins do not contain smooth muscle cells. Collagen I and elastin provide the arteries with their mechanical strength. These extracellular matrix proteins are found in large arteries where these vessels need more supportive strength to adapt to the high pressure of the blood (Truskey, 2011). SMCs play an active role in controlling the mechanical properties of arterial walls, with contraction allowing dynamic regulation of vascular resistance and thus blood flow to the downstream tissues (Aird, 2007). The tunica adventitia is the outer layer of the blood vessel. It mainly consists of loose connective tissue, collagen and fibroblasts, and the nerves and blood vessels that supply the main blood vessel. It has been reported that adventitial fibroblast cells contribute to maintaining the blood vessel

tone with SMCs and playing a pivotal role in the repair process after vascular injury (Truskey, 2011).

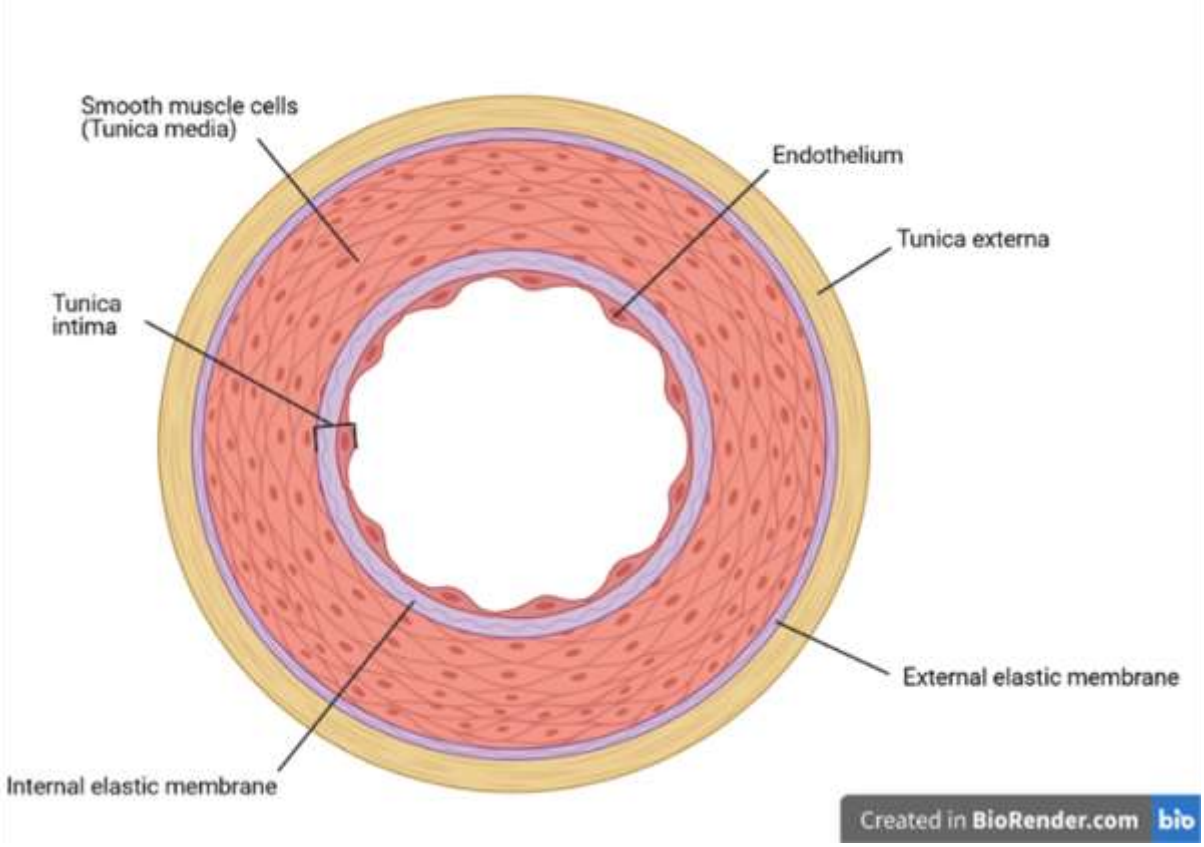

Figure 1.1. Cross-sectional view of a normal artery. The normal structure of the artery consists of three main layers: the tunica intima which is composed from a monolayer of endothelial cells. Tunica interna is separated from the tunica media by internal elastic membrane. Tunica media is the second layer which is composed mainly from VSMCs. Tunica adventitia is the most outer layer of the blood vessel that contains connective tissues, nerves, and the vasa vasorum.

1.3.2 Mechanisms of atherosclerotic plaque formation

Atherosclerosis is chronic vascular inflammation that can started early in childhood as fatty streaks. The development of these initial lesions continues for decades, creating an advanced and highly thrombogenic plaque. In some circumstances, these might rupture, leading to fatal heart attacks.

1.3.3 Endothelial cell dysfunction

Endothelial cell dysfunction is an early precursor of atherosclerosis. This is thought to occur due to hypercholesterolemia and abnormal blood flow at specific vulnerable areas of the arterial system (Braunwald *et al.*, 2002). For instance, a blood vessel in which there are low shear stress, or are exposed to turbulent blood flow in branched or curved segments of the vessel are known to be vulnerable to plaque formation (Robert *et al.*, 2013). This endothelial dysfunction can also be worsened by other cardiovascular risk factors such as high blood cholesterol, smoking, diabetes mellitus and hypertension (Yang *et al.*, 2020). Each of these trigger structural changes that cause a disruption in the permeability of the intercellular junctions that lay between ECs. The function of the transmembrane proteins occludins and cadherin to seal the paracellular junctions between endothelial cells are affected by the inflammatory mediators released during atherosclerosis. Initially, during the early stage of atherosclerosis, there will be a localized loss for the selective barrier function of these junctions. This disruption to the barrier function of the intimal layer allows an influx of LDL

cholesterol particles into the subendothelial matrix (Gallo *et al.*, 2018). These particles are trapped and eventually modified and oxidized. Accumulation of oxidized LDL particles in the subendothelial area will enhance the endothelial dysfunction. The loss of normal endothelial cell function leads to a reduction in the production of NO (nitric oxide) and Prostacyclin (PGI_2) removing the normal inhibitory influence of the endothelial cells on platelet aggregation favouring platelet activation in these regions (Cyr *et al*.,2020; Zuchi *et al*., 2020). Additionally, through increasing expression of the VCAM1 (vascular cell adhesion molecule 1) and ICAM1 (intercellular adhesion molecule 1) cell surface markers it promotes increasing the recruitment of circulating monocytes and T- lymphocytes to the affected segment. In later stages of atherosclerosis, the endothelial cell dysfunction will also promote the migration and proliferation of vascular smooth muscle cells within the subendothelial space (Xue *et al.*, 2020).

1.3.4 Foam cell formation

Endothelial dysfunction will promote the recruitment of circulating monocytes towards the injured area through increased endothelial permeability and monocyte adhesion. Several studies have reported that a considerable monocytes migration will happen across the endothelium without a significant disruption in the endothelial barrier (Navab *et al.*, 1988). Moreover, this monocyte movement across the endothelial membrane will also accelerate albumin flux into the subendothelial space (Territo *et al*., 1984). Once recruited to the subendothelial area, the monocytes will differentiate into macrophages. As a result of the inflammatory process, the LDL particles moved from the circulation to the sub-endothelial matrix will be modified and then oxidised, mainly because of myeloperoxidase oxidation

products, an inflammatory enzyme secreted by the macrophage. As an anti-inflammatory response, the macrophages will start to engulf the oxidized LDL particles. At this point, the macrophages become enriched with intracellular lipid droplets and are known as foam cells because of their appearance. The accumulation of foam cells in the subendothelial space creating an early stage of atherosclerosis referred to as fatty streaks (Anastasia V. Poznyak *et al.*, 2020)(Figure 1.2). This new layer formed in the subendothelial space is known as the neointima.

1.3.5 The role of platelets in the development of the atherosclerotic plaque

Although platelets are principally known to play a role in thrombus formation, recent studies have demonstrated a vital role for platelets in the initiation and progression of the atherosclerotic lesion. This appears to occur through a mechanism independent of that used for thrombus formation. According to Huo and colleagues, platelets will adhere to the dysfunctional endothelial membrane even before the adherence and migration of monocytes into the subendothelial matrix (Huo *et al*., 2003). Although the mechanism by which platelets adhere to the inflamed endothelium is not fully understood, studies have reported that this occurs via integrin $\alpha_{IIb}\beta_3$ and the platelet vWF receptor, glycoprotein Iα (GPIbα). This binding triggers platelet activation at the dysfunctional endothelial segments (Massberg *et al*., 2002; Gawaz *et al*., 2005). At healthy segments of the endothelium, platelets cannot be adhered or activated because of the inhibitory effects of endothelial PGI_2 and NO. In areas of dysfunctional endothelium, these cells produce lower levels of PGI_2 and NO, which facilitate platelet adhesion and activation. The adherent activated platelets will express P-selectin and CD40L on their cell surface. These adhesive receptors play a crucial role in mediating platelet-

endothelial adhesion and platelet-platelet aggregation (Gąsecka *et al.*, 2021). Gawaz and colleagues demonstrated in mice that chronic blockade of GPIbα decreased subendothelial leukocyte recruitment and consequently slowed atherosclerosis progression in mice (Gawaz *et al.*, 2005). After platelets became activated, they release monocyte attracting protein (MAP-1). This stimulates monocyte adhesion, invasion, macrophage differentiation and conversion to foam cells (Massberg *et al.*, 2002). These macrophages propagate the inflammatory process by secreting Interleukin-1 (IL-1), Tumour necrosis factor-α (TNF-α) and monocyte chemotactic protein 1 (MCP-1), which elicits further leukocyte recruitment.

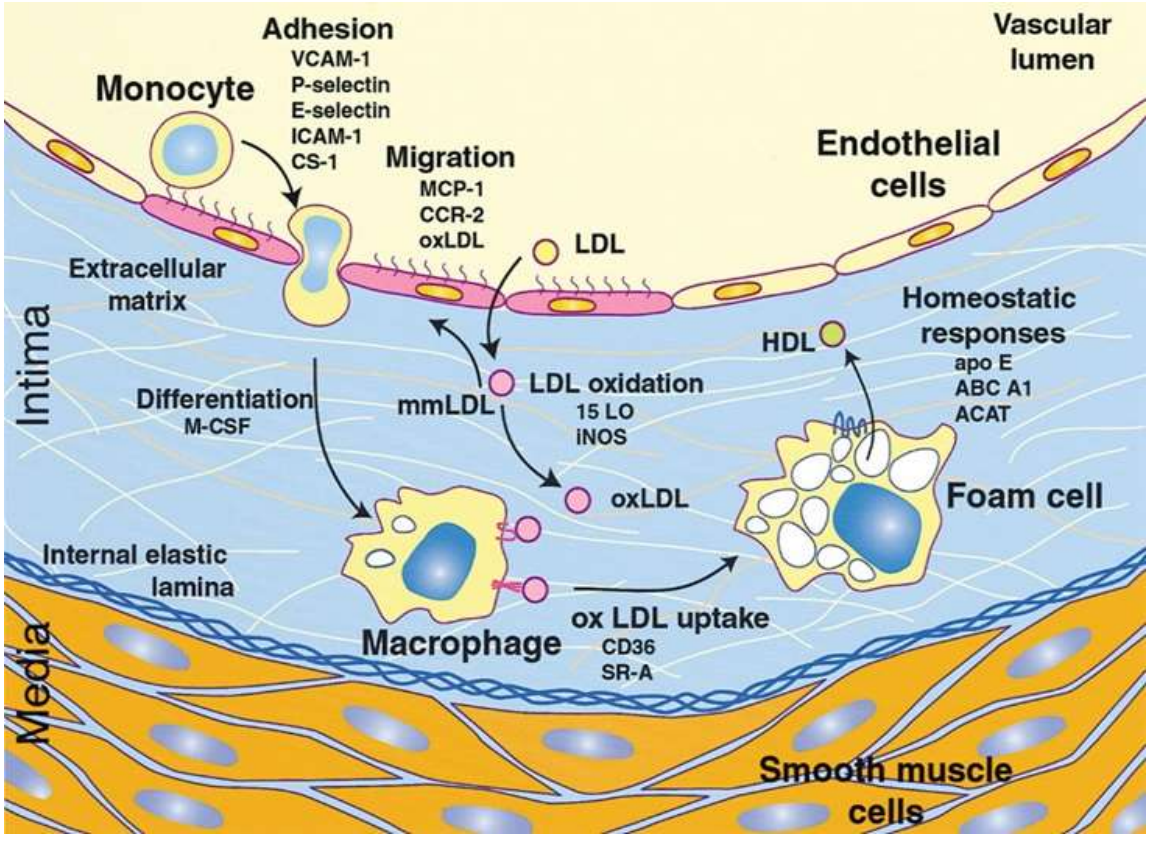

Figure 1.2 Foam cell formation. Monocytes and LDL emigrate through the dysfunctional endothelium toward the subendothelial space where the monocytes will differentiate to macrophages, and LDL will be oxidized. Figure reproduced from Glass & Witztum, (2001).

1.3.6 T-lymphocyte recruitment

Previous studies have demonstrated that T-lymphocytes play an essential role in the initiation and progression of atherosclerosis (Jonasson *et al*., 1985). T helper lymphocytes will move toward the subendothelial space after being activated by the human leukocyte antigen-DR-positive (HLA-DR-positive) endothelium. In the subendothelial matrix, T helper 1 (Th1) lymphocytes will contribute to the inflammatory process by secretion of cytokines such as interferon-gamma (IFN-γ) and tumour necrosis factors (TNF), whose receptors have been detected on the surface of foam cells of mouse models. TNF-α and IFN-γ can enhance the rate of atherosclerosis progression by further increasing the permeability of the endothelial barrier leading to an acceleration of the influx of monocytes and LDL-cholesterol into the subendothelial space (Pober and Sessa, 2007). T helper 2 (Th2) lymphocytes also have a role in plaque formation by secreting another group of cytokines that contribute to foam cells formation and smooth muscle proliferation through secretion of IL-4 and IL-13 (Folick *et al*., 1997). These findings demonstrate a role for cellular immunity in promoting atherosclerosis. On the other hand, there was no detected significant role for humoral immunity in atherosclerosis, as previous work had seen little contribution of the B lymphocytes in this inflammatory process (Hansson and Jonasson, 2009). However, Galigiuri and colleagues reported that splenectomy in mice would accelerate the atherosclerotic plaque formation compared to control animals, demonstrating the vital role of humoral immunity in the pathogenesis of atherosclerosis (Galigiuri *et al*., 2002).

1.3.7 Infiltration and proliferation of smooth muscle cells

As a result of the pro-inflammatory condition that the early stages of atherosclerosis have created, SMCs originating from the tunica media will be modified from their normal contractile phenotype to proliferative phenotype, and migrate to the intima, where they can assist in the thickening of the neointimal layer. This occurs both through the loss of inhibitory signals from the dysfunctional endothelium and due to the localized release of cytokines such as IL-1β and platelet-derived growth factor (PDGF) from endothelial cells and macrophages (Sheikine and Hansson, 2006). Besides, platelets have also been seen to invade through the endothelial barrier and accumulate in the subendothelial matrix. Here they become activated by collagen and other agonists in the subendothelial matrix and start to secrete PDGF and lysophosphatidic acid (LPA) which stimulates SMC migration and proliferation at the subendothelial space (Schafer and Bauersachs, 2008). Once SMCs invade the neointimal space, they will begin to produce and release a range of extracellular matrix molecules such as collagen and proteoglycans, leading to the formation of a fibrous cap that lies between the endothelium and the accumulated foam cells (Figure 1.3). The SMCs also take up lipids similarly to macrophages (Cadsuda *et al*., 1992). with recent studies demonstrating that 50% of all foam cells in human atherosclerotic plaques are of smooth muscle origin (Wang *et al.*, 2019). Additionally, they have reported that Smooth Muscle Cell-derived foam cells (SMCDFCs) express less ABCA1 than macrophage-derived foam cells. ABCA1 (ATP-binding cassette transporter 1) is a transporter that facilitates the expulsion of LDL particles from foam cells, and so facilitates regression of atherosclerosis. The downregulation of ABCA1 in SMCDFCs makes them more resistant to regression than macrophages-derived foam cells (Q *et al*., 2020). Research has also shown that SMC migration is influenced by a number of

proteins. For example, CEMIP (cell migration-inducing and hyaluronan-binding protein) plays an essential role in enhancing VSMCs proliferation and migration through activation of the Wnt-Beta-Catenin signalling pathway (Chong *et al.*, 2020). This group has reported that CEMIP level is upregulated in plasma of patients with atherosclerosis, compared to that observed in a matched group of healthy people. Similarly, overexpression of C-X-C motif chemokine 12 (CXCL12) was associated with a high rate of VSMCs proliferation and their transformation to foam cells (Li *et al*., 2020). Any intervention that decreases the expression of CEMIP or CXCL12 may help prevent VSMCs proliferation and maturation within the plaque (Xue *et al*., 2020; Q *et al*., 2020; Li *et al*., 2020) pointing to a potential new therapeutic strategy in atherosclerosis. On the other hand, Ursodeoxycholic acid (UDCA), a natural bile acid that is used for the treatment of cholestatic hepatic pathologies, has been reported to prevent intimal hyperplasia and SMC migration, principally through inducing apoptosis. So, UDCA may be a useful therapeutic substance to treat atherosclerosis (Huang *et al.*, 2020)

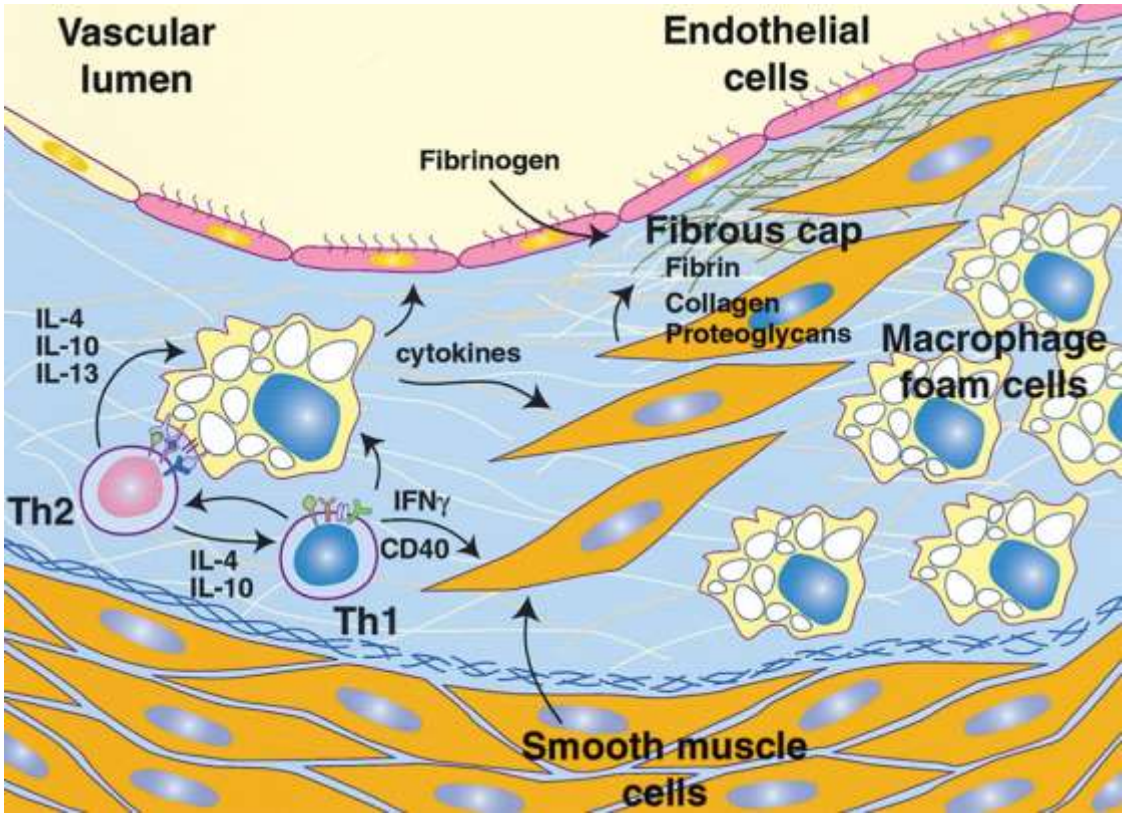

Figure 1.3 Fibrous cap formation. The fibrous cap results from the migration of SMCs between the endothelial cells and macrophage-derived foam cells. Here they proliferate and lay down fibrin, collagen and proteoglycans that will form the fibrous cap of the atherosclerotic plaque. Figure reproduced from Glass and Witztum (2001).

1.3.8 Formation of the necrotic core

The size of the neointima is controlled in early atherosclerotic lesions by apoptosis of foam cells (Liu *et al*., 2005). This apoptotic response is driven by several different chemical messengers such as TNF-α and oxLDL. Additionally, induction of endoplasmic reticulum stress is a crucial mediator of foam cell death (Seimon and Tabas, 2009). Whilst this cell death initially acts to limit the size of the plaque, in more advanced lesions, there is a reduced ability of phagocytic cells to clear apoptotic foam cells (called defective efferocytosis). Due to the reduced clearance rate, these apoptotic cells start to become necrotic – with the cells become swollen and have increased membrane permeability (Gaultier *et al*., 2009). This allows the

lipid contents to leak into the extracellular space alongside cytokines and other cytotoxic compounds. For instance, IL-1β, TNF-α and IFN-γ all work to propagate the growth of the plaque by increasing the size of the necrotic core (Andres *et al*., 2012). This creates a necrotic lipid-filled core of the plaque flanked on either side by a shoulder region, containing T-lymphocytes, macrophages, and SMCs, underneath the fibrous cap (Figure 1.4). At this stage, the entire structure is referred to as a fibroatheroma, and if unperturbed, will often lead to no observable clinical symptoms (Bentzon *et al.*, 2014). Further growth of the fibroatheroma causes progressive narrowing of the arterial lumen, which can cause angina by limiting blood supply to the cardiac muscle. However, plaque size does not correlate with the likelihood of its ability to trigger acute cardiovascular events (Jaberi *et al*., 2018).

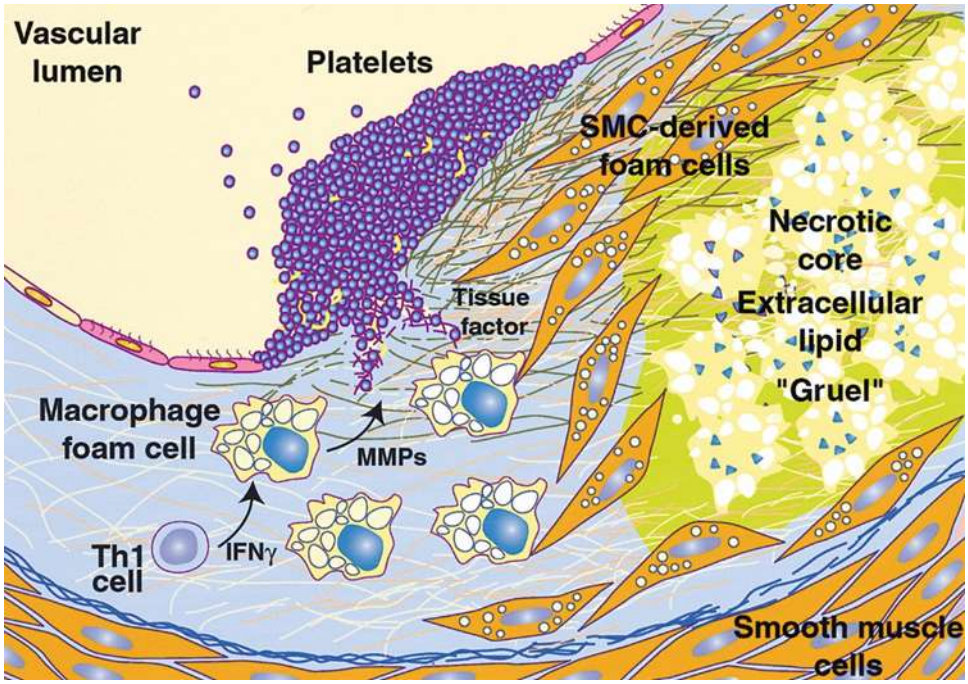

Figure 1.4 Formation of the necrotic core. Macrophage-derived foam cells and SMC-derived foam cells, and other ECM contents will accumulate and form the necrotic core. Figure reproduced from Glass and Witztum (2001).

1.3.9 Mechanisms of atherosclerotic plaque disruption

An atherosclerotic plaque is often clinically silent and often will cause no notable symptoms for the affected individual throughout their entire life. However, some plaques may become disrupted decades after their formation, leading to exposure of the blood to the highly-thrombogenic material contained within. There are three types of plaque disruption that can lead to the onset of clinical symptoms: Plaque rupture (PR), plaque erosion (PE), and plaque fissuring (PF). Although, some investigators consider PE and PF as subtypes of PR (Asada *et al.*, 2020).

1.3.9.1 Plaque Rupture

Plaque rupture (PR) is the most common cause of acute coronary syndrome (Khandkar *et al.*, 2021). In plaque rupture, the fibrous cap of the atherosclerotic plaque will thin and progressively weakened till it breaks, leading to an opening that is large enough to release most of the highly atherogenic contents of the plaque into the circulation (Okuyama *et al*., 2015). The exact mechanism that triggers atherosclerotic PR is unclear, with several suggested hypotheses (Fuster *et al*., 1988). Badimon and Vilahur have reported that the current consensus is that PR is a multifactorial process that involves biomechanical, hemodynamic and physical factors (Badimon and Vilahur, 2014). In support of this evidence has suggested that mechanical disruption of the plaque caused by vasospasm and increased blood shear stress can contribute to rupture. Abela *et al* have also reported that cholesterol crystals penetrating the thin cap of the atherosclerotic plaque might be responsible for the PR (Abela *et al.*, 2016). However, the principal player in this event seems to be continuation of the inflammatory processes (Van Der Wal *et al.*, 1994).

Collagen is an essential source of atherosclerotic plaque cap strength. Type I, II and III collagen are found in the atherosclerotic matrix in unequal concentrations, with type I collagen being the most abundant (Wolf and Ley, 2019). Over time, the macrophages inside the stabilized plaque will start to secrete matrix metalloproteinases (MMP), which will digest the collagen in the fibroatheroma (Gough *et al.*, 2006). This will lead to thinning of the plaque wall, especially at the shoulder region. This type of fibroatheroma is called a thin cap fibroatheroma, or unstable plaque (Figure 1.5; Davies, 2000). However, it is still unclear how long it takes the stabilized fibroatheroma to convert into a thin cap fibroatheroma (Cao *et al*, 2020). Other researchers have also raised several questions about the relationship between PR and thrombo-embolic phenomenon, as several post-mortem studies in cases of deaths due to non-cardiac causes have reported observing signs of PR without thrombosis. This might mean that the thrombosis could happen without the need for direct exposure of the luminal blood with the constituents of the plaque. It also suggests that the causative relationship between PR-induced thrombosis with ACS and sudden cardiac death could be overestimated, and might actually be incidental (Virmani *et al.*, 2000). According to several post-mortem studies conducted on patients who died as a result of acute coronary syndrome, ruptured atherosclerotic plaques also contain less smooth muscle cells in comparison to intact plaques, making the wall of the plaque thinner, weaker and more vulnerable to rupture, especially at the shoulder area (Lee *et al.*, 1991). At this stage, the SMCs will be the most abundant constituents of the atherosclerotic fibroatheroma (Islam *et al.*, 2016). They will start to engulf the oxidized LDL particles akin to macrophages, creating smooth muscle-derived foam cells (Bentzon *et al.*, 2014). The immune system will begin to target both of these distinct foam cell populations, which engulf the modified lipid particles using several enzymes such as cathepsins and matrix metalloproteinase (Katsuda *et al*.,1992), triggering their destruction

and leading to the formation of a large necrotic core (Clarke and Bennett, 2009). Additionally, these enzymes will also work to weaken the plaque by degrading collagen. Interestingly, the apoptosis rate among these SMCs is significantly higher than that of the local macrophages, which are especially pronounced in advanced and late atherosclerotic lesions. Although some researchers have suggested that the apoptotic rate might be the same for both cells, but the macrophages that undergo apoptosis are rapidly replaced by new macrophage cells from circulation giving the appearance of a slower turnover rate (Clarke and Bennett, 2009). Macrophage apoptosis may ameliorate or decrease the atherosclerosis progression, mainly by reducing the size of the plaque. However, SMC apoptosis will adversely affect the strength and stability of the atherosclerotic plaque architecture. It will lead to thinning of the fibrous cap of the plaque, making it more vulnerable to rupture (Figure 1.5). IFN-γ, which is mainly secreted from macrophages and T-lymphocytes, has been shown to increase SMC apoptosis and reduce their collagen synthesis, which would also contribute to the weakening of the fibrous cap. So, inflammation is likely to play an essential role in triggering this loss of SMC, which could eventually lead to plaque rupture if this becomes too extensive (Lippy *et al*., 2013).

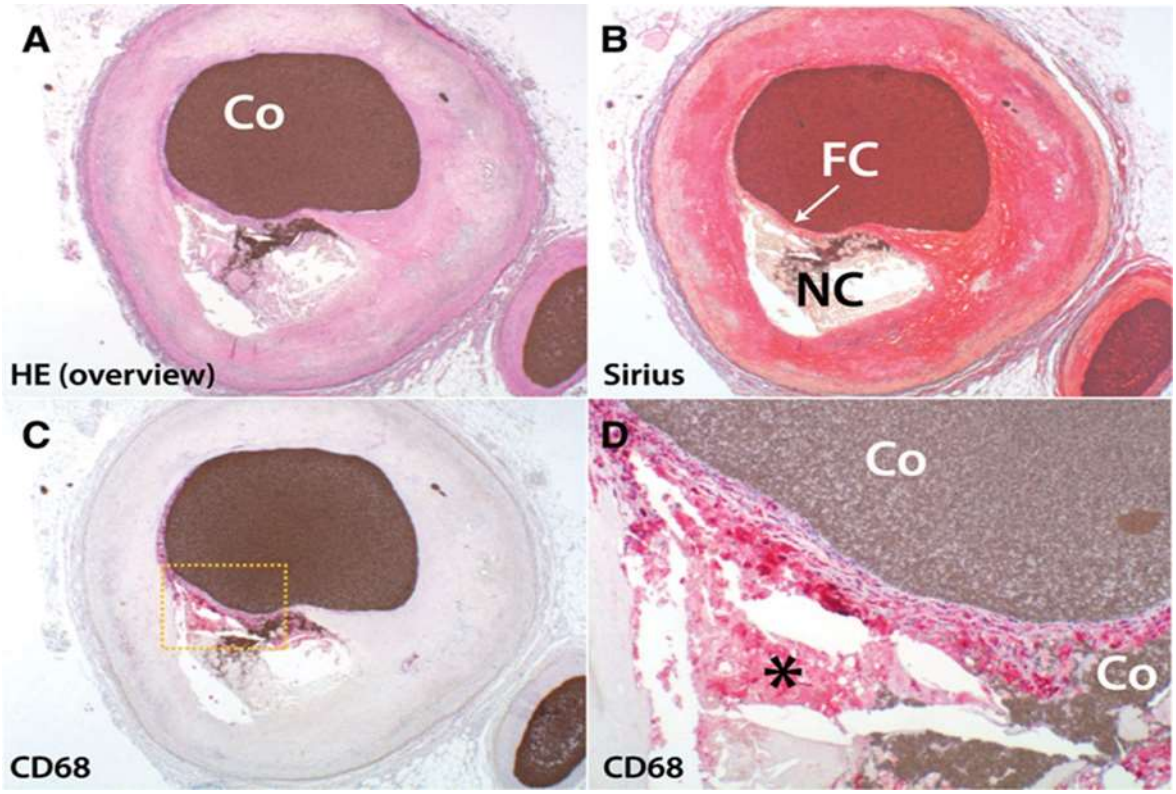

Figure 1.5 Thin-cap atherosclerotic plaque. Immunohistochemical staining of a segment of artery taken post-mortem. Co: contrast medium, (Fc) thin fibrous cap, NC: necrotic core. The vulnerable thin fibrous cap is about to rupture. In such case, the highly thrombogenic content of the necrotic core (NC) will be released to circulation leading to the thrombo-embolic phenomenon, most of the cells inside the NC were positive for CD68 antibody. Figure reproduced from Bentzon *et al*., (2014)

1.3.9.2 Plaque erosion

In plaque erosion (PE), the endothelial membrane is disrupted; however, the contents of the necrotic core are still not in contact with the circulation (Jia *et al.*, 2013). Plaque erosion (PE) is caused by a different mechanism from that of plaque rupture. Some studies have reported that the endothelium beneath the thrombus on an eroded plaque is either severely damaged or absent. However, both the internal and external elastic lamina are intact, and the medial layer is normal, with SMCs showing a contractile phenotype. In contrast, the internal elastic lamina is damaged in plaque rupture, and the media layer is thin with disrupted architecture

(Hao *et al*., 2006). Additionally, whilst smooth muscle cell number was reported to be lower in both lesions, the number in areas of PR was significantly lower than that found in areas undergoing PE (Van Der Wal *et al.*, 1994). Also, the necrotic core in PE is smaller than that of PR, and the density of inflammatory cells is lower than that in PR. Furthermore, some studies have reported that several PE lesions have no necrotic core (White *et al*.,2016). In addition, Although several studies have reported that patients who have PE are less likely to develop acute coronary syndrome (ACS) in comparison with those patients with PR, other studies have suggested that the causative relationship between PE and ACS were underestimated owing to the difficulties in using common diagnostic tools such as standard coronary angiography and intravascular ultrasonography in which this superficial lesion that is easily missed (Shahar *et al*., 2003; Virmani *et al*., 2000). Furthermore, several post-mortem studies have reported that PE is responsible for about 40% of all sudden cardiac deaths (SCDs; Bentzon *et al*., 2014). Other studies have suggested considering PE as a cause for SCD when thorough microscopic examination fails to detect PR (Virmani *et al*., 2000). In addition, they have reported that young women have a significantly higher rate of PE lesions than other samples of patients (Shahar, 2003). The mechanism that is responsible for thrombus formation in PE is currently the subject of debate. How can there be a thrombus on top of the plaque in PE when a thick and intact fibrous cap prevents contact with the blood? This indicates that the highly-thrombogenic constituents of the atherosclerotic plaque matrix may not always be the primary trigger for thrombosis in atherosclerotic disease (Arbustini *et al*.,1991). However, other investigators have documented that the constituents of thrombi caused by PE differ significantly from those triggered by PR. Although thrombi caused by PE and PR are both composed mainly of fibrin and platelets, platelets are the principal constituent of PE thrombi,

whilst fibrin was seen to be the major constituent of PR thrombi (Sato *et al.*, 2005). These data indicate that the mechanisms of PR thrombosis differ from those triggered by PE.

Some studies have suggested that the inflammatory process that accompanies PE or PR differs from that found in the intact plaque. As stated previously, it is rare to detect neutrophil cells among the inflammatory cells during the formation of the intact plaque formation (Hansson and Jonasson, 2009). However, in the case of PE and PR, there are abundant neutrophil cells observed at the site of the lesion. As the neutrophil cells can secrete certain lytic enzymes, they may have a role in initiating plaque wall erosion or ulceration (Weiss *et al*., 1989). Some researchers have reported that collagenase I is mainly secreted from neutrophil cells. Activation of neutrophil will cause the secretion of this enzyme, which will degrade type I collagen leading to weakening and thinning of the fibrous cap. High expression of collagenase I is also known to be a risk factor for atherosclerotic plaque rupture, potentially further suggesting a role for neutrophils in this process (Herman *et al.*, 2001). This localized neutrophilia also has been observed following coronary angioplasty-induced laceration (Van Der Wal *et al*., 1994). However, other studies have suggested that neutrophils play no role in plaque erosion or rupture, as they only accumulate at the lesion site after these events have occurred (De Servi *et al.*, 1990) . In addition to the above local risk factors for PR and PE, there are other systemic factors, for instance, procoagulant conditions, recurrent infections, and systemic inflammation.

1.3.9.3 Plaque fissuring

Sometimes the thin plaque cap can tear, break, or crack, especially at the weaker shoulder regions of the plaque (Davies and Thomas, 1985). These plaque fissures (PF) have been seen

to be associated with thrombosis, and in some cases, with fatal heart attacks (Davies and Thomas, 1981). Usually, PF is associated with intraplaque haemorrhage into the necrotic core (Virmani *et al*., 2000). Some researchers have suggested that the source of this haemorrhage is from the flow of the luminal blood through the tears or the cracks that are associated with PF (Davies & Thomas, 1985). However, other studies have hypothesized that the intraplaque haemorrhage is mainly caused by neovascularisation of the medial layer (Paterson, 1938). Plaque fissuring has also been considered a precursor for PR or an incidental lesion (Arbustini *et al*., 1991).

1.4 The mechanisms of atherothrombosis

Atherothrombosis is the term applied to the haematological process that leads to thrombosis in the setting of atherosclerosis. In the intact blood vessel, antithrombotic factors significantly outweigh any procoagulant thrombotic factors. However, after rupturing of atherosclerotic plaque, this balance will be disrupted, and the procoagulant effects will exceed the anticoagulant effects, ending with the formation of a thrombotic clot (Junt *et al*., 2007).

1.4.1 Formation of a platelet aggregate

After rupture of the atherosclerotic plaque, platelets start to accumulate and adhere to the exposed collagen at the site of the ruptured plaque. The adhesion of the platelets is mainly triggered by collagen in the subendothelial matrix, either directly or indirectly, via bound vWF (Kaplan and Jackson, 2011). The binding of platelets to these adhesive ligands activates them, but this can be amplified further by influencing soluble agonists such as thrombin,

thromboxane A_2, and adenosine diphosphate (ADP) produced or released at the site of injury. After activation of the platelets, the inactive form of integrin αIIbβ3 will convert to its active form, enabling the activated platelets to bind with fibrinogen and vWF. Activated platelets begin to cohere to one another via the bound fibrinogen, leading to the formation of a platelet aggregate. (Kaplan and Jackson, 2020).

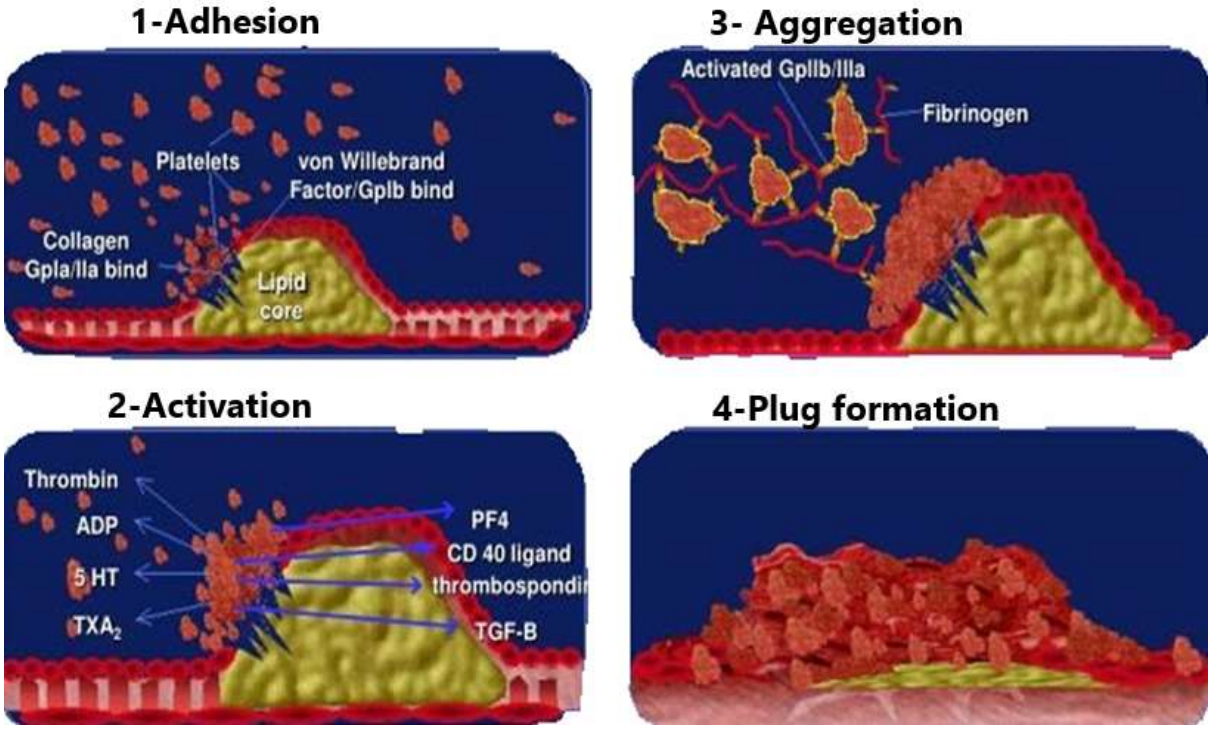

Figure 1.6 Platelet activation in atherosclerosis. After rupture of the atherosclerotic plaque, platelets start to accumulate and adhere to the exposed collagen at the site of the ruptured plaque. (1) The adhesion of the platelets is mainly triggered by collagen in the subendothelial matrix, either directly or indirectly, via bound vWF. (2) Adherent platelets become activated through intracellular signalling pathways caused by binding to vWF or collagen. This activation triggers platelet production of thromboxane A_2, secretion of ADP and 5-HT, and production of a catalytic surface for thrombin production. These platelet agonists can then activate other circulating cells to recruit them to the growing thrombus. (3) Activation also triggers the activation of integrin $\alpha_{IIb}\beta_3$ on the platelet surface. This allows these cells to bind fibrinogen. Cohesion of platelet through fibrinogen bridges helps trigger aggregation of platelets. (4) This aggregation then can then contract and create a plug covering the surface of the ruptured plaque. Figure modified from Kumar, (1997).

1.4.2 Activation of the blood coagulation cascade

Blood coagulation is a highly regulated and complex process. It plays a crucial role in keeping the blood in a highly hemodynamic balanced situation. Under normal physiological conditions, when vascular wall injury happens, the endothelial lining is interrupted, and sub-endothelial collagen and tissue factor will expose to blood at the injury site. Collagen will stimulate aggregation and activation of the platelets at the site of vascular injury resulting in the formation of a platelet aggregate. Exposed tissue factor in the subendothelial matrix will stimulate a cascade triggering activation of plasma-derived coagulation factors. The final product for the activated coagulation cascade is the formation of Thrombin from prothrombin, which can cleave soluble plasma-derived fibrinogen into insoluble fibrin mesh. This, in turn, will enmesh the unstable platelet aggregate forming a stable thrombus (Asada *et al*., 2020). Classically, the coagulation cascade was divided into three pathways - the extrinsic, intrinsic, and common pathway (Figure 1.7). This classical model of blood coagulation can interpret the results of *in vitro* coagulation screening tests (the prothrombin time and the activated partial thromboplastin time). However, it does not require a role for cell surfaces in the coagulation process, and it fails to provide appropriate explanations for several bleeding disorders. For example, it is unable to explain why people with FIX and FVIII deficiency (haemophilia A and B) suffer from significant bleeding episodes, despite the extrinsic and common pathway being unaffected. This lead to the development of the cell-based model of haemostasis (Hoffman, 2003).

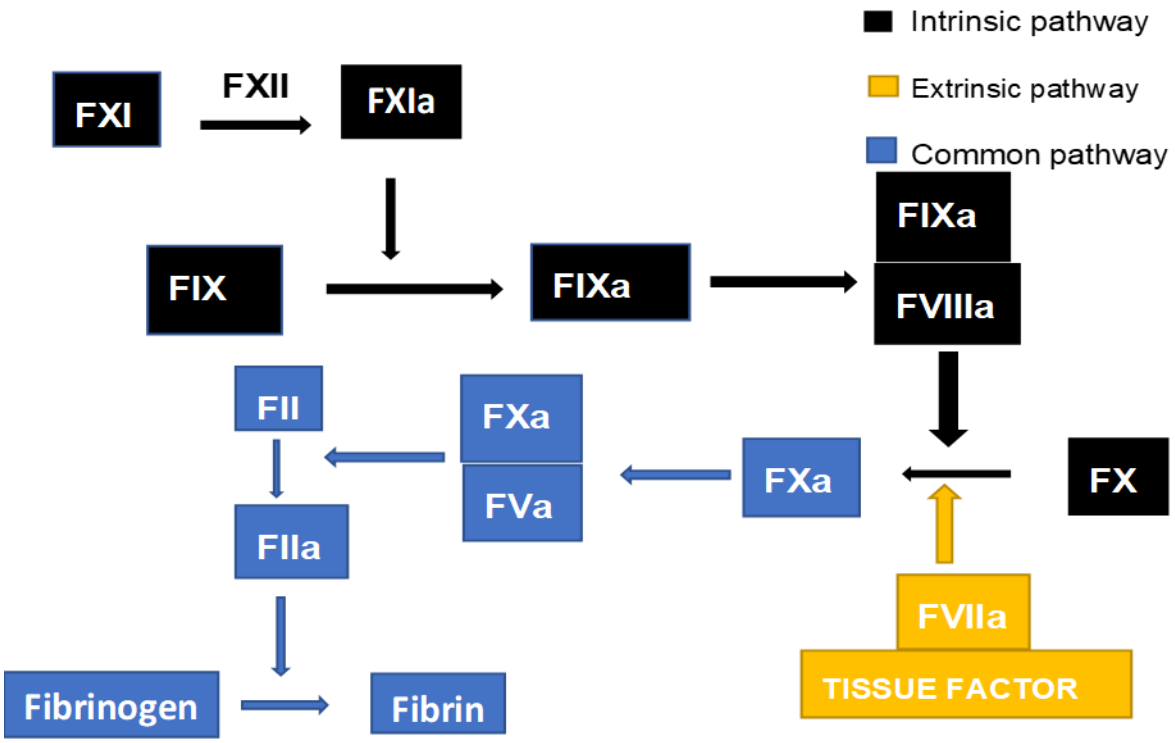

Figure 1.7 The classic interpretation of the coagulation cascade. Classically, the coagulation cascade consists of three pathways - the extrinsic, intrinsic, and common pathways. According to this cascade, FXII is the main initiator of the intrinsic pathway, activating XI to XIa. Activation of FXIa will lead to activating FIX to IXa. In corporation with FIIIa, FIXa will activate FX to FXa. FXa with FVa will activate prothrombin (FII) to thrombin (FIIa). Thrombin will transform the soluble fibrinogen to more stable and insoluble fibrin.

1.4.2.1 The cell-based model of haemostasis

More recently, there has been a move away from the traditional conception of the extrinsic, intrinsic, and common coagulation pathways as three independently regulated parts of the coagulation cascade. Instead, the cell-based model of haemostasis proposes that these pathways work together to create three temporally overlapping stages that illustrate the activation of the coagulation pathway *in vivo* and provides a thorough understanding of

certain bleeding disorders (Zaidi and Green, 2019). The three stages are known as the initiation, amplification, and propagation stages.

1.4.2.2 Initiation phase

Under normal physiological conditions, specific cells outside of the blood vessel, such as fibroblasts, macrophages, smooth muscle cells, and mononuclear cells express tissue factor (TF). This is why this step was traditionally referred to as the extrinsic pathway. Normally TF is not present on the surface of endothelial cells, but this can be triggered when cells are exposed to specific inflammatory mediators (e.g., TNF-α). TF is also expressed by endothelial cells in response to vascular wall injury.

Immediately after vascular wall injury, inactive FVII in the plasma will be in direct contact with subendothelial TF at the site of vascular injury (Figure 1.8). Here, TF plays an essential role in initiating the coagulation cascade to activate FVII to FVIIa. This TF-FVIIa complex will activate FX to FIXa, which can then trigger the formation of thrombin from prothrombin. Moreover, it has been reported that TF-bearing cells secrete a small amount of thrombin even under normal physiological conditions, which may further contribute to the initiation phase of the coagulation cascade (Hoffman, 2003).

1.4.2.3 Amplification phase

During the amplification phase, the initial spark of thrombin formation that occurred in the initiation phase can be used to trigger a significant amplification of thrombin production. This occurs upon the surface of activated platelets, which have begun to form an aggregate upon

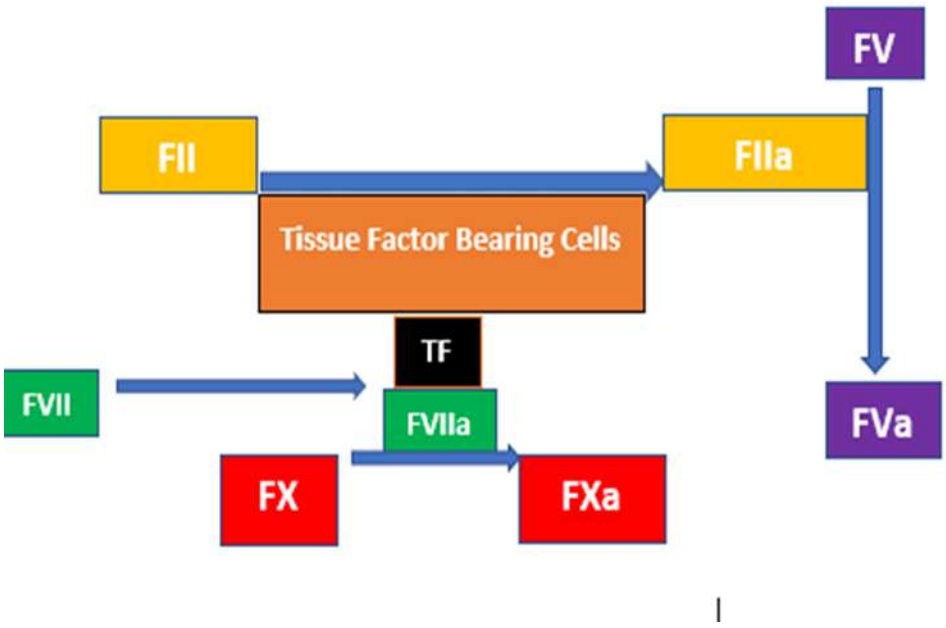

Figure 1.8 The initiation phase of the cell-based model of haemostasis. After vascular wall injury, inactive FVII in the plasma will be in direct contact with subendothelial TF at the site of vascular injury. TF plays a vital role in initiating the coagulation cascade as it works to activate FVII to FVIIa. This TF-FVIIa complex will activate FX to FXa, which can then trigger the formation of thrombin from prothrombin. Moreover, It has been reported that TF- bearing cells secreted a small amount of thrombin (FIIa) even under normal physiological conditions, which may further contribute to the initiation phase of the coagulation cascade by converting FV to FVa.

the exposed subendothelial collagen at the site of vascular injury. This aggregate formation is further reinforced by the ability of the initial thrombin spark to trigger further local platelet activation through cleavage of the proteas -activated receptor 1 (PAR1) and protease activated receptors 4 (PAR4) on the surface of human platelets, as well as their indirect binding to GPIb (Lordan *et al*., 2021). This high-level platelet activation allows platelets to expressed phosphatidylserine on its external face of its plasma membrane. These procoagulant lipids can bind clotting factors bringing them together at a catalytic surface where they can more effectively activate one another than when free in the bloodstream.

Simultaneously, thrombin produced in the initiation phase can cleave and activate Factor V, VIII and XI upon the surface of the activated platelets. These helps increase local thrombin production as Factor XI activates Factor IX. This FIXa works together with Factor VIIIa from a second tenase complex that can cleave and activate Factor X on the surface of the activated platelets.

1.4.2.4 Propagation phase

On the surface of the activated platelets, activated FVIIIa will combine with activated FIXa. The FVIIIa-FIXa complex will be a cofactor for the activation of FXa, which will later bind to FVa (Figure 1.9). After that, the FXa-FVa complex will play an essential role in activating prothrombin to thrombin, converting fibrinogen to more stable and insoluble fibrin. The amount of thrombin formed during the propagation phase is much more than that during the initiation phase. Consequently, Thrombin will activate more FVa and platelets, form more fibrin, and so on (Hoffman, 2003)

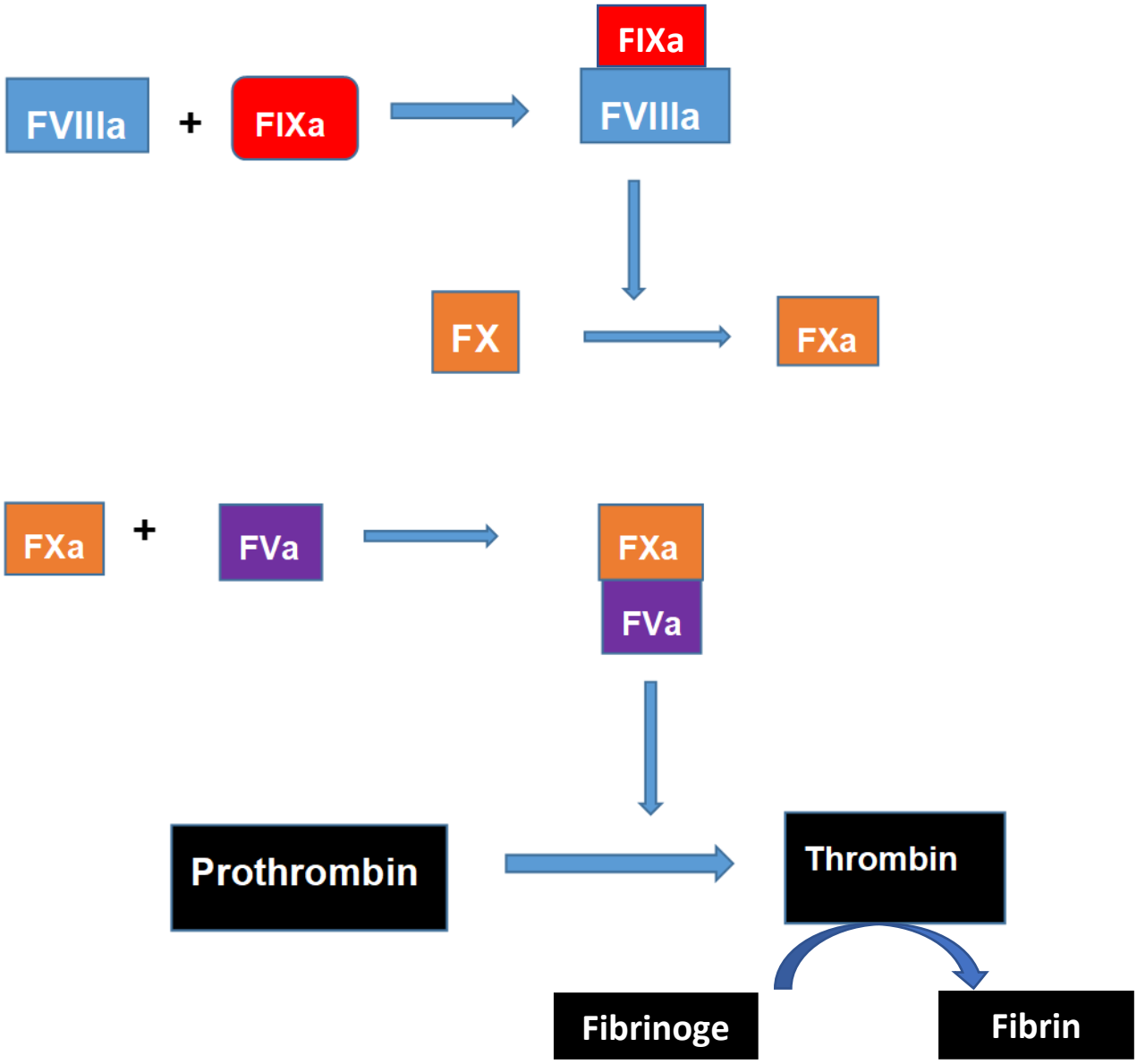

Figure 1.9 Propagation phase of the cell-based model of haemostasis. On the surface of the activated platelets, activated FVIIIa will combine with activated FIXa. The FVIIIa-FIXa complex will be a cofactor for the activation of FXa, which will later combine with FVa. After that, the FXa-FVa complex will activate prothrombin to Thrombin, converting fibrinogen to more stable and insoluble fibrin.

1.4.2.5 Fibrinolysis

This system acts to remove fibrin allowing the clot to be resolved once the vascular injury is patched. As mentioned above, there is a fine balance between the coagulation pathway and the fibrinolysis system. Once fibrin is formed, this will act as a physiological signal for fibrinolysis to begin. Initially, tissue plasminogen activator (tPA) and plasminogen accumulate over the surface of the fibrin clot. Thereafter, tPA will react with plasminogen activating it to plasmin which will act to lyse fibrin, creating fibrin degradation products such as D-dimer (Mybin and Critchley, 2016).

1.5 Animal studies of atherosclerosis initiation and progression

1.5.1 Clinical monitoring of the progression of atherosclerosis in humans is difficult

Atherosclerosis is a chronic, longstanding disease. The natural history of atherosclerosis is a process that may extend over decades, therefore monitoring this disease may need to extend over similar timescales (Charo *et al*., 2011). Several studies have monitored a significant correlation between the intimal-medial thickness of the carotid artery (IMTC) and the progression of atherosclerosis (Urbina *et al*., 2006). The most common method to measure IMTC is by using Doppler ultrasonography. It is a non-invasive and cost-effective method but requires a specialist team to perform. This technique works by identifying areas of high-velocity blood flow, indicating arterial stenosis or obstruction (Stein *et al*., 2008). Magnetic resonance imaging (MRI) studies can also measure IMTC but with higher sensitivity and specificity than Doppler ultrasonography (Grant e*t al*., 2003). MRI also allows us to accurately measure the atherosclerotic plaque size, although it is not the most cost-effective method

(Sam *et al*., 2005; De Groot *et al*., 2008). Monitoring of atherosclerosis progression can also be done via monitoring of several plasma biomarkers such as C-reactive protein (CRP), cardiac troponin, tumour necrosis factor-α (TNF-α), IL-6, IL-8, MMPs 1,3,8, and 9, myeloperoxidase (MPO). Several studies have reported a proportional relationship between the level of these biomarkers and the severity of atherosclerosis. In addition, there was a significant correlation between the severity and number of cardiovascular attacks and the levels of the inflammatory biomarkers (Brown and Bittner, 2009). However, the specificity of some of these biomarkers is low. For example, CR-protein is an acute phase reactant, so, any inflammation whether vascular or non-vascular can increase its level. IL-6, IL-8 is nearly similar to CR-protein, however, MMPs and MPO are more specific for atherosclerotic inflammation as they are contributing to plaque thinning and rupture(Wang *et al.*, 2017). Beyond this, it is difficult to study atherosclerotic plaques in live humans, with much of the research performed on post-mortem examination of arterial specimens. Through documenting the histochemical and histopathological features of atherosclerosis at people who have died at different ages, it has been possible to study the natural history of this disease, which has helped investigators to monitor atherosclerosis among live people (Zhdanov and Sternby, 2004). However, this does not allow us to study the molecular and cellular events that lead to plaque formation, progression, and rupture directly in humans.

Therefore, most of our knowledge about the pathology and pathogenesis of atherosclerosis has been obtained from *in vivo* animal studies. The animals that have been most used to study atherosclerosis are mouse, rabbits, and pigs. These animal models allow researchers to study the mechanism of atherosclerosis within the complex cellular, chemical, and physical environments found within the body and throughout all stages of the disease progression.

However, each of these different animals offers distinct advantages and disadvantages when modelling human atherosclerosis.

1.5.2 Rabbit models

Rabbits were the first animal models used to explore the biological, molecular, and immunological mechanisms of atherosclerosis. Rabbits are an attractive model as they are relatively small, easily handle, available, and cheap to maintain (apart from mice models). The first study in rabbits was conducted in 1908 by Ignatowski to assess the influence of a protein-rich diet on atherosclerosis (Ignatowski, 1908), followed by a similar study which was conducted in 1913 to study the effects of hyperlipidaemia on changes in the structure of rabbits' blood vessels (Antischkow, 1913). Both demonstrated foam cell formation in the intima, demonstrating that rabbits can be susceptible to some degree of diet-induced atherosclerosis like humans. Kolodgie and his colleagues reported that to initiate an early atherosclerotic lesion with monocyte infiltration and foam cells forming in the subendothelial similar to that found in humans, investigators needed to feed rabbits for a long time a low cholesterol diet (Kolodgie *et al.*, 1996). However, to elicit more advanced atherosclerotic lesions in rabbits, high cholesterol diets need to be used for long periods (6 months - years) alongside the induction of an artificial endothelial lesion (Aikawa *et al.*, 1998).In addition to the need for mechanical intervention, the diets needed to induce abnormally high plasma cholesterol levels leading to the accumulation of dietary lipid in multiple additional organs which make this disease appear different from that seen in humans (Fan *et al.*, 2001).Besides, the low levels of hepatic lipase in rabbits lead to significant mortality due to hepatotoxicity during the feeding period suggesting more systemic effects of these interventions (Fan *et al*.,

1997). Therefore, whilst rabbits have some similarities in plasma lipoproteins to humans, they are not identical, and they can struggle to fully recreate the human phenotype with dietary interventions alone fully. The development of genetically modified rabbits resulted in better models of human like atherosclerosis models. In 1980, Watanabe succeeded in creating a line of rabbits with a hereditary hyperlipidaemic disorder by breeding rabbits with a natural mutation in the LDL receptor. Most of these rabbits developed spontaneous atherosclerotic lesions across the aortic intima, similar in structure to those found in human patients with familial hypercholesterolemia. These mutant transgenic models demonstrated the power of transgenic models for *in vivo* studies of the genetic factors involved in the development of the *in vivo* atherosclerotic studies (Watanabe, 1980). Despite rabbits not being as easy to genetically modify as mice, there have been a number of transgenic models of altered lipid metabolism produced to try to model human cardiovascular disease (as reviewed in Watanabe, 1980); however, they are still unrelevant for more lifestyle-induced image (Tylor, 1997). Additionally, due to their larger size, they are more accessible to medical imaging techniques to track atherosclerotic lesion formation and development. For example, previous studies in rabbits have demonstrated the possibility of using MRI over six months to monitor atherosclerosis formation. This group concluded that an MRI scan is a non-invasive technique that might be possible to use to monitor and follow the human atherosclerotic plaque formation and progression (Worthley *et al*., 2000). Rabbit models have supplied the investigators with huge and valuable information regarding atherosclerosis. However, some authors have reported some limitations of this model (Kolodgie *et al.*, 1996) These include differences in the anatomical distribution of atherosclerotic lesions in rabbits (aortic arch and descending thoracic aorta) compared to those seen in humans coronary arteries and abdominal aorta (Tylor, 1997).

1.5.3 Murine models

Whilst rabbit models were the first animal models used; mice models have become the principal model used in this field. This because of the ease in which it is possible to genetically modify this species, which coupled with its rapid breeding rate, small size and low cost of maintenance – makes this a powerful model system in which to work (Veseli *et al.*, 2017). However, haemodynamic factors have significantly differed between mice and humans, which may alter mechanical aspects of plaque development and rupture between these species (Feintuch *et al*., 2007). Initial studies examined the impact of feeding wild-type mice with lipid-rich diets. These discovered that mice are relatively resistant to atherosclerosis because of differences in their lipid profile compared to humans. In humans, most of the plasma cholesterol is carried in LDLs, which are pro-atherogenic particles. However, in mice, most of the plasma cholesterol is naturally maintained in the bloodstream by high-density lipoproteins (HDLs), whilst LDLs carries only a small percentage of the total plasma cholesterol (Getz and Reardon, 2012). Thus, the study of transgenic mice has played a crucial role in exploring the influence of atherosclerosis's genetic and environmental factors. This includes transgenic mice with LDL receptor (LDLR) deficiency, creating a Watanabe hereditary hypercholesterolemic rabbit model. These transgenetic mice have a significantly higher plasma LDL cholesterol than normal mice and are more prone than wild-type mice to developing atherosclerotic lesions(Ishibashi *et al.*, 1993) .The main advantages are the plasma lipid profile of these mice are like human plasma lipid profile with the preservation of the apolipoprotein E (ApoE) protein. However, the main disadvantage of this model is that it is still necessary to feed these mice a heavily lipid-laden diet to observe an advanced

atherosclerotic lesion. Crucially these atherosclerotic lesions do not rupture spontaneously, erode or fissure, meaning that they cannot naturally replicate the crucial pathological event involved in triggering acute cardiovascular events in humans. Another widely used mouse model is the ApoE knockout mouse. ApoE is an essential protein within lipoprotein particles which allows them to be cleared from the plasma by the liver through binding bound to the LDLR. Plump and his colleagues reported that ApoE-deficient mice have significantly higher plasma cholesterol (mainly in the form of VLDL and IDL) than normal mice. After twenty weeks of normal diet feeding, these ApoE-deficient mice developed atherosclerotic lesions across the aorta and pulmonary artery – providing a model that does not require lipid-over-enriched diets to generate atherosclerosis. Unfortunately, these atherosclerotic lesions also do not rupture spontaneously or get thrombosis even with a longer feeding period (Plump *et al*., 1992).

Further attempts to create a transgenic mouse with a vulnerable atherosclerotic plaque led to developing a transgenic mouse deficient in both LDLR and ApoE. This double knockout mouse model presents severe hyperlipidaemia and spontaneous development of atherosclerotic lesions even with normal diet feeding. However, like the respective single knockout mouse models, the atherosclerotic lesions do not rupture spontaneously (Bontu *et al*., 1997).

The only transgenic mice models that have been shown to develop spontaneous plaque rupture are the ApoE/Fibrillin-1 double knockout mouse (Van Der Donckt *et al.*, 2015). Fibrillin-1 is a key glycoprotein that helps stabilize elastic microfilaments in the arteries, such that loss of this protein leads to filament destabilization and increased arterial stiffness. These animals developed an aspect of advanced plaque instability and could be seen to develop

thrombotic complications such as myocardial infarction and stroke. This appeared due to mechanical induction of increased plaque progression caused by the increased pulse pressure found in the stiffened arterial wall (figure 1.10; Van Herck *et al.*, 2009); Van der Donckt *et al*., 2015). Although fibrillin-1 mutations have been shown to increase atherosclerotic plaque development and cardiovascular risk in humans (Medley *et al*., 2002), this may not represent a normal causative event. Further studies will be required to see if this model fully replicates human plaque rupture.

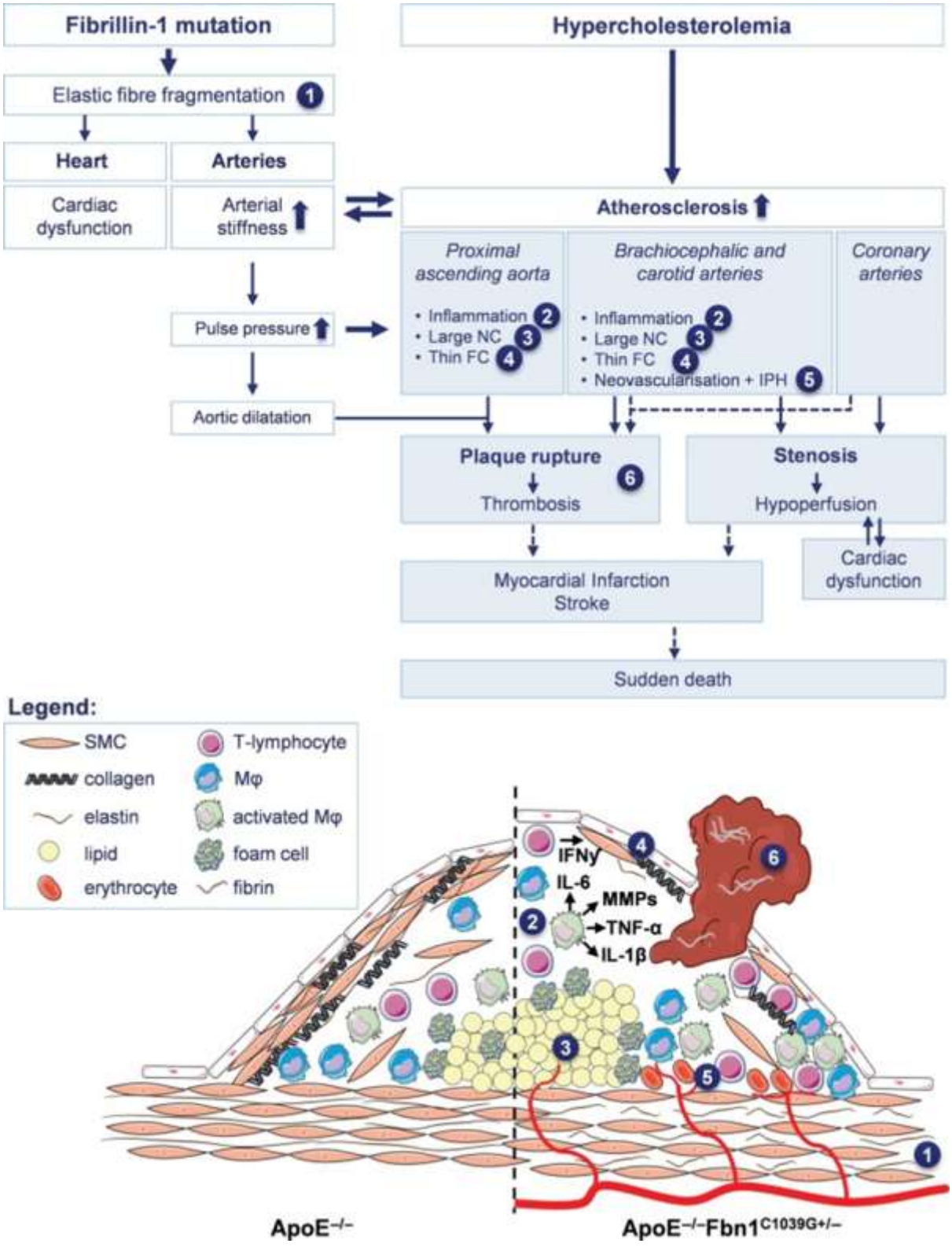

Figure 1.10 Mechanisms of Fibrillin-1/ApoE knockout plaque rupture. Rupture of the atherosclerotic plaque in Apo E/Fibrillin1 mice will release highly thrombogenic contents to the circulation leading to either myocardial infarction or stroke. Reproduced from van der Donckt *et al*., (2015).

1.5.4 Porcine models

Pigs have an anatomy and physiology that are more like humans than mice and rabbits. More than two-thirds of the total body energy requirement of the pig is derived from the metabolism of non-esterified fatty acids, which is like that of a human. Furthermore, the size of the heart and other great vessels are similar to those of humans (Kaplan *et al*., 1982). The heart's electrical circuitry, the coronary circulation, and the morphology and structure of mitral, tricuspid, and aortic valves are like those found in humans. The heart rate of human (60-100 beat per minutes) and pigs (91-167 beat per minutes) are also mimic to that of human (Lelovas *et al*., 2014). The predominant plasma lipoprotein are LDLs, while high-density Lipoproteins (HDL) comprise about one-quarter of the total plasma lipoprotein, which is similar to that found in humans. This has perhaps made the natural history of atherosclerosis in pigs and humans appear to be similar (Getz and Reardon, 2012). Bloor and White (1992) reported that ageing pigs might develop atherosclerosis spontaneously. For these reasons, many scientists have recommended pigs as the most appropriate animal for studying atherosclerosis. Under a normal diet, swine do not develop atherosclerosis; however, using a high lipid diet they will develop hypercholesterolemia and atherosclerosis. The speed of the atherosclerotic progression depends on dietary cholesterol intake, a period of feeding, and other coexistence risk factors (for example, diabetes mellitus). Usually, the atherosclerotic lesions that are seen in the hypercholesterolaemic model are simple, like those seen in fatty streaks of humans as they are distributed focally and over unpredictable locations. Advanced atherosclerotic lesions in these hypercholesterolaemic models are uncommon, and they require a prolonged period of high dose cholesterol intake (6-9 months) for this to occur (Nakashima *et al.*, 1994). Like rabbits, there have been attempts to use vascular trauma to

shorten the time required to induce plaque formation. However, after about 2-3 months, most of the lesions were only early stages of plaque development, with only foam cell accumulation observed. After one year, they reported some advanced atherosclerotic lesions in the form of fibroatheroma, with necrotic core and intraplaque haemorrhage. Although intravascular trauma could help develop advanced atherosclerotic lesions, this did not decrease the time of the experiment (Mihaylov *et al*.,2000). The large size of pigs makes them easier to image atherosclerotic plaques. Therefore, they have played an important role in assessing and evaluating some novel imaging techniques, such as CT and MRI angiography (Granada *et al.*, 2009). Unlike mice, the genetic modification of pigs is not as easy to achieve. However, a knockout of models of the LDLR has been developed. This resulted in pigs with a metabolic disease that is similar to human familial hypercholesterolemia. Pigs with this mutation developed atherosclerosis while they were fed their normal diet. After one year from the onset of the experiment, there were early atherosclerotic lesions in the form of fatty streaks. After two years, there were more advanced human-like atherosclerotic lesions in form of fibroatheroma with a necrotic core. Moreover, there was a thin cap membrane and multiple spots of haemorrhages distributed within the fibroatheroma. The coronary arteries were the most affected vessels, especially at low shear segments. After three years of follow up, thin cap membrane rupture could be observed to happen in some pigs. Therefore, these pigs provide an excellent tool for modelling human disease. The most important disadvantages of this model are the long period of observation required to see these changes, which means experiments take time and are expensive to perform. In addition, these large and heavy animals are more challenging to handle than the smaller mouse or rabbit models (Davis *et al.*, 2014).The large size of the pigs represents a considerable challenge for the scientists, so recently, genetically engineered minipigs have resolved these important

practical issues facing this model. It has allowed the imaging studies to become more feasible with better resolution, as the thick fatty tissues of the normal pig were a barrier against ultrasound and other imaging studies. Researchers have now prepared several atherosclerotic models from this type of pig with good results and with low cost (Gal *et al*., 1990).

1.5.5 The limitations of using animal models to study human atherosclerotic plaque formation and development

Animal models can develop an atherosclerotic plaque like those found *in vivo* in humans, with similar cellular components to human plaque. However, differences in gene expression were observed between the two types of plaques (Poznyak *et al.*, 2020). Navab and colleagues have stated considerable molecular and biological differences between the inflammatory processes found in human and animal atherosclerotic plaques (Navab *et al.*, 1988). Furthermore, the plasma lipid profile in most animal models is known to differ from that of the human. Also, there are other important molecular differences between these species that may alter atherosclerotic plaque development. For example, it has been reported that macrophages of mice do not have ApoE. This protein plays an essential role in the development and propagation of atherosclerosis in humans. This could make mice an unsuitable place for drug experiments that will be used to treat human atherosclerosis (Lindmark *et al.*, 2004). Therefore, an alternative to using animal studies is to examine the atherosclerotic process using tissue-engineered human cell models of atherosclerosis (Navab *et al*., 1988). Whilst many atherosclerosis drugs trials have reported successful results on pre-clinical animal studies, they have failed to reproduce these findings when applied to human

volunteers in later clinical studies. For example, Torcetrapib is a drug designed to treat atherosclerosis by raising plasma HDL levels and lowering LDL levels. The results that have been collected from the animal studies were successful. However, after about one year of the human clinical trial, this medication was stopped abruptly because of its serious adverse side effects. These data suggested that biological, molecular, and physiological differences between animals and humans may impact the ability of animal models to be used to perform pre-clinical drug testing successfully. As such, it might be unsafe to translate the results of some animal drug experiments to humans (de Haan *et al.*, 2008).

1.6 Developing tissue-engineered models of human atherosclerosis

1.6.1 The use of human *in vitro* models for the study of atherosclerosis

Since Virchow made the first description of an atherosclerotic plaque in 1856, there has been an ambition to create realistic atherosclerotic models to increase our understanding for the pathological aspects of this disease. This must lead to many different *in vivo* and *in vitro* models having been created. Initial atherosclerotic *in vitro* models were limited to simplified 2D models consisting of a monolayer cell culture. This included models incorporating monocyte-macrophage, endothelial cells, and SMCs using either primary or human cell lines (Gualtero *et al*., 2018). However, these models did not reflect the normal *in vivo* environment. For example, these models fail to replicate the physical conditions of blood flow which are known to play a key role in modulating endothelial cell function *in vivo* during the onset of atherosclerosis, as they lacked the pulsatile wall pressure changes present in the native tissues (Hosseini *et al.*, 2021; Yurdagol *et al*.,2016). Additionally, these 2D culture models are cultured upon stiff plastic surfaces of cell culture flasks, which are usually made from

polystyrene. This stiff wall differs considerably from the mechanical properties of the natural *in vivo* environment. This type of model does not reflect the dynamic interactions between the endothelial cells with other cellular and molecular components of the subendothelial matrix. Furthermore, the phenotype, proliferation, and protein expression of these cells differ from that of the cells found *in vivo* (Timraz *et al.*, 2015). Due to these limitations of 2D cell culture these models have been deemed unsuitable to replace the animal models as they either assess a single cell type or a monolayer of incorporating cells cultured in a non-dynamic environment (Robert *et al*., 2013). Therefore, researchers have developed 3D cell cultures that used components from the extracellular matrix as a scaffold. Most of these extracellular substances like collagen, gelatin, fibrin and proteoglycan derived either from animal sources or the human placenta. This allows investigators to co-culture multiple cells in the same construct to better replicate the normal blood vessel tissues. For example, Navab and colleagues created an *in vitro* human co-culture model to study monocytes migration in atherosclerosis. In this experiment, they used human aortic endothelial cells and smooth muscle cells isolated from the ascending aorta of a donor. They reported a considerable monocytes migration across the endothelium toward the subendothelial space, thus replicating the early stages of atherosclerotic plaque development and demonstrating the potential of human co-culture models. (Navab *et al*.,1988). Culturing within 3D models has been shown to prolong the viability of the cell (Gualtero *et al*., 2018). On the other hand, they have been reporting that the expression of cytokines, chemokines, and the pro-inflammatory responses of cells in 3D culture models differs from that in 2D culture models (Gualtero *et al*., 2018).

1.6.2 The use of human *ex vivo* models for the study of atherosclerosis

In vitro human models have provided novel information about the formation of atherosclerotic plaque. However, most of this information is restricted to the initial stages of the disease, and not the advanced stages responsible for acute coronary syndrome and other acute cardiovascular events. This limits their ability to be used for pre-clinical studies of these pathologies. For instance, these models cannot assess the effects of specific molecules or enzymes on the development and stability of atherosclerotic plaque. This has led investigators to establish *ex vivo* models. The ex vivo and the in vitro atherosclerotic studies complement each other – with each having advantages and limitations over the other. Human ex vivo models have also been used to explore more detail about the pathology and pathogenesis of atherosclerosis. These models utilize samples from endarterectomy surgeries to collect atherosclerotic plaques from human donors. The main advantage of ex vivo models is that as primary tissue, they fully recreate the complex inflammatory milieu of the atherosclerotic plaque, which is not entirely played in current in vitro models (Erbel *et al*., 2014). Several studies have used primary human tissue specimens from the carotid artery of patients who have undertaken carotid endarterectomy. In 1989, Goran and colleagues documented the presence of T-lymphocytes in the atherosclerotic plaque. They reported that activated T-lymphocytes play an essential role in the pathogenesis of atherosclerosis by secretion of cytokines such as IFN-γ transforming growth factor-β and tumour necrosis factor-β. These cytokines affect the proliferation and differentiation of smooth muscle cells and macrophages in atherosclerotic plaque. IFN-γ was observed to be a potent activator for macrophage differentiation and proliferation. However, it harms phenotype differentiation

of smooth muscle cells(Hansson *et al*., 1989). Similarly, in 2007, Meissner and his colleagues reported that IFN-α could stimulate T-lymphocytes to be more effective in killing smooth muscle cells, leaving the atherosclerotic plaque weak and liable to rupture (Niessner *et al*., 2007). Other studies have utilized human atherosclerotic tissue samples from carotid and femoral arteries of patients undergoing revascularization to create ex vivo models. For example, previous work used these samples to show that the activated form of the NF-κβ (nuclear factor kappa B)transcription factor is associated with unstable atherosclerotic plaque rupture (Monaco *et al.*, 2004). However, there are also several limitations of *ex vivo* models. Whilst it is easy for us to grow and culture primary human cells *in vitro* in a reproducible manner, the performance and the functions of these cells can differ significantly from the same human cells found *in situ* (Yang *et al*., 2007). Investigators using *ex vivo* models have encountered difficulties in sustained culturing the tissue sections obtained from patients-with the optimal culture period of the primary human tissue often being restricted to one day (Nakashima *et al.*, 1994) .Attempts to culture these cells for longer have led to the disruption in the architecture of the obtained section of the human atherosclerotic artery, leading to difficulties in the interpretation of the results obtained. The short survival period and donor-to-donor variability of the sectioned human tissue creates practical and experimental difficulties. It is also more challenging to recreate physiological blood flow conditions and other *in vivo* conditions in an *ex vivo* culture model than *in vitro* models. Lastly, as the endarterectomy samples are taken from patients at various stages of atherosclerosis, they represent a very heterogeneous array of tissue samples. This variance between endarterectomy samples will cause intrinsic variability in the results of these studies, and these can confound the results of cellular, protein and genetic analysis (Erbel *et al*., 2014). Additionally, the inaccessibility of endarterectomy samples to all research groups acts as a

critical limiting factor in their widespread uptake by the scientific community and usefulness in drug testing (Lebedeva *et al*., 2017). Therefore, finding a more standardized human model of atherosclerosis could help us better understand the cellular and molecular basis and better predict the effect of prophylactic and therapeutic drugs to reduce the incidence and severity of acute cardiovascular events.

1.6.3 The potential of vascular tissue-engineering techniques to create a novel *in vitro* model of human atherosclerosis

Creating an *in situ* atherosclerotic plaque model requires the creation of a realistic replica of the arterial wall. For a quarter of a century, regenerative medicine has been developing tissue-engineered arteries as alternatives to autologous donor grafts in revascularization surgery for conditions such as coronary artery bypass graft surgery, congenital heart anomalies corrective surgery and arterio-venous anastomosis of renal dialysis (Matsumura and Shin, 2005). The tools and techniques used for creating clinical grafts have also paved the way for creating realistic replication of human arteries that may be adapted to develop artificial human arterial tissues, which can replicate thrombosis and haemostasis under near-physiological conditions found in the human body. Recent studies have reported that vascular tissue engineered (VTE) arterial constructs can be used as alternatives to the traditional *in vivo* models to assess and evaluate the effectiveness of anti-platelet and anti-thrombotic therapies. For example, pre-clinical trials have previously successfully used a VTE model instead of *in vivo* animal models to assess the efficacy of the hemodynamic properties of anti-platelet therapy (Copes *et al.*, 2019). These methods can be adapted to develop a healthy arterial model into which can be incorporated a neointimal layer to create a full tissue-engineered human atherosclerosis model.

Tissue engineering comprises 3 main pillars that will determine the effective replication of both the morphological and functional properties of the tissue. These are the cell source, the scaffolds used to structure these cells, and the use of chemical and physical stimuli to direct the proliferation, differentiation, and maturation of the tissue. Vascular tissue engineering studies have principally utilised primary human endothelial and smooth muscle cells to generate the key intimal and medial layers of the artery. However, the variability in proliferation and phenotypic properties between batches of these cells have caused investigators to consider other cell sources including the use of bone marrow cells, mesenchymal stem cells and induced pleuripotent stem cells with which to develop tissue-engineered arteries (Bajpai and Andreadis, 2012; Mallone *et al*., 2021).

Vascular tissue engineering has achieved the development of artificial arteries using a variety of scaffold-based and scaffold-free approaches. Scaffold-based tissue engineering uses a range of synthetic (e.g., expanded polytetrafluoroethylene, Dacron) or endogenous extracellular matrix (e.g., collagen, fibrin) materials to create a structure supporting growth and development of the component cells within a 3D cell culture environment. These scaffolds can be made in several different ways, including through electrospinning, hydrogel formation, 3D printing, or decellularisation of endogenous tissue (Gualtero *et al*., 2018). Alternatively, scaffold-free engineering using the creation of self-supporting cell sheets can also be used to create effective tissues. Each of these methodologies provides distinct advantages and disadvantages with regards to their ability to effectively replicate the biochemical, cellular, anatomical, physiological, and mechanical properties of blood vessels.

1.6.3.A Scaffold-based VTE

1.6.3.A.1 Hydrogels

Collagen hydrogels scaffold are one of the most common applications for the scaffold -based tissue engineering. Collagen and fibrin are commonly used as an extracellular matrix to support the growth of the cells (Ovsianikov *et al*., 2018; Ovsianikov *et al*., 2020). These scaffolds provide great flexibility in modifying the size and morphology of the resulting tissue-engineered blood vessel according to the requested grafting situation and the ability to direct cell colonization and proliferation through a pathway (Ovsianikov *.,2020)*.However, specific challenges face this technique's the scaffold base technique progress, for example, the heterogeneous distribution and low concentration cells density, mainly when a large, porous 3D construct is used. However, this disadvantage is less pronounced with hydrogel scaffolds, as the cells will be distributed more homogenously with somewhat higher density (Copes *et al*., 2019). The main disadvantage of hydrogel scaffold is its relatively weak consistency. Water represents more than 90% of the composition of a collagen hydrogel, so whilst these models are good at mimicking the local extracellular environment, from a mechanical point of view, they are weak and lack the stiffness of native tissues. This may cause the cell behaviour and inflammatory cytokines secretion to be different from that of the native human environment (Brown *et al*., 2005; Yang *et al*., 2009). To improve the biological realism of 3D hydrogel cultures, collagen hydrogels can be made more mechanical strong through a process of plastic compressed, where the aqueous component of the intercellular medium is squeezed from the gel through application of a mass atop of the gel, and the extruded liquid can then be absorbed. Consequently, the water content of the gel is reduced, and the density of the

collagen and cells contained within will be increased, making the collagen hydrogel stronger and denser, and improving its similarity to the native tissue (Cheema and Brown, 2013). The mechanical stiffness of the collagen hydrogels also influences cell behaviour, with vascular smooth muscle cells adopting proliferative phenotypes in stiffer gels and a contractile phenotype in more compliant hydrogels and can promote angiogenic behaviours in endothelial cells (Ryan and O'Brien, 2015; McDaniel *et al*., 2017; Mason *et al*., 2013). Thus, modulating the stiffness of gels can significantly alter the effectiveness of 3D cell culture models.

1.6.3.A.2 Decellularized vascular tissue engineering

To create a biologically relevant scaffold in vascular tissue engineering, some researchers have utilised decellularized vascular tissue. This involves treating segments of veins or arteries with detergents or other chemicals to remove the cellular content and leave the extracellular matrix proteins largely intact. These can then be seeded with cells to create a healthy blood vessel that can be utilised for implantation. This is particularly helpful for creating vascular grafts for patients using their own cells to seed the construct and thus decrease the recipient's immunological reactions to the vascular implant. However, the availability of vascular tissue is limited, and so the most common source of material is from xenogenic sources (Chih-hsun Lin, 2018). Therefore, this is unlikely to provide a viable alternative to current *in vivo* atherosclerosis models.

1.6.3.A.3 Electrospun scaffolds

Electrospinning is a production process that utilised high voltage electrical forces to charge a droplet of polymer solutions. Due to the electrostatic repulsion elicited by the applied voltage, this can trigger a stream of liquid to arise from this droplet, which as it dries can then be elongated to form nanofibers that can be collected onto frames. Depending on the parameters used this can be set-up to produce meshes of randomly orientated or highly aligned fibres. These meshes of nanofibers have been used to create 3D scaffolds that resemble the fibrous nature of the extracellular matrix, and thus provides an artificial replacement for decellularized vein scaffolds. Through choice of the appropriate polymer for electrospinning, as well as choice of coating this can create strong scaffolds with a high capacity for cellular binding. Electrospinning is a promising tissue engineered technique that has been used to produced cellular scaffold with mechanical and biological properties that are nearly similar to that of natural *in vivo* blood vessel (Anwarul hasan *et al*., 2014; Karkan *et al.*, 2019).

1.6.3.A.4 3D bioprinting

During the past decade, there have been great progress in the development of 3D bioprinting technology in tissue engineering. In this process specialised bioinks are produced in which cells and natural or synthetic scaffold molecules to create the basis for the bioink, then printing this drop-by-drop onto a substrate using either inkjet, extrusion, or laser-assisted printing techniques (Gungor-Ozkerim *et al*., 2018). Due to the high spatial resolution possible through this deposition, this allows the tissue to be micropatterned to closely-resemble the structure of the native tissue. A particular advantage is the ability to build up hollow 3D organs through this manner, which allows the production of tubular blood vessel constructs

that closely resemble the native artery. The limitations of this method revolve around the potential cell stress induced by the bioprinting process can lead to lower cell viability, however as the bioinks and printer technology have improved this has become less of an issue (Wang *et al*., 2021)

1.6.3.4 Scaffold-free blood vessel models

One of the disadvantages of scaffold-based tissue engineering is the difficulty in distributing cells at high density evenly through the construct. Cell sheet-based tissue engineering provides the ability to fabricate highly organised, functional, structurally complex tissues or organs without using scaffolds. This strategy of tissue engineering is based on the assembly of cell spheroids or cell sheets. Matrix materials are thermoresponsive surfaces that provide a base for the growth of the vascular cells into cell sheets. Once confluent, the cell can then be harvested through changing the temperature to reversibly detach the sheets in a non-invasive manner (Figure 1.11). From here they can be assembled into more complex tissues, whilst maintaining their highly regular structures (Imashiro and Shimizo, 2021). This procedure allows researchers to build up complex tissues through stacking of cell sheets to create 3D models with comparable cell density and depth to the native tissues (Moschouris *et al*., 2016).

1.6.3.5 Perfusion bioreactors and cellular stimuli

Whilst vascular tissue engineering initially involved the development of tissues under static conditions, these do not recreate the local physical environment encountered by cells. In the

case of vascular tissue engineering, it is widely appreciated that the phenotypic properties of both endothelial and smooth muscle cells are heavily affected by the presence of shear stresses elicited by the flow of blood over the intimal surfaces, as well as the circumferential and longitudinal forces elicited by arterial blood pressure exerted on the wall of the blood vessel (Mironov *et al*., 2003). Therefore, perfusion bioreactors are utilised which allow

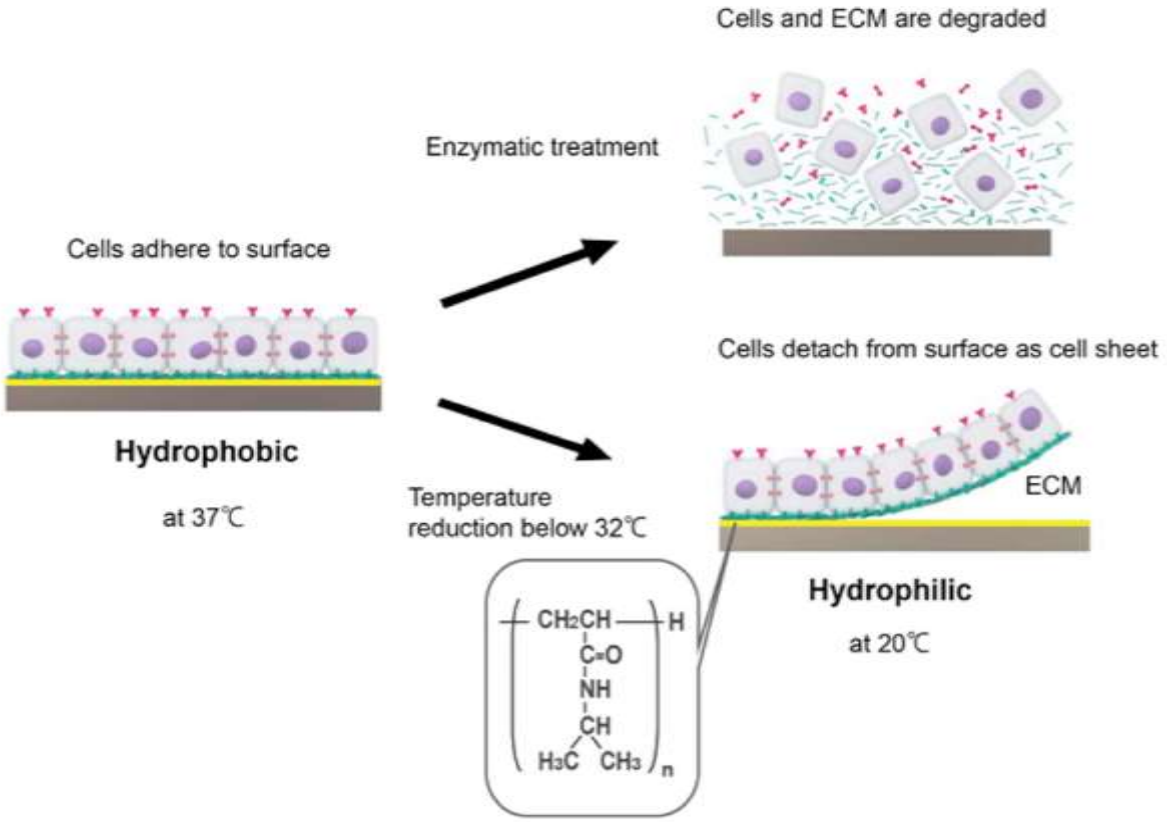

Figure 1.11 An example of scaffold-free tissue engineering. Adhesion and detachment of the confluent cultured cells can be controlled by modifying the temperature. At 37°C, the surface of the matrix material (PolyN-isopropyl acrylamide) is hydrophobic and so adheres well to the cell sheet. By decreasing the temperature below 32°C, the properties of the matrix material changes and becomes hydrophilic, allowing easy detachment of the cell sheets. This allows their harvesting where they can be incorporated into tissue-engineered models. Figure reproduced from Sekine and Okano (2021).

continuous flow of culture media over the construct during the culture period (Selden and Fuller, 2018). These can therefore be used to help refine the local environment that cells are

exposed to during the culture period. To help this better they do this by delivering key biochemical signals for cell differentiation, maintaining oxygen and nutrient concentration within desired levels, as well as deliver the mechanical cues that cells are exposed to in the body (Paez-Mayorga, 2019). In vascular tissue engineering, the ability to mimic fluid flow has been shown to prevent endothelial cells adopting a pro-inflammatory phenotype and helps maintain smooth muscle cells in a contractile phenotype (Chiu *et al*., 2004; Bennett *et al*., 2016). The major disadvantages of this approach are the costs and availability of perfusion bioreactors, as this requires specialist equipment, and a steady supply of specialist culture media which could make this approach inaccessible to some groups. Recent studies have demonstrated that it may be possible to mimic the effect of flow on endothelial cells by artificially triggering the activation of mechanosensitive channels using chemical agonists. This has been shown to induce the same anti-inflammatory responses as the application of fluid flow (Davies *et al*., 2019) therefore may offer an alternative approach to continuous perfusion.

1.6 Aims and Objectives

Previous work by Musa and colleagues has succeeded in developing a three-dimensional tissue-engineered human arterial construct using a layer-by-layer methodology (Musa *et al*., 2016). The arterial construct was made by culturing separate intimal and medial layers, which were then subsequently co-cultured together. The intimal layer was made through culturing human umbilical vein endothelial cells (HUVECs) on top of an aligned mesh of fibronectin-coated PLA nanofibres, whilst the medial layer was produced through culturing human coronary artery smooth muscle cells (HCASMCs) in a type I collagen hydrogel. Upon combining these into a single co-construct through gluing them together using a collagen hydrogel as an

adhesive, this single arterial construct was able to replicate the pro- and anti-aggregatory functions of native human intact and damaged artery. These data therefore demonstrated the potential for utilising tissue engineered human arterial models to study thrombosis and haemostasis in a healthy human artery under near-physiological conditions.

The layer-by-layer methodology used to produce this model makes it possible to modify each layer independently of each other, as well as develop and introduce additional layers to be included within the model systems. This opens the possibility of creating a 3D neointimal cell culture construct to introduce within the tissue engineered arterial construct to represent various stages of atherosclerosis. Through adapting and developing the techniques previously used by Musa *et al*., (2016), it should be possible to assess the impact of these constructs on the activation of primary and secondary haemostatic systems. This would form the basis of a humanised testing platform for anti-atherosclerotic and anti-thrombotic therapies used to treat patients at risk of acute cardiovascular events.

Previous studies have shown that it is possible to use tissue-engineered arteries to study the first stages of plaque formation through assessing migration of monocytes and development of foam cells (Robert *et al.*, 2013; Zhang *et al*., 2020). Additionally a hanging drop cell culture has been used to generate a fibroatheroma model, however this exists outside of the structure of a blood vessel (Mallone *et al.*, 2018). Furthermore, there has been no previous attempt to use tissue engineered blood vessels to create a more advanced stage model of atherosclerosis.

In this project, we aim to develop and validate a simple 3D cell cultured neointimal model that can be inserted into the previously developed tissue-engineered arterial construct to begin to develop a tissue-engineered atherosclerotic plaque model.

The objectives of this project are:

1) Develop a 3D neointimal culture model that is compatible with the pre-existing tissue-engineered arterial constructs

2) Assess the ability of the 3D neointimal culture model to activate the primary and secondary haemostatic system

3) Assess the ability of the 3D neointimal culture model to modulate the behaviour of co-cultured smooth muscle and endothelial cells in the developed tissue engineered arterial constructs

Chapter 2: Materials and Methods

2.1 Materials

Name of the material	Name of the supplier
Proliferating THP-1 cells	European Collection of Authenticated cell cultures (Porton Down, UK).
Phorbol 12–myristate 13-acetate (PMA), paraformaldehyde, trypan blue and copper sulfate pentahydrate, Nile-Red, and Hoechst 33342, formaldehyde solution, Oil Red O powder, Lipopolysaccharide (LPS), Ascorbic acid, Acid citrate dextrose (ACD), 85 mM sodium citrate, Fibronectin from bovine plasma, N-N-dimethyl formamide (DMF), Isopropanol, Iron III chloride (FeCl3), Fibrinogen from human plasma, Bovine Thrombin	Sigma Aldrich (Gillingham, UK)
RPMI 1640 with L-glutamine, fetal bovine serum (FBS) , phosphate-buffered saline (PBS), Penicillin/Streptomycin (AA), Cell scrapers, Whatman filter paper, Scalpel blades, Polytetrafluoroethylene (PTFE), 99.9% Ethanol, Trypan blue, CORNING Collagen type 1 Rat Tail (low concentration), Collagen type 1 Rat Tail High Concentration (high concentration), Copper sulphate (CuSO4.5H2o)	Scientific Laboratory Supplies (Nottingham, UK).
Phycoerythrin-conjugated CD68 mouse monoclonal antibody, FITC-conjugated CD86 mouse monoclonal antibody, phycoerythrin-conjugated CD163 mouse monoclonal antibody, ethylenediaminetetraacetic acid (EDTA), MEM-α Medium powder, Slide-lyzer dialysis cassetes (gamma-irradiated, 10K MWCO), and Corning high concentration rat tail collagen	Fisher Scientific (Loughborough, UK)

Monoclonal recombinant human full-length CD80 protein and polyclonal CD206 Mannose Receptor Antibody	Novus Biologicals (Abingdon, UK)
The goat anti-mouse secondary antibody, the goat anti-rabbit secondary antibody, and the FITC-conjugated anti-CD36 antibody, Human IL-1, PDGF-BB, IL-6 and TNF-α ELISA Kits, oxLDL assay kit, Recombinant Anti-ICAM1 antibody, Goat F(ab')2 Anti-Rabbit IgG - H&L (FITC), pre-adsorbed, Anti-CD31 antibody, Anti-alpha smooth muscle Actin antibody	Abcam (Cambridge, UK).
Human IFN-γ and IL-4 cytokines	Peprotech (London, UK).
Sterile low-density lipoprotein	2B Scientific (Upper Heyford, UK).
Live/Dead Staining Kit ‖ accutase	PromoCell GmbH (Heidelberg, Germany),
macrophage detachment solution	VWR international Ltd (Leicestershire, UK).
Human Coronary Artery Smooth Muscle cells (HCASMCs), Human umbilical vein endothelial cells (HUVECs), Gibco medium 231, Medium 200, Gibco smooth muscle growth supplement (SMGS), Low serum growth supplement (LSGS), α-MEM medium powder and Corning TM, 5-(and-6) carboxyfluorescein diacetate, succinimidyl ester, mixed isomers (CFSE)	Fisher Scientific (Loughborough, UK),
SN-17a	Cambridge Bioscience (Cambridge, UK).
Human FVII and Human plasmin	Enzyme Research Laboratories (Swansea, UK).
Atorvastatin Calcium Trihydrate (5g)	Active Pharma Supplies Ltd. (Leyland, UK)
Acetate sheets	Ryman's
Aspirin, Apyrase and luciferin-luciferase	Sigma Aldrich (Dorset, UK)

Nunc™ Cell Scrapers, CellTrace™ Violet Cell Proliferation Kit, for flow cytometry	Thermo Fisher Scientific. (Paisley, UK)
Eppendorf cell culture dishes, 35 mm	Eppendorf UK Limited
Silicon glue	RS
Watson-Marlow 505 series peristaltic pump	Watson-Marlow
Leica inverted fluorescence microscope (MSV269)	Leica
UV cabinet	BioRad
3D SLA printer	Elego mars

2.2 Methods

2.2.1 2D Culture

2.2.1.1 2D THP-1 cell culture

$1x10^5$ THP cells were seeded in each well of 24-well plates in RPMI 1640W media supplemented with 10% fetal bovine serum (FBS), penicillin and streptomycin. To induce differentiation into M0 macrophages, THP-1 cells were treated with 50nM PMA (Phorbol 12-myristate 13- acetate) in a humidified incubator at 37°C, 5% CO_2, for 48 hours. To further polarize the M0 cells into M1 and M2 macrophages, the media was then replaced with a PMA-free media for 24 hours and cells were then treated with either 100 ng/mL lipopolysaccharide (LPS) and 20 ng/mL IFN-γ (for M1 macrophages) or 20 ng/mL IL-4 (for M2 macrophages) at 37°C, 5% CO_2 for 72 hours.

2.2.1.1.1 Trypan Blue Cell Viability Assay

Cell viability of M0, M1 and M2 macrophages was assessed by removing the cell culture medium and adding 400 µl of PBS containing 5% [v/v] trypan blue stain into each well. Cells assessed by light microscopy using a 20x objective. Three pictures were captured in the centre, left and right side of each well using Q-Capture/Pro7 software. Live, dead, and total cells were counted, and the percentage of live cells was used to quantify cell viability for each condition.

2.2.1.1.2 Light microscopy

The THP-1-derived cells were assessed and photographed under light microscopy using a 20x objective. Q-Capture/Pro7 software was used to photograph the cells using Olympus brightfield microscope (CKX41).

2.2.1.1.3 Immunofluorescent staining of M0 macrophages

Cells from M0 cultures were fixed with either a 4% [w/v] paraformaldehyde or 10% [w/v] formalin solution overnight at 4°C. The fixatives were then removed, and each well was blocked by the addition of HEPES-buffered saline (HBS; 10 mM HEPES, 145 mM NaCl, 5 mM KCl, 1 mM $MgSO_4$, pH 7.4) supplemented with 1% [w/v] bovine serum albumin (BSA) for 1 h at room temperature. Afterwards, the blocking solution (1% [w/v] BSA in HBS) was removed and cells resuspended in the blocking solution to which a 1:100 dilution of either a phycoerythrin-conjugated anti-human CD68 antibody or the FITC-conjugated anti-human CD36 antibody was added. The plates were incubated with this staining solution at 4ºC overnight. The staining solution was removed, and the cells were washed with the blocking solution for five minutes at room temperature. This was repeated 3 times in total. The cells

were resuspended in the blocking solution was added to each well, and then the cells were examined using the 20x objective on a Nikon ECLIPSE Ti fluorescent microscope. The FITC filter set was used for cells stained with the CD36 antibody, whilst the TRITC filter set was used for cells stained with the CD68 antibody. Immunofluorescence signals were also analyzed from the 24-well plates using a BioTek 2 synergy microplate reader using excitation wavelengths of 475-495 nm excitation for both antibodies and emission at either 518-538 nm for CD36 staining or 607-621 nm for CD68 staining.

2.2.1.1.4 Immunofluorescent staining of M1 and M2 macrophages

M1 and M2 polarized THP-1 cells were fixed with either 4% paraformaldehyde or 10% [w/v] formalin solution and incubated overnight at 4°C. The fixatives were then removed, and each well was blocked by the addition of blocking solution of 1% [w/v] BSA in HBS for 1 hour at room temperature. Afterwards, the blocking solution was removed, and cells resuspended in the blocking solution containing either 200 µg/mL CD80 or 1 µg/mL CD206 primary antibody. The plates were then incubated at 4ºC overnight. The staining solution was removed, and the cells were washed and incubated with the blocking solution for five minutes at room temperature. This was repeated 3 times in total and then labelled by incubation with either a 1:5000 dilution of FITC-conjugated anti-mouse (CD80), or 1:7500 dilution of anti-rabbit (CD206) secondary antibodies in the blocking solution for 1 hour at room temperature. The wells then washed three times with HBS with 1% [w/v] BSA three times for 5 minutes. After that, the sample was resuspended in HBS with 1% [w/v] BSA was analyzed using a Fluoview FV1200 laser scanning confocal microscope (Olympus, UK) using 473 nm excitation wavelength and emission at 490-520 nm.

2.2.1.1.5 Preparation of oxidized low-density lipoproteins.

A commercially available preparation of sterile low-density lipoprotein (LDL) isolated from human plasma was diluted to 5 mg/mL using sterile PBS. Half of this stock was aliquoted and stored at -80°C before its use in experiments as a non-oxidized LDL preparation. LDL oxidation was performed as previously described by Wraith *et* al., (2013). 10 µM copper sulphate was added to the remaining LDL solution and incubated for 24 hours at 37ºC to allow for its oxidation. Excess copper sulphate was then removed from the sample solution through dialyzing the sample against a PBS buffer containing 100 µM of EDTA for 24 hours at room temperature under sterile conditions. Dialysis was performed using a Slide-a-Lyzer dialysis cassette (gamma-irradiated 10K MWCO; Fisher Scientific) according to the manufacturer's instructions. Aliquots of this sample were then preserved at -80 ºC before its use in experiments.

2.2.1.1.6 Validation of oxidation of low-density lipoprotein

The oxidized Low-density lipoprotein samples were characterized through a comparison of the absorbance of the oxidized and native low-density lipoproteins at 300 nm, as well as through an oxidized LDL ELISA assay kit from Abcam. Samples were run on the ELISA kit as per the manufacturer's instructions. Oxidized LDL Assay ELISA Kit was designed to be used for the measurement of oxidized phospholipids associated with human LDL in plasma, serum, or other biological fluid samples. The kit has an OxLDL Standard and has a detection sensitivity limit of ~100 ng/mL. Each kit provides sufficient reagents to perform up to 96 assays including standard curve and unknown samples. For the absorbance readings, oxidized and native LDL samples were loaded into a 96-well plate and their absorbance was read at 300 nm on a BioTek 2 synergy microplate reader.

2.2.1.1.7 THP-1-derived foam cell production

To create macrophage-derived foam cells, M1 macrophage cell cultures were supplemented with 50 µg/ml oxidized LDL (see section 2.2.A.1.G below for further details) and they were incubated at 37°C, 5% CO_2 for 72 hours. Control samples were also made at the same time by incubating cells with either non-oxidized LDL or an equivalent volume of PBS and incubated for the same time under the same conditions.

2.2.1.1.8 Oil Red O staining of THP-1-derived foam cells

After the culture period, cells were fixed by incubation with 4% paraformaldehyde solution for one hour at room temperature. The paraformaldehyde was removed, and the cells were washed with distilled water two times to remove any excess solution. A 60% isopropanol solution was then added to each well, and the cells were incubated for five minutes at room temperature. This was then removed, and then the cells were stained with 0.5% Oil Red O solution for 20 minutes at room temperature. The staining solution was removed, and cells were washed five times with distilled water. Cells were then photographed using Q-Capture/Pro7 software using a 20x objective on an Olympus brightfield microscope (CKX41), or the EVOS brightfield microscope using the 10x objective.

2.2.1.1.9 Detachment of THP-1-derived foam cells

THP-1-derived foam cells were prepared inside a T25 flask (using 6-8x10^6 THP-1 cell concentration) using the same methodology stated in 2.2.1.1.7. Cells were then attempted to be attached using either Macrophage detachment solution, accutase, trypsin/EDTA and cell scraper.

2.2.1.2 2D Human coronary artery smooth muscle cell culture

2.2.1.2.1 Preparation and proliferation of the HCASMCs

HCASMCs were cultured in accordance with the supplier's instructions. $3x10^5$ cells suspended in Medium 231 supplemented with SMGS were seeded in a T75 flask. The cells were grown in a humidified incubator at 37ºC, and 5% CO_2 and the media were changed every 48 hours until the HCASMCs were 80-90% confluent. HCASMCs used in experiments did not exceed passage 5.

2.2.1.2.2 Preparation and fluorescent imaging of HCASMCs-derived foam cells

HCASMCs were seeded into 24-well plates with 5 x 10^5 /mL cell seeding density and incubated at 37ºC, 5% CO_2 in a humidified incubator for 48 hours. The culture media was then supplemented with either 50 µg/mL of either oxidized or native LDL and incubated at 37°C and 5% CO_2 in a humidified incubator for an additional three days. After culturing, HCASMCs-derived foam cells were fixed with a 10% [w/v] formalin solution overnight at 4°C. The fixatives were then removed, and the cells were washed with PBS for 1 h at room temperature. The washing solution was then removed, and cells were resuspended in 400 µL PBS containing 100 µg/mL Nile-Red and 5 µg/mL Hoechst 33342 stain solution. After 45 minutes of incubation at room temperature, the staining solution was removed and then the collagen hydrogels were washed with PBS. The cells were imaged using the Fluoview FV 1200 laser scanning confocal microscope (Olympus, UK) using 473 nm excitation wavelength and emission at 490-520 nm.

2.2.1.3 2D Endothelial Cell Culture

Human umbilical vein endothelial cells (HUVECs) were cultured according to the suppliers'

instructions in Medium 200 that was supplemented with low serum growth supplement (LSGS), penicillin and streptomycin. The cells were incubated in the 37°C, 5% CO_2, humidified conditions. The media was changed every 48 hours. HCASMCs used in experiments did not exceed passage 5.

2.2.2 3D culture methods

2.2.2.1 3D THP-1 cell culture

2.2.2.1.1 Culture of THP-1 cells on top of non-compressed collagen hydrogels

Collagen hydrogel was prepared by mixing the following materials: type I rat tail collagen hydrogels, 10x DMEM, cell suspension, 1M Sodium Hydroxide, and 50 nM PMA using the following equations:

Volume of Collagen (µL) = [(final solution volume x final [collagen] of hydrogel)] ÷ stock [collagen]

Volume of 10x DMEM (µL) = final solution volume ÷ 10

Volume of 1M NaOH (µL) = volume of collagen added x 0.023

Volume of cell suspension (µL) = Final solution volume - (volume of 10x DMEM + Volume of collagen + volume of 1M NaOH)

The final concentration of the collagen desired is 3 mg/mL. All materials were kept pre-chilled on ice to prevent early gelation. The solution was mixed carefully and slowly to avoid air bubble formation, until a homogenous solution was formed. THP-1 cells were pelleted by centrifugation at 200 x *g* for 5 minutes, and then resuspended into completed RPMI media to give a cell density of 1.8 x 10^6 cell/mL. The THP-1 cells were then seeded in a 24-well plate (6x

10^5 cells/mL cell seeding density, and then each well supplemented with 200 µL of completed RPMI media. The collagen hydrogels were incubated at 37°C, 5% CO_2, for 4 days. Media was changed every 48 hours. The cells were then assessed by light microscopy using Q-Capture/Pro7 software and a 20x objective.

2.2.2.1.2 Preparation of the 3D human neointimal cell culture construct

To trigger M0 differentiation - THP-1 cells were mixed at a cell density of 3.6 x 10^6 cells/mL into a neutralized solution of 3 mg/mL type I collagen (Figure 2.1). 0.2 mL of the THP-1/collagen mixture was then loaded under sterile conditions onto a 1 x 1 cm (6x 10^5 cells/mL cell seeding density, sterile filter paper frame prepared on a PTFE base inside a petri dish. The collagen-cell mixture was left to set for 30 minutes at 37°C, 5% CO_2. The hydrogel was then transferred to 6-well plates and covered with RPMI medium containing 10% [v/v] FBS,

Penicillin, Streptomycin, and 50 nM PMA, and then incubated for 48 h at 37℃, 5% CO_2 to trigger differentiation of the cells into M0 macrophages.

To trigger M1 differentiation – The M0-containing hydrogels were then placed into PMA-free, supplemented RPMI media (containing 10% [v/v] FBS, Penicillin and Streptomycin), and incubated for 24h. The RPMI media was then changed to a fresh supplemented RPMI media containing 100 ng/mL LPS &20 ng/mL IFN-ɣ. The gels were then incubated at 37°C, 5% CO_2 incubator for 3 days.

To generate THP-1 derived foam cells. The media was exchanged with a fresh, supplemented RPMI media that contained either 50 µg/mL oxLDL, 50 µg/mL LDL or an equivalent volume of PBS. The different samples of the collagen hydrogels were incubated at 37°C, 5% CO_2 for a

further 3 days.

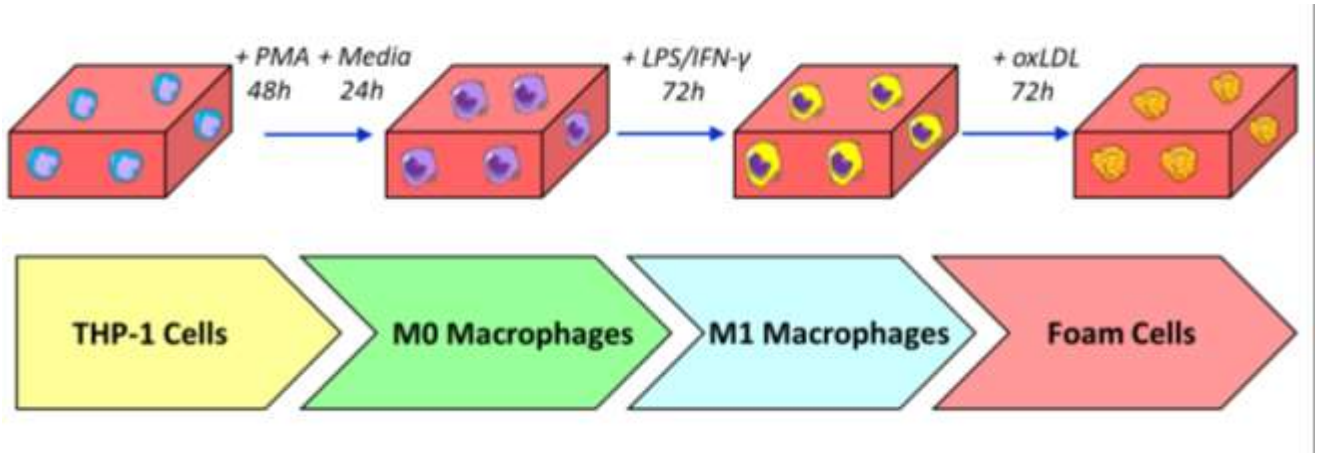

Figure 2.1 – A summary of the culturing of the 3D neointimal cell culture model. A THP-1-containing compressed hydrogen gel was cultured with 50 nM PMA for 48 h to induce THP-1 differentiation to M0 macrophages. Following this the media was changed for 24 h followed by incubation with Lipopolysaccharide and IFN- for 72 h to induce differentiation to M1 macrophages. Finally, the M1 macrophages were treated with oxLDL for 72 h. The resultant hydrogels on day 10 of the culture were then used for experiments. Monocyte, macrophage, and foam cell icons were obtained from bioicons.com.

2.2.2.1.3 Immunofluorescent staining of the M1-containing hydrogels

To assess M1 differentiation within the collagen hydrogels, collagen hydrogels cultured to contain M0 and M1 macrophages were prepared as stated above in Section (2.2.2.1.2). The hydrogels were then fixed with a 10% [w/v] formalin solution overnight at 4°C. The fixatives were then removed, and each frame of the collagen hydrogels was blocked by the addition of HBS supplemented with 1% [w/v] bovine serum albumin (BSA) for 1 h at room temperature. Afterwards, the blocking solution was removed, and the frames of the collagen hydrogels were resuspended in a labelling solution made up of the blocking solution containing 0.2 mg/mL CD80 primary antibody. The collagen hydrogels were incubated with this staining solution at 4ºC overnight. The staining solution was removed, and the collagen hydrogels were

washed three times with the blocking solution for five minutes at room temperature. After the third wash, the collagen hydrogels were stained by the addition of blocking solution containing varying concentrations of FITC-conjugated anti-mouse secondary antibodies (using a dilution concentation of 1:5000) for 1 hour at room temperature. The collagen hydrogels were then washed 3 times with HBS containing 1% [w/v] BSA for five minutes at room temperature. The collagen hydrogels were then analyzed by confocal microscopy using the Fluoview FV 1200 laser scanning confocal microscope (Olympus, UK) using 473 nm excitation wavelength and emission at 490-520 nm. Fluorescent intensity was assessed using ImageJ.

2.2.2.1.4 Fluorescent imaging of THP-1 derived foam cells in the 3D neointimal constructs

After culture, the tissue-engineered neointimal layer was fixed with a 10% [w/v] formalin solution overnight at 4°C. The fixative was then removed, and the collagen hydrogels were washed with PBS for 1 h at room temperature. Afterwards, the PBS was removed, and the collagen hydrogels were resuspended in 400 µL of PBS containing 100 µg/mL Nile-Red and 400 µg/mL Hoechst 33342. After incubation for 20 minutes at room temperature, the staining solution was removed, and the collagen hydrogels were washed with PBS. The samples were then imaged with a Fluoview FV 1200 laser scanning confocal microscope (Olympus, UK) using 473 nm excitation wavelength and emission at 490-520 nm.

2.2.2.1.5 Plastic compression of tissue-engineered neointimal constructs

The collagen hydrogel was prepared as described previously. Two 1x1 cm filter paper frames were placed inside either 2x1x1cm metallic or plastic moulds. Two mL of hydrogel were put in each mould, and then placed inside 9.6 cm^2 petri dish. They were incubated in a humidified incubator at 37°C, 5% CO_2 overnight. The next day the mould was flipped, and the gel

extracted onto a nylon sheet with tissue paper underneath. A 50g metal weight was applied atop of the hydrogel for 5 minutes. The compressed collagen hydrogels were then separated into two 1cm x 1cm frames (Brown *et al*., 2005, Yang *et al*., 2009). Each compressed collagen hydrogel has $5x10^5$ cells. Thereafter, the compressed collagen hydrogels were transferred to 24-well plates containing completed RPMI media. The culture media was exchanged for PMA-free RPMI media, and the hydrogels were incubated for 24 hours at 37°C, 5% CO_2. RPMI media was then exchanged again for fresh RPMI media containing 100 ng/mL LPS and 20 ng/mL IFN-ɣ was added, and then incubated for a further 3 days in an incubator at 37°C, 5% CO_2. The media was changed for fresh RPMI media containing either 50 µg/mL Ox LDL or 50 µg/mL non- oxidized LDL and placed in the incubator for a further 3 days prior to experimentation. In some experiments, 20 µg/mL of atorvastatin, or an equivalent volume of its vehicle, methanol, was added alongside the OxLDL.

2.2.2.1.6 Assessing cell viability of 3D culture of THP-1-derived cells

After culture, the collagen hydrogels were initially photographed by light microscopy using Q-Capture/Pro7 software and 20x objectives. The size and the morphology of the THP-1 cells were evaluated. The collagen hydrogels were then transferred to 24-well plates and the collagen hydrogels were stained using the Live-Dead Staining Kit II (Promocell) according to the manufacturer's instruction. Cells viability was assessed for fluorescent staining within the collagen hydrogels using a Fluoview FV 1200 laser scanning confocal microscope (Olympus UK) using a 10x objective and with excitation at 473 nm (Calcein staining of live cells) or 543 nm (EthDIII staining of dead cells) and emission at 490–520 or 590–620 nm respectively.

2.2.2.1.7 Measuring oxLDL uptake into 3D neointimal cell cultures

0.5% [w/v] Oil Red O solution dissolved in isopropanol was filtered on the day ten of the experiment. Each hydrogel was incubated with 500 µL Oil Red O solution for 30 minutes at room temperature on an orbital shaker (100 rpm). After this the gels were washed three times with PBS. After this the hydrogels were restrained by addition of 500 µL isopropanol to each gel and rocked on an orbital shaker for 30 minutes. From this solution, 100 µL was placed into a 96-well plate and absorbance was read at 570 nm to quantify the amount of neutral lipids present in the sample.

2.2.2.2 Preparation of the tissue engineered medial layer (TEML) construct

This was performed as previously described by Musa *et al*., (2016). To prepare the tissue engineered medial layer, the collagen hydrogel was prepared according to the manufacturer's instructions. To prevent early gelation of the collagen hydrogels, all constituents of the

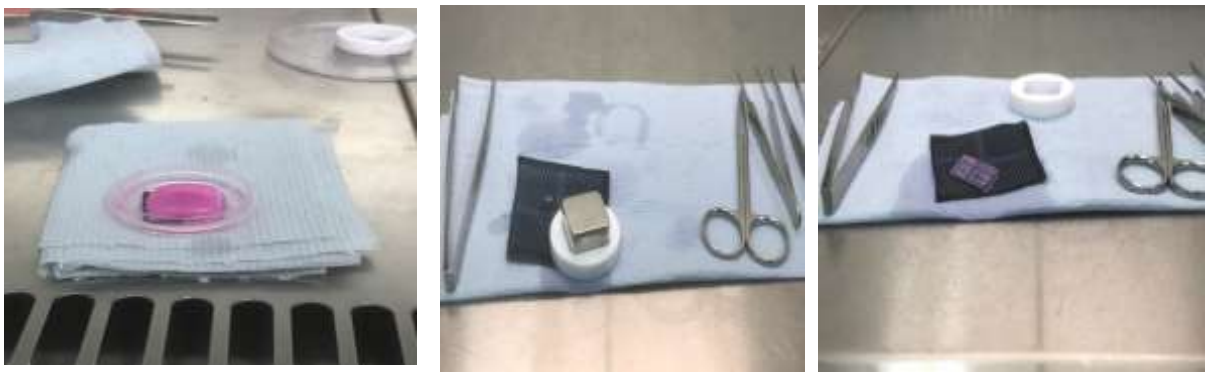

A **B** **C**

Figure 2.2. Plastic compression of the collagen hydrogels of THP-1 derived foam cells. This technique was specifically initiated to be used in the atherosclerotic models to increase the cell density and mechanical stiffness of the collagen hydrogels and to make the culture environment more suitable with the inflammatory condition that is initiated by the pro-inflammatory macrophages and foam cells. A. the collagen hydrogels before compression, B. During compression, and C after compression.

collagen hydrogel (αMEM, 1M NaOH, and rat tail type I collagen) were placed in ice. HCASMCs

were mixed into a neutralized solution of 3 mg/mL type I collagen. 200 µL of this solution was then pipetted into 1x1cm^2 filter paper frames to create hydrogels containing 1x10^5 cells. The hydrogels were set by incubation for 40 minutes at 37°C, 5% CO_2. The hydrogels were subsequently transferred into 24-well plates and cultured in completed Medium 231 supplemented with 50 µg/ml ascorbic acid. The media was changed daily with fresh ascorbic acid supplemented media. After this the culture media was removed and exchanged with fresh completed Medium 231 that contained either 50 µg/mL OxLDL, 50 µg/mL of non-oxidized LDL or an equivalent volume of PBS. The hydrogels were incubated for another 72 hours at 37°C, 5% CO_2 for a total culture period that did not exceed 6 days.

2.2.2.3 Optimizing media to allow co-culture of the 3D neointimal mode with layers of the tissue engineered arterial construct

Tissue-engineered neointimal constructs were made as stated above in Section 2.2.2.1. After day 10 of culture, the cell culture media was switched to RPMI media, Medium 231 or Medium 200. The cells were then incubated at 37°C, 5% CO_2, for 48 h. Cell viability was then assessed as stated in Section 2.2.2.1

2.2.2.4 Fibrin polymerization assay

Monitoring of thrombin-induced polymerization of fibrin gel was monitored in 96-well plates through measuring changes in sample turbidity using a modification of the method of Stabenfeldt *et al*., (2012). A 3 mg/mL human fibrinogen solution was pipetted into 100 µL samples in a 96-well plate, where it was mixed with various concentration of thrombin to give final concentrations of 0.01U/mL, 0.05 U/mL, 0.1 U/mL, 0.5 U/mL, 1 U/mL, and 5 U/mL. Immediately after mixing thrombin into the fibrinogen solution, the absorbance of the

sample was read at 350 nm every minute for 1 hour using a BioTek 2 Synergy microplate reader.

2.2.2.5 Neointimal-medial co-cultures

The neointimal and TEML cultures were prepared as previously described in sections 2.2.2.1 and 2.2.2.2. Upon day 2 of the TEML culture and day 10 of the neointimal culture, the two constructs were attached via a fibrin gel. Immediately prior to use, a 3 mg/mL human fibrinogen solution was mixed with a 50 U/mL thrombin. This gelating solution was then distributed over the four corners (20 µL) of the non-compressed collagen hydrogel of the media layer, and then the neointima layer was placed on top of it for one hour at room temperature to ensure it had fully gelated. The hydrogels were subsequently transferred into 24-well plates and cultured in completed Medium 231 for 4 days at 37°C, 5% CO_2 prior to use in experiments.

In the cell migration experiments, the HCASMCs were tracked through labelling with CFSE (Carboxyfluorescein succinimidyl ester) by incubation with 5 µM CFSE in fresh media for 30 minutes at 37°C and then replaced with fresh media. In some experiments, foam cells were labelled with CellTracker™ Violet by incubation with fresh RPMI containing 15 µM dye for 20 minutes at room temperature under gentle agitation.

2.2.2.6 Shear-induced separation of fibrin-coupled hydrogels

A compressed collagen hydrogel and non-compressed collagen hydrogel were made using the method described above and set in 10 mm x 5 mm filter paper frames. These were then attached to one another using a fibrin gel created by mixing a 3 mg/mL human fibrinogen solution with a 0.5 U/mL thrombin. This gelating solution was then used to attach the

compressed acellular gel atop of the non-compressed collagen hydrogel of the media layer, and then the neointima layer was left on top of it for one hour at room temperature to ensure full gelation. After this, samples were either incubated with either a plasmin-free HBS (as a control sample) or HBS-containing (30nM) plasmin for one hour at room temperature.

After the treatment, the construct was placed inside a custom-made 3D printed flow chamber to allow exposure to shear stress (Figure 2.3). The flow chamber was prepared using an Elegoo Mars 3D SLA printer. After printing the printed chamber was treated twice with isopropyl alcohol for 5 minutes in an ultrasonic cleaner. These were then dried and cured in ultraviolet light (405 nm) for one hour under rotation.

The combined hydrogel model was placed inside the 3D printing template and held in place using a coverslip and silicone grease to ensure the hydrogel was tightly held within the flow chamber (Figure 2.3). The flow chamber was connected to a Watson-Marlow 505 series peristaltic pump and perfused at maximum flow speed with distilled water (0.07 cm^2/s; Figure 2.4). The quantification of the generated shear stress was calculated according to the following equation:

$$\tau = \frac{6uQ}{bh^2}$$

Where the τ is the shear stress, u is the viscosity of the fluid, Q is the flow rate, b is the width of the flow space, and h is the height of the space between the hydrogel model and the coverslip. While width of the chamber is 0.5 cm, its height is 0.5 cm and the value of water viscosity at room temperature is 0.7 CP (Centipoise), leading to a calculated shear stress on the hydrogel model of 4.7 $dyne/cm^2$.

2.2.2.7 Intimal-neointimal co-cultures

The neointimal model was prepared according to protocol detailed in Section 2.2.2.1.2. On day 10 of the culture, the collagen hydrogels were sprayed twice with a 10 ng/ml fibronectin solution and then left to air dry for 45 minutes at room temperature. The fibronectin-coated surface of the neointimal constructs were then seeded with 200 µL of a HUVEC seeding density suspension ($3X10^5$ cells/mL). The coculture samples were incubated at 37°C, 5% $CO_2$for one hour to allow for HUVEC cell attachment. The samples were then placed into Medium 200 supplemented

with low serum growth supplement, penicillin and streptomycin and incubated for 37°C, 5% CO_2 for 4 days. The media was changed after 48 hours.

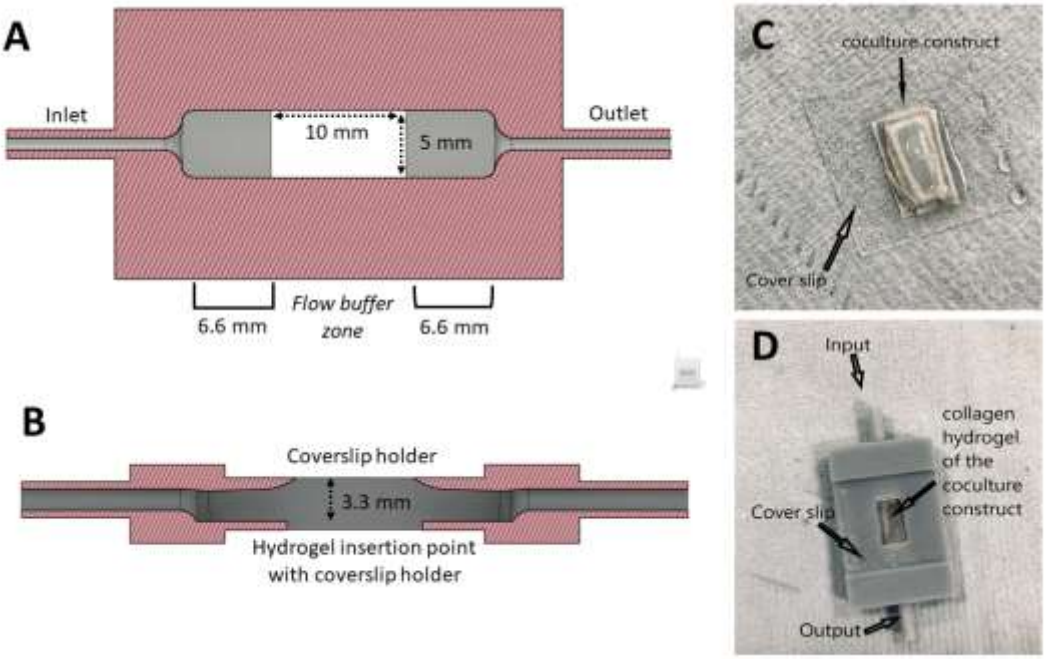

Figure 2.3 3D printed flow chamber for shear-induced hydrogel construct disassembly experiment. These 3D printing templates were prepared using a 3D Elegoo mars printer. (A) A top-down view of the flow chamber. The flow chamber was designed to create a 10 mm x 5 mm x 5 mm (L x w x d) space in which to insert the hydrogel model into the flow chamber. This is flanked either side a flow buffer zone, which provides a space to ensure laminar flow occurs across the construct. (B) A side on slice through the flow chamber. In the centre of the template, there is a chamber in which we put the collagen hydrogels of the co-culture construct held in place by a coverslip. (C) Silicone grease was used around the edge of the coverslip to hold the coverslip onto the surface of the 3D printed flow chamber. The hydrogel model is then placed in the centre of the coverslip to ensure that it aligns with the insertion space in the flow chamber design. (D) The completed model.

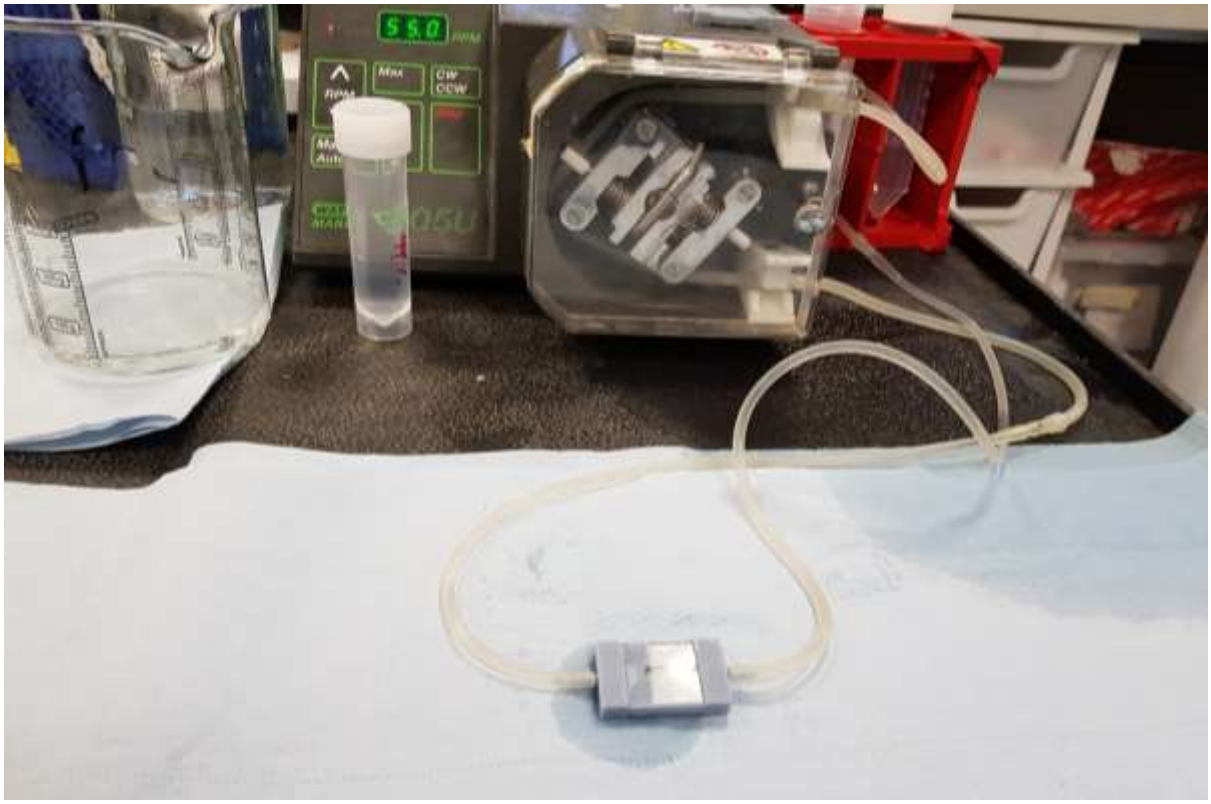

Figure 2.4. The set-up of the shear stress-induced hydrogel disassembly experiment. A Watson-Marlow 505 series peristaltic pump machine (Fluid Technology, UK) was attached to the 3D printed flow chamber and set to pump from a water reservoir at maximum speed.

2.2.2.8 $FeCl_3$ injury of Neointima-HUVECs co-cultures

Filter paper strips were soaked in a 10% $FeCl_3$ solution. This was placed upon a PTFE board and the neointimal surface of the co-culture not coated with HUVEC cells was placed on top of this for 5 minutes at room temperature. The co-culture was then washed 3 times for 1 minute, 2 minutes and 5 minutes in PBS prior to exposure to washed platelet suspensions (see figure 2.5 below). Uninjured constructs were also washed with PBS for the same time prior to exposure to human platelet suspensions.

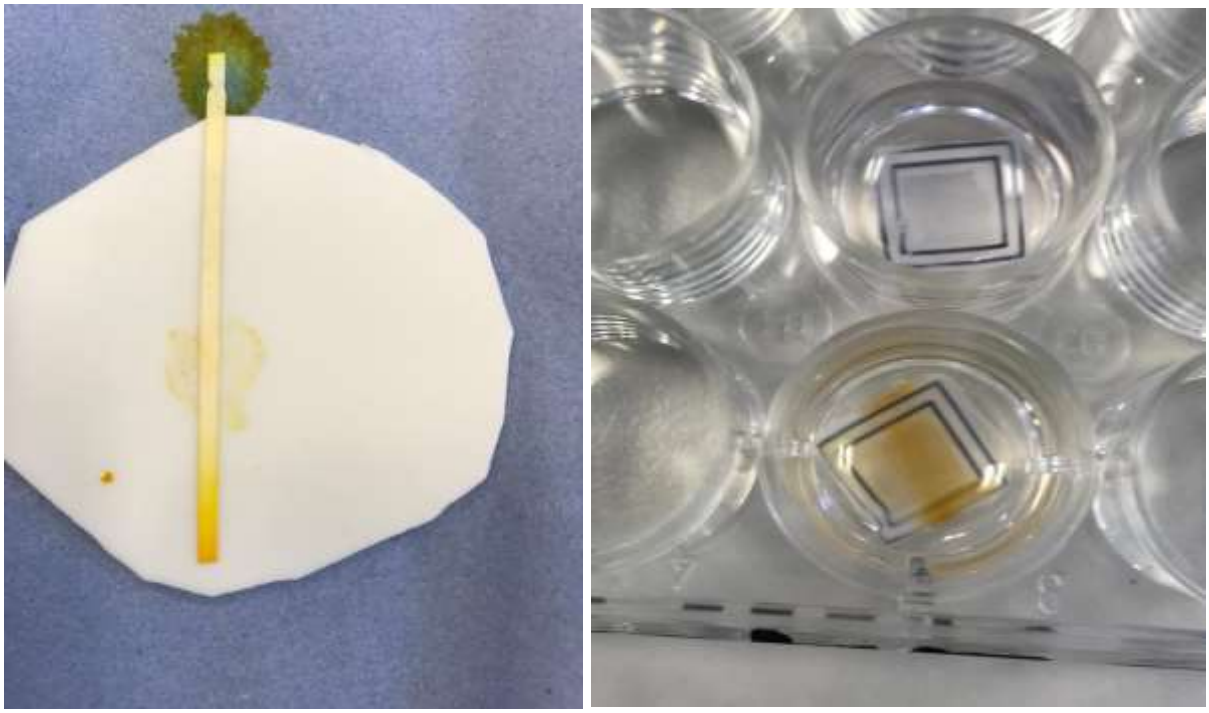

Figure 2.5 $FeCl_3$-induced neointimal injury. (A) Filter paper strips were soaked in 10% $FeCl_3$ solution for at least 1 hour prior to use. These were then removed, wiped of extraneous FeCl3 solution, and placed on a sterile PTFE plate. (B) The collagen hydrogels of the neointima coculture were placed on the $FeCl_3$-soaked filter paper on the neointimal surface of the co-culture for 5 minutes. The samples were then washed 3 times in PBS and then photgraphed to demonstrate the permeation of $FeCl_3$ through the complete construct.

2.2.3 Conditioned Media ELISA experiments

Conditioned media samples from atorvastatin-treated neointima-SMCs and neointima-HUVEC co-cultures samples were collected at the end of their incubation period including three conditions, foam cells-SMCs, M1-SMCs, and SMCs alone, and the same was applied for HUVECs co-culture experiments. Four kits for four inflammatory cytokines have been assessed which were IL-1β, TNF-alpha, IL-6, and PDGF. The cell samples were processed according to the manufacturers' instructions and read at 450 nm wavelength on a BioTek 2 Synergy microplate reader.

2.2.4 Preparation of Cryosections

A few formalin-fixed hydrogels were cut into 10 µm thickness sections by a cryostat (Leica CM

3050 S). To prevent ice crystal, the hydrogels were infiltrated by 15% sucrose until the specimens sunk down in the container, then infiltrated by 30% sucrose until the specimens sunk down in the container embedded, then 50:50 30% sucrose and Optimal Cutting Temperature compound (OCT), then OCT before mounting for section. After sectioning, the cryosections were then affixed to Superfrost microscope slides. Slides were stored at 4°C until staining. To enhance the adhesion of the sections to the slide, samples were then heated in a slide over for 60°C for 45 minutes. Samples were allowed to cool prior to use.

2.2.4.1 Staining of Cryosections

2.2.4.1.A Haematoxylin and Eosin Staining

Samples were washed twice with PBS to dissolve the residual OCT from the cryosections. Samples were then stained in freshly filtered Harris Haematoxylin solution for 5 minutes, followed by washing under running tap water. Samples were then differentiated in 0.3% acid-alcohol solution for 45 seconds. After washing under running tap water, samples were then blued through addition of Scott's tap water for 45 seconds. After washing with running tap water, samples were then incubated with Eosin solution for 3 minutes. After washing with running tap water, sample were then imaged using an EVOS brightfield microscope using a 10x and 20x objective.

2.2.4.1.B Nile Red Staining

Samples were washed twice with PBS to dissolve the residual OCT from the cryosections. Samples were then covered with 1 µg/mL Nile Red solution dissolved in a PBS solution containing 0.1% [v/v] acetone. Samples were protected from light and incubated for 30

minutes at room temperature on an orbital shaker set for 100 rpm. Samples were then washed 3 times with PBS, and then were mounted with a coverslip in fluoroshield mounting medium containing DAPI (Abcam, UK). Samples were then imaged using the 10x and 20x objectives on an Fluoview FV1200 laser scanning confocal microscope (Olympus, UK) using 405 nm and 473 nm excitation wavelength and emission at 430-455 nm and 490-520 nm.

2.2.4.4 Immunostaining

Samples on the slide were separated by a hydrophobic barrier pen (Pap Pen, Scientific Laboratory Supplies), and then washed 3 times with PBS to remove residual OCT. After washing, the samples were blocked by incubation in PBS containing 0.1% [v/v] Tween 20, 1% [w/v] Bovine serum Albumin, 0.3M glycine and 10% [v/v] Normal goat serum for 1 hour at room temperature. The blocking solution was then removed, and the samples were then incubated overnight at 4°C in a humidified slide staining tray with either mouse anti-type I collagen (1:100 dilution), rabbit anti-tissue factor (1:100 dilution), mouse anti-α Smooth muscle actin (1:1000 dilution), or mouse anti-CD31 (1:1000 dilution). The antibody solution was then removed, and the samples were washed three times with PBS containing 0.1% [v/v] Tween 20 and 1% [w/v] Bovine serum albumin (PBST-BSA) for 10 minutes at room temperature. After washing, the samples were incubated with a PBS solution containing 1% [w/v] Bovine serum albumin and either 2 µg/mL of either goat anti-mouse-Alexa Fluor488 (α Smooth muscle actin), goat anti-mouse-Alexa Fluor 647 (CD31, collagen), or goat anti-rabbit anti Rabbit-Alexa Fluor488 (tissue factor). After incubation with the secondary antibodies, samples were washed 3 times with PBS-BSA for 10 minutes at room temperature. After this samples were then mounted with a coverslip in fluoroshield mounting medium containing

DAPI (Abcam, UK). The slides were then imaged using the 10x and 20x objectives on an Fluoview FV1200 laser scanning confocal microscope (Olympus, UK) using 405 nm, 473 nm and 635nm excitation wavelength and emission at 430-455 nm, 490-520 nm and 655-755nm respectively.

.

2.2.5 Assessment of the hemostatic effects of the 3D neointimal layer and derived co-cultured constructs

2.2.5.1 Preparation of human platelet-poor plasma (PPP)

Blood donations were approved by the Keele University Research Ethics Committee. Blood was taken from healthy medication-free volunteers. Each one-part blood was mixed with 9 parts 3.8 % [W/V] sodium citrate solution. Thereafter, the blood was centrifuged at 700 x *g* for 8 minutes to separate blood into its constituents. Platelet-rich plasma (PRP) was isolated and 100 µM aspirin, and 0.1 U/mL apyrase were added. Isolated PRP was centrifuged again at 350 x *g* for 20 minutes to pellet platelets. The coagulation experiments were done using the supernatant of the platelet poor plasma.

2.2.5.2 Preparation of washed human platelet suspension

Blood donations were approved by the Keele University Research Ethics Committee. Blood was donated by healthy medication-free volunteers who gave written informed consent. Whole blood was mixed in a 5:1 ratio with acid citrate dextrose anticoagulant (85 mM sodium citrate, 78 mM citric acid and 111 mM d-glucose). The PRP was obtained by centrifugation for 700 x g for 8 minutes. After extraction this was treated with 100 µM aspirin and 0.1 U/mL apyrase. Platelets were then collected by centrifugation at 350 g for 20 minutes. Washed

platelets were re-suspended into supplemented HEPES –Buffered Saline (HBS) to a final cell density of to 2x108 cells/mL. To make supplemented HBS, HBS (pH 7.4, 145 mM NaCl, 10 mM HEPES, 10 mM d-glucose, 5 mM KCl, 1 mM MgSO4), was supplemented on the day of the experiments with 1 mg/mL BSA, 10 mM glucose, 0.1 U/mL apyrase and 200 µM CaCl2. Immediately prior to all experiments the $CaCl_2$ concentration of the washed human platelet suspension was increased to 1 mM.

2.2.5.3 Prothrombin time measurement

Citrated PPP (0.5 mL) was aliquoted into cuvettes and recalcified by addition of 20 mM $CaCl_2$. The samples were then incubated for 10 minutes prior to the experiment in a water bath held at 37°C. The tissue-engineered neointimal constructs were washed with PBS, and then inserted into sodium acetate frames to allow the surface of the neointimal constructs to be placed in contact with PPP (Figure 2.6). Prothrombin time was measured as the time taken between construct contact with PPP and the observation of the formation of fibrin crystals within the PPP sample.

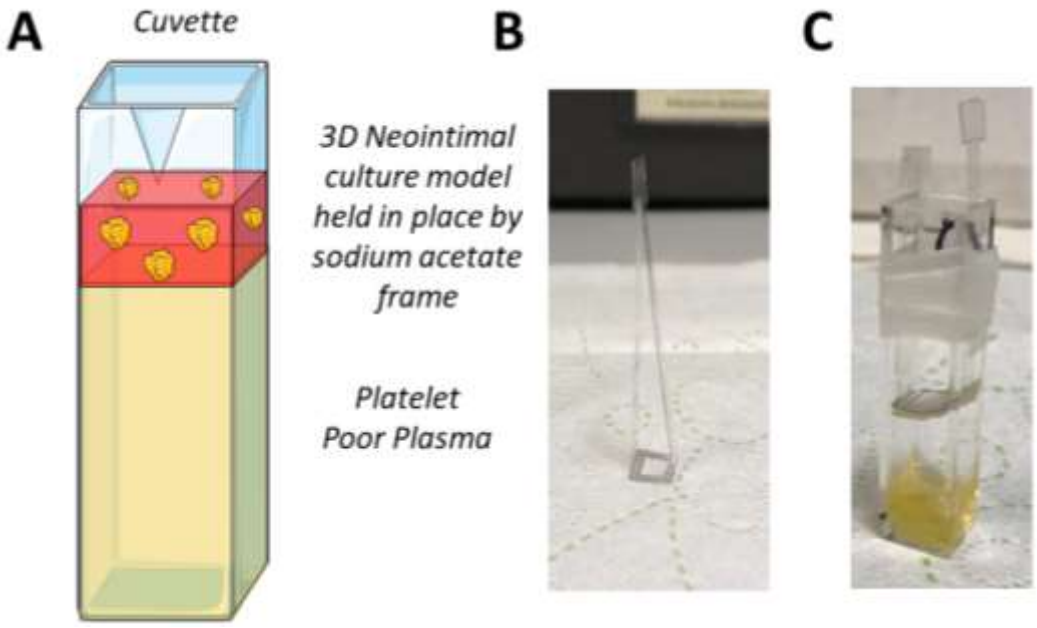

Figure 2.6 Experimental Set-up for assessing prothrombin time stimulated by 3D neointimal culture models. (A) Diagram demonstrating the experimental set-up. Washed human platelets or platelet-poor plasma (PPP) was placed in contact with the luminal surface of the 3D neointimal culture model held in position using a sodium acetate frame. The cuvette was then held in a water bath held at 37°C under constant magnetic stirring. (B) Picture of the sodium acetate frame. (C) Photos of complete set-up with frame not fully inserted. Parafilm is placed around the outside of the cuvette to help hold it in a cuvette holder in the waterbath. Cuvette and Foam cell icons obtained from Bioicons.com.

2.2.5.4 Tissue factor assay

Tissue factor activity of the tissue-engineered neointimal constructs were assessed by measuring tissue factor-dependent activation of FVII. THP-1 cells were mixed at a cell density of 6 x 10^5 cells/mL into a neutralized solution of 3 mg/mL type I collagen, and then 200 µL of this sample was then set into 48-well plates. These cells were then cultured in RPMI media over 10 days to foam cells as detailed in Section 2.2.2.1.2 through sequential addition of PMA, IFN-γ and LPS, and oxLDL or native LDL. On day 10 of the culture, were treated with 100 µL of a PBS solution containing 1 mM $CaCl_2$, 100 nM FVII and 10 µM SN-17a (the fluorogenic

substrate - 6-amino-1-naphthalenesulfonamide-based , ANSN) . Cleavage of the SN-17a which is the fluorescent indicator of FVIIa activity) was then measured fluorometrically using a BioTek 2 synergy microplate reader using excitation wavelengths of 340-380 nm, and emission wavelengths of 518-538 nm. Readings were taken every 10 seconds for 10 minutes at 37°C.

2.2.5.5 Platelet aggregometry

Platelet aggregation was measured using a ChronoLog light transmission aggregometer. The baseline for 0% aggregation was set at the start of experiment against a tube filled with 450 µL of unused washed human platelet suspension, and for 100% aggregation was set using a tube filled with 450 µL supplemented HBS. The neointimal constructs were placed into sodium acetate frames and placed into contact with 0.8 mL washed human platelet suspension. These were incubated for 10 minutes at 37°C under constant magnetic stirring (Figure 2.7). Following this the construct was removed, and in some experiments was fixed in 4% paraformaldehyde. 450 µL of the platelet suspension was transferred into glass aggregometry tubes containing magnetic stir bars. Stirring was set to 1200 rpm and temperature of the aggregometry tube holder was maintained at 37°C. Changes in light transmission was recorded during constant stirring of the samples at 37°C for 10-16 minutes.

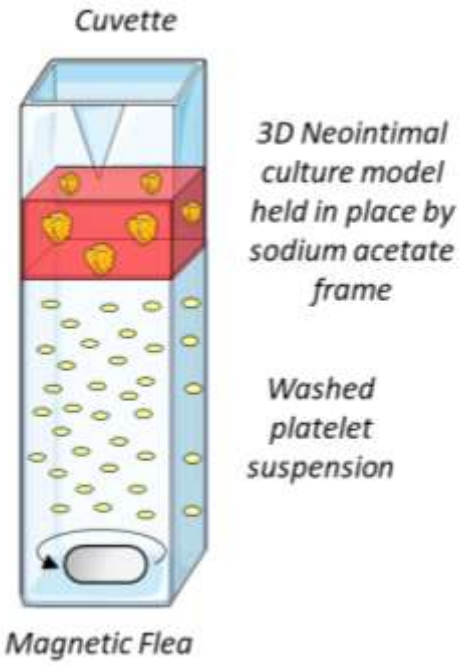

Figure 2.7: Experimental Set-up for assessing aggregatory responses to 3D neointimal culture models. Diagram demonstrating the experimental set-up. A cuvette containing 800 µL washed human platelet suspension containing 1 mM $CaCl_2$ was placed in contact with the luminal surface of the 3D neointimal culture model held in position using a sodium acetate frame. The cuvette was then held in a water bath held at 37°C under constant magnetic stirring. Cuvette and Foam cell icons obtained from Bioicons.com.

2.2.5.6 ATP secretion assay

A Luciferin-luciferase assay was used to assess secretion of ATP from platelet dense granules. After incubation with the neointimal construct for 10 minutes at 37°C, the construct was removed, and samples of the washed platelet suspension were extracted for aggregometry analysis as stated above in 2.2.3.4. The remaining washed platelet suspension was incubated without the construct for a further 10 minutes at 37C. 80 µL of the washed platelet suspension was then placed into a 96-well plate and mixed with 20 µL luciferin-luciferase assay mixture (Sigma Aldrich, UK) immediately prior to reading. A BioTek Synergy 2 microplate reader was then used to measure ATP-induced luminescence from the sample over 1 minute.

2.3 Statistical Analysis

Values stated are mean ± SEM of the number of observations (n) indicated. For experiments comparing two variables, a Student's T-test was used. Statistical analysis of experiments in which multiple comparisons between variable were made simultaneously was assessed by using one-way analysis of variance (ANOVA) followed by a post hoc Tukey test. A $P < 0.05$ was considered statistically significant.

Chapter 3: Development of a neointimal layer for 3D human tissue-engineered arterial constructs

3.1 Introduction

The atherosclerotic artery is distinguished from the normal vessel by the presence of an abnormal thickening of the intimal layer of the blood vessel, leading to the formation of a neointima. This neointima is formed from the infiltration of monocytes and smooth muscle cells at sites of endothelial dysfunction (See Figure 1.1). Monocytes migrate to the site of the inflamed endothelial lining and migrate into the subendothelial space where they transform into macrophages (Gawaz *et al*., 2005). These macrophages start to engulf the oxidized low-density lipoproteins (ox LDL) forming specialized macrophage-derived foam cells. These foam cells are then covered by a fibrous cap that is made up by smooth muscle cells migrating from the medial layer – leading to the fibroatheroma stage of plaque development (Virmani *et al*., 2003). Beneath this fibrous cap, there will be apoptotic death of some of the foam cells, leads to the formation of a necrotic core characterized by live and dying foam cells as well as an accumulation of extracellular lipids. This creates a proinflammatory environment which appears to propagate atherosclerosis plaque development and then to potential plaque rupture. Therefore, to create a realistic model system in which to study advanced developmental stages of atherosclerosis requires the production of tissue-engineered model with the potential to elicit a fibrous cap and a necrotic core (Seimon and Tabas, 2009).

As development of atherosclerotic plaques occurs over decades and in a manner that is unpredictable in different individuals, it is infeasible and unethical to study much of the process of atherosclerotic plaque development and rupture at the cellular and molecular level in humans (Almeida & Budoff, 2019). Current studies are principally limited to the assessment

of tissue samples collected post-mortem, as well as imaging studies conducted in patients who have or who died because of ischemic heart disease (Beausire *et al*., 2018: Precht *et al*.,2018: Gallo *et al*., 2018). Whilst these studies have advanced our understanding of large-scale morphological changes in plaque structure, they do not provide an accessible model in which to study the cellular and molecular changes underlying plaque development (Yonetsu and Jang, 2018). Furthermore, human *ex vivo* studies have also contributed to progressing the advantages of human studies. The main advantage of *ex vivo* studies is their ability to analyse the complex inflammatory milieu of the atherosclerotic plaque which is not fully recreated in current in vitro models (Erbel *et al*., 2014). On the other hand, the very short period that human tissue can be maintained in culture significantly limits the usefulness of these models, as well as the difficulty in researchers obtaining these samples, and standardising these tissues to allow for reproducible biological study.

Therefore, most of our current knowledge about the pathology and pathogenesis of atherosclerosis has been obtained from *in vivo* animal studies. The animals that have been most using to study atherosclerosis *in vivo* are mouse, rabbits, pigs, as well as non-human primates. These animal models provide a method to study the mechanism of atherosclerosis within a complex cellular, chemical, and physical environment found within the animal body as well as non-human primates and allows investigators to study atherosclerosis throughout all stages of the disease progression. However, each of these models presents with different issues in fully recreating human atherosclerotic plaque development and treatment. These include differences in anatomical locations of plaques, the need for transgenic animals to mitigate for interspecies differences in lipid metabolism, failure for plaque rupture to occur spontaneously in some species, and failure to translate preclinical drug testing findings from

model organisms into humans during clinical trials (Veseli *et al*., 2017). These differences necessitate the use of multiple experimental models to create reliable findings.

The limitations of animal models have led to some researchers examining the possibility of recreating human atherosclerosis in *in vitro* human cell models (De Haan *et al*., 2008). However, traditionally these models either replicate the early stages of atherosclerosis ahead of foam cell formation, in which monocyte and lipids are recruited to the subendothelial compartments or represent isolated atherosclerotic plaque models created outside the cellular context of the vasculature (Mallone *et al*., 2017). As later stages of plaque development are clinically relevant, there is a need for an *in vitro* human atherosclerosis blood vessel model which can be used to examine plaque development, rupture, and subsequent thrombosis.

Initially, researchers used *in vitro* human models instead of animal models to study the pathogenesis and pathology of atherosclerosis. These have focussed heavily on the initial formation of the plaque with aims based around creating models to study monocyte infiltration and foam cell formation (Islam *et al*., 2016). Initial work focussed on the use of 2D culture methods using monolayers of endothelial cells, smooth muscle cells and macrophage/foam cells to simulate the initial stages of atherosclerosis. However, all these models did not reflect the normal *in vivo* environment due to limited realism of these 2D monolayer. More recently, Noonan *et al*., (2019) have reported the use of a triple-cell 2D atherosclerosis model in which human coronary artery endothelial cells and smooth muscle cells were culture on opposite sides of a transwell insert. To finish the model, THP-1 cells were differentiated in 6-well plates to M0 macrophages by treatment for 72 h with phorbol esters. This provide a model in which the cellular signalling and subsequent changes in cell

phenotype between the 3 cell types can be assessed but does not provide a method for studying further development of the plaque (Noonan *et al*.,2019). Another significant disadvantage of these 2D models is that they devoid of any relevant physical stimuli found *in vivo*, such as the shear forces that the blood vessel is exposed to by blood flow (Yurdagol et al.,2016).

These limitations lead to the development of 3D cultures to more effectively model. These initial stages of atherosclerosis, for example, (Liu *et al*., 2017) developed a model in which human coronary artery smooth muscle cells (HCASMCs) were cultured within a collagen hydrogel, atop with human coronary artery endothelial cells were plated to create a simple tissue engineered coronary artery model. After activation of the model with oxidised low-density lipoprotein, these cultures could be seen to trigger effective transmigration of THP-1 cells into the subendothelial compartments. Similar experiments in these models have been improved using stretchable microfluidic channels (Gu *et al*., 2019), or through incorporation of tissue-engineered blood vessels into microfluidic chambers (Robert *et al*., 2013; Zhang *et al*., 2020) to allow for physical stimulation of the models. The primary endpoints of these projects have been to examine the effects of experimental conditions and pharmacological agents upon the accumulation of foam cells within the neointima. However due to the limited time of monocyte exposure, the degree of foam cell infiltration observed is limited in these models.

Production of a more comprehensive fatty streak, as well as development of later stage models of atherosclerosis within these tissue-engineered blood vessels is difficult because it involves the effective maintenance of the viability of the surrounding blood vessel cells, whilst neointimal foam and smooth muscle cells undergo differentiation and degradation.

Recreating the full development and breakdown of an atherosclerotic plaque within an *in vitro* model would be extremely technical challenging, time-consuming and expensive. An alternative approach is to begin to create tissue-engineered blood vessels in which more developed atherosclerotic plaques are engineered directly into them. Previously Musa *et al.*, (2016) created tissue-engineered blood vessel constructs using a layer-by-layer building methodology – with a medial layer being made through culturing HCASMCs within a type I rat collagen hydrogel, and an intimal layer developed through culturing human umbilical vein endothelial cells (HUVECs) atop of an aligned PLA nanofibers mesh through creating independently cultured constructs representing the intimal and medial layers which are able to effectively replicate the primary haemostatic properties of arteries. The modularity of this design provides the potential to directly incorporate a pre-developed fatty streak, fibroatheroma or unstable plaque between the intimal and medial layers of the construct. This construct could allow the *in vitro* development of a range of different stages of the atherosclerotic plaque ranging from the fatty streak, to the fibroatheroma, to plaque rupture.

As macrophage-derived foam cells play a principal role in the pathology of atherosclerosis, human monocytes have been used in *in vitro* experiments as a source to culture human macrophages and human foam cells for atherosclerosis studies. However, as monocytes comprise only 2-8% of all leukocytes, this separation requires a complex and expensive process to separate and isolate these cells from other types of leukocytes from fresh human blood (Huo *et al*., 2003). Therefore, previous studies have used human monocytic cell lines such as U937, HL-6p or THP-1 cells. THP-1 cells are human monocytic cells obtained from a patient with acute monocytic leukaemia and are the most used cell type as they share many structural, biochemical, and physiological properties with that of primary human monocytes

(e.g., expression of CD14, and LDL receptors; Mallone *et al*., 2017). In addition, they share a similar cytokine production response upon polarization, especially IL-6, IL1-ß, TNF-ὰ, and PDGF. Furthermore, upon polarization of M1 cells, both types of cells exhibit a similar expression level of CD80. However, human primary monocytes exhibit a higher expression level of CD206 upon M2 polarisation in comparison with that of THP-1-cells. Additionally, human primary monocytes produce significantly higher levels of IL-2, IL-7, IL-8, and IL-9 upon polarization in comparison with that of THP-1 cells (Tedesco et al.,2018). Furthermore, it has been reported that the phagocytic activity of primary human monocytes derived macrophages is higher than that of THP-1-derived macrophages (Madhvi *et al*.,2019).Despite these differences in behaviour, THP-1 cells have been widely used as a viable alternative to human monocytes in the culture of macrophage-derived foam cells as they can be readily differentiated to macrophages when artificially stimulated upon treatment with phorbol 12-myristate 13-acetate (PMA) and provide a more sustainable supply of foam cells possible than when using fresh peripheral blood monocytes (Daigneaul *et al*.,2010).

Human macrophages are not a homogenous cell type *in vivo* as they can significantly change their phenotype depending on the local tissue environment. This has traditionally led to macrophages being divided into two main groups, M1 and M2 macrophages (Figure 2). M1 cells are characterized by their pro-inflammatory activity, while M2 by their phagocytic, anti-inflammatory activity. These different phenotypes can be artificially induced in culture using different combination of cytokines and other chemical signals. For example, polarisation of M1 macrophages can be achieved by culturing in the presence of lipopolysaccharide and IFN-gamma, leading to these cells expressing certain pro-inflammatory cytokines, for instance, TNF-α, IL-1β, IL-6 and IL-12. On the other hand, if we activate macrophages with IL-4 or IL-13,

this will lead to a polarisation to an M2 macrophage phenotype leading to these macrophages secreting certain anti-inflammatory cytokines, for instance, IL-10 (Via *et al*., 1989). More recently it has become clear that the M1/M2 polarisation is a simplification with multiple distinct M2 subgroups having been demonstrated (Yuan *et al*., 2015). Both M1 and M2 macrophages are found in human atherosclerotic plaques, but with M1 macrophages predominating in more rupture prone plaques, whilst M2 macrophages are observed in more stable plaques (Genin *et al*., 2015). Therefore, being able to replicate mixed populations of M1 and M2 macrophage may be required to best replicate atherosclerotic plaques. Furthermore, although macrophage-derived foam cells have been traditionally considered to be the principal source of foam cells within the neointima, this has been challenged by data demonstrating that smooth muscle cell-derived foam cells contribute around about 50% of all the foam cells present in atherosclerotic plaques found in human arteries (Allahverdian *et al*., 2014). Interestingly, these cells show reduced expression of the cholesterol efflux transporter ABCA1 in later stage atherosclerotic lesions, whereas macrophage-derived foam cells show upregulated expression (Wang *et al*., 2019). This loss of this lipid-exporting transporter prevents the regression of smooth muscle cell derived foam cells back to its original form, facilitating its accumulation within the plaque. As previous 3D culture models of atherosclerosis have not investigated the incorporation of this cell type, experiments were also performed to investigate whether smooth muscle derived foam cells could be developed within a 3D culture. Due to the complexity of the cellular and biochemical environment contained within the atherosclerotic plaque, this chapter has focussed on developing a 3D culture model of a foam cell-rich neointimal layer containing either macrophage- or smooth muscle cell-derived foam cells that can be incorporated within our previously developed tissue engineered arterial construct.

3.2 Aims and Objectives

The aim of this chapter is to develop a novel 3D neointimal construct within a collagen hydrogel that can be incorporated into our previously developed tissue-engineered arterial model.

Objective 1: Establish a 2D culture of THP-1-derived foam cells, and assess whether these can be successfully detached from the culture plastic for introduction into a 3D hydrogel

Objective 2: Incorporate THP-1 cells into a 3D collagen hydrogel and assess the ability of using the 2D culture protocol to produce THP-1-derived foam cells within the scaffold. Evaluate whether 3D cultures of THP-1-derived foam cells through differentiation within the 3D gel or following culture in a 2D environment.

Objective 3: Assess the potential for utilising plastic compression of the 3D culture containing construct to increase the mechanical support from the 3D gel and to increase foam cell density within the gel

Objective 4: Assess the potential for incorporating human coronary artery smooth muscle cell-derived foam cells within the 3D culture for co-culturing.

3.3 Results

To create an *in vitro* 3-dimensional atherosclerotic plaque inside the tissue-engineered human blood vessel constructs, it was necessary to be able to develop a neointimal layer representing the accumulation of macrophage-derived foam cells into the fatty streak. This can then be transferred between the intimal and medial layers of our current construct to create a neointimal layer, which can be used to create a tissue-engineered model of atherosclerosis.

Firstly, it was necessary to establish a reliable culture methodology to allow the scalable production of macrophage-derived foam cells within a 3D collagen hydrogel. Whilst it is possible to culture foam cells from monocytes derived from human blood, this would require a significant supply of fresh human blood and the use of expensive cell isolation methods to allow for the extraction of sufficient human monocytes to make this a viable route. Therefore, instead, it was decided it was more sensible to establish the foam cell culture using THP-1 cells, a human monocytic cell line derived initially from a leukemic patient. To develop a neointimal layer for a blood vessel construct it was necessary to create and characterise a reliable *in vitro* foam cell culture from THP1 cells. This was initially attempted in 2D culture to allow for the establishment of methods to assess cellular differentiation prior to beginning work on developing 3D culture techniques.

3.3.1 Establishing a reliable methodology for creating a proliferating THP-1 cell suspension culture

Initial work involved establishing a reliable methodology for culturing THP-1 cells. THP-1 cell cultures require high-seeding density to allow them to reach a proliferative stage of rapid growth. This typically takes 1-2 weeks of maintenance in culture to reach this stage. The initial

experiment cell culture was established using a proliferating THP-1 cell culture received directly from the supplier. This culture could be seen to rapidly expand upon incubation and was used to establish the initial THP-1 cell culture, as well as provide aliquots of low passage cells that were placed into cryostorage (Figure 3.1A). The first attempt to revive a frozen cryovial of THP-1 cells led to a non-proliferating culture, despite cells being seeded at the recommended cell density and culture conditions, with the cell density in the culture remaining below 2.5 x10^5 THP-1 cells/mL (Figure 3.1B). This culture was established according to the supplier's instruction in which the thawed cells should be rapidly diluted into a large volume of RPMI containing 10% [v/v] FBS to facilitate rapid removal of DMSO from the cells and prevent toxic effects of this solvent. Therefore, a different strategy was used to attempt to establish a method of successfully reviving the cryovials of THP-1 cells. The thawing procedure was changed to reduce the possibility of osmotic swelling of the THP-1 cells and increasing the nutrients available for them by slowly adding RPMI media supplemented with 20% [v/v] FBS. This attempt proved successful, leading to cells achieving a rapid phase of proliferation after 10 days in culture (Figure 3.1C). This technique has been successfully applied to subsequent revived cryovials of THP-1 cells throughout the project.

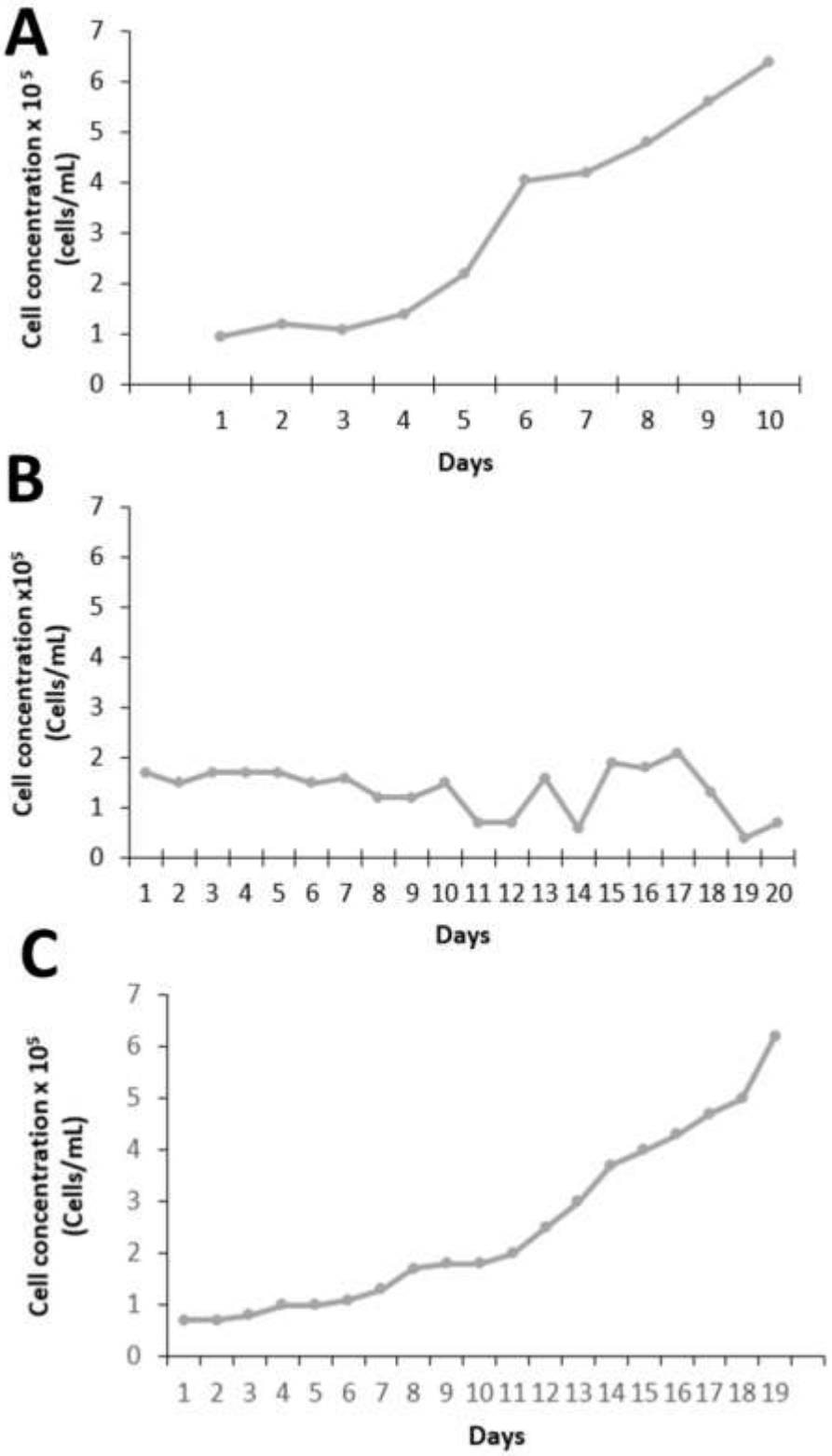

Figure 3.1. Proliferation curves of differentially revived THP-1 cell cultures. (A) Upon arrival, the cells were incubated at 37°C, 5% CO_2 as per the supplier's instructions. (B) Upon defrosting the cryoprotected THP-1 cells were rapidly mixed with RPMI with 10% [v/v] FBS and incubated at 37°C, 5% CO_2 as per the manufacturer's instructions. (C) Upon defrosting, the cryoprotected THP-1 cells were slowly mixed with RPMI with 20% [v/v] FBS and incubated at 37°C, 5% CO_2 as per the supplier's instructions. Viable cell density was then daily measured using trypan blue and a haemocytometer under a light microscope, n=49. * = $P < 0.05$ between indicated conditions using a one-way ANOVA with post hoc Tukey test).

Values are shown as

Mean ±SEM

3.3.2 Differentiation of THP-1 into M0 macrophage cells in 2D culture

Having established a proliferating THP-1 cell suspension, experiments were performed to differentiate M0 macrophage cells from THP-1 cells in 2D culture. This has traditionally been achieved by treating the cells with phorbol 12-myristate 13-acetate (PMA). However, there is great variability in the differentiation protocols used between labs, with no consensus on a standardised protocol for this stage of cell culture. Different labs use a variety of PMA concentrations and incubation periods, with these variables ranging between 6 – 500 nM for the PMA concentration, and between 3-72 hours for the incubation period (Lund *et al.*, 2016). Therefore, experiments were performed to assess the optimal conditions for M0 macrophage culture in the laboratory. Previous studies have suggested that 48h incubation with PMA was the optimal period for THP-1 differentiation (Daigneault *et al.*, 2010); Aldo *et al.*, 2013), and so experiments investigated the effect of using different PMA concentrations incubated for 48 h to induce an M0 phenotype in 2D cultures of THP-1 cells. THP-1 cells were cultured in 24-well plates at a seeding density of 1x 10^5 cells/well. The cells were treated with either completed RPMI media alone or completed RMPI media containing either 25, 50 or 100 nM PMA, and then incubated for 48 h. Cells were imaged by light microscopy to look for morphological signs of differentiation. At the end of the incubation period, adherent cells in the culture were then labelled with a fluorescence antibody to CD68, a cell surface marker for macrophages and assessed by fluorescent microscopy (Jensen *et al.*, 2009). The fluorescent readings from each well were then measured using a microplate reader. PMA treatment induced morphological differentiation of the THP-1 cells during the incubation period. Most notable was the transition of the monocytic cell suspension into an adherent macrophage

phenotype, with minimal, weak cell adhesion seen in cells not treated with PMA (Figure 3.2). Additionally, PMA-treated cells also showed a difference in their size as they differentiated from THP-1 monocytic cells to THP-1-derived macrophages (the mean cell diameter increasing from 8.5 µm to 21 µm). Furthermore, as THP-1 cells differentiate to macrophage, distinct morphological changes appear. The cells started to change from round to oval-shaped and could be seen to form some elongated, spindle-like cells (Figure 3.3). As THP-1 cells differentiated to macrophages, they become larger and either rounded or elongated to form spindle-like structures.

To assess macrophage differentiation, experiments were performed to examine the cell surface expression of CD68. CD68 is a member of the lysosomal-associated membrane proteins (LAMPs). Previous studies have demonstrated that the cell surface expression of this marker can be seen to be increased in THP-1 cells derived macrophages(Genin *et al.*, 2015) . This marker is also of interest due to previous studies that have demonstrated that CD68 may also play a role in the uptake of oxidised low-density lipoproteins (ox LDL), and as such, may be necessary for foam cell formation (Biros, Reznik and Moran, 2021). PMA-treatment also increased the fluorescent labelling of CD68 Expression on the cell surface of THP-1 cells. However, limited fluorescence signals could be expressed by the THP-1 cells that have not

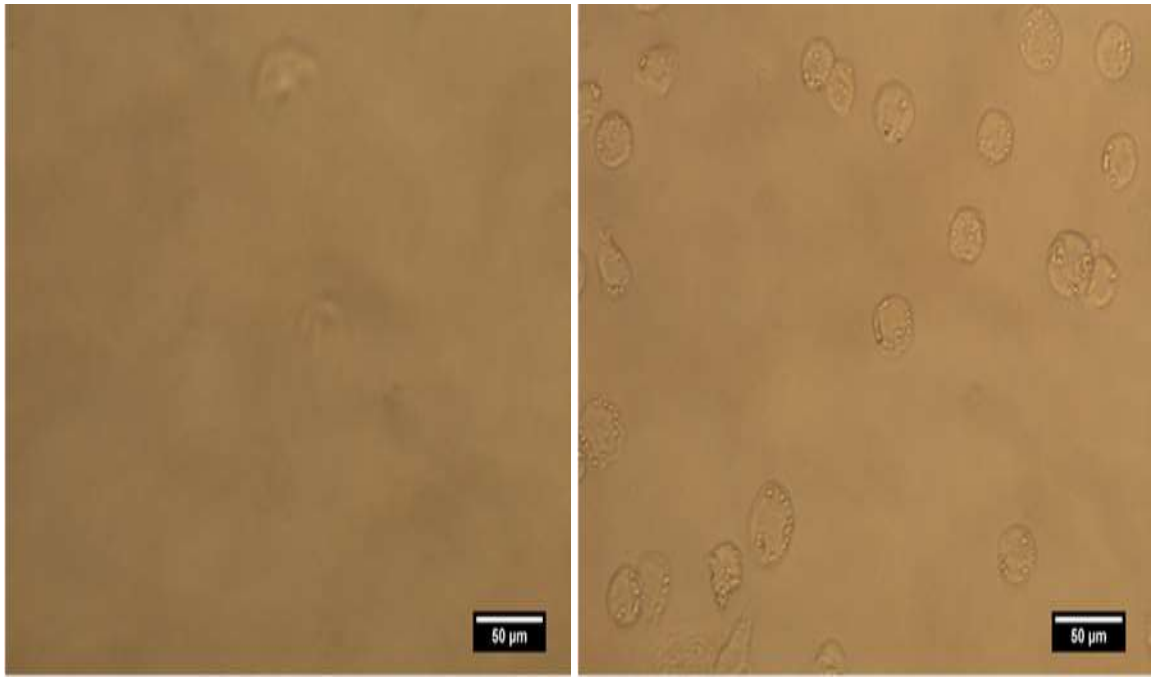

Figure 3.2 THP-1 cells become adherent after PMA stimulation. THP-1 cells were treated with either completed RPMI media alone (Left) or completed RMPI media containing either 25, 50 or 100 nM PMA, and then incubated for 48 h (Right, the PMA concentration for this image was 50nM). The cells were then fixed and imaged using light microscopy. Cells treated without PMA were found to attach in low-density. Most of the remaining cells were dislodged during the washing process and were therefore difficult to get into focus (Left). PMA-treated THP-1 cells became firmly adhere to the surface of the 24-well plate during the culture period (Right), n=6.

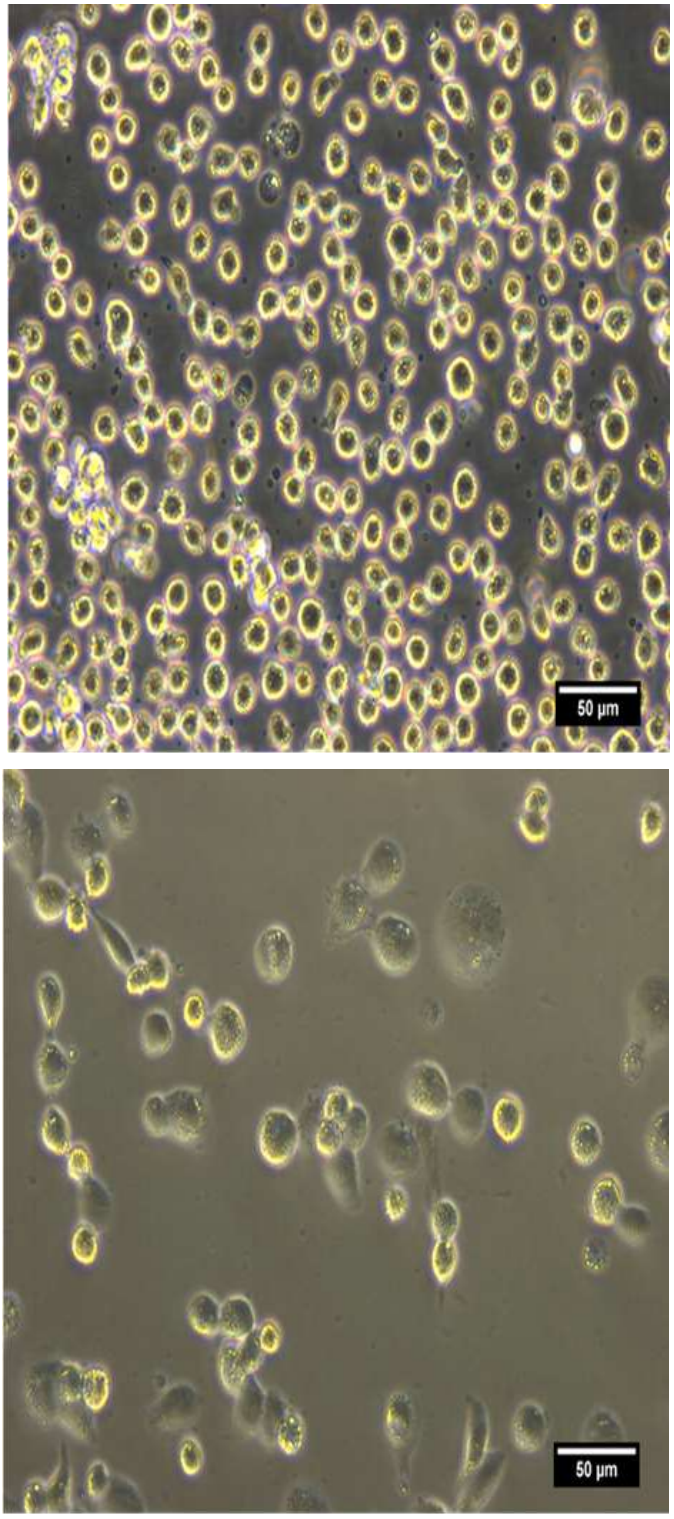

Figure 3.3. PMA stimulation of THP-1 cells induces an increase in size, and a transition of a population into more elongated, spindle-like forms. THP-1 cells either before (Top panel) or after (Bottom panel) treated with PMA (25nM) for 48 h at 37°C, 5% CO_2 (Right). The cells were found to become larger, and some were seen to take up rounded or elongated cellular morphologies, indicative of a macrophage differentiation, n=6.

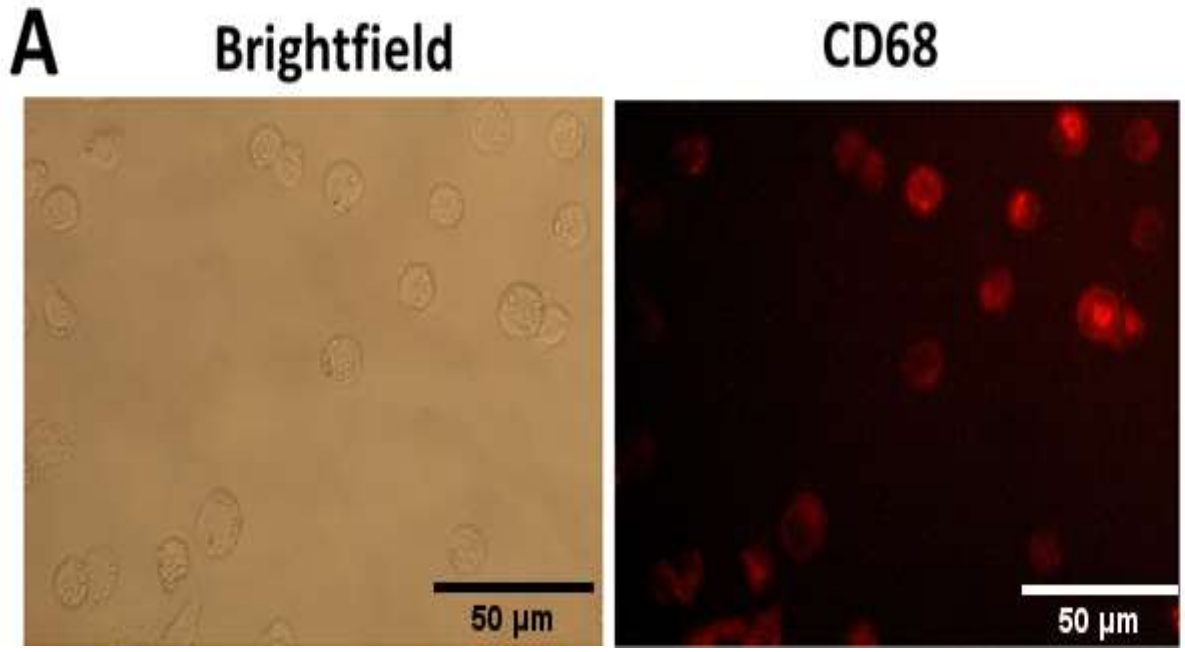

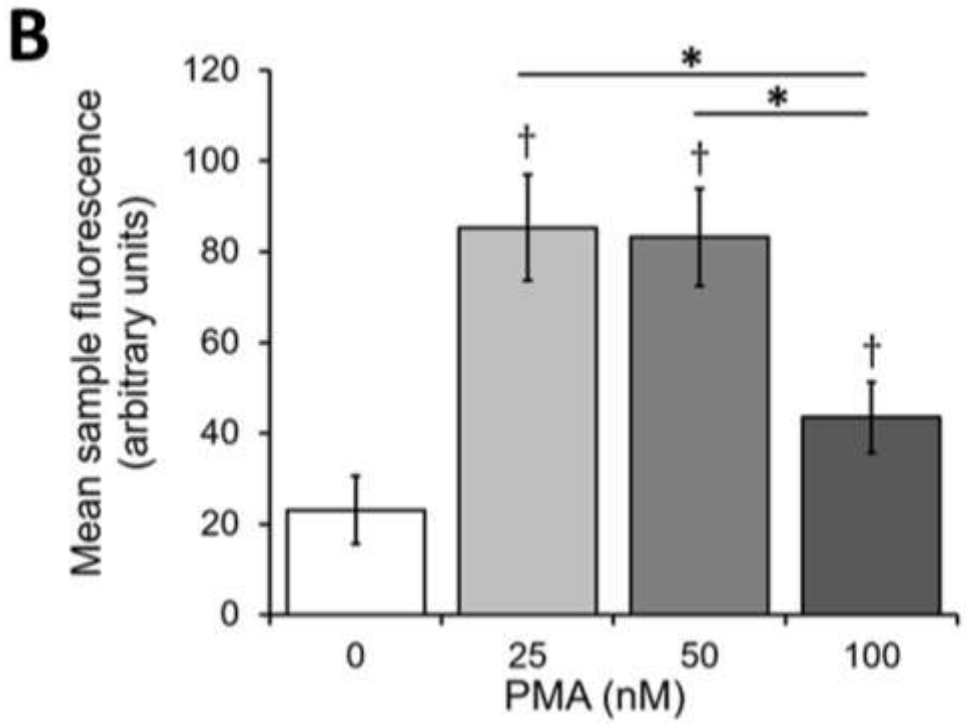

Figure 3.4. PMA induces CD68 Expression in THP-1 cells. THP-1 cell suspensions were seeded at $1x10^5$ cells/well in 24-well plates in RPMI media with varying concentrations of PMA. Cells were then incubated at 37°C, 5% CO_2 for 48 h. Adherent cells were then stained with a fluorescent CD68 antibody. The immunofluorescence signals were read by a microplate reader. Then fluorescence was read by a microplate reader. (A) Brightfield and (B)

fluorescence image on fluorescence microscope of cells treated with 25 nm PMA. The brightness and contrast of the fluorescent image was amended to improve clarity of the image. (C) Fluorescence reading from the microplate reader. † = P < 0.05 compared to 0 nM PMA, * = P < 0.05 between indicated conditions using a one-way ANOVA with post hoc Tukey test). Values shown are Mean ± SEM of 10 experiments

been treated with PMA. This could be explained by the lack of THP-1 cell adherence on the culture plastic when cultured in the absence of PMA (Figure 3.2).

Interestingly stimulation with 25 and 50 nM appeared to create the optimal environment for macrophage differentiation, whilst stimulation with 100 nM appeared to create a weaker response (Figure 3.4). One possibility is that prolonged treatment of THP1 cells with high concentrations of PMA might adversely affect cell viability. Therefore, a trypan blue assay was done to assess if there was any effect on cell viability in these cultures. As shown in figure 3.5, none of the treatment condition adversely affected cell viability, with all conditions showing cell viability of around 99%.

To further confirm this, additional studies examined the expression of the CD36 protein, which is known to be upregulated during the differentiation of monocytes to macrophages (Tontonos *et al*., 1998). CD36 is also an essential mediator of ox LDL uptake during foam cell formation, thus higher expression of this protein would help us increase the changes of forming THP-1-derived foam cells (Biros *et al.*, 2021). Experiments were therefore performed to assess the PMA concentration that optimally upregulated expression of CD36 cell surface expression in THP-1 cells. These data demonstrated a similar pattern to CD68 expression, with expression highest in cells treated with 50 nM PMA (Figure 3.6). Although this increase was found to not be statistically significant over that observed when cells were stimulated with

25 nM PMA, it was decided that THP-1 cell differentiation into macrophages would be performed by treating with 50 nM PMA for 48 h in all future studies.

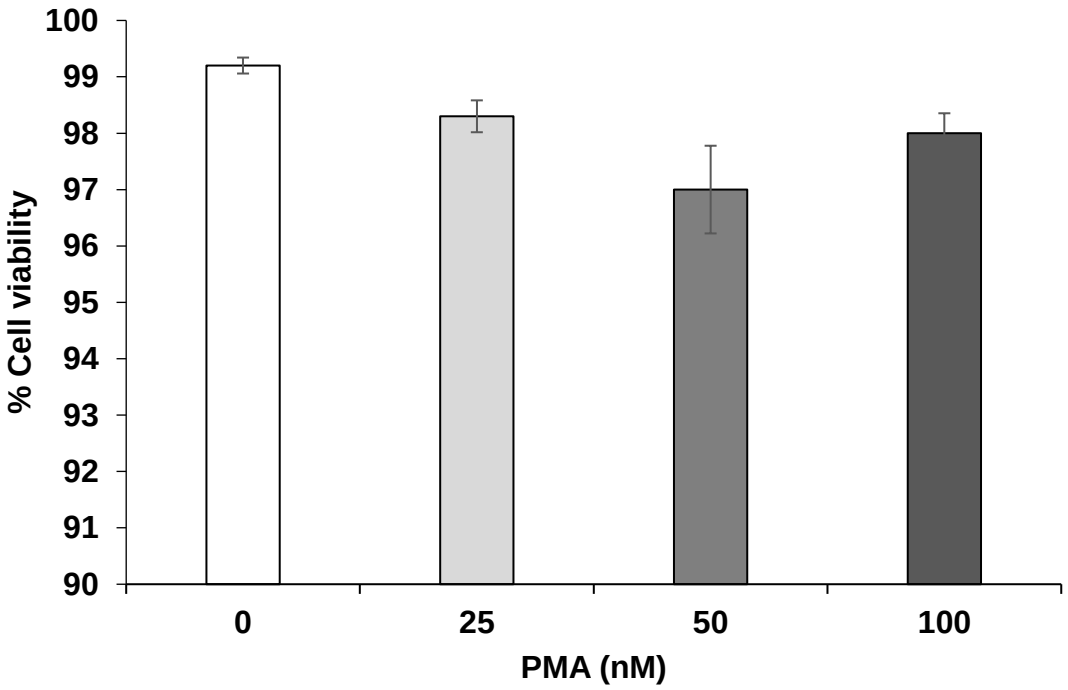

Figure 3.5: Incubation with PMA does not affect cell viability significantly in THP-1 cell cultures. THP-1 cell suspensions were seeded at $1x10^5$ cells/well in 24 well plates in RPMI media with varying concentrations. Cells were then incubated at 5% CO_2 at 37°C for 48 h. At the end of the culture trypan blue was added to the well and live and dead cells were counted across 5 different parts of the well to assess cell viability. Values shown are Mean ± SEM of 12 experiments. (* = $P < 0.05$ between indicated conditions using a one-way ANOVA with post hoc Tukey test).

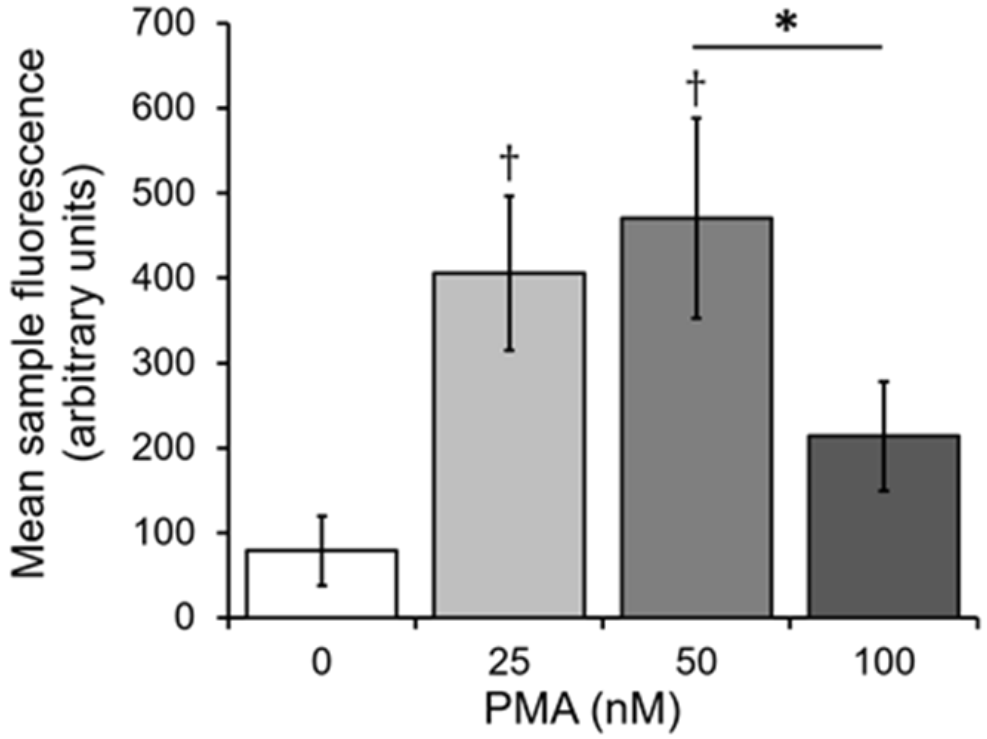

Figure 3.6. PMA treatment increases cell surface expression of the oxLDL receptor, CD36 in THP-1 cells. THP-1 cell suspensions were seeded at $1x10^5$ cells/well in 24-well plates in completed RPMI media with various concentrations of PMA. Cells were then incubated at 5% CO2 20% O2 at 37°C for 48 h. Adherent cells were then stained with a fluorescent CD36 antibody. Then the immunofluorescence signals were read by a microplate reader. † = P < 0.05 compared to 0 nM PMA. Values shown are Mean ± SEM of 10 experiments. (* = P < 0.05 between indicated conditions using a one-way ANOVA with post hoc Tukey test)

3.3.3 Differentiation of M0 THP-1 derived macrophages into M1 macrophages in 2D cultures

Macrophages can polarise further into multiple alternative phenotypes. The most common of these different polarisations are the M1 and M2 macrophages – with M1 macrophages generally considered to be pro-inflammatory, whilst the alternatively-activated M2 macrophages are often regarded as an anti-inflammatory (Murray *et al.*, 2014). Both macrophage types have been previously observed to be present in human atherosclerotic lesions (Bouhlel., 2007). Crucially M1 macrophages have been found to be associated with

rupture-prone lesions and able to form foam cells (Stoger *et al*., 2012). whilst M2 macrophages are associated with more stable plaques, are resistant to oxLDL uptake and have been shown to be associated with atherosclerosis regression (Chinetti-Gbaguidi *et al.*, 2011). Therefore, it would be ideal to be able to create atherosclerotic plaques with differing compositions of M1 and M2 macrophages to assess their impact on the biological function of the tissue-engineered arteries. To be able to do this, experiments were performed to assess the potential of our PMA-differentiated macrophage cells to be polarised using further treatment with commonly-used cytokine cocktails such as lipopolysaccharide (LPS) and Interferon-γ (IFN- γ) for M1 macrophages, and IL-4 for M2 macrophages (Yang *et al.*, 2020). To assess effective polarisation of our M0 macrophages to M1 macrophages, experiments were performed to assess whether treatment of our macrophages with 100 ng/ml LPS and 20 ng/ml IFN-γ could induce an increase in M1 macrophages in our cell population. This was assessed by examining immunoflorescent staining of adherent cells with CD80, a widely used cell surface marker for M1 macrophages (Xu *et al*., 2019).

An initial optimisation experiment was performed to select the best dilution for the FITC-lablled secondary antibody. In this experiment we stained the cells directly with four different dilutions of the secondary antibody (1:2500, 1:5000, 1:7500 and 1:10000) without using the primary antibody. From this experiment, 1:5000 was observed to provide minimal observable background staining in the absence of the primary antibody (data not shown). This antibody concentration was then used to stain THP-1-derived M0 macrophages that had been treated with 100 ng/ml LPS and 20 ng/ml IFN-γ (or an equivalent volume of their vehicle, DMSO). As shown in Figure 3.6, LPS and IFN-γ treatment significantly increased the CD80 expression on

the surface of the THP-1-derived macrophages – demonstrating that it is possible to successfully differentiate the M0 macrophages to THP-derived M1 macrophages

3.3.4 Differentiation of M0 THP-1 derived macrophages into M2 macrophages in 2D culture

To assess effective polarisation of the M0 macrophages to M2 macrophages, experiments were performed to assess whether treatment of the M0 macrophages with 20 ng/mL IL-4 could induce M2 macrophage differentiation. This was initially assessed by examining the staining of adherent cells with an indirect labelling method using a primary antibody to CD206 and a FITC-conjugated secondary antibody. Initial optimisation experiments assessed the optimal FITC-conjugated anti-rabbit secondary antibody concentration to provide the lowest non-specific secondary antibody binding by treating cells with different dilutions of the secondary antibody (1:2500, 1:5000, 1:7500 and 1:10000) without using the primary antibody. The lowest background staining was observed with the 1:10000 dilution, so this was used for the subsequent experiments. Treatment of THP-1-derived M0 macrophages with IL-4 elicited an increased cell surface expression of the M2 macrophage cell surface marker, CD206 compared to M0 macrophages treated the vehicle control, PBS (Figure 3.7). Thus, the M0 macrophages can be differentiated into either M1 or M2 macrophages using appropriate cell culture conditions.

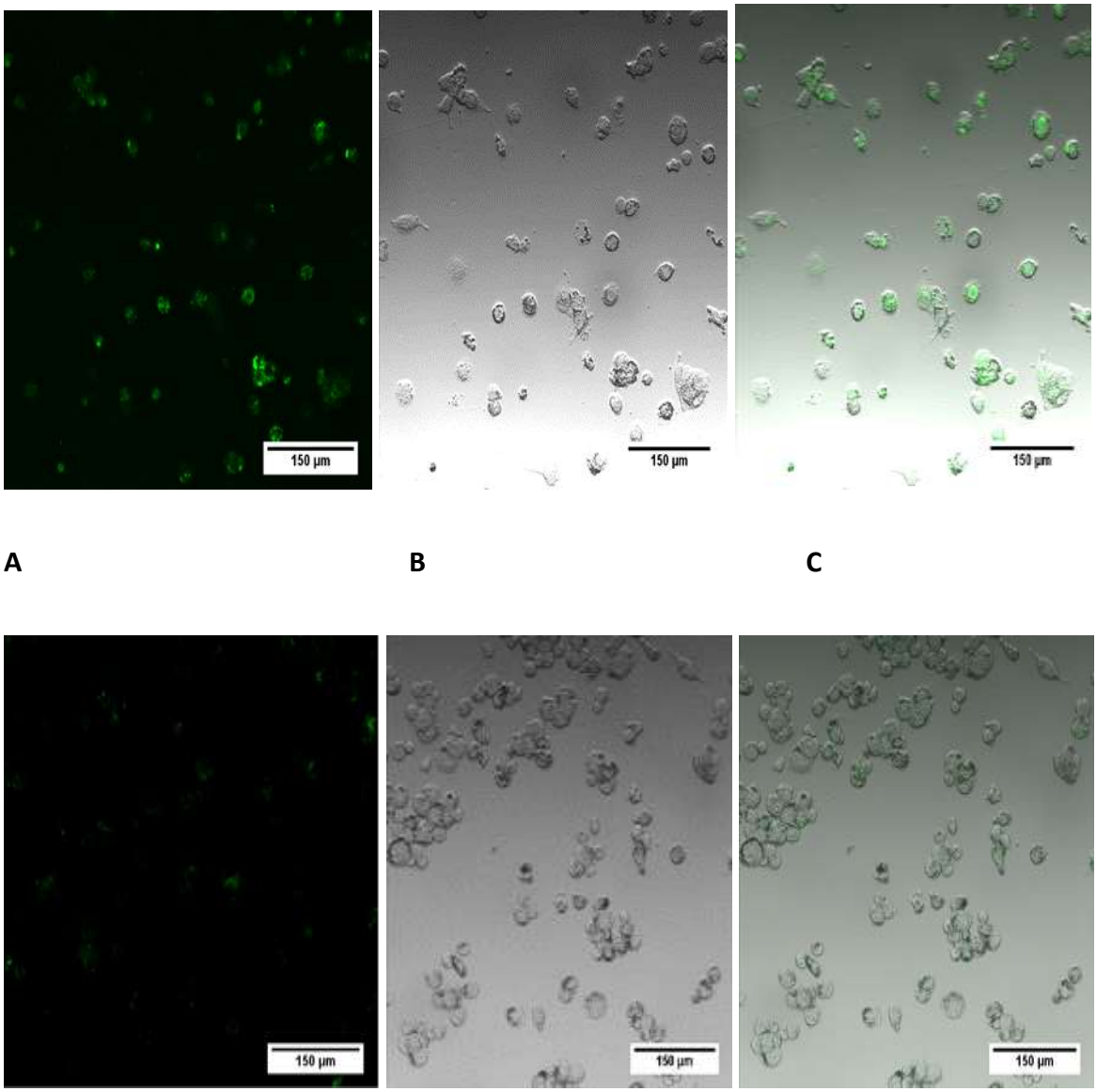

Figure 3.7 THP-1 derived M1 cells could be generated by treatment of M0 macrophages with LPS and IFN-γ. THP-1 cell suspensions were seeded at $1x10^5$ cells/well in 24-well plates in completed RPMI media with various concentrations of PMA. Cells were then incubated at 5% CO_2 20% O2 at 37°C for 48 h. The RPMI media was then replaced with a PMA-free media for 24 hours and cells were then treated with either 100 ng/mL lipopolysaccharide (LPS) and 20 ng/mL IFN-γ (A-C), or an equivalent volume of their vehicle, DMSO (D-F), at 37°C, 5% CO_2 for 72 hours. Cells were then fixed and labelled with a mouse anti-CD80 antibody, followed by a FITC labelled anti-mouse secondary antibody. Samples were then imaged using a Fluoview laser confocal scanning microscope. (A, D) FITC fluorescence (B,E) Brightfield image of samples (C,F) Overlay of the two images. n = 6.

3.3.5 Generation of THP-1 derived foam cells from M1 macrophage in 2D cultures

Finally, to establish the protocol for creating THP-derived foam cells, experiments were performed to assess the ability of the M1 macrophage cells to form foam cells in 2D culture. Previous studies have found that macrophage cells will transform to foam cells after taking up oxLDL from the culture medium (Poznyak *et al.*, 2020). Sterile oxLDL samples were created through a copper sulphate oxidation process (Section 2.2115). The oxidation state of the LDL samples was first validated via reading of the absorbance spectrum. As shown in Figure 3.8A, the oxidised samples were visibly cloudy compared to the non-oxidised aliquots taken from the same sample. Previous studies have demonstrated that oxidised LDL has a different absorbance property to the non-oxidised LDL (Levitan *et al*., 2010). A notable difference in the absorbance spectra with differences could also be observed at every wavelength in our samples. This indicated that oxidation state had been effectively changed. To definitively validate the oxidation of the LDL samples, these were via an oxLDL ELISA kit, which showed a significant increase in the presence of oxLDL within the samples compared to the non-oxidised LDL, although a small basal oxidisation of this sample was unexpectedly observed (Figure 3.8C). These data therefore indicate that copper sulphate-mediated oxidation of the samples was effective and could be used to trigger foam cell formation in the THP-1-derived M1 macrophages. M1 macrophages were chosen to create

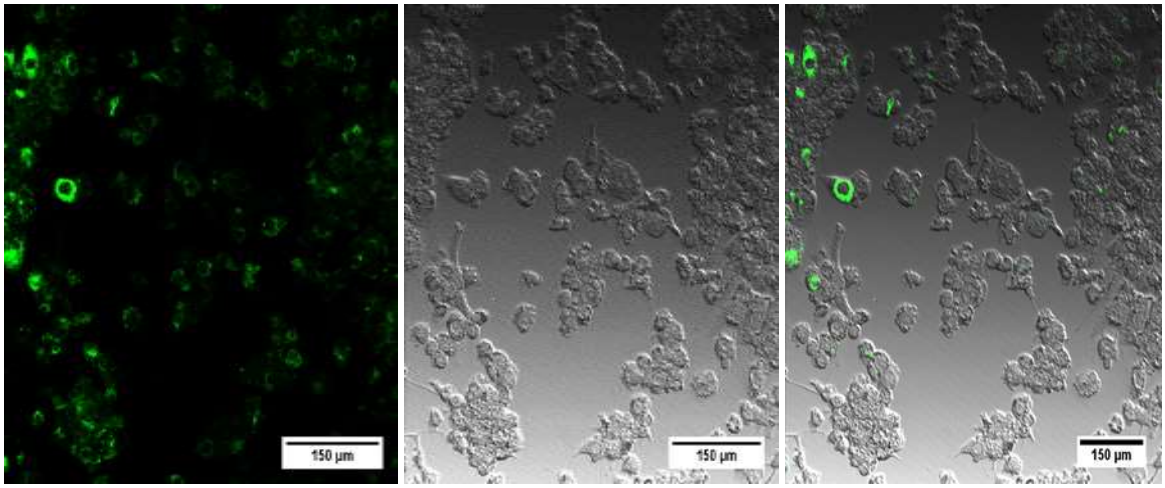

A **B** **C**

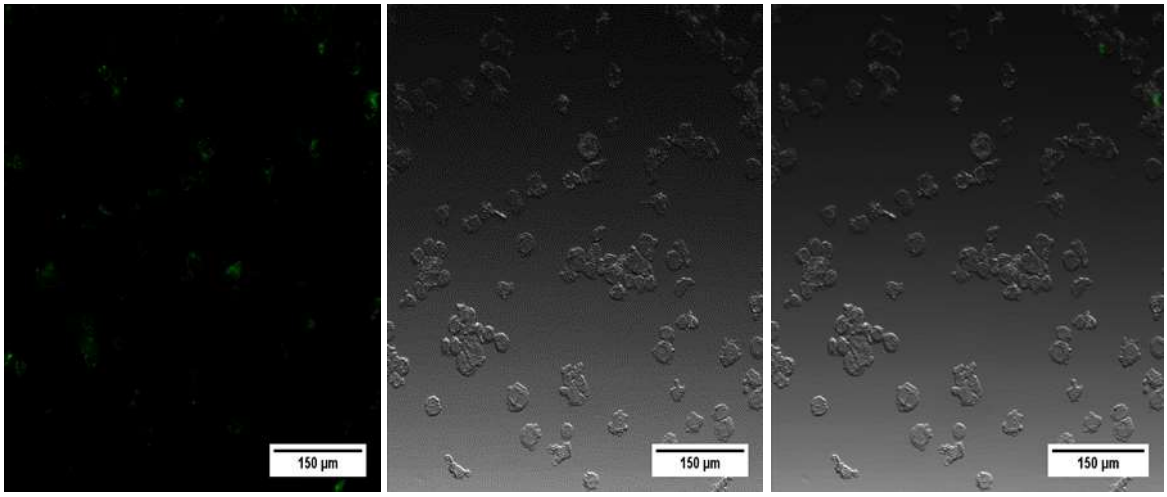

D **E** **F**

Figure 3.8 IL-4 treatment of THP-1-derived M0 macrophages elicits increased expression of CD206. THP-1 cell suspensions were seeded at $1x10^5$ cells/well in 24-well plates in completed RPMI media, cells were then incubated at 5% CO_2, 37°C for 48 h .Cells were then rested by incubation in a PMA-free media for 24 h, and then treated with either 20 ng/mL IL-4 (A-C) or an equivalent volume of PBS (D-F). Adherent cells were then stained with the primary CD206 antibody and then with its secondary antibody. (A, D) Fluorescent imaging of CD206 (B, E) Brightfield images of the cells (C, F) Overlay of the fluorescent and brightfield images. n=4.

the foam cells are they are found to predominate in rupture-prone plaques (Genin *et al.*, 2015).

M1 macrophage cells were cultured in 24-well plates as previously described, but at the same time of IFN-γ and LPS addition for M1 polarization, the media was also supplemented with either 50 µg/ml LDL and 50 µg/ml oxLDL or an equivalent volume of their vehicle, PBS. Following the incubation for 72h, the samples were fixed and subject to Oil red O staining to assess whether M1 macrophages treated with oxLDL could be observed to have developed the intracellular accumulations of lipids observed in foam cells. As shown in Figure 3.9, Whilst most oxLDL-treated M1 macrophages could be seen to have developed intracellular lipid accumulations, neither those treated with LDL or PBS could be seen to have any significant Oil Red O staining indicating that intracellular neutral lipid deposits had developed specifically in the oxLDL-treated macrophages. These data demonstrate that we have developed the techniques to generate THP-1-derived foam cells in 2D culture, as well as the methods to assess each of the stages of THP-1 differentiation into these cells.

3.3.6 Assessment of strategies to develop a 3D hydrogel culture of THP-1 cells

Having established the methodology for culturing THP-1-derived foam cells in 2D culture, two distinct strategies were considered for developing a 3D hydrogel culture of THP-1-derived foam cells. The first was to detach the cells generated through the 2D culture system and then seed these into 3D collagen hydrogels, whilst the second was to seed THP-1 cells directly into the 3D hydrogels and then use the culture conditions developed in 2D culture to elicit THP-1 differentiation within the hydrogel scaffold. Initial experiments cultured foam cells

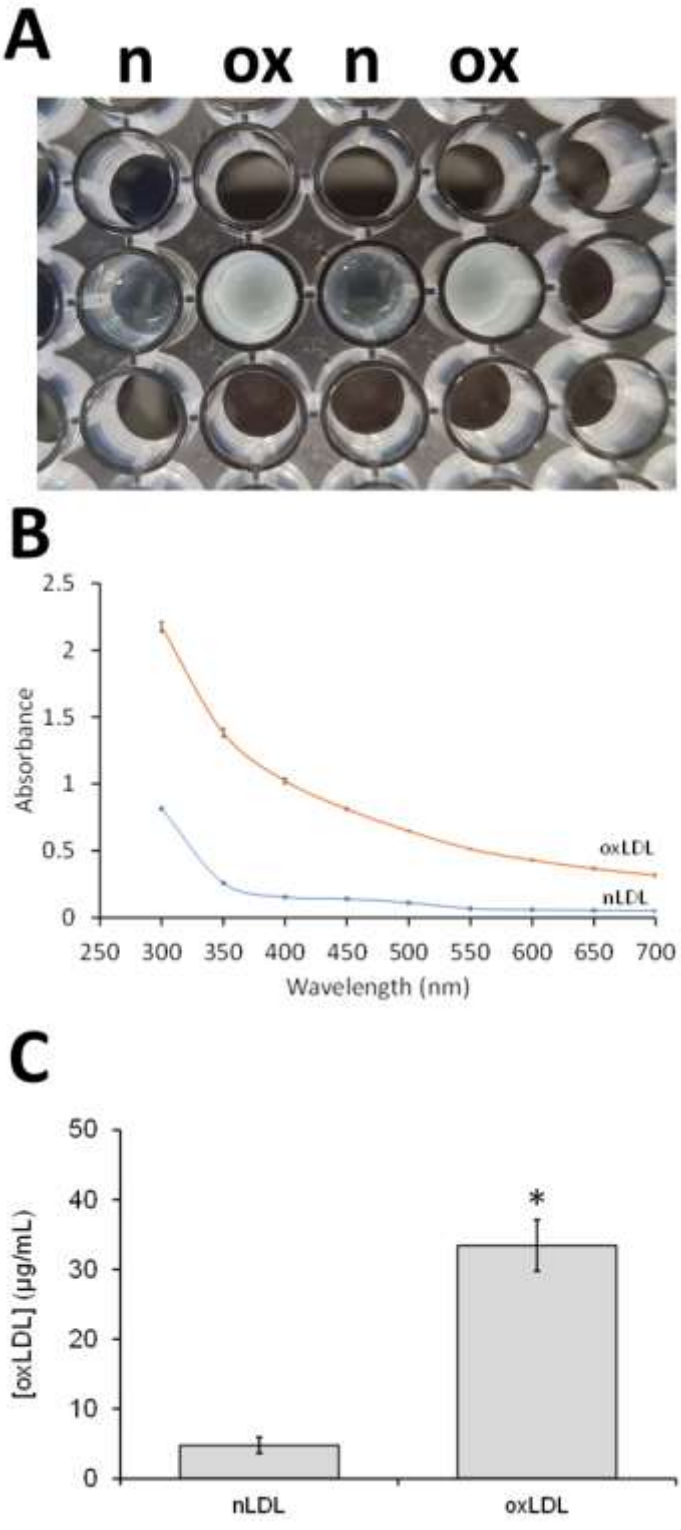

Figure 3.9. Validation of the oxidation of the LDL samples. Oxidised and non-oxidised LDL samples were assessed to validate effective oxidation of the LDL particles. (A) Picture of the oxidised (ox) and non-oxidised (n) samples when loaded in 96-well plate (B) Absorbance spectra of the oxidised (oxLDL) and non-oxidised (nLDL) samples. Data are shown as mean ± SEM (n = 2). (C) Measurement of oxidative state using an oxLDL ELISA assay kit. n = 4. (* = $P < 0.05$ relative to the nLDL control using a student's T- test)

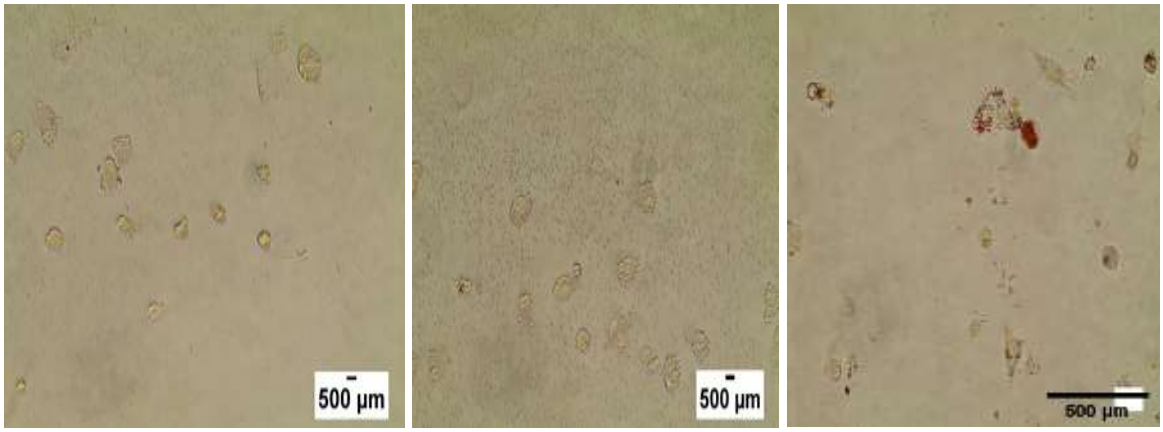

A B C

Figure 3.10 Oil Red O staining of M1 macrophages treated with LDL and oxLDL. THP-1 cell suspensions we reseeded at $1x10^5$ cells/well in 24-well plates in RPMI media with 50 nM PMA. Cells were then incubated at 5% CO_2, 37°C for 48 h. Cells were rested by incubation in a PMA-free media for 24 h, and then cells were treated with LPS and IFN-γ and either 50 µg/mL LDL (B), 50 µg/mL oxLDL (C) or an equal volume of their diluent PBS (A) at 5% CO_2, 37°C for 72 h. After this period, cells were fixed and stained with Oil Red O to assess intracellular accumulations of neutral lipids, n=6.

within T25 flasks to provide sufficient cells to make hydrogel culture viable, and then attempted to detach viable foam cells from 2D cultures using either a commercial Macrophage Detachment Solution (Promocell), accutase, EDTA/Trypsin or cell scrapers. After treatment, the cell suspension extracts were collected and number of viable and non-viable cells was assessed using trypan blue. The cells remaining in the flask were stained with Oil Red O and imaged. These studies found that none of the treatments identified above were successful in detaching significant numbers of THP-1-derived foam cells from the flask, with the majority being found remaining on the surface of the flask. Assessment of cells found in the cell suspension were found to be mainly non-viable (Data not shown). Therefore, efforts

focussed on seeding THP-1 cells into collagen hydrogels and attempting to differentiate these into THP-1-derived foam cells.

3.3.7 Establishing a 3D culture by seeding THP-1 cells on top of a collagen hydrogel

Pilot experiments assessed whether THP-1 cells could successfully attach, proliferate, and differentiate in contact with a collagen hydrogel. This was assessed by assessing cell attachment and differentiation under PMA treatment when seeded onto the top of a 3D collagen hydrogel. This experiment is an intermediate stage between the 2D-THP-1 cells culture and the typical 3D-hydrogel culture of the THP-I cells. To do this, collagen hydrogels were set into 24-well plates, and THP-1 cells were then seeded in a small volume of RPMI media containing either 0, 25, 50 or 100 nM PMA. As can be seen in Figure 3.10, cells not stimulated with PMA stayed rounded and showed none of the morphological indicators of macrophage differentiation seen in our earlier experiments on cell culture plastic. In contrast, cells treated with PMA showed considerable morphological changes ranging from more oval-shaped and elongated cells with some showing spindle-like shapes, indicative of successful M0 differentiation (Figure 20B-D). These studies, therefore, indicated that PMA-induced differentiation of THP-1 cells is possible when PMA cells are cultured within 3D collagen hydrogels.

3.3.8 Establishing a method for THP-1 cell culture within a 3D collagen hydrogel

Following these pilot experiments, further experiments assessed the potential of THP-1 cells to be differentiated into macrophages within a type I collagen hydrogel both in the presence and absence of PMA stimulation. PMA was added to ensure the final concentration within

the hydrogel solution prior to setting was 50 nM. Light microscopy experiments of PMA treated hydrogels showed the presence of cells with an elongated or stretched morphology within the 3D hydrogel which indicates the possibility of differentiation of the THP-1 cells into M0 macrophages (Figure 3.11). Following the end of the culture period, these collagen hydrogels were then subject to live/dead cell staining and found that almost all cells within the gel were live (91.1% ± 1.7 % and 96.1 ± 0.8 % viability for cells treated with and without PMA respectively), with no differentiation between the cells at different depths within the gel or between cells incubated with or without PMA. These indicated that THP-1 cells could be successfully treated with PMA within the hydrogels, without altering cell viability.

3.3.9 Differentiation of THP-1 derived M1 macrophages within the collagen hydrogels

To assess if it was possible to generate M1 macrophages following PMA stimulation of THP-1 cells in 3D cultures, collagen hydrogels were prepared using the same method which was used for THP-1 derived M0 macrophages. To be sure that PMA treatment did not affect Cells growing and viability, the collagen hydrogels were assessed using microscopic monitoring and live/dead cell staining respectively (Figure 3.12 and 3.13). After that we proceeded in the experiment using the same protocol that have been used for the 2D culture experiments. Following PMA treatment, the collagen hydrogels were rested by incubation in a PMA-free media for 24 h. The RPMI media was changed to a fresh RPMI media containing 100 ng/mL LPS and 20 ng/mL IFN-γ to induce differentiation to M1 macrophages, as previously demonstrated in the 2D culture experiments.

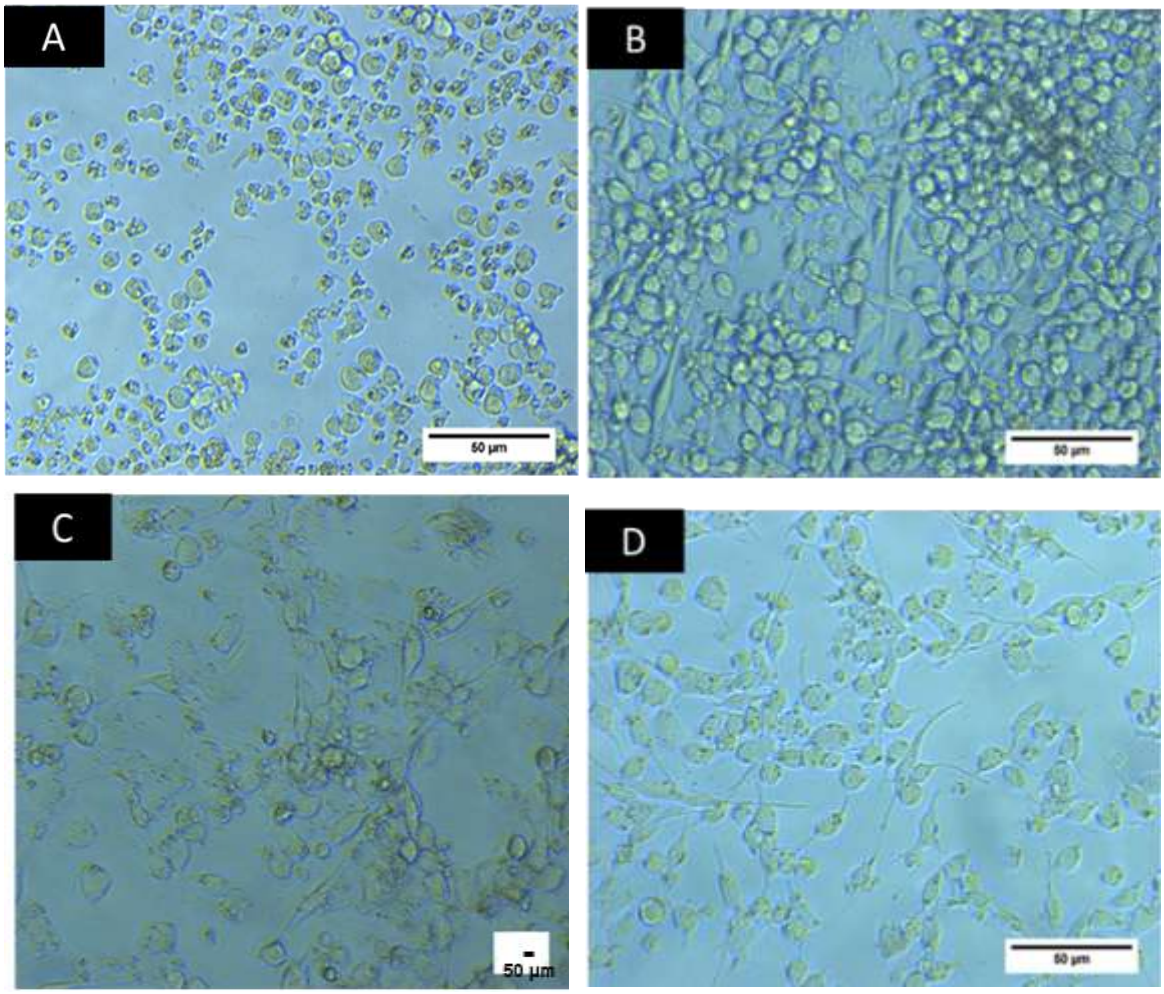

Figure 3.11 PMA-induced differentiation of THP-1 cells cultured on top of a type I collagen hydrogel. Two groups of modified 3D-hydrogel were prepared, those which did not treat with PMA (A), and those which were treated with 25 nM B, 50 nM C, 100 nM of PMA D. THP-1 cells in first group (A) stay rounded in shape and small in size, however, the second group (B,C,D) as they differentiated to macrophage, they elongated or stretched and form spindle-like cells and become larger in size consistent with them differentiating into M0 macrophages, n=2.

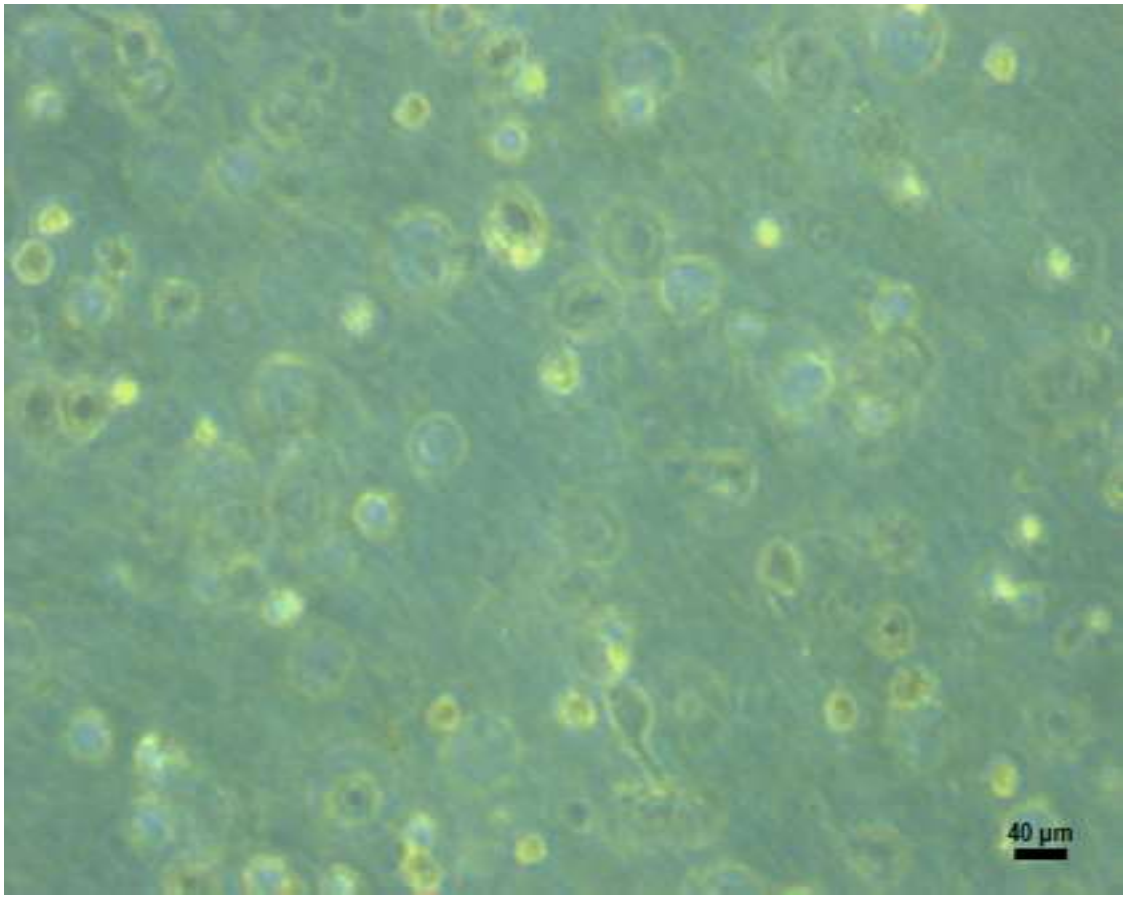

Figure 3.12. THP-1 cells undergo morphological change when stimulated with PMA when cultured in a 3D collagen hydrogel. THP-1 cells were mixed at a cell density of 3 x 10^6 cells/mL into a neutralized solution of 3 mg/mL type I collagen. The THP-1/collagen mixture was then loaded under sterile conditions onto a 1 x 1 cm, sterile filter paper frame prepared on a PTFE base inside a petri dish. The collagen-cell mixture was left to set for 30 minutes at 37°C, 5% CO2. The hydrogel was then covered with RPMI medium containing 10% [v/v] FBS, Pencillin, Streptomycin and 50 nM PMA, and then incubated for 48 h at 37˚C, 5% CO_2. Cell morphology was then observed using light microscopy, n=6.

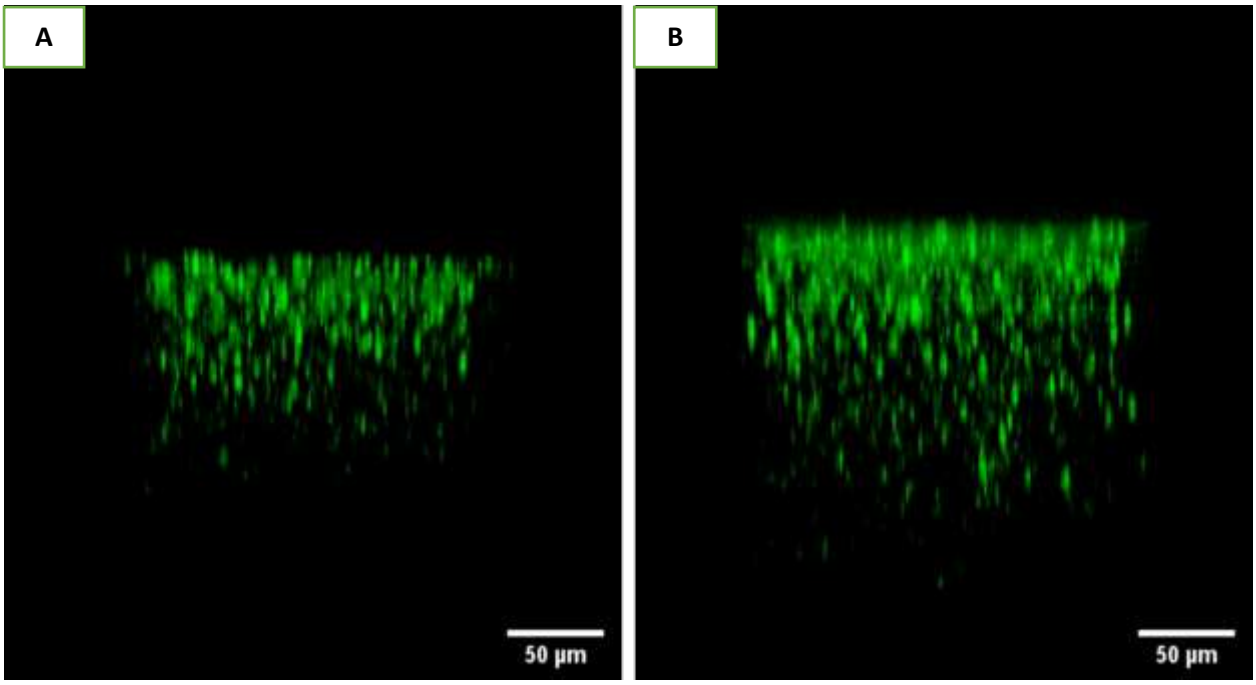

Figure 3.13 THP-1 cell viability was not affected by PMA treatment within the collagen hydrogels. THP-1 cells were mixed at a cell density of 3 x 10^6 cells/mL into a neutralized solution of 3 mg/mL type I collagen. The THP-1/collagen mixture was then loaded under sterile conditions onto a 1 x 1 cm, sterile filter paper frame prepared on a PTFE base inside a petri dish. The collagen-cell mixture was left to set for 30 minutes at 37°C, 5% CO_2. The hydrogel was then covered with RPMI medium containing 10% [v/v] FBS, Penicillin, Streptomycin and either with 50 nM PMA (A) or an equivalent volume of DMSO (B), and then incubated for 48 h at 37˚C, 5% CO_2. Cell morphology was then observed using light microscopy. On the sixth day of the experiment, the cytokines completed media was changed by a live/dead stain solution, and then the collagen hydrogels were imaged by the confocal microscopy, PMA sample A, PMA free sample B, n=6.

The hydrogels were then subject to immunolabelling with the unconjugated primary antibody to CD80 and a FITC-labelled secondary antibody previously used in the 2D culture experiments. Pilot studies retested the secondary antibody to find a concentration that did not induce significant non-specific staining in the absence of a primary antibody. Four different dilutions of the secondary antibody were used (1:2500, 1:5000, 1:75000 and 1:10000). From this experiment, a 1:10000 dilution was found to produce the lowest background (data not shown). Using this and the CD80 primary antibody concentration previously utilised in the 2D cultures, it was possible to identify strong labelling of cells within the 3D construct indicating that M1 differentiation had successfully occurred (Figure 3.14).

To ensure that the CD80 labelling was specific for M1 macrophages, experiments compared immunofluorescent labelling achieved in M1 and M0 macrophages cultured within the 3D hydrogels. As shown in Figure 3.14A, B, whilst M1 macrophages showed strong immunofluorescent labelling, weaker staining was observed in the M0 macrophages not stimulated to differentiate with LPS and IFN-γ. The fluorescent labelling of CD80 within the hydrogel constructs was quantified using Image J and was found to be consistently and significantly greater in M1 macrophage-containing hydrogels compared to those containing M0 macrophages (Figure 3.15C). These data therefore demonstrate that the CD80 staining is specific for M1 macrophages, and that it is possible to generate M1 macrophages within the 3D collagen hydrogel culture.

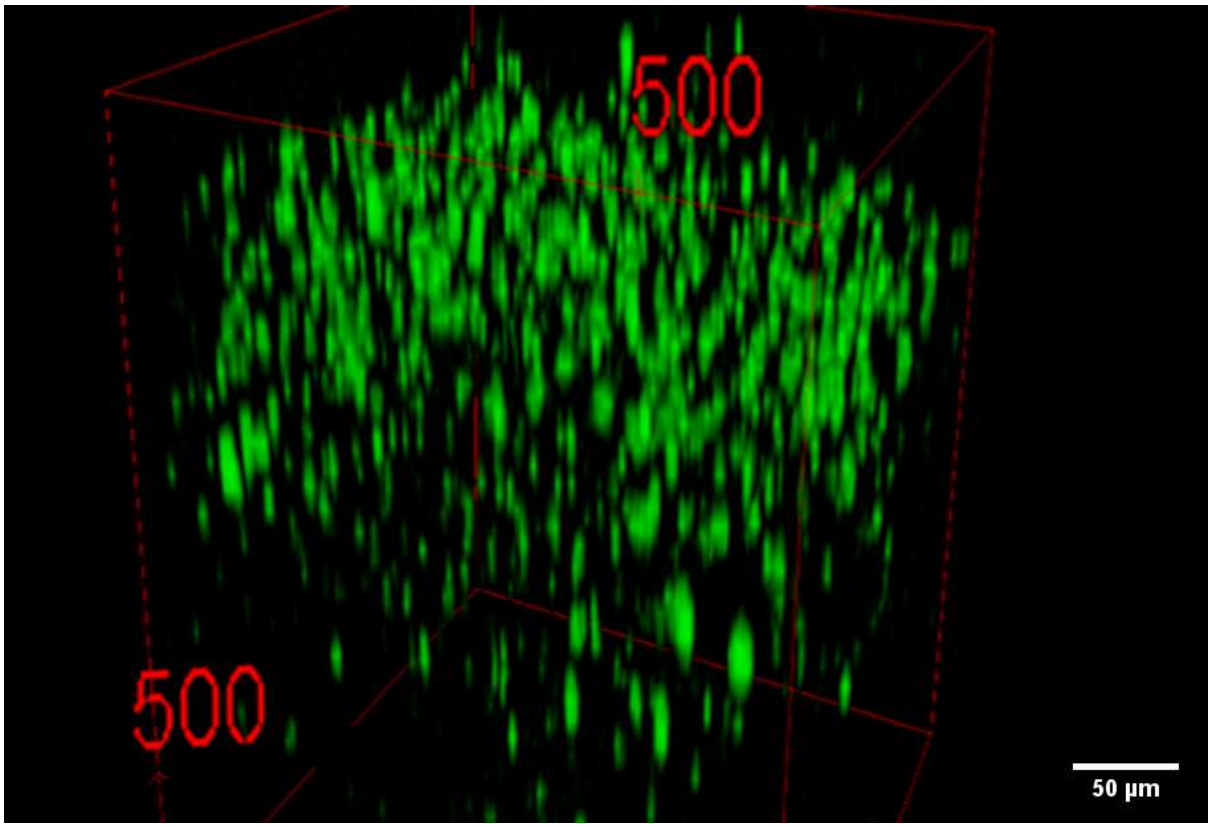

Figure 3.14 LPS and IFN-γ can induce M1 macrophage differentiation in 3D cultures. THP-1 cell suspensions were seeded at $6x10^5$ cells/hydrogel in RPMI media with 50 nM concentration PMA. Cells were then incubated at 5% CO_2, 37°C for 48 h. Cells were rested by incubation in a PMA-free media for 24 h, and then cells were transferred into fresh RPMI containing 100 ng/mL LPS and 20 ng/mL IFN-γ for a further 72 h. Collagen hydrogels were then fixed and then immunolabelled using an unconjugated CD80 antibody and a FITC-labelled secondary antibody. Samples were then subject to z-stack imaging using a confocal microscope, n=6.

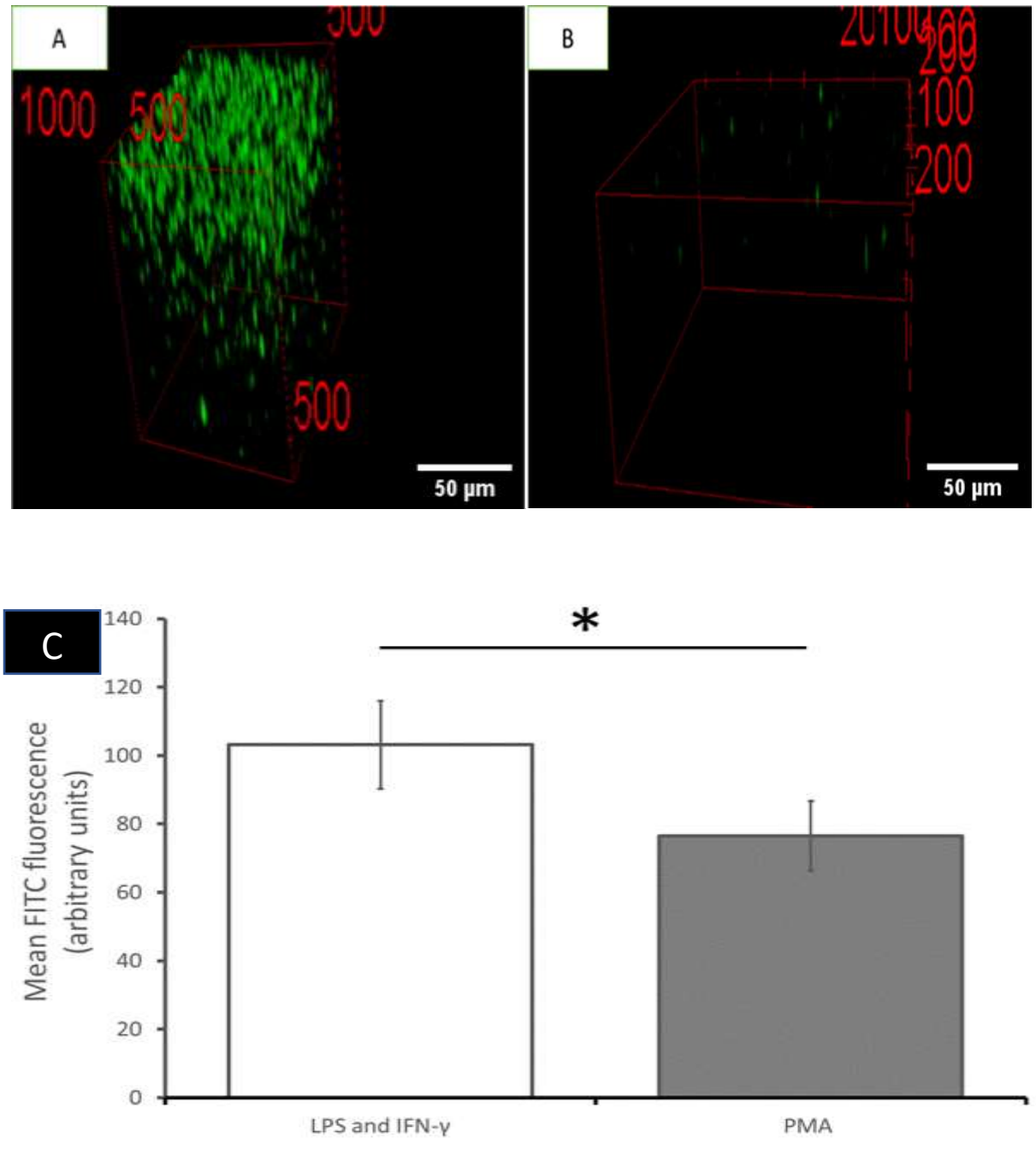

Figure 3.15 CD80 antibodies stain M1-differentiated macrophages but not M0 macrophages within the 3D collagen hydrogels. (A-C) THP-1 cell suspensions were seeded at $6x10^5$ cells/hydrogel in RPMI media with 50 nM concentration PMA. Cells were then incubated at 5% CO_2, 37°C for 48 h. Cells were rested by incubation in a PMA-free media for 24 h, and then cells were transferred into fresh RPMI containing either (A) 100 ng/mL LPS and 20 ng/mL IFN-γ or their vehicle, DMSO (B) for a further 72 h. Collagen hydrogels were then fixed and then immunolabelled using an unconjugated CD80 antibody and a FITC-labelled secondary antibody. Samples were then subject to z-stack imaging using a confocal microscope.

(Bottom) Image J analysis of the total FITC fluorescence observed through the entire hydrogel. * = P < 0.05 between indicated conditions using a student's T-test. Values shown are Mean ± SEM of 3 experiment.

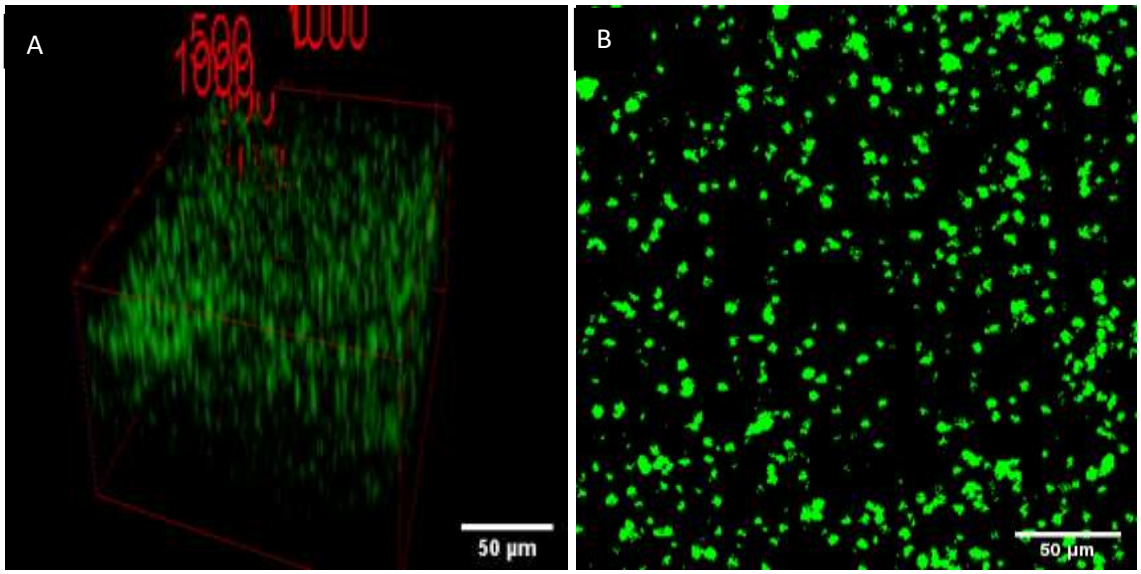

Figure 3.16. Live/dead staining of THP-1 derived foam cells. THP-1 cell suspensions were seeded at density of $6x10^5$ cells/collagen hydrogel in completed RPMI media with 50nM PMA concentration RPMI media. Collagen hydrogels were then incubated at 5% CO_2 20% O_2 at 37C for 48 h. Cells were rested by incubation in a PMA-free media for 24 h, and then cells were treated with LPS and IFN-γ for 72 h. Lastly, collagen hydrogels were treated with 50 µg/mL oxLDL at 5% CO_2, at 37°C for 72 h. Cells were then stained using a live/dead cell staining kit. Samples were then subject to z-stack imaging using a confocal microscope with green pseudocolouring indicating live cells, whilst red indicates non-viable cells, n=6.

3.3.10 Differentiation of THP-1 derived foam cells in the 3D collagen hydrogel

Following successfully demonstrating the ability to differentiate THP-1 cells into M1 macrophages within the collagen hydrogels, the next experiments assessed whether subsequent treatment of the M1 macrophage-containing 3D cultures with 50 µg/mL oxLDL was able to elicit the formation of THP-1-derived foam cells within the collagen hydrogels. After the culture of the M1 macrophages, fresh RPMI media containing 50 µg/ml of oxLDL was added to the cells for 72 hours. After this, the cell viability of THP-1 cells was assessed using live/dead staining. Cells were found to be 95% ± 1.5 % viable (Figure 3.15).

Experiments were next performed to confirm the presence of foam cells within the 3D culture. This was achieved using nile red, a fluorescent stain that labels intracellular neutral lipids and has previously been used to characterise lipid uptake in the cultured macrophages (Greenspan *et al*., 1985). As shown in Figure 3.16, the droplets of the intracellular, neutral lipids appear as red dots surrounding the Hoechst-stained nuclei of the THP-1 derived foam cells (pseudocoloured blue). These data therefore indicated that oxLDL treatment was able to elicit the production of THP-1-derived foam cell production within the collagen hydrogels.

To assess the specificity of the Nile Red staining, THP-1-derived M1 macrophages were produced and treated with 50 µg/mL oxLDL, 50 µg/mL of non-oxidised LDL, or RPMI media with an equivalent amount of PBS. The collagen hydrogels were re-incubated for another 72 hours. The cells were then fixed and stained with Nile Red and Hoechst-33342. Nile Red fluorescence in THP-1-derived M1 macrophages that were treated with oxLDL, was found to be significantly higher than those treated either with non-oxidised LDL or PBS (Both $P < 0.05$). These data indicate that the Nile Red fluorescence was specifically labelling THP-1-derived foam cells within the 3D culture. This construct therefore represents a prototype 3D

neointimal model that could be incorporated within the previously developed tissue-engineered blood vessel construct.

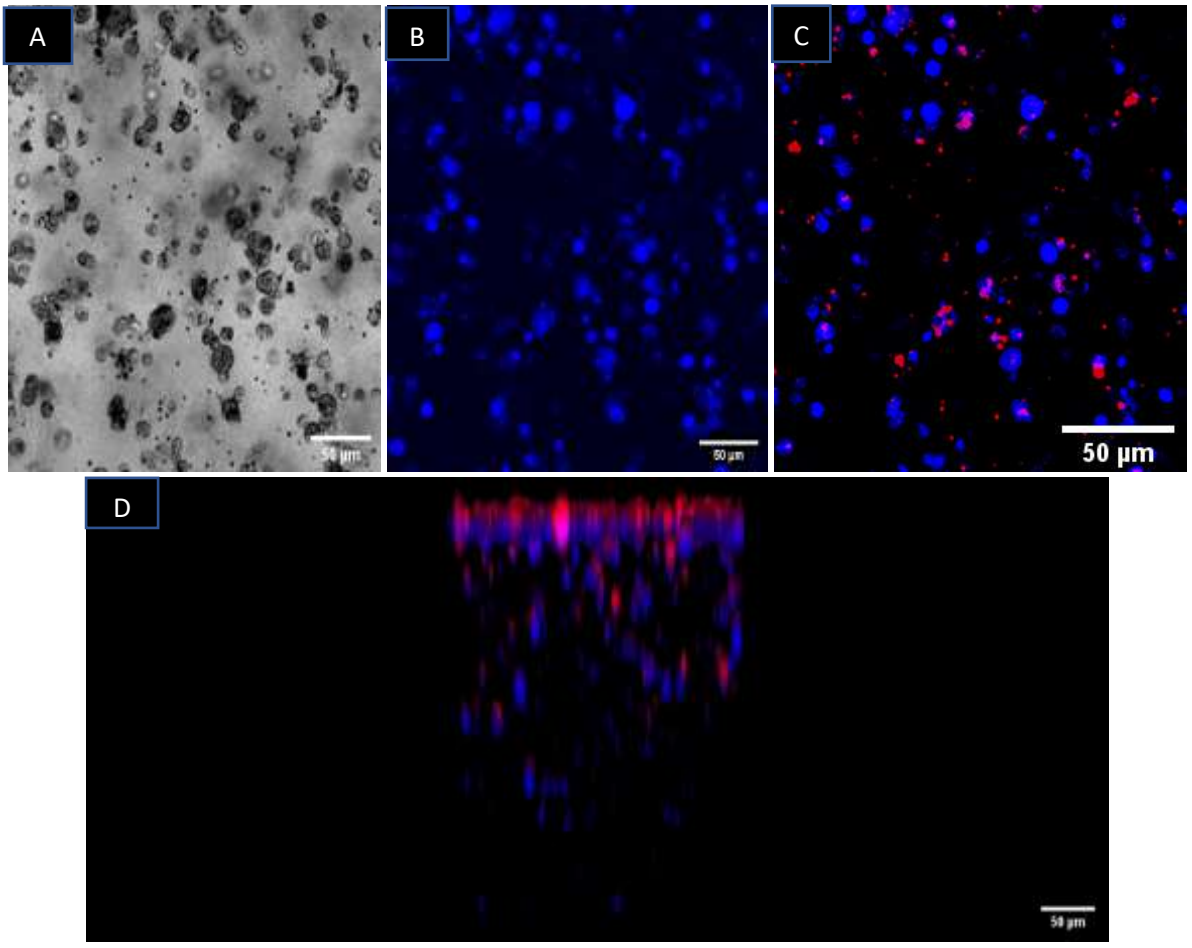

Figure 3.17 Nile Red staining indicates oxLDL loading of THP-derived macrophages can induce foam cell formation in 3D culture. THP-1 cell suspensions were seeded at 6x10^5 cells/collagen hydrogel in RPMI media with 50 nM PMA concentration RPMI media. Collagen hydrogels were then incubated at 5% CO_2, 37°C for 48 h. Cells were rested by incubation in a PMA-free media for 24 h, and then cells were treated with LPS and IFN-γ for 72 h. Then collagen hydrogels were treated with 50 µg/mL oxLDL at 5% CO_2, 37°C for 72 h. On the tenth day of the experiment, the collagen hydrogels were fixed with10% formalin overnight and then were stained with Nile Red and Hoechst-33342 to assess the intracellular accumulation of neutral lipid. (A) Brightfield image (B) Hoechst-33342 fluorescence (C) Overlay of the Hoechst-33343 and Nile Red fluorescence (D) A -stack imaging using a confocal microscope,n=6.

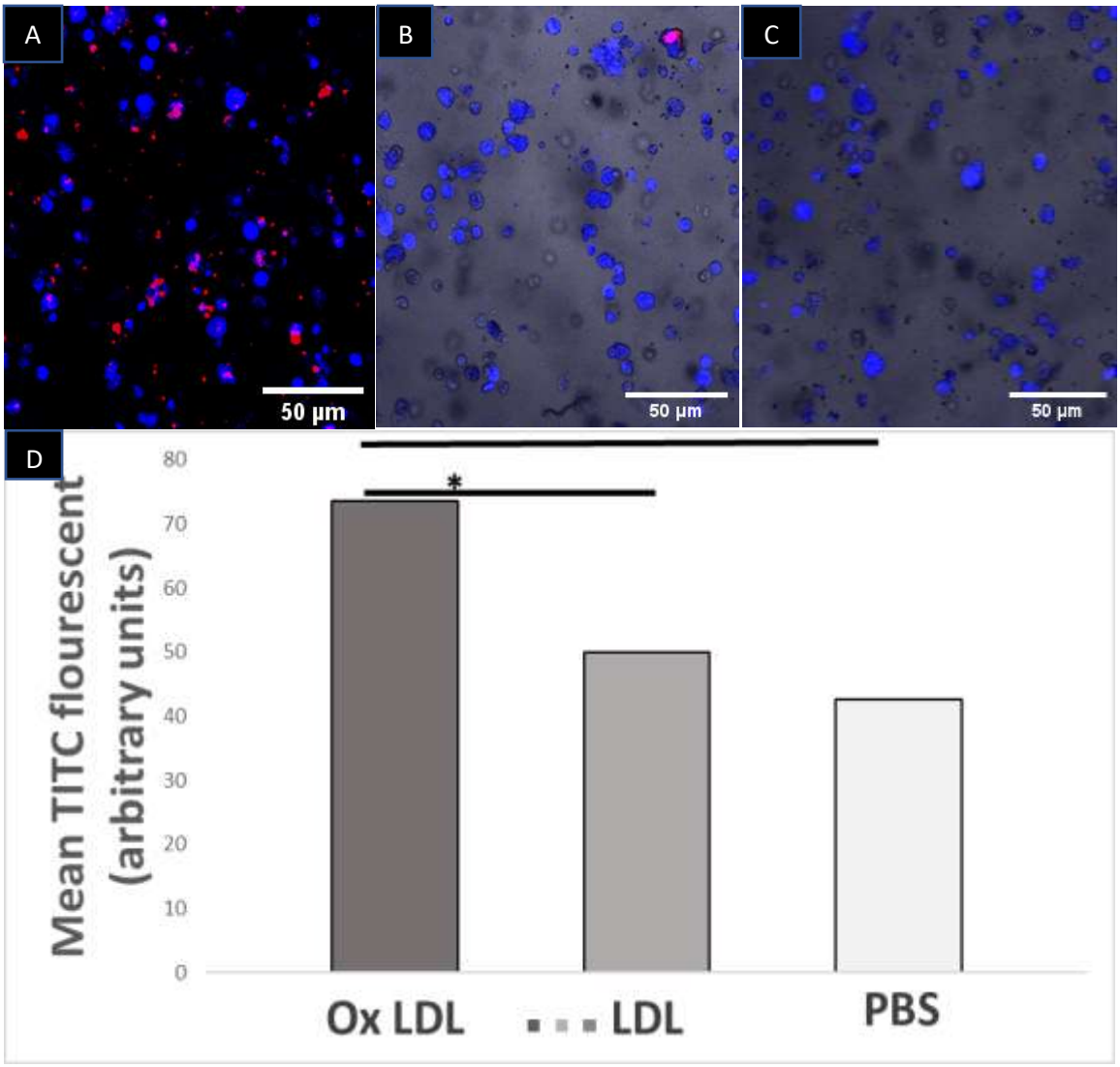

Figure 3.18. Nile Red specifically labels intracellular neutral lipid accumulation with THP-1-derived foam cells, but not M1 macrophages. THP-1 cell suspensions was seeded at $6x10^5$ cells/collagen hydrogel in RPMI media with 50 nM PMA. Collagen hydrogels were then incubated at 5% CO_2, 37°C for 48 h. Cells were rested by incubation in a PMA-free media for 24 h, and then cells were treated with LPS and IFN-γ for 72 h. Then the cells were treated with and either 50 µg/mL OxLDL (A), 50 µg/mL LDL (B) or an equal volume of their vehicle, PBS (C) at 5% CO_2, 37°C for 72 h. After this period, cells were fixed and stained with Nile-Red/Hoechst stain to assess intracellular accumulations of neutral lipids. Image J analysis of the Nile Red fluorescence present within the entire hydrogel. Values shown are Mean ± SEM of 5 experiments. (* = $P < 0.05$ between indicated conditions using a one-way ANOVA with post hoc Tukey test).

3.3.11 Plastic compression experiment

Whilst the neointimal culture model developed in a simple collagen hydrogel could be used to introduce an atherosclerotic plaque into the tissue-engineered arterial construct, the

density of the THP-1-derived foam cells within these constructs is relatively low compared to that observed in a fatty streak or more advanced lesions. Additionally, the collagen construct is relatively mechanically weak, which could be a disadvantage when trying to incorporate this into the tissue-engineered arterial construct. Plastic compression can be used to improve the mechanical properties by increasing the collagen content, through squeezing excess aqueous fluid out of the gel, leaving the cells and collagen present at a higher density increasing the stiffness of the construct (Braziulis *et al*., 2012). Plastic compression is performed by placing a sterile weight on top of the hydrogel for a short period of time, with filter paper underneath to absorb any extracted fluid. As previous studies have shown that reduced substrate stiffness reduces the phenotypic properties of M1 macrophages (Okamoto *et al*., 2018), experiments were therefore performed to assess whether viable THP-1-derived foam cells could be successfully developed within a collagen hydrogel after plastic compression. In these studies, the THP-1 cells were seeded into collagen hydrogels and set in a mould. The samples were than subject to plastic compression, and then placed back into RRPMI media where it was then treated with PMA, LPS, IFN-γ and oxLDL as described previously. Initial live/dead cell staining images demonstrated that the process of plastic compression did not significantly reduce cell viability, with viability found in the compressed hydrogels to be 89.3% ± 0.7% (Figure 3.18A, B)

To assess foam cell production within the compressed collagen hydrogels, THP-1-derved M1 macrophages were prepared in compressed collagen hydrogels using the same cultured method which was used for the non-compressed method. The samples were then treated wither either complete RPMI media containing either 50 µg/mL oxLDL or 50 µg/mL of non-oxidised LDL, and then incubated for a further 72 hours. The gels were then fixed and stained

with Nile-Red/Hoechst stain using the same protocol which was used for the non-compressed hydrogels previously. As shown in Figure 3.19, intracellular neutral lipid droplets (red dots) could be observed in most of the cells in samples treated with oxLDL, but not in those treated with non-oxidised LDL. Image J assessment of the fluorescent intensity through the hydrogels was found to be significantly higher in the oxLDL-treated samples than those treated with non-oxidised LDL ($P < 0.05$; Figure 3.20)

3.3.12 TNF-α and IL-6 secretion is upregulated in THP-1-derived foam cells generated within the compressed 3D collagen hydrogel

M1 macrophages are characterised by the secretion of a variety of pro-inflammatory cytokines such as TNF-α, IL-6 and IL-1β (Biswas and Mantovani, 2010). The expression of these pro-inflammatory cytokines has previously been shown to be upregulated by treatment of THP-1-derived macrophages with oxLDL (Wang *et al*., 2015; Zhong *et al*., 2020; Liu *et al*., 2014). Therefore, experiments were conducted to assess whether the foam cells within the compressed collagen hydrogel were able to replicate these effects, by assessing cytokine secretion of these cytokines into the conditioned media taken from compressed hydrogels

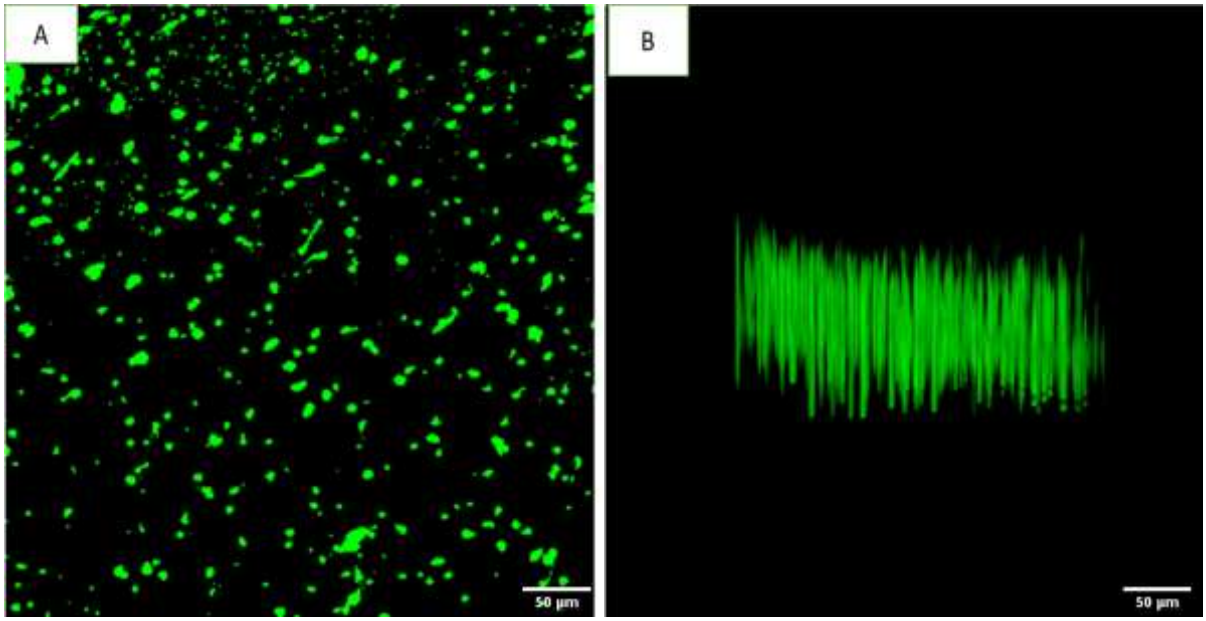

Figure 3.19. Live/dead stain of the THP-1 derived foam cells in compressed collagen hydrogels. THP-1 cell suspensions were seeded into compressed collagen hydrogels, and then incubated in RPMI media with 50 nM PMA at 5% CO_2, 37°C for 48 h. Cells were rested by incubation in a PMA-free media for 24 h, and then cells were treated with LPS and IFN-γ for 72 h. The samples were then treated with 50 µg/mL OxLDL at 5% CO_2, 37°C for 72 h. After this period, cells were stained with Live/Dead Cell staining kit stain to assess cell viability. Images were taken using confocal microscopy. (A) a single slice through the gel (B) A projection of the z-stack through the whole hydrogel, n=6.

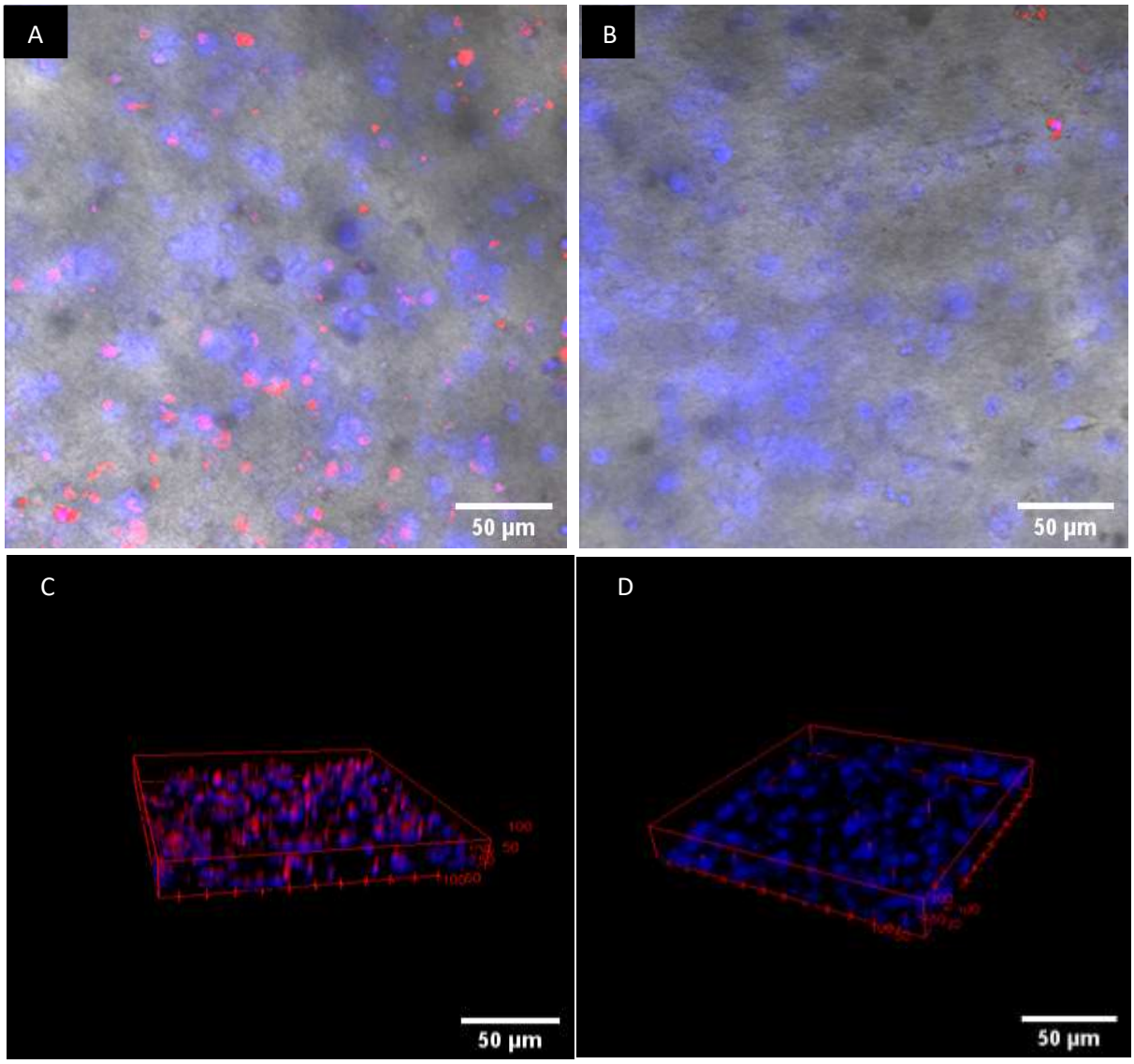

Figure 3.20 THP-1-derived foam cells could be produced within compressed collagen hydrogels. THP-1 cell suspensions were seeded into compressed collagen hydrogels, and then incubated in RPMI media with 50 nM PMA at 5% CO_2, 37°C for 48 h. Cells were rested by incubation in a PMA-free media for 24 h, and then cells were treated with LPS and IFN-γ for 72 h. The samples were then treated with either 50 µg/mL OxLDL (A) or 50 µg/mL LDL (B) at 5% CO_2, 37°C for 72 h. After this period, cells were fixed and stained with Nile-Red/Hoechst stain to assess intracellular accumulations of neutral lipids, n=6.

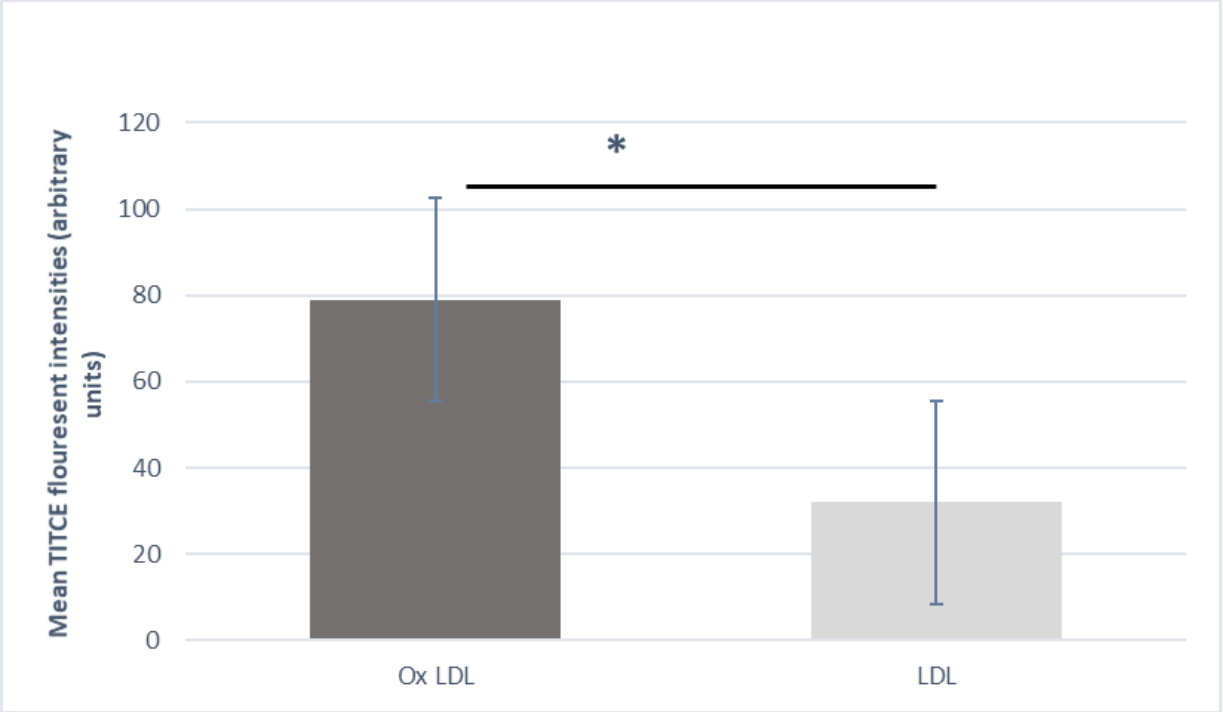

Figure 3.21. THP-1-derived foam cells are produced in compressed collagen hydrogels treated with oxLDL, but not non-oxidised LDL. THP-1 cell suspensions were seeded into compressed collagen hydrogels, and then incubated in RPMI media with 50 nM PMA at 5% CO_2, 37°C for 48 h. Cells were rested by incubation in a PMA-free media for 24 h, and then cells were treated with LPS and IFN-γ for 72 h. The samples were then treated with either 50 µg/mL OxLDL (A) or 50 µg/mL LDL (B) at 5% CO_2, 37°C for 72 h. After this period, cells were fixed and stained with Nile-Red/Hoechst stain to assess intracellular accumulations of neutral lipids. Bar chart shows Image J analysis of the Nile Red fluorescence present within the entire hydrogel. Values shown are Mean ± SEM of 5 experiments. (* = $P < 0.05$ between indicated conditions using a student's T-test).

containing either THP-1-derived-foam cells or M1 macrophages. Conditioned media samples exposed for the same time frame to an acellular collagen hydrogel was used to control for basal presence of these cytokines in the FBS-supplemented media. In addition to the 3 proinflammatory cytokines assays were also assessed for the presence of PDGF-BB, a cytokine not widely known to be secreted by M1 macrophages but has been demonstrated to play a role in triggering vascular smooth muscle cell migration to the atherosclerotic plaque (Cheng *et al*., 2020). Therefore, we examined whether oxLDL stimulation of the M1 macrophages could trigger synthesis of this cytokine.

As shown in Figure 3.21, conditioned media samples taken from THP-1-derived foam cells could be observed to secrete significantly increased amounts of IL-6 and TNF-α into the conditioned media compared to the acellular collagen hydrogel. The M1 macrophages were found to secrete IL-6 and TNF-α into the conditioned media, but only IL-6 was found to be significantly greater than that observed from the conditioned media from the conditioned collagen hydrogel. The oxLDL loading of the THP-1-derived foam cells was seen to enhance the secretion of both pro-inflammatory cytokines compared to M1 macrophages consistent with previous research, but this was only found to be significantly higher for IL-6. Unexpectedly, it was not possible to detect any IL-1β secretion from the conditioned media of any of the samples (Figure 3.22A). Absorbance readings taken from the zero-concentration standard were found to be consistently and significantly higher than that obtained from any of the samples. These data therefore indicate the possibility that the complete RPMI media may contain chemicals that interfere with the ELISA plate. Similarly, test for PDGF-BB within the conditioned culture media found no evidence of secretion of this cytokine, consistent with the cytokines being measured being specifically produced by the THP-1-derived cells.

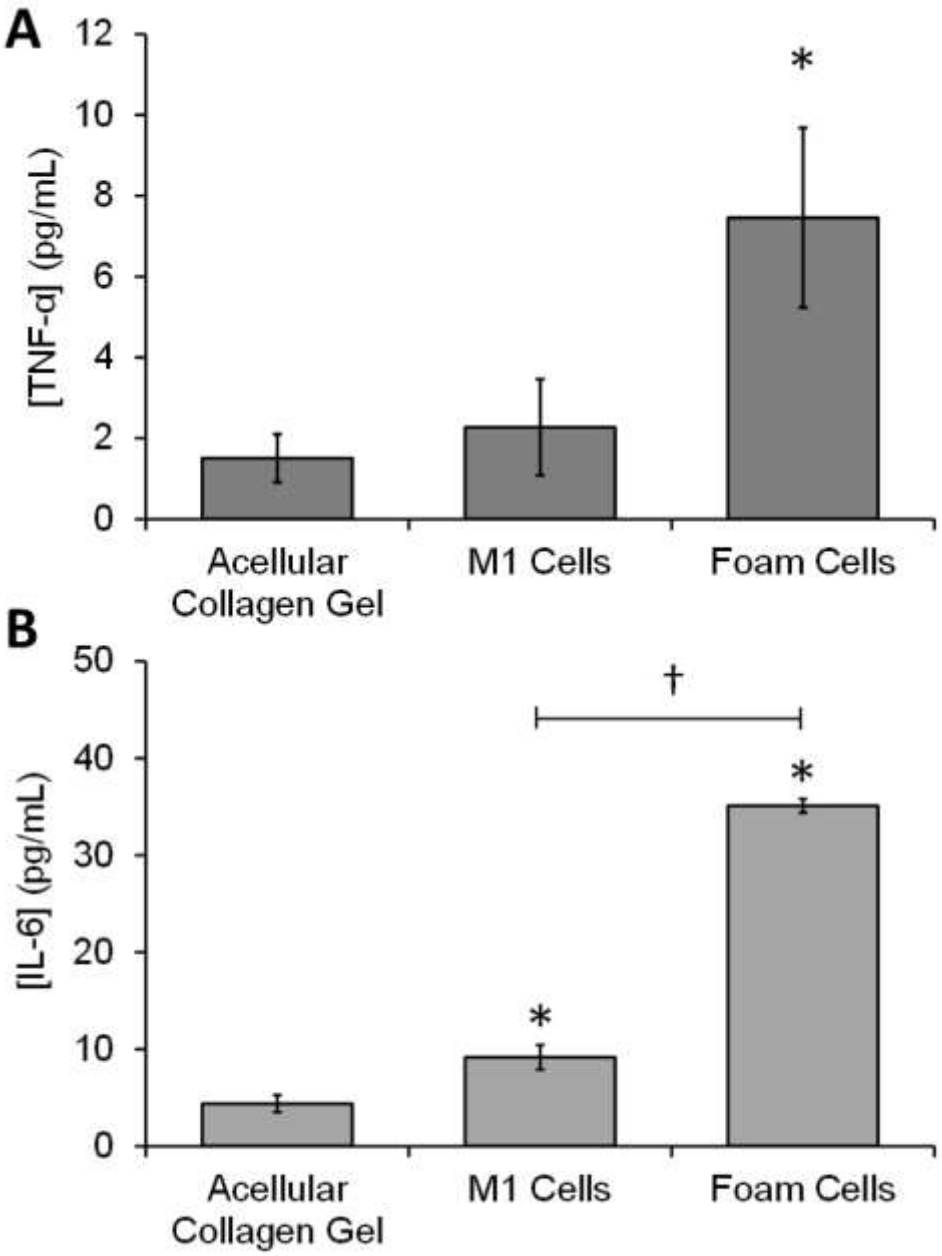

Figure 3.22. TNF-α and IL-6 secretion is upregulated in foam cells generated within the compressed 3D collagen hydrogel THP-1 cell suspensions were seeded into compressed collagen hydrogels, and then incubated in RPMI media with 50 nM PMA at 5% CO_2, 37°C for 48 h. Cells were rested by incubation in a PMA-free media for 24 h, and then cells were treated with LPS and IFN-γ for 72 h. The samples were then treated with either 50 μg/mL OxLDL (Foam cells) or an equivalent volume (M1 cells) at 5% CO_2, 37°C for 72 h. Acellular collagen gels were also placed in culture alongside these constructs as a control sample. Conditioned media samples were then extracted and subjected to ELISA analysis of either TNF-α (A) or IL-6 (B) contained within the samples. * Indicates $P<0.05$ relative to the acellular gel control † = $P<0.05$ relative to the indicated samples using a one-way ANOVA with post hoc Tukey test, n=6.

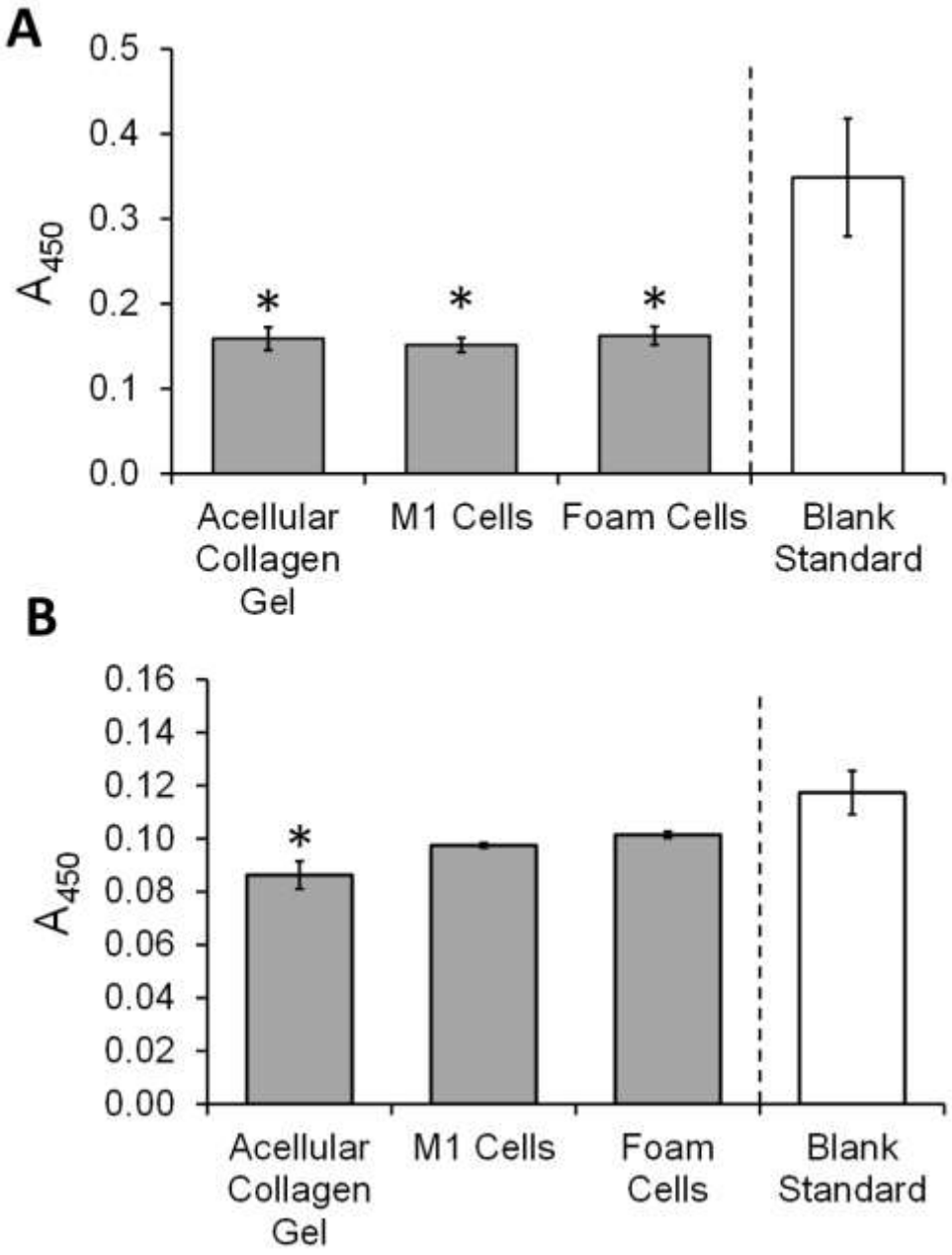

Figure 3.23. IL-1β and PDGF-BB could not be detected within the conditioned media extracted from compressed 3D collagen hydrogels containing THP-1-derived cells. THP-1 cell suspensions were seeded into compressed collagen hydrogels, and then incubated in RPMI media with 50 nM PMA at 5% CO_2, 37°C for 48 h. Cells were rested by incubation in a PMA-free media for 24 h, and then cells were treated with LPS and IFN-γ for 72 h. The samples were then treated with either 50 µg/mL OxLDL (Foam cells) or an equivalent volume (M1 cells) at 5% CO_2, 37°C for 72 h. Acellular collagen gels were also placed in culture alongside these constructs as a control sample. Conditioned media samples were then extracted and subjected to ELISA analysis of either IL-1β (A) or PDGF-BB (B) contained within the samples. * Indicates $P<0.05$ relative to the zero concentration (blank) standard using a one-way ANOVA with post hoc Tukey test, n=6.

Overall, these data indicated that the foam cells are not just viable but maintain their significant pro-inflammatory phenotype when cultured with the compressed collagen hydrogels.

3.3.13 Development of 2D cultures of human coronary artery smooth muscle cell-derived foam cells.

Previous studies have demonstrated that that smooth muscle cell-derived foam cells contribute around about 50% of all the foam cells present in atherosclerotic plaques found in human arteries (Allahverdian *et al*., 2014). Therefore, an accurate model of the neointima would also incorporate this cell type. Therefore, initial experiments assessed the possibility of culturing human coronary artery smooth muscle-derived foam cells (HCASMC-DFCs) in 2D culture. Human coronary artery smooth muscle cells (HCASMCs) were seeded in 24-well plates in complete Medium 231 and incubated for 48-72 h to provide time for cell proliferation and maturation. At the end of this period, the samples were seen to become elongated and spindle-shaped, consistent with the morphology expected of these cells (Figure 3.22). The media was then changed to a fresh sample containing 50 µg/mL oxLDL and incubated for a further 72 h. After this period cells were fixed and stained with Nile Red and Hoechst-33342 to assess intracellular accumulations of neutral lipids. As Figure 3.23 shows, Nile-Red stain labelled intracellular neutral lipid droplets inside smooth muscle cells (red droplets) indicating that it was possible to create HCASMC-DFC in 2D culture.

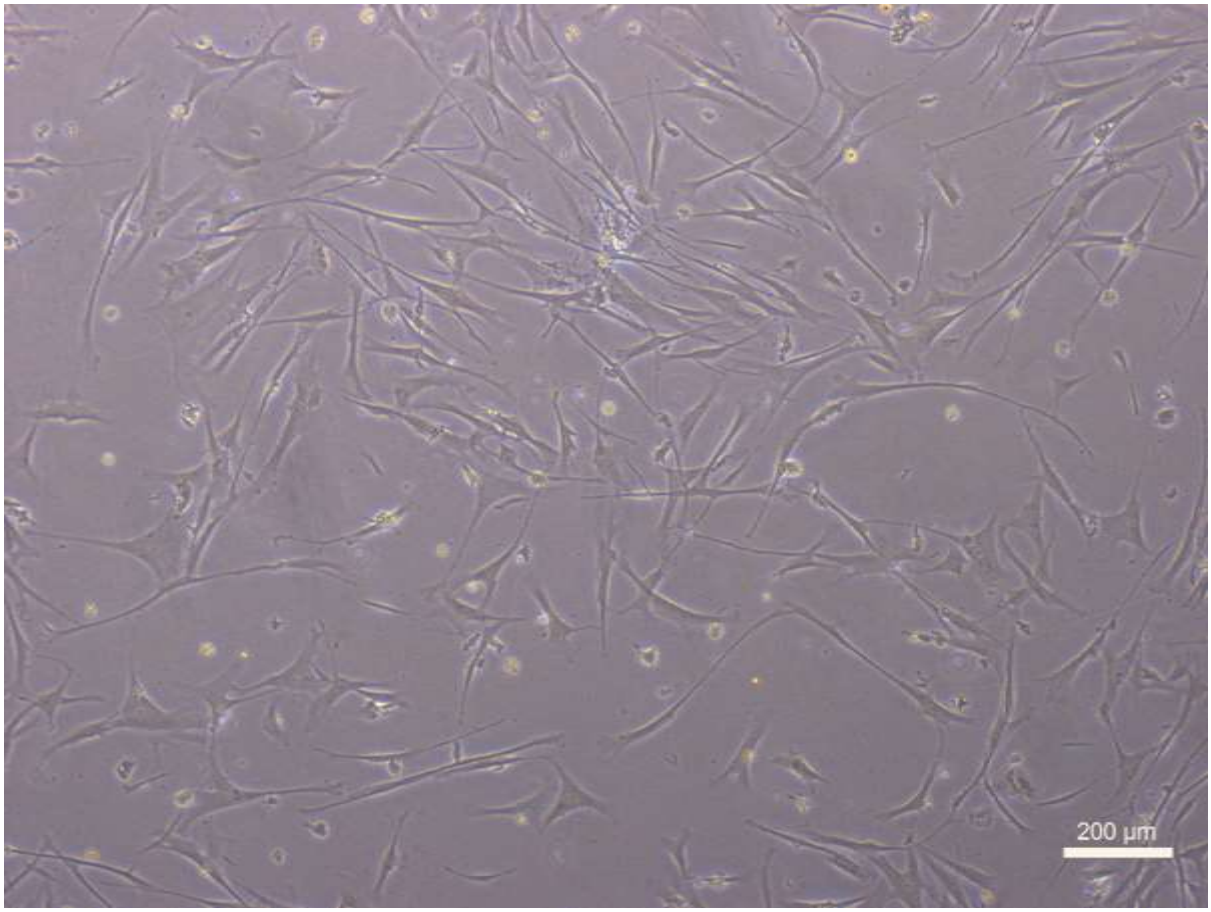

Figure 3.24. 2D culture of HCASMCs. HCASMCs were cultured according to the manufacturer instructions. The cells were seeded at a cell density of $1x10^5$ cells/well in 24-well plates in completed Medium 231 and incubated at 5% CO_2 at 37°C for 48 h-72 hours. Images were then taken by light microscopy, n=6.

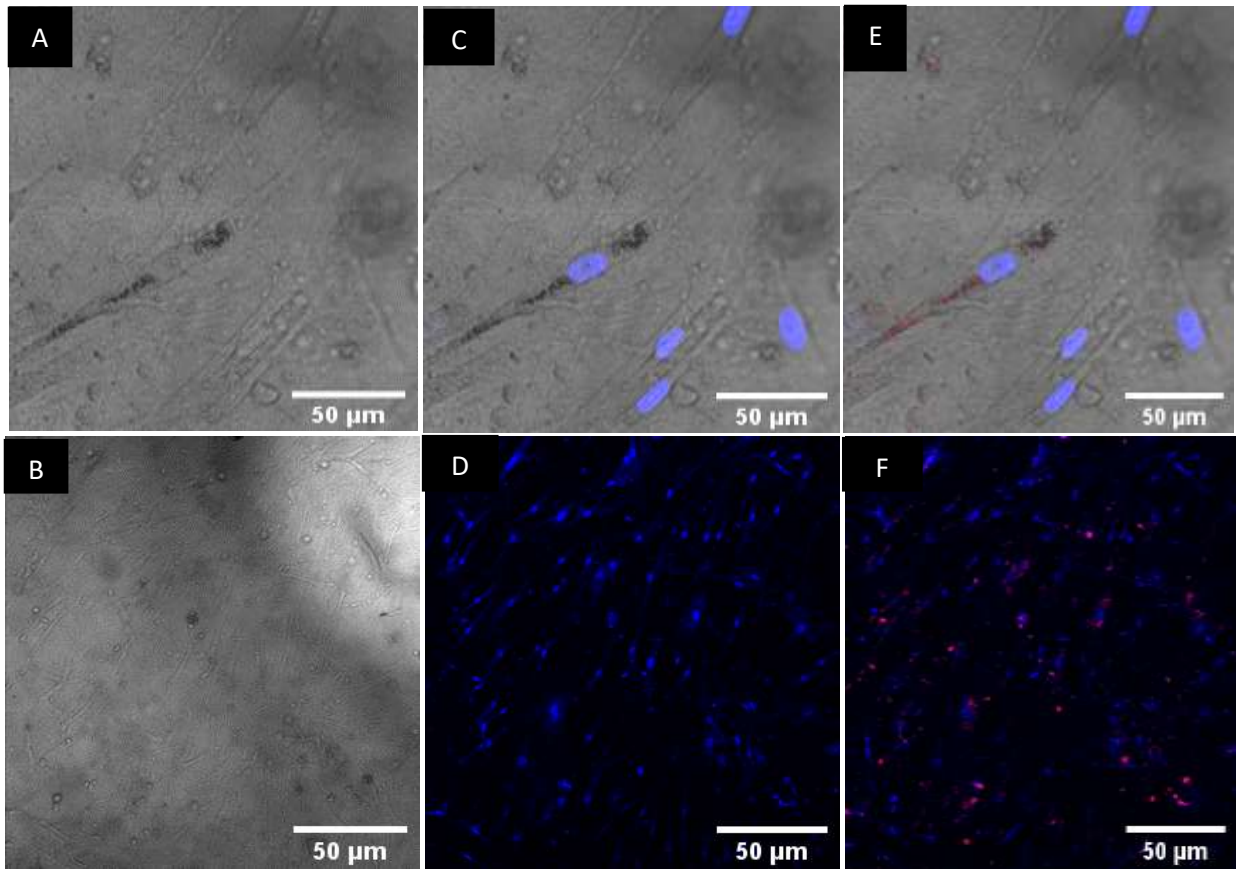

Figure 3.25. Culturing of HCASMC-DFC in 2D cultures. HCASMCs were seeded in 24-well plates in completed 231 media at a density of $1x10^5$ cells/well for 48 hours. The cells were then treated with 50 µg/mL oxLDL at 5% CO_2, 37°C for 72h. After this period, cells were fixed and stained with Nile-Red and Hoechst-33342 to assess the intracellular lipid droplets. Smooth muscle cells stained with Hoechst-33342 dye, (Right panel) Overlay of Nile-Red and Hoechst fluorescence. Samples were assessed at high (A-C) and low (D-F) magnification. (A, D) Brightfield images (B,E) Hoechst-33342 fluorescence (C,F) An overlay or Nile Red and Hoechst fluorescence, n=4.

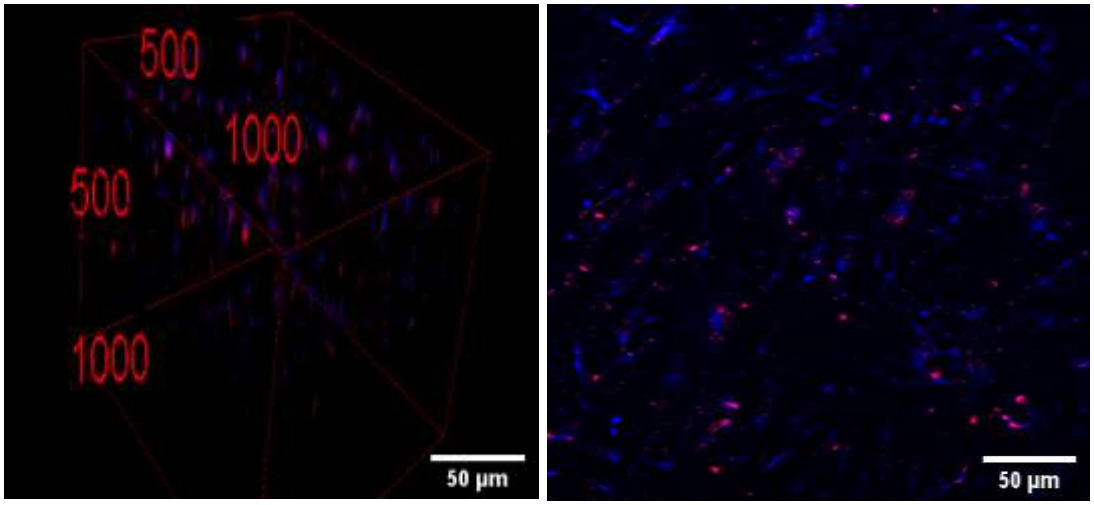

A B

Figure 3.26. HCASMC-DFC can be cultured successfully within 3D collagen hydrogels. HCASMCs were seeded at $1x10^5$ cells/collagen hydrogel and set with 1x1cm filter paper frames. The collagen hydrogels were then treated with fresh RPMI media contain 50 µg/mL ox LDL in 5% CO_2, 37°C for 72h. Following this the collagen hydrogels were stained with Nile-Red and Hoechst stains to assess intracellular accumulations of the lipids. Z-stack imaging was conducted using a confocal microscope. (A) Z-stack image (B) single slice image, n=6.

3.3.14 Preparation of SMC derived foam cells in collagen hydrogels

HCASMCs were seeded within collagen hydrogels and then incubated with fresh media containing 50 µg/mL oxLDL for 72 hours. HCASMCs within the samples were shown to stain positively for Nile Red (Figure 3.24D-F). Higher magnification imaging demonstrated that the HCASMC could be observed to have accumulated granules that stained positively for Nile Red, indicating the presence of the intracellular lipid deposits characteristic of foam cells.

3.3.15 Cell viability assessment of HCASMC-DFC

To ensure that the viability of the HCASMC-DFCs was not impacted by culturing within 3D hydrogels or exposure to oxLDL, a cell viability assessment was performed through live/dead

staining of the samples. As shown in Figure 3.25, the HCASMCs remained a high level of viability after culture with 50 μg/mL oxLDL within a 3D collagen hydrogel with 92.4% ± 0.9 of cells found to be viable.

3.3.16 HCAMSC-DFCs accumulate greater lipid deposits when cultured with oxLDL than with non-oxidised LDL.

Macrophage-derived foam cells take up oxLDL with a higher affinity than the native, non-oxidised LDL particles (Chistiakov *et al.*, 2017). Experiments were performed to assess whether oxidation of the LDL particles impacts on the rate of foam cell formation in our 3D collagen hydrogels. After seeding of HCASMCs within a collagen hydrogel, the cells were incubated with complete Medium 231 supplemented with either 50 μg/mL oxLDL or 50 μg/mL of non-oxidised LDL and incubated for 72 hours. The cells were fixed and stained with Nile red and Hoechst-33342. The samples were then subject to z-stack imaging and the mean Nile red fluorescence for all slices was compared for cells treated with oxLDL and non-oxidised LDL. As shown in Figure 3.27A, B, nile red staining of lipid deposits was seen more frequently in HCASMCs treated with oxLDL than non-oxidised LDL. This was confirmed by an ImageJ analysis of the mean Nile red fluorescence observed through the hydrogels that showed that this was significantly greater oxLDL-treated samples ($P < 0.05$; Figure 3.27C). These data suggest that oxidation of the LDL particles facilitates the formation of HCASMC-DFCs, in a manner similar to that seen for macrophage-derived foam cells.

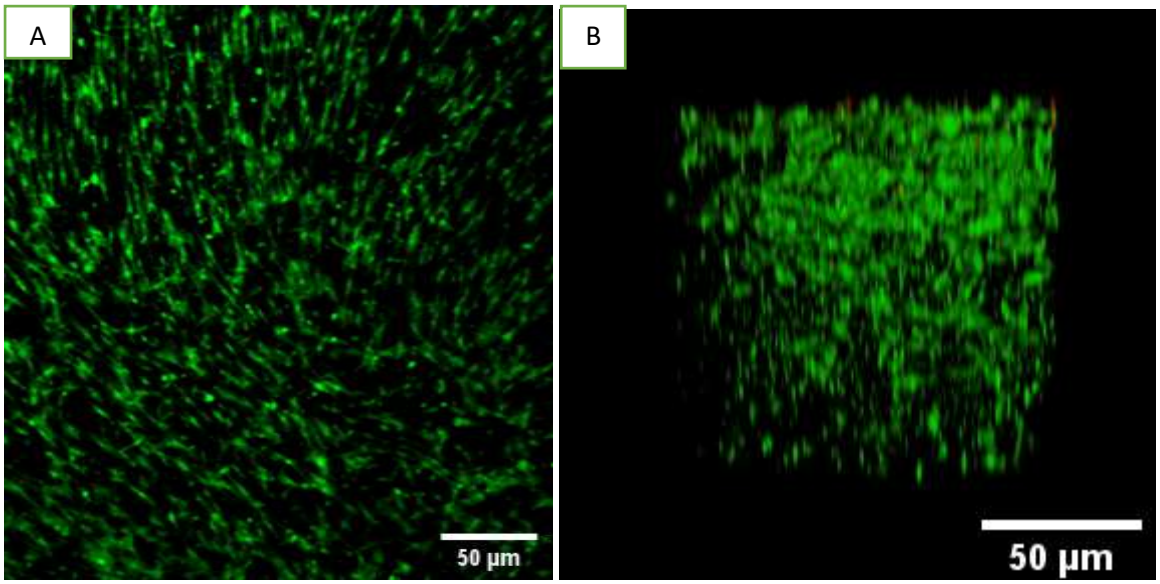

Figure 3.27 HCASMCs maintain a high level of viability when cultured with 3D collagen hydrogels. HCASMCs were seeded at $1x10^5$ cells/collagen hydrogel and set with 1x1cm filter paper frames. The collagen hydrogels were then treated with fresh RPMI media contain 50 µg/mL ox LDL in 5% CO_2, 37°C for 72h. Following this the collagen hydrogels were stained with a lead/dead cell stain. Single slice image (A) and Z-stack (B) imaging were conducted using a confocal microscope.n=5

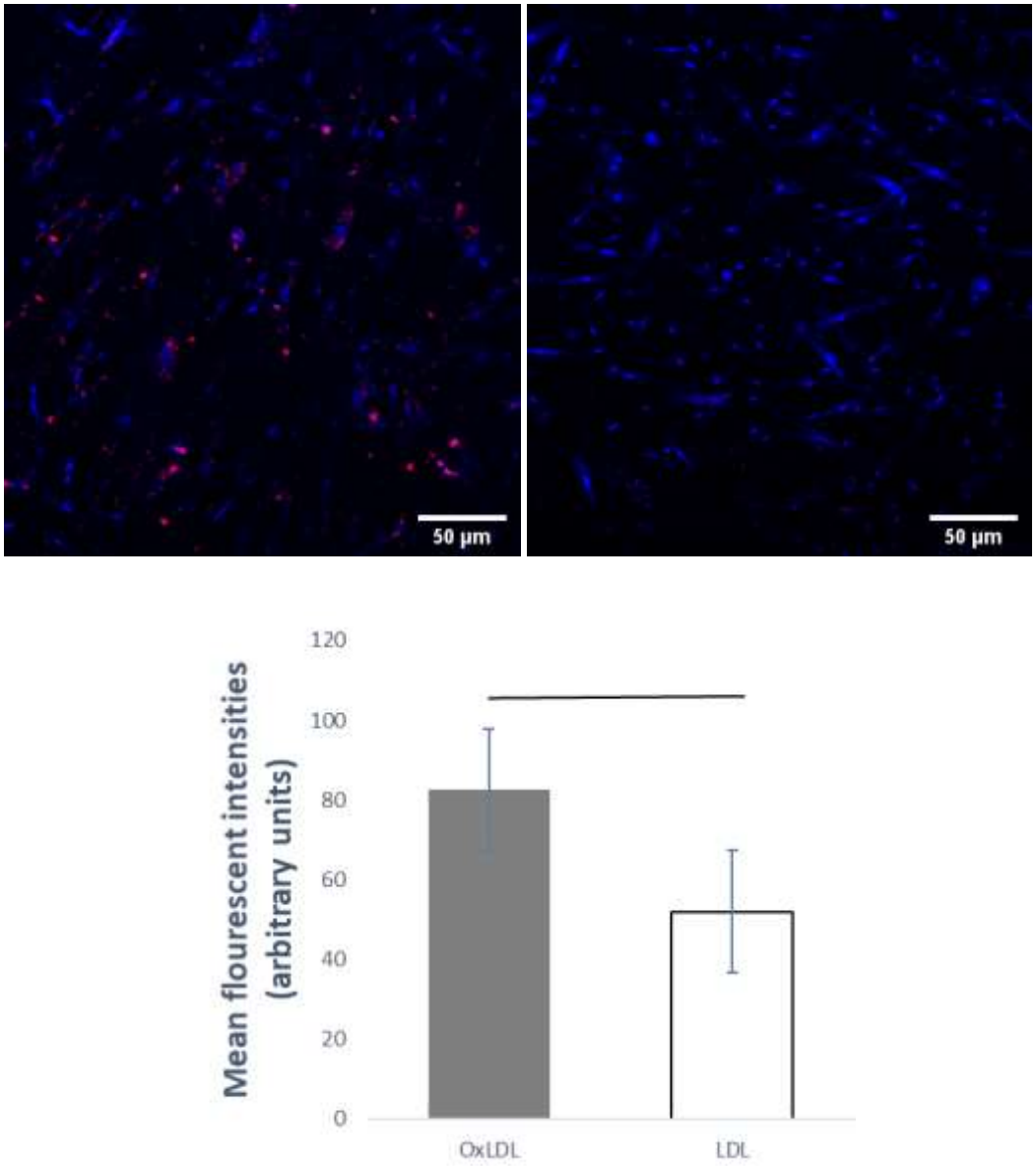

Figure 3.28 Nile Red staining was significant greater in samples loaded with oxLDL than non-oxidised LDL. HCASMCs were seeded at $1x10^5$ cells/collagen hydrogel and set with 1x1cm filter paper frames. The collagen hydrogels were then treated with fresh RPMI media contain either 50 µg/mL ox LDL (Top, left) or 50 µg/mL non-oxidised LDL (Top, right), and incubated at 5% CO_2, 37°C for 72h. Following this the collagen hydrogels were stained with Nile-Red and Hoechst stains to assess intracellular accumulations of the lipids. Z-stack imaging was conducted using a confocal microscope. (Lower panel) The mean fluorescence through the sample was measured using Image J. * $P < 0.05$ using a student's T-test. Values shown are Mean ± SEM of 3 experiments.

3.4. Discussion

In this chapter it has been demonstrated that it is possible to successfully create a 3D neointimal culture model through the differentiation of THP-1 cells into foam cells within a compressed collagen hydrogel. Through assessing the ability to develop THP-derived foam cells within both 2D and 3D cultures, it was found that it was optimal to trigger the differentiation of the THP-1 foam cells within the collagen hydrogel, rather than prior to seeding into the gel. Importantly cell viability of the THP-1-derived foam cells remained high through all stages of the process and retained their ability to produce and secrete proinflammatory cytokines such as IL-6 and TNF-α into the surrounding medium.

By carefully assessing the effectiveness of each stage in this multi-step culture system, it has been possible to develop a reliable and reproducible culture method that can be used to produce an ex vivo humanised model of atherosclerotic plaque formation. Whilst this was an original process at the time this was completed in the model, another group has recently reported achieving the same feat (Garcia-Sabate *et al*., 2020). Although this group has also demonstrated the ability to culture THP-1 cells into foam cells within a collagen hydrogel, this chapter still represent the first demonstration of producing foam cells within a compressed collagen hydrogel. As macrophage proinflammatory responses improve as stiffness of the extracellular matrix increases (Zhuang *et al*., 2020), it is likely that the stiffer compressed collagen hydrogel will provide an optimal environment for culturing foam cells.

The neointimal culture model detailed in this chapter represents a different strategy to previous attempts to create a tissue-engineered model of human atherosclerosis, that have revolved around triggering monocyte recruitment and transendothelial migration into the neointimal space of a healthy blood vessel model (Robert *et al*., 2013; Liu *et al*., 2017; Zhang

et al., 2020). In contrast our strategy is to develop the neointimal environment outside of the blood vessel and then adapt our layer-by-layer fabrication strategy to introduce the tissue-engineered artery once this has been fully developed. This process allows us to artificially introduce a high density of foam cells directly into the model system without having to recruit and differentiate these from perfused blood samples. Of the previous attempts, only Zhang *et al*., (2020) have demonstrated that monocytes recruited into the subendothelial space were able to undergo transformation into foam cells. Whilst this is an important step in recreating atherosclerosis in tissue-engineered human arteries, it is important to note that both our model and that of Zhang *et al*., (2020) only provide a replica of the fatty streak, an early, clinically silent stage of atherosclerotic plaque development. Therefore, further development of the model will be required to create more advanced lesions with the construct to ensure that it is able to trigger the later stages that undergo the clinically relevant events of plaque rupture and erosion. With this in mind, the demonstration that it is possible to effectively develop HCASMC-DFCs within the collagen hydrogels should allow us in future to develop more advanced models encompassing this key cell in the atherosclerotic plaque (Allahverdian *et al*. 2014). Through incorporating the HCASMC-DFC alongside in the hydrogels alongside the THP-1-derived foam cells, it is likely that it will be possible to develop models that better replicate the cellular environment of the advance atherosclerotic plaque. However additional efforts will be needed to replicate both the necrotic core of the plaque and the fibrous cap, both of which are characteristic of advanced fibroatheroma stages of plaque development. Modifications of the methods to trigger targeted cellular apoptosis or necrosis within the neointimal would provide a basis for developing a necrotic core, however further engineering will be required to ensure this does not adversely affect surrounding cells. The fibrous cap could be developed either exogenously seeding the intimal surface of the

construct with HCASMCs or via the ability of the model to trigger endogenous vascular smooth muscle cell migration with cultured within the construct. The latter of these options is explored further in chapter 5. Therefore, it should be possible to utilise this initial prototype to develop more advanced stage neointimal models.

One of the major disadvantages of the neointimal culturing system developed here is the prolonged culture period required, with this culture system requiring the THP-1 cells to be cultured for 10 days to produce THP-1-derived foam cells. This extended period creates both cost implications as well as practical difficulties in that it slows down the rate at which this *in vitro* model can be made. Future research will be required to assess whether the development of THP-1-derived foam cells can be speed up within the compressed collagen hydrogels. During the development of the model, we principally optimised the concentration of cytokines and LDL particles used during the culture, but it is likely that similar effects can be observed at much shorter durations. For example, there has traditionally been no standardised protocol to differentiate THP-1 cells to macrophages, with the concentration of the PMA used and duration of treatment differing widely between labs (Park *et al*., 2007) (Starr *et al*., 2018; Chanput *et al*., 2014; Spano *et al*., 2007; Lund *et al*., 2016; Feng *et al*., 2004; Daigneault *et al*., 2010). For example, investigators have used between 3-72 h of PMA stimulation to initiate M0 macrophage differentiation. In this study we utilised 48 h , this has previously been shown to be the optimal period for THP-1 differentiation in specialist studies (Daigneault *et al.*, 2010); Aldo *et al.*, 2013), however ; future studies should investigate whether it is possible to develop effective THP-1-derived foam cell cultures after 24 h or less. Similarly, whilst we have used 72 h incubation to induce both M1 polarisation and foam cell formation, other groups often perform this incubation for as little as 24 h (e.g., Greenspan *et*

al., 1997; Genin *et al*., 2015). This could therefore reduce the culture length from 10 days down to as little as 4 days, which could significantly reduce the culture costs and enhance the rate at which these constructs could be made.

3.5 Conclusion

This chapter details an effective and reproducible system for developing a 3D culture model of the neointimal lining of the atherosclerotic human artery. The foam cells contained within can be shown to be highly viable and maintain their proinflammatory properties such that they have the potential to influence the cellular behaviour of endothelial and smooth muscle cells when cultured together within a tissue-engineered arterial model. Although this model currently represents an early stage of atherosclerotic plaque development, through development of a protocol for the development of HCASMC-DFC within 3D collagen hydrogels it should be possible to produce more advanced models in future.

Chapter 4: Assessing the prothrombotic potential of the 3D neointimal constructs

4.1 Introduction

Disruption of the atherosclerotic plaque triggers the onset of acute cardiovascular events such as myocardial infarction and ischemic stroke. Through disruption of the anti-thrombotic endothelial barrier, plaque rupture and erosion expose the complex biochemical and cellular environment contained within the atherosclerotic plaque to the bloodstream. This triggers both the activation of circulating platelets as well as the blood coagulation system (Khandkar *et al*., 2021; Libby *et al*., 2019). The resultant thrombi formed can occlude the affected blood vessel, causing ischemic damage to the downstream tissue. However, the mechanisms underlying these thrombotic events are variable depending on the mechanisms of plaque disruption. Post-mortem imaging has demonstrated that plaque rupture is the pathological event responsible for most of all fatal myocardial infarctions, whilst plaque erosion (in which the plaque is not ruptured) is responsible for fatal coronary thrombi in around a third of all patients (Khandkar *et al*., 2021; White *et al*., 2016). However, the thrombotic response was seen to be distinct in these different pathological events, with ruptured plaques causing the formation of thrombi which were more fibrin-rich, whilst plaque erosion lead to thrombi which were more platelet-rich (Sato *et al.*, 2005). Importantly, studies have demonstrated that patients presenting with plaque rupture tend to have a larger infarct area and reduced left ventricular function (Higuma *et al.*, 2015). Additionally, the prognosis of patients who had experienced plaque rupture was found to be worse than those whose acute cardiovascular event had been triggered by plaque erosion (Yonetsu and Jang, 2018). These results indicate that the method of plaque breakdown plays a key role in determining the type of thrombotic response observed, and thus play a significant role in determining the prognosis

of these patients. Through better understanding the mechanisms of atherothrombosis we may be able to improve the functional outcomes for patients undergoing myocardial infarction.

In plaque rupture, the mechanical breakdown of the atherosclerotic plaque brought about through the weakening of the fibrous cap leads to direct exposure of components of the neointima to the bloodstream. Contained within this layer are a number of components that can trigger the activation of platelets. Assessment of lipid-rich atheromatous plaques taken from patients with carotid stenosis found the presence of significant quantities of type I and III fibrillar collagen (Reininger *et al*., 2010; Penz *et al*., 2005). Antibody blockade of Glycoprotein VI (GPVI) in human platelets, or genetic knockdown of GPVI in murine platelets, prevented platelet activation when exposed to plaque samples. Similarly, collagenase treatment of plaque material or exposure to antibodies to type I and III collagen inhibited platelet activation in response to the excised atherosclerotic plaques, providing clear evidence that collagen plays a role in triggering platelet activation. This effect of collagen is likely supported by the presence of other adhesive ligands present in atherosclerotic plaques, such as von Willebrand Factor (vWF) and fibronectin (Gencer *et al*., 2021; Matter *et al*., 2004). Fibronectin has been suggested to trigger platelet activation at plaques through activation of GPVI in *in vitro* studies, however the significance of these findings is unclear as there has been limited study of the role of this protein in *in vivo* studies (Cho and Mosher, 2006). Von Willebrand Factor is known to play a key role in mediating platelet activation to collagen under conditions of high shear stress, consistent with a role for this protein in assisting in platelet adhesion to a ruptured plaque (Mastenbroek *et al*., 2015; Savage *et al*., 2021). Antibody blockade of the vWF receptor, Glycoprotein Ib, was found to significantly prevent

ex vivo platelet activation on material taken from human atherosclerotic plaques obtained by surgical endarterectomy (Reininger *et al*., 2007; Reininger *et al*., 2010). Interestingly, high levels of plasma vWF have been found to be a risk factor for patients in developing recurrent myocardial infarction, indicating that this protein facilitates the progression of atherothrombosis (Badimon and Vilahur, 2014; Sakai *et al*., 1999).

Alongside these adhesive ligands, the soluble chemical constituents of atherosclerotic plaques may also sensitize human platelets through the presence of oxidized low-density lipoproteins (oxLDLs). This may also be enhanced further by the presence of additional oxLDL within the bloodstream of individuals suffering from dyslipidemia. Previous studies have demonstrated that increased oxLDL content of plaques from patients with symptomatic carotid disease was associated with symptomatic disease (Nezu *et al.*, 2016) due to the enhanced thrombogenic properties of these plaques upon rupturing. Previous studies have demonstrated that the CD36 scavenger receptors are responsible for sensitizing human platelets exposed to oxLDL, and therefore responsible for the prothrombotic platelet phenotype connected to atherothrombosis (Asada *et al*., 2020; Podrez *et al*., 2007). oxLDL activation of CD36 triggers a tyrosine kinase- and protein kinase C-dependent signalling pathway which activates phosphodiesterases to cleave cAMP, as well as triggering the formation of reactive oxygen species which inhibit Protein Kinase G (Wraith *et al*., 2013; Berger *et al*., 2020). This therefore removes the dampening effects of platelet inhibiting compounds such as prostacyclin and nitric oxide produced by endothelial cells, enhancing the activity of human platelets. Additionally, the core of atherosclerotic plaques have been demonstrated to be rich in lysophosphatidic acid, which has also been demonstrated to trigger platelet activation through activation of LPA1 and LPA3 receptors (Siess *et al.*, 1999).

Although some evidence has demonstrated that prostaglandin E2 (PGE_2) is produced within human atherosclerotic plaques and could trigger arterial thrombosis (Gross *et al.*, 2007; Gross *et al*., 2014), studies performed on *ex vivo* human plaques have indicated that blockade of this receptor has limited impact on plaque-induced thrombosis (Yang and Chen, 2016). However, this discrepancy has been suggested to be due to the limited timeframe in which the reactive PGE_2 remains active after plaque dissection (Mastenbroek *et al.*, 2015). Overall, these studies demonstrate that release of atherogenic lipids from the interior of the plaque into the bloodstream can facilitate platelet activation during atherothrombosis. Beyond platelet activation, atherothrombosis has also been demonstrated to involve activation of the blood coagulation system (Mastenbroek, 2015). Tissue factor is the key extracellular activator of the extrinsic pathway through its ability to activate Factor VII. This enzyme is known to be abundantly expressed in atherosclerotic plaques, with this enzyme associated both with foam cells and vascular smooth muscle cells, as well as microparticles created by apoptosis of foam cells (Grover and Mackman, 2020; Marmur *et al*., 1996). The degree of expression of tissue factor within the plaque had been shown to be a key determinant of the thrombogenicity of this structure (Grover and Mackman, 2020; Toschi *et al*., 1997). Blocking tissue factor activity by incubation with tissue factor pathway inhibitor or an anti-tissue factor antibody was shown to significantly reduce the thrombogenic potential of human atherosclerotic plaque samples (Badimon and Vilahur, 2014; Badimon *et al*., 1999), supporting the idea that activation of the extrinsic pathway of coagulation plays a significant role in determining the occlusive potential of a disrupted plaque. However activation of the intrinsic pathway of coagulation also supports the growth of thrombi formed upon plaque rupture, as genetic knock-out of factor XII have also been shown to reduce the longer-term stability of the thrombus triggered by Tissue Factor-Factor VII activity (Mastenbroek *et al.*, 2015; Kuijpers *et al*., 2014) Importantly,

the activation of the blood coagulation system and human platelets by disrupted plaques are not independent, with evidence suggesting interplay between these two events. For example, platelets can be seen to be observed to colocalize with fibrin and tissue factor in atherosclerotic plaques, suggesting that tissue factor-dependent activation of coagulation helps recruit platelets, facilitating the growth of the thrombus (Hoshiba *et al.*, 2006). Similarly, platelet recruitment on plaque-coated surfaces has been shown to trigger a second wave of fibrin formation in ex vivo studies, suggesting that the exposure of phosphatidylserine on the activated platelet surface plays a key role in progression of the clotting response by acting as a catalytic surface for clotting factors (Reininger *et al.*, 2010). Therefore, this self-propagating interplay between primary and secondary haemostatic responses is responsible for the uncontrolled clotting response which is the hallmark of ischemic heart disease and stroke. Any 3D culture model of the neointima must be capable of triggering these atherothrombotic properties to be considered a valid model of the human atherosclerotic plaque. Previous studies of tissue-engineered blood vessel constructs have demonstrated that they can replica the inflammation of endothelial cells and begin to accumulate foam cells when exposed to oxidized LDL and pro-inflammatory mediators. However, none of these previous studies have assessed the pro-thrombotic potential of these model system, therefore making it uncertain if they can be used as valid replacements of current animal models of atherothrombosis. Atorvastatin is currently recommended by the National Institute for Clinical Excellence (NICE) as both for primary prevention of cardiovascular events in people at high risk of experiencing an acute cardiovascular event, as well as secondary prevention to prevent further cardiovascular events (NICE, 2016). Although statins are primarily used to reduce the dyslipidemia found in patients at risk of acute cardiovascular events, statins are well known to have pleiotropic effects on a variety of different aspects of

cardiovascular function (Davignon, 2004). Atorvastatin has been shown to impact on the functional properties of platelets, endothelial progenitor cells, endothelial cells, monocytes and foam cells (Hilgendorf *et al*., 2003; Tekten *et al*., 2004; Gorabi *et al*., 2019; Sandhu *et al*., 2017; Sanguini *et al*., 2005). Due to the complex interactions between platelets, the coagulation cascade, and cells of the plaque and blood vessel wall, it is difficult for clinical and *in vivo* studies to dissect the importance of each of the various effects of statins on each of these cells in eliciting the thrombotic response to a ruptured or eroded plaque. The layer-by-layer fabrication model utilized in these experiments provides us with the ability to assess the impact of this drug on the interaction between human platelets and macrophage-derived foam cells within the atherosclerotic plaque. In this chapter, experiments were performed to assess whether the 3D neointimal culture model can function as an effective ex vivo replica for a ruptured atherosclerotic plaque by triggering activation of human platelets and tissue factor dependent coagulation upon exposure to human blood samples. We also examined whether treatment with atorvastatin could reduce the prothrombotic properties of the neointimal construct.

4.2 Results

4.2.1 The 3D neointimal cell culture model containing THP-1-derived foam cells can trigger coagulation of human platelet poor plasma

Ruptured atherosclerotic plaques are able to trigger activation of the blood coagulation cascade through the presence of tissue factor present within the neointimal layer(Owens and MacKman, 2012). Tissue factor has been shown to be localised within foam cells present within the plaque (Mast, 2016; de Oliveira *et al.*, 2020). Additionally, previous studies in 2D

cultures of THP-1 cells have demonstrated that tissue factor activity of these cultures can be upregulated by treatment with either lipopolysaccharide (Guha *et al.*, 2001) or oxidised low density lipoprotein (Owens *et al*., 2012). However there does not appear to have been similar studies conducted in THP-1 cells cultured within a 3D cell culture model – therefore it is uncertain whether the 3D neointimal model developed in chapter 3 will be able to trigger blood coagulation, and thus be a valid model of the human atherosclerotic plaque. Previously Musa *et al*., (2016) developed a testing platform to assess the ability of tissue engineered arterial constructs to activate human platelets. This was achieved through using a custom-made sodium acetate frame to hold the luminal surface of the construct on top of a washed human platelet suspension (Musa *et al*.,2016). This method was adapted to assess whether the 3D neointimal construct could initiate the activation of the blood coagulation cascade by performing a prothrombin time measurement on human platelet-poor plasma samples exposed to the luminal surface of neointimal constructs containing either THP-1-derived foam cells or M1 cells. As previous experiments have demonstrated an ability for fibrillar collagen to activate Factor XII (van der Meijden *et al*., 2009), it is possible that the compressed collagen could trigger activation directly. Therefore, the cellular constructs were also compared against an acellular compressed collagen hydrogel as a control. As shown in Figure 4.1, the foam cell-containing construct had the shortest prothrombin time (87 ± 5s). This was significantly quicker than both the M1 cell-containing gel (158 ± 3s; n = 6; $P < 0.05$) and the acellular collagen hydrogel (376 ± 6s; n = 6; $P < 0.05$). These data indicate that foam cells are able to effectively trigger the blood coagulation system, consistent with previous studies in 2D cultures that showed the atherogenic transformation of foam cells (Owens *et al*., 2012). Additionally, the M1 cells were found to trigger coagulation significantly faster than the

acellular collagen hydrogel ($p < 0.05$) indicating that the LPS-stimulated M1 cells have also developed tissue factor activity.

4.2.2 Plastic compression of the 3D neointimal culture model does not affect its procoagulant properties

Plastic compression increases the stiffness and the collagen concentration of the collagen hydrogels (Ahearne, 2014). Previous studies have demonstrated that THP-1 cells take on a more pro-inflammatory phenotype when cultured upon stiffer collagen gels (Sridharan *et al*., 2019) suggesting that compression could enhance the pro-coagulant expression of the THP-1-derived foam cells. To assess this possibility, experiments were performed to compare the procoagulant properties of compressed or non-compressed collagen hydrogels. These were compared against a control in which a PPP (platelet poor plasma) sample alone was recalcified. As shown in Figure 4.2, compression of the collagen hydrogel did not significantly alter the prothrombin time (116 ± 12s vs 90 ± 5s for compressed and non-compressed gels respectively; both $n = 5$; $P > 0.05$). These are both significantly longer than the prothrombin time measured from the control samples (735 ± 12s; $n = 3$; both $P<0.05$ compared to compressed and non-compressed hydrogels). These data indicate that the stiffness or collagen concentration of the hydrogel does not alter the procoagulant properties of the 3D neointimal culture model.

4.2.3 The 3D neointimal culture model possesses measurable tissue factor activity that is enhanced by incubation with oxLDL.

It has been established that macrophages and foam cells within atherosclerotic lesions possess significant tissue factor activity and this activity is a key determinant of the thrombotic potential of these structures (Mastenbroek, 2015). As the prothrombin time measurements on the M1- and foam cell-containing neointimal constructs demonstrate a

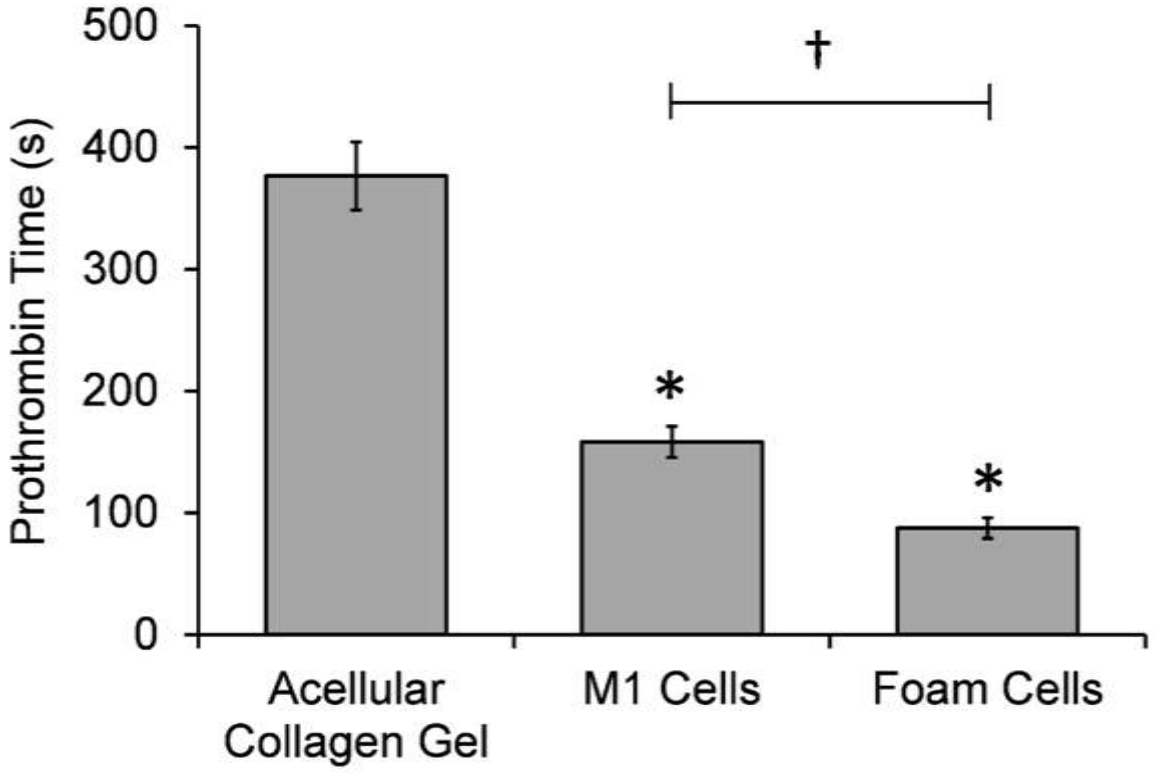

Figure 4.1: The 3D neointimal culture model with THP-1-derived foam cells induces the fastest coagulation of PPP. 3D neointimal culture models were produced in which THP-derived foam cells or M1 cells were cultured, as well as a cell-free collagen hydrogel. Samples were then placed onto sodium acetate frames and placed into contact with the surface of prewarmed, recalcified human platelet-poor plasma (PPP). The sample is kept warm in a 37°C water bath. The time taken for fibrin formation after addition of the 3D neointimal cultures models was recorded for each sample. Values shown are Mean ± SEM of 6 independent experiments. * Indicates $P < 0.05$ vs the control sample. † Indicates $P < 0.05$ relative to the indicated sample using one-way ANOVA with post hoc Tukey test.

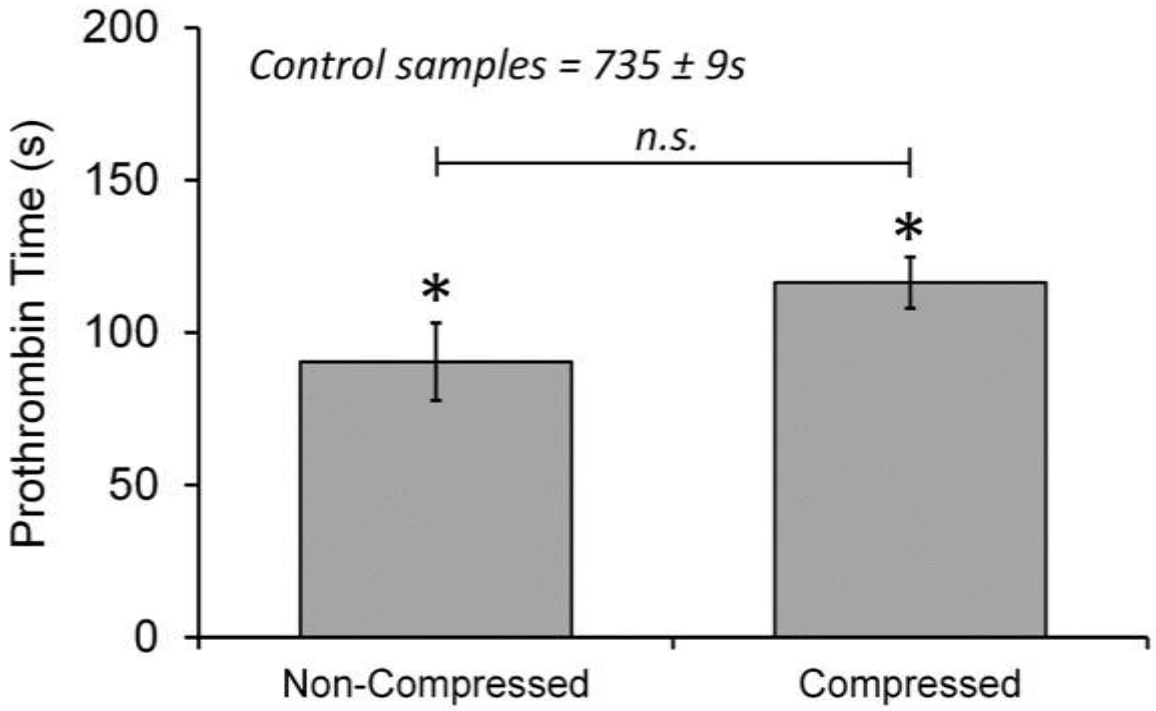

Figure 4.2: Compression of the 3D neointimal culture model does not affect its procoagulant properties. THP-1-derived foam cells were cultured within either a compressed or a non-compressed collagen hydrogel. Samples were then placed onto sodium acetate frames and placed into contact with the surface of prewarmed, recalcified human platelet-poor plasma (PPP). The sample is kept warm in a 37°C water bath. The time taken for fibrin formation after addition of the 3D neointimal cultures models was recorded for each sample. Values shown are Mean ± SEM of 5 independent experiments. * Indicates $P < 0.05$ vs the control sample using a student's T-test. n.s. indicates not statistically significant.

significant capacity for triggering the activation of blood coagulation, experiments were next performed to assess the tissue factor activity of the neointimal constructs. A novel microplate assay of tissue factor activity developed by our lab to assess tissue factor activity in 3D cell culture models was used on the 3D neointimal culture model. This assay involves incubating the constructs with a solution containing the target of tissue factor, inactive Factor VII, and a fluorescent indicator of activated factor VII (FVIIa) activity, SN-17a.

When digested by FVIIa, SN-17a becomes more fluorescent, and so the rate of fluorescence increase can be used to assess the tissue factor activity contained within each construct (Figure 4.3A). Previous experiments have demonstrated that this fluorescence increase is dependent upon both the presence of a tissue factor-bearing construct and the presence of inactive Factor VII, thus demonstrating it is the presence of tissue factor that is principally responsible for this fluorescence increase (Ranjbar & Harper, Personal communication). As can be seen in Figure 4.3B, when both the M1- and foam cell-containing neointimal models were incubated with Factor VII and SN-17a, they both elicited a significantly enhanced fluorescence increase during the incubation period compared to the acellular collagen gel. These data confirm that a tissue factor bearing construct is required to trigger the cleavage of SN-17a. Interestingly, the fluorescent increase was found to be significantly enhanced for neointimal constructs containing foam cells (29524 ± 2974 arbitrary units) then those containing M1-macrophages (21960 ± 1823 arbitrary units; $n = 12$; $P < 0.05$). These results are consistent with previous studies have demonstrated that oxLDL treatment of THP-1 cells significantly enhanced their tissue factor activity (Owens and Mackman, 2012). They are also consistent with the prothrombin time measurements made on these constructs, with the foam cell-containing construct demonstrating both the fastest prothrombin time and highest

tissue factor activity, whilst the avascular collagen hydrogel samples have got the lowest values.

4.2.4 Human Coronary Artery Smooth Muscle Cell-derived foam cells have greater tissue factor activity than untreated smooth muscle cells

In chapter 3, the possibility of developing 3D models incorporating HCASMC-derived foam cells into the neointimal culture was demonstrated. Vascular smooth muscle cells in the tunica media are known to be a significant source of tissue factor (Mackman *et al*., 2007). As vascular smooth muscle derived foam cells comprise around half of the cells in the human atherosclerotic plaque, experiments were performed to investigate if these cells could also contribute a significant source of

tissue factor to a neointimal culture model. As shown in Figure 4.4, both the 3D HCASMC- or HCASMC-derived foam cell-containing cell culture construct were found to trigger coagulation of platelet-poor plasma significantly faster than the acellular collagen gel. However, the HCASMC-derived foam cells were found to have a significantly shorter prothrombin time (100 ± 10s) compared to those containing untreated HCASMCs (199 ± 24s; $n = 6$; $P < 0.05$).

To confirm whether this related to changes in tissue factor activity in these constructs, experiments were performed using the SN17a-based tissue factor activity. These experiments demonstrated that both the neointimal constructs containing both untreated HCASMCs and HCASMC-derived foam cells (Figure 4.5). These data suggest that incorporating smooth muscle cells and smooth muscle cell-derived foam cells alongside THP-1-derived foam cells to

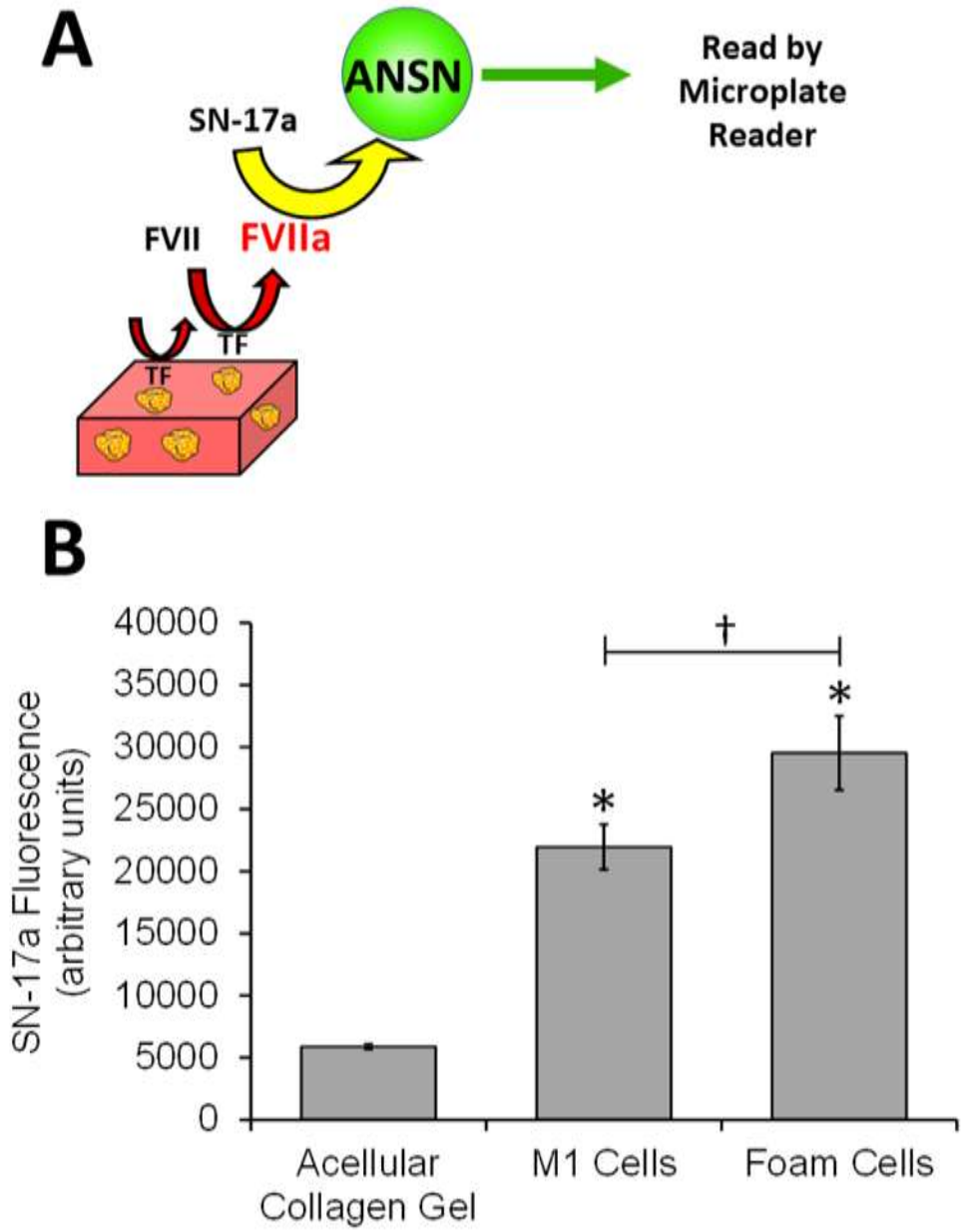

Figure 4.3: The 3D neointimal culture model possesses measurable tissue factor activity, which is enhanced by incubation with oxLDL. (A) Tissue factor assay methodology. A solution of inactive factor VII, CaCl2 and the fluorescent Factor VIIa indicator, SN-17a, was added onto foam cell and M1-containg neointimal culture models, or an acellular collagen set within 48-well plates immediately before the start of the recording. Tissue factor in the sample activates Factor VII to Factor VIIa, which in turn can cleave SN-17a, releasing the fluorescent moiety ANSN (6 amino-1-naphthalenesulphonamide) moiety which can be measured by the microplate reader. (B) Culture media was removed and an HBS solution containing 25 nM inactive Factor VII, 1mM $CaCl_2$, and 2.5 µM SN-17a was added to acellular collagen gels, or M1- or THP-1-containing 3D neointimal culture models. The well plate was then read fluorometrically for 10 minutes. The mean change in SN-17a fluorescence observed between the initial reading and that observed after 10 minutes for TEML. Values shown are Mean ±

SEM of 12 independent experiments. * Indicates $P < 0.05$ vs the control sample, † Indicates $P < 0.05$ relative to the indicated sample using one-way ANOVA with post hoc Tukey test.

produce a model more consistent with a fibroatheroma, could further enhance the prothrombotic potential of the 3D neointimal constructs, consistent with the higher thrombogenicity of this plaque stage (Fernández-Ortiz *et al.*, 1994).

4.2.5 THP-1-derived foam cells can trigger a slow platelet activation and aggregation

Ruptured atherosclerotic plaques expose the bloodstream to several adhesive and soluble ligands that can trigger platelet aggregation, as described in the introduction. For the 3D neointimal culture model to be an effective model of the human atherosclerotic plaque, the model needs to be capable of triggering human platelet activation and aggregation. Due to the complex cellular and biochemical environment present in the plaque it has not been possible to identify if foam cells play a role in providing this pro-aggregatory response of the atherosclerotic plaque. Due to the ability to engineer the cellular composition of the neointimal culture model, it has been possible to assess whether THP-derived M1- and foam cells are able to increase the pro-aggregatory potential of the neointimal construct. This was assessed using a cuvette-based system to expose our 3D neointimal culture models to washed human platelet suspensions (Figure 2.7). Washed platelets were utilised to remove the potential for platelet activation caused by thrombin generation elicited by the extrinsic coagulation pathway. Washed human platelet suspension were preincubated in contact with

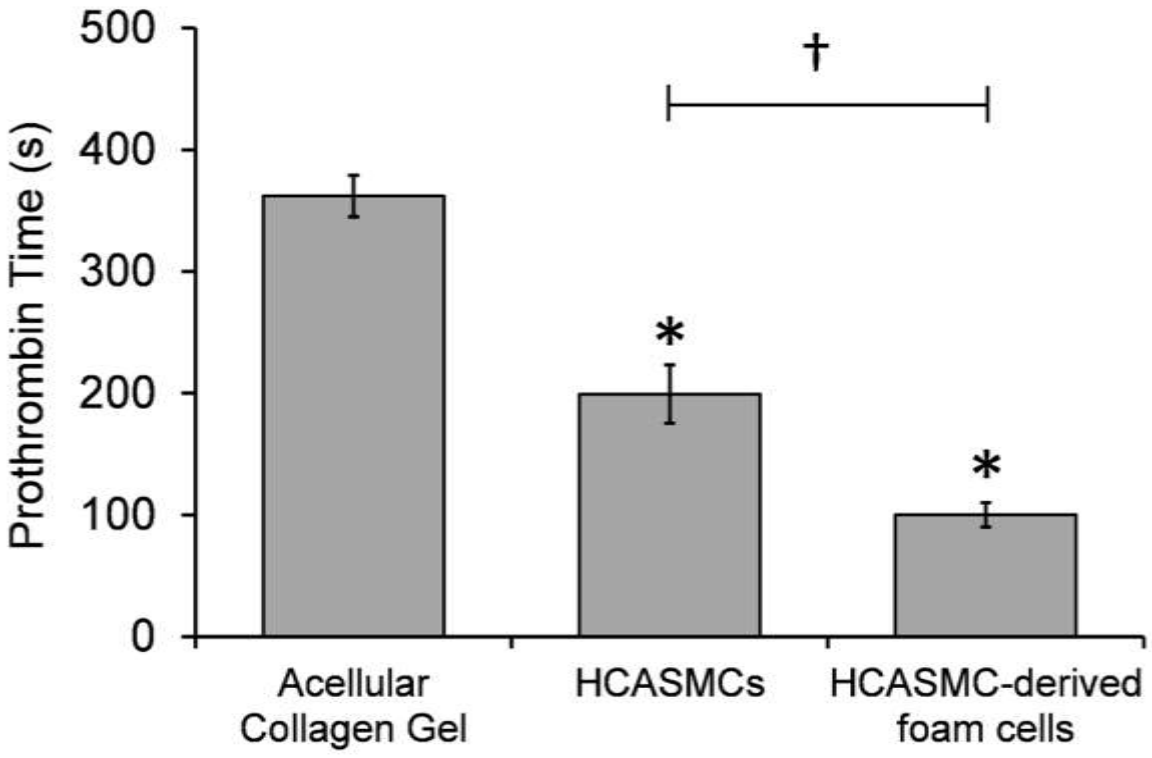

Figure 4.4: A neointimal culture containing human coronary artery smooth muscle-derived foam cells. 3D neointimal culture models were produced in which HCASMC-derived foam cells or untreated HCASMCs were cultured. Additionally, a cell-free collagen hydrogel was used as a control sample. Samples were loaded onto sodium acetate frames and placed into contact with the surface of prewarmed, recalcified human platelet-poor plasma (PPP). The sample is kept warm in a 37°C water bath. The time taken for fibrin formation after addition of the 3D neointimal cultures models was recorded for each sample. Values shown are Mean ± SEM of 6 independent experiments. * Indicates $P < 0.05$ vs the control sample, † Indicates $P < 0.05$ relative to the indicated sample using one-way ANOVA with post hoc Tukey test.

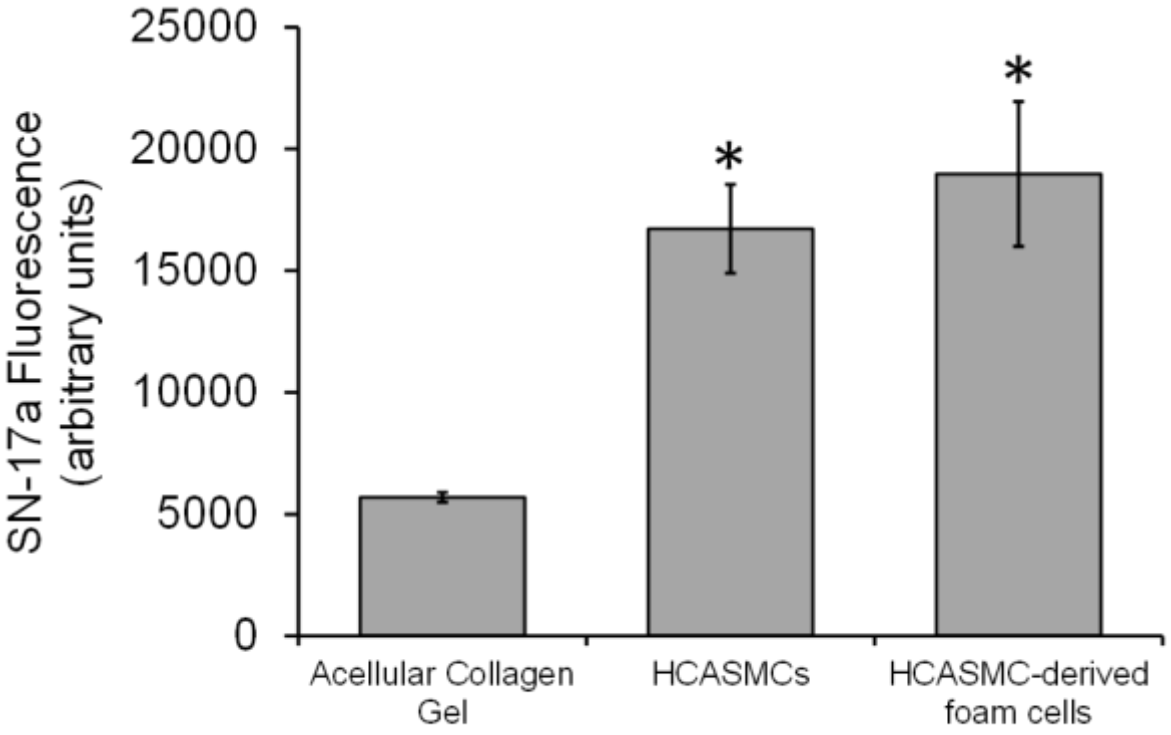

Figure 4.5: A neointimal culture model containing HCASMC-derived foam cells possesses measurable tissue factor activity, which is enhanced by incubation with oxLDL. Culture media was removed and an HBS solution containing 25 nM inactive Factor VII, 1mM $CaCl_2$, and 2.5 μM SN-17a was added to acellular collagen gels, or M1- or THP-1-containing 3D neointimal culture models. The well plate was then read fluorometrically for 10 minutes. The mean change in SN-17a fluorescence observed between the initial reading and that observed after 10 minutes for TEML. Values shown are Mean ± SEM of 9 independent experiments. * = $P < 0.05$ vs the control sample using one-way ANOVA with post hoc Tukey test.

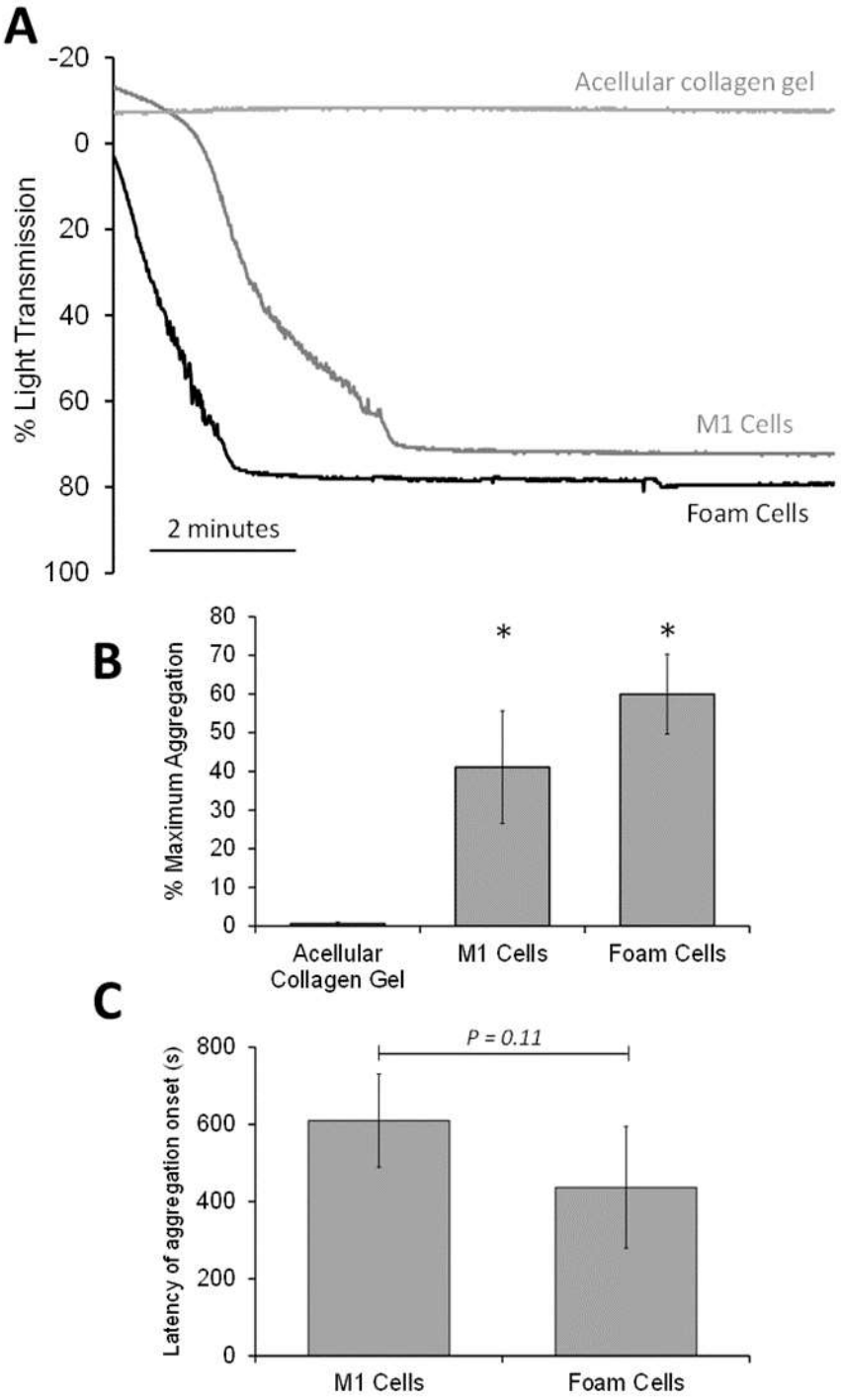

Figure 4.6: The 3D neointimal constructs trigger slow, weak platelet activation. (A) Washed human platelet suspensions resuspended in supplemented HBS containing 1 mM $CaCl_2$, were exposed to either an acellular compressed collagen hydrogel, or a 3D neointimal culture model containing either THP1-derived M1 or foam cells. The constructs were incubated for 10 minutes at 37°C under constant magnetic stirring. The gel was then removed, and the samples was transferred for monitoring on a light transmission aggregometer at 37°C under constant magnetic stirring for up to 16 minutes. (B, C) Bar charts summarising the mean maximum % aggregation observed during the recording period (B) and the mean time taken for the samples to begin to aggregate (C). Values shown are Mean ± SEM of 7 experiments,

*= P<0.05 relative to the acellular collagen hydrogel using a one-way ANOVA with post hoc Tukey test for (B) and a student's T-test for the indicated samples for (C).

the luminal surface of the construct for 10 minutes at 37°C under constant magnetic stirring. The sample was then transferred from the cuvette into a Chronolog aggregometer for further monitoring by light transmission aggregometry. As can be seen in Figure 4.6A, the acellular collagen hydrogel was not observed to elicit any significant platelet aggregation in any of the experiments (0.6 ± 0.4%), consistent with previous observations by Musa *et al*., (2016). In contrast, preincubation with either the M1- or foam cell-containing constructs was able to elicit platelet aggregation – however it was found to be slow in onset, with the time taken to transition from shape change into aggregatory responses occurring slowly after onset of monitoring on the aggregometer. On average this transition occurred earlier for foam cell-containing gels (437 ± 157s) compared to M1-cell containing constructs (610 ± 320s), although this effect was not significant (n = 7; P = 0.11; Figure 4.6B). Similarly, the maximum % aggregation measured over the 15-minute recording period was found to be greater in the foam cell-containing constructs (59.9 ± 10.3%), this was not found to be statistically greater than that elicited by the M1-containing constructs (41.0 ± 14.6%; n = 7; P > 0.05; Figure 4.6C). These data therefore indicate that whilst both foam cell- and M1 macrophage-containing gels can consistently elicit aggregation, but these responses are generally slow and variable in their time of onset – suggesting that these gels are only able to weakly activate human platelets in the absence of thrombin generation. A luciferin-luciferase dense granule secretion assay was performed on samples of the washed human platelet suspensions exposed to the 3D neointimal culture models to further assess the degree of platelet activation. As activated human platelets secrete ATP-containing dense granules into the extracellular medium, the light production by the luciferase solution added to the extracellular medium can be used to

indicate the extent of platelet activation. As shown in Figure 4.7, foam cell-containing gels elicited a significant increase in luciferase luminescence

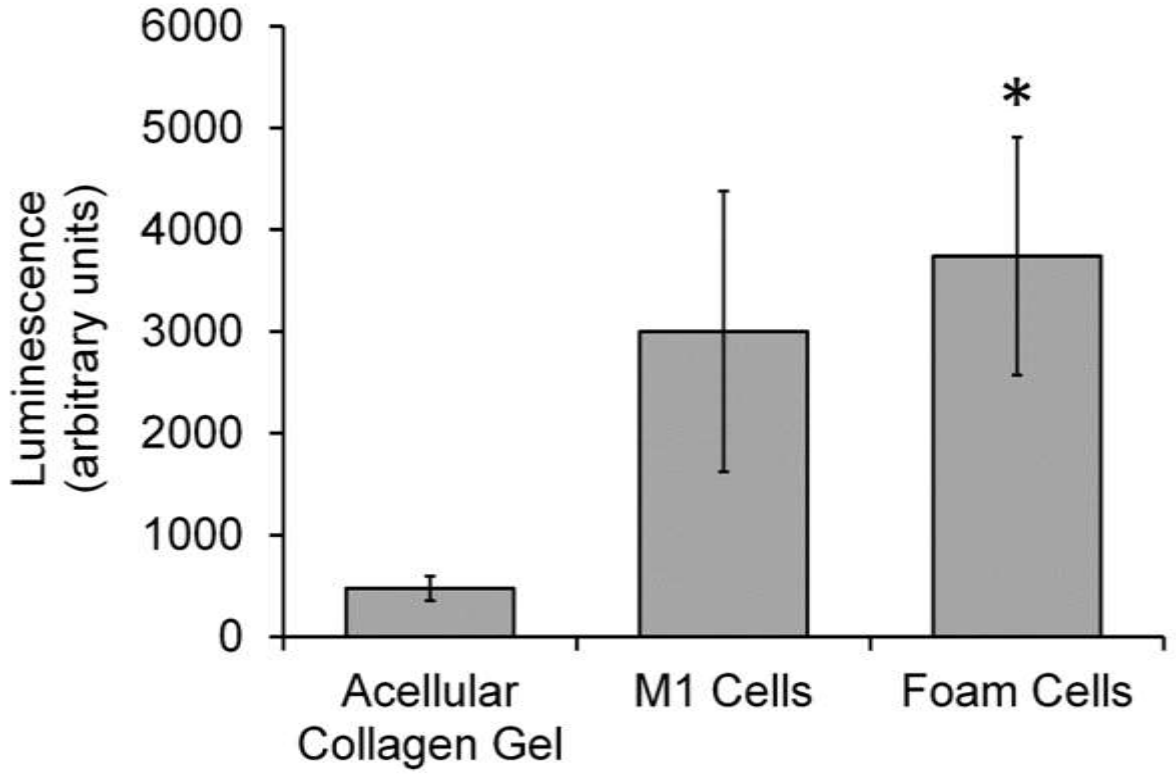

Figure 4.7: THP-1-derived foam cell containing hydrogels induces significant platelet dense granule secretion. Washed human platelet suspensions resuspended in supplemented HBS containing 1 mM $CaCl_2$, were exposed to either an acellular compressed collagen hydrogel, or a 3D neointimal culture model containing either THP1-derived M1 or foam cells. The constructs were incubated for 10 minutes at 37°C under constant magnetic stirring. The gel was then removed, and samples taken for aggregometry. The remaining platelet solution was transferred back to the water batch and incubated for a further 10 minutes. After this a sample was pipetted into a 96-well platelet and mixed with 20% [v/v] luciferin-luciferase, and luminescence read for 1 minute on a BioTek2 synergy microplate reader. n = 7, * = $P<0.05$ relative to the acellular collagen hydrogel using one-way ANOVA with post hoc Tuckey test. Values shown are Mean ± SEM of 3 experiments.

in washed human platelet suspensions (3740 ± 1169 arbitrary units) compared to samples exposed to acellular collagen gels (476 ± 121 arbitrary units; n = 7; P <0.05). M1-containing gels also elicited an intermediate increase in luciferase light production (3000 ± 1380 arbitrary units) compared to the foam cell-containing and acellular collagen hydrogels respectively, however this difference was insignificant compared to both other samples (P > 0.05 for both). These results are consistent with the aggregation data, with the greatest increase in luciferin luminescence elicited by foam cell containing gels correlating with the most rapid platelet aggregation.

4.2.6 Atorvastatin reduces the pro-aggregatory properties of the 3D neointimal constructs

Atorvastatin is widely used in the primary and secondary prevention of acute cardiovascular events in patients at risk of suffering thrombotic events. Previous studies have demonstrated that atorvastatin and other statins can inhibit tissue factor expression in monocytes and vascular cells (Hilgendorff *et al*., 2003; Owens and MacKman, 2012; Zheng *et al*., 2021; Eto *et al*., 2002; Bruni *et al*., 2003). Additionally, atorvastatin has been shown to reduce human platelet function (Tekten *et al*.,2003; Sanguigni *et al*., 2005). Therefore, 3D neointimal cell culture constructs were treated during the oxLDL loading period either with 20 µM atorvastatin or an equal volume of its vehicle, methanol (MeOH). As shown in Figure 4.8C, prior treatment with atorvastatin tended to reduce the extent of the maximum platelet aggregation observed (35.0 ± 2.0%) compared to the methanol control sample (72.0 ± 17.6%; n = 6), although this effect was not statistically significant (P = 0.07). Atorvastatin was found to significantly increase the latency of the onset of platelet aggregation (681 ± 140s vs 434 ± 129s for atorvastatin- and MeOH-treated constructs respectively; P < 0.05; Figure 4.8D).

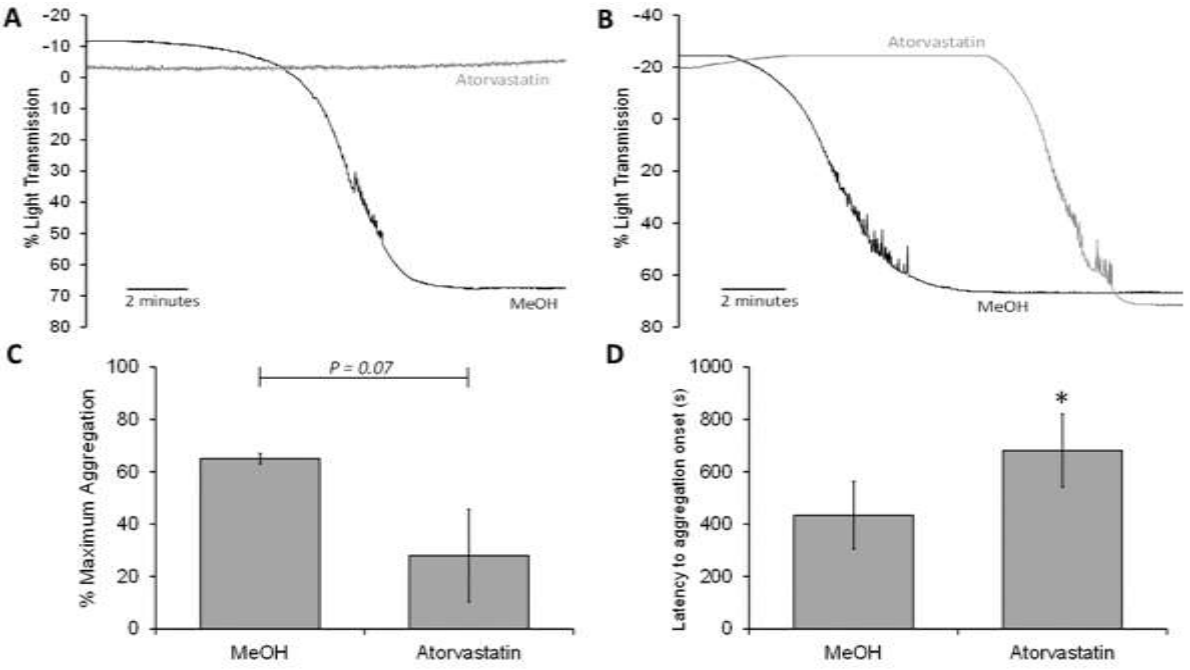

Figure 4.8 Treatment with atorvastatin reduces the pro-aggregatory properties of the 3D neointimal constructs. Washed human platelet suspensions resuspended in supplemented HBS containing 1 mM $CaCl_2$, were exposed to either an atorvastatin- or methanol (MeOH)-treated neointimal construct containing foam cells. The constructs were incubated for 10 minutes at 37°C under constant magnetic stirring. The gel was then removed, and the samples was transferred for monitoring on a light transmission aggregometer at 37°C under constant magnetic stirring for up to 16 minutes. Prior treatment of the 3D neointima with Atorvastatin has decreased the percentage of the maximum platelet aggregation in comparison with that of Methanol (35.0 ± 2.0% vs 72.0 ± 17.6%), although this was statistically insignificant (A &C). In addition, Atorvastatin has increased the latency of the platelet aggregation in comparison with that of Methanol (681 ± 140s vs 434 ± 129s), (A&D), * indicates p value< 0.05 using a student's-T test. Values shown are Mean ±SEM of 6 experiments.

In some experiments, the neointimal constructs that were exposed to the washed human platelet suspensions were fixed immediately after extraction to allow for assessment of platelet adhesion and aggregation upon the surface of the construct exposed to the washed human platelet suspension. To do this the samples were stained with Hoechst-33342 and a FITC-conjugated CD41a antibody that should specifically bind to human platelets and imaged using confocal microscopy to isolate the surface layer of the construct. Despite blocking with normal goat serum prior to the exposure to the antibodies, the primary antibody was found to bind non-specifically to the foam cells within the gel. Due to this limitation, platelet populations upon the surface of the construct were identified through counting cellular material stained with the CD41a antibody (Pseudocoloured red in Figure 4.9), but not Hoechst 33342 (pseudocoloured blue) as platelets are anucleate. Using this methodology, it was possible to identify platelet populations closely associated either above or adjacent to the nucleate foam cells on the surface of the construct. The density of these CD41+, Hoechst- populations on the surface of the construct were found to be significantly greater for methanol-treated samples (23.4 ± 4.6 populations/image) compared to atorvastatin-treated samples (9.0 ± 1.4 populations/image, $n = 4$; $P < 0.05$). As we have previously shown that the acellular collagen hydrogel alone does not support platelet activation (Musa *et al*., 2016), these data indicate that foam cells can trigger platelet a small upregulation of platelet binding to the neointimal construct in a manner that can be inhibited by atorvastatin pre-treatment. Further work will be required to confirm these findings in samples in which platelets have been differentially labelled from foam cells

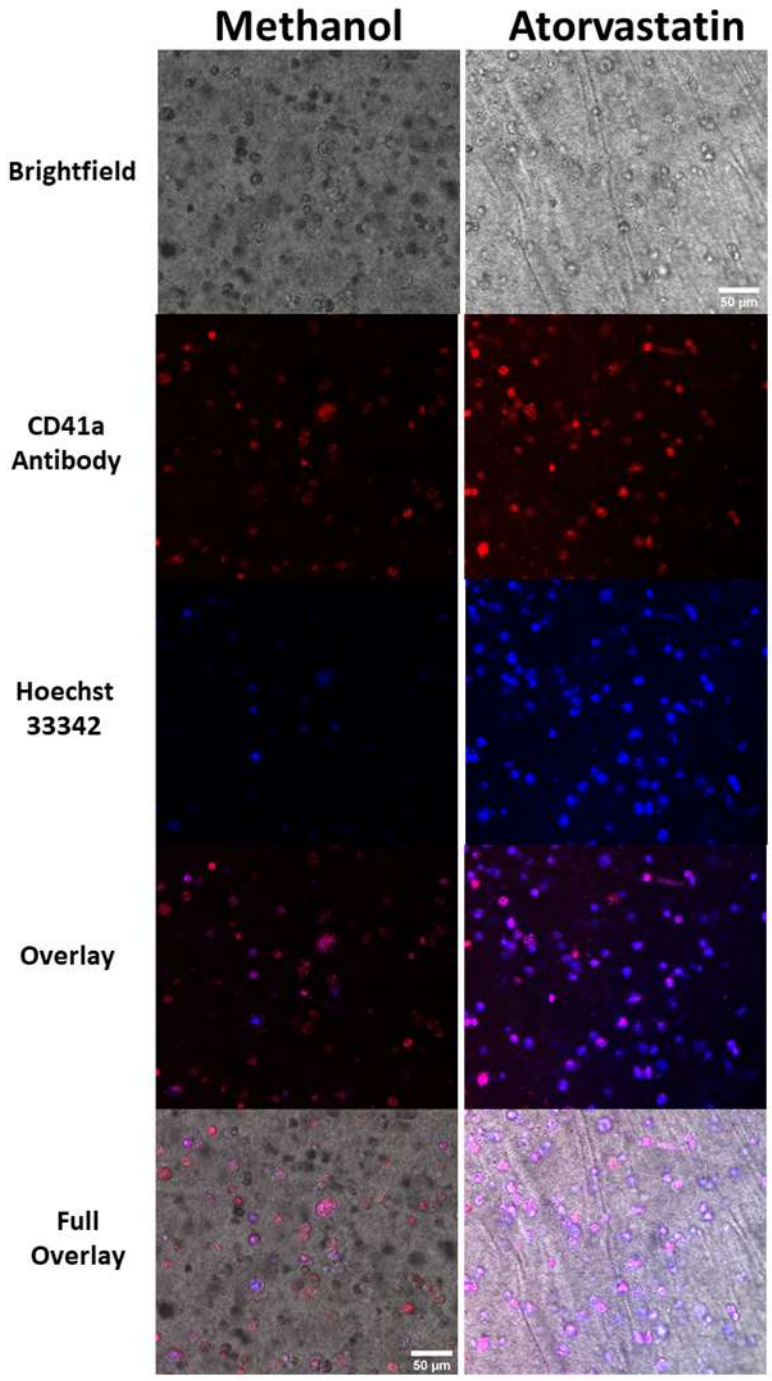

Figure 4.9 Treatment with atorvastatin reduces the interaction of human platelets with the 3D neointimal constructs. (A, B) Washed human platelet suspensions resuspended in supplemented HBS containing 1 mM $CaCl_2$, were exposed to either an atorvastatin- or methanol (MeOH)-treated neointimal construct containing foam cells. The constructs were incubated for 10 minutes at 37°C under constant magnetic stirring. The gel was then removed and fixed with paraformaldehyde. Samples were then stained with a FITC-labelled anti-CD41a antibody (red) and Hoechst 33342 (blue). The surface of the construct exposed to the washed human platelet suspension was then imaged using confocal microscopy. n=10

Luciferin-luciferase measurements also showed that atorvastatin treatment tended to reduce the dense granule secretion elicited by the foam cell construct, however this was currently insignificant due to the variability of the measurements (2385 ± 600 vs 1068 ± 398; Figure 4.10) for MeOH- and Atorvastatin-treated constructs respectively; n = 6; P = 0.14). These data indicate that atorvastatin treatment can reduce the pro-aggregatory potential of the 3D neointimal constructs, although further experimental repeats will be needed to confirm these initial data.

4.2.7 Atorvastatin reduces the pro-coagulant properties of the 3D neointimal constructs

Experiments also assessed the procoagulant properties of the foam cell-containing constructs after being treated with either atorvastatin or its vehicle, methanol. As shown in Figure 4.11, treatment with atorvastatin significantly increased the measured prothrombin time of the constructs compared to methanol-treated control samples 567 ± 93s vs 109 ± 34s for atorvastatin- and MeOH-treated constructs respectively; n = 3; $P < 0.05$; Figure 4.11). Control samples in which the platelet poor plasma was treated with calcium alone failed to induce visible fibrin formation after 30 minutes in two of the three samples tested, whilst the other sample took 1267s (1622 ± 177 s) – demonstrating that the faster fibrin formation is due to exposure to the constructs. Further repeats will be required to ensure the repeatability of the results. However, these initial studies indicate the likelihood that the develop 3D neointimal construct is able to replicate previous findings that show that atorvastatin treatment can reduce the tissue factor expression of monocyte-derived cells (Owens *et al*., 2012).

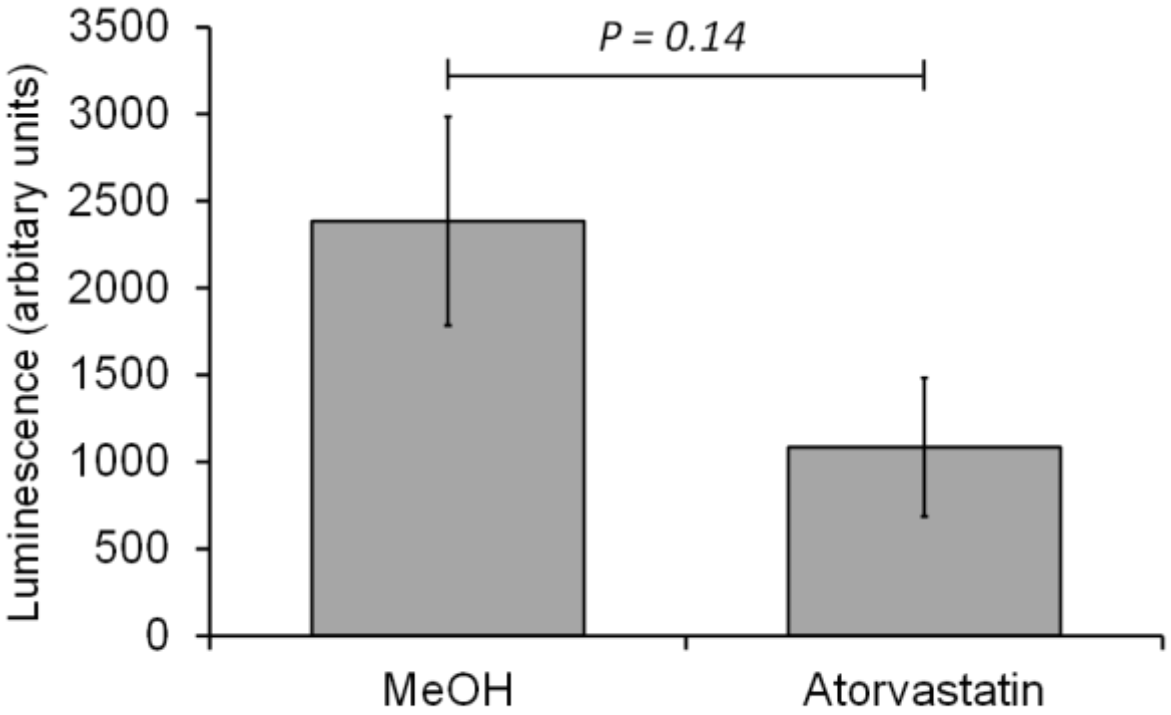

Figure 4.10 Treatment with atorvastatin did not significantly inhibit platelet dense granule secretion elicited by exposure to the 3D neointimal construct. Washed human platelet suspensions resuspended in supplemented HBS containing 1 mM $CaCl_2$, were exposed to either to either an atorvastatin (20 µM)- or methanol (MeOH)-treated neointimal construct containing foam cells. The constructs were incubated for 10 minutes at 37°C under constant magnetic stirring. The gel was then removed, and samples taken for aggregometry. The remaining platelet solution was transferred back to the water bath and incubated for a further 10 minutes. After this a sample was pipetted into a 96-well platelet and mixed with 20% [v/v] luciferin-luciferase, and luminescence read for 1 minute on a BioTek2 synergy microplate reader. Values shown are Mean ± SEM using a student's T-test. n= 6.

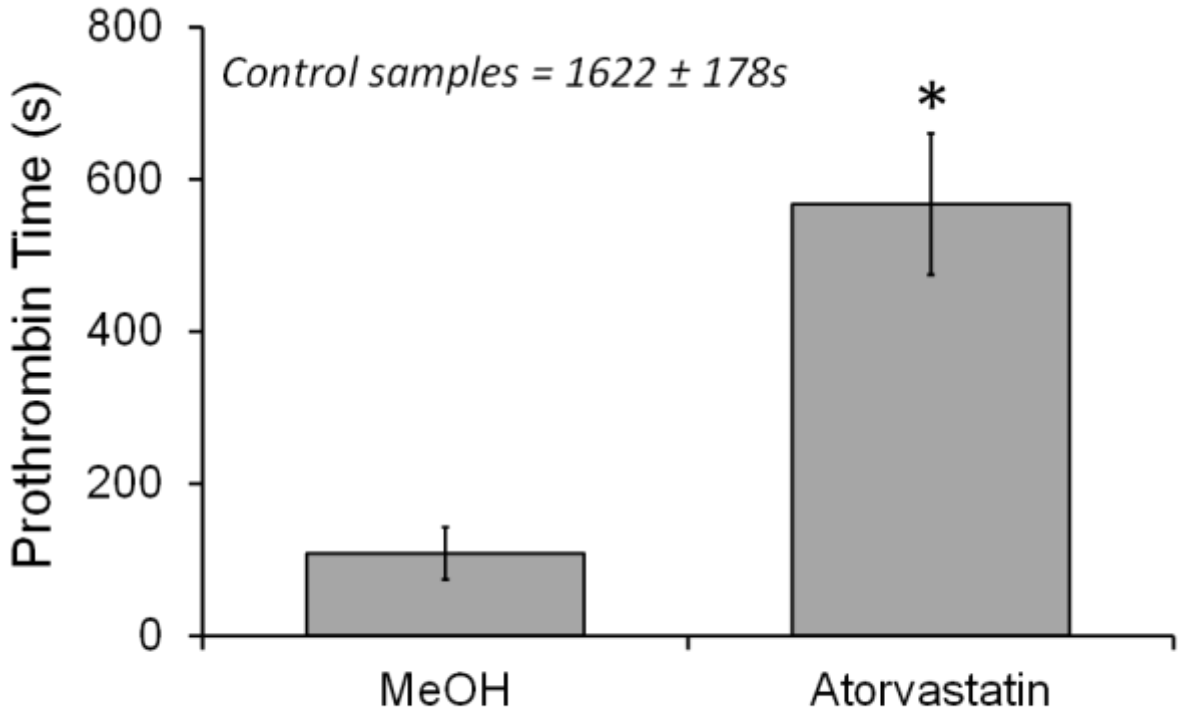

Figure 4.11 Treatment with atorvastatin reduces the procoagulant properties of the THP-derived foam cell constructs. 3D neointimal culture models were produced with THP-derived foam cells which were either treated with methanol (MeOH) or 20 µM atorvastatin at the same time as the oxLDL. At the end of the culture period, samples were placed onto sodium acetate frames and placed into contact with the surface of prewarmed, recalcified human platelet-poor plasma (PPP). A negative control was also conducted in which acellular collagen hydrogels were also monitored for procoagulant activity (data shown only in caption). The sample is kept warm in a 37°C water bath. The time taken for fibrin formation after addition of the 3D neointimal cultures models was recorded for each sample. Values shown are Mean ± SEM of 3 experiments. * Indicates $P < 0.05$ vs the methanol-treated sample using a student's T-test.

To further investigate the procoagulant properties of the atorvastatin-treated constructs, conditioned media samples were collected after the end of the final incubation with oxLDL and either atorvastatin or methanol and assessed for tissue factor activity using the SN-17a assay. As can be seen in Figure 4.12, conditioned media from both methanol- and atorvastatin constructs possessed observable tissue factor activity. No such activity was observed in samples in which Factor VII and SN-17a was added to HBS alone (ΔSN-17a fluorescence = -834 ± 246 ; n = 3). The tissue factor activity was found to be consistently greater in samples taken from Methanol-treated constructs (ΔSN-17a fluorescence = 46844 ± 3653) compared to atorvastatin-treated constructs (42258 ± 3821 increase; n = 6; $P < 0.05$) indicating that atorvastatin treatment reduces the expression of tissue factor expression in these THP-1-derived foam cell cultures.

4.2.8 Treatment with atorvastatin reduced the accumulation of lipids into THP-1-derived foam cells

Previous studies have demonstrated that statins are able to inhibit the uptake of oxidised LDLs by foam cells. This potentially occurs due to a number of differing effects including regulation of foam cell scavenging receptor expression, a tendency for lipids with lower oxidation potential to be loaded into LDLs, and the direct antioxidant properties of statins reducing the oxidative state of the LDLs (Hofnagel *et al*., 2009). To examine whether atorvastatin-mediated inhibition of oxLDL uptake could be replicated in our model, and if it could be responsible for the impact of this statin on inhibiting the activation of human platelets by the foam cell-containing neointimal construct, experiments were performed to

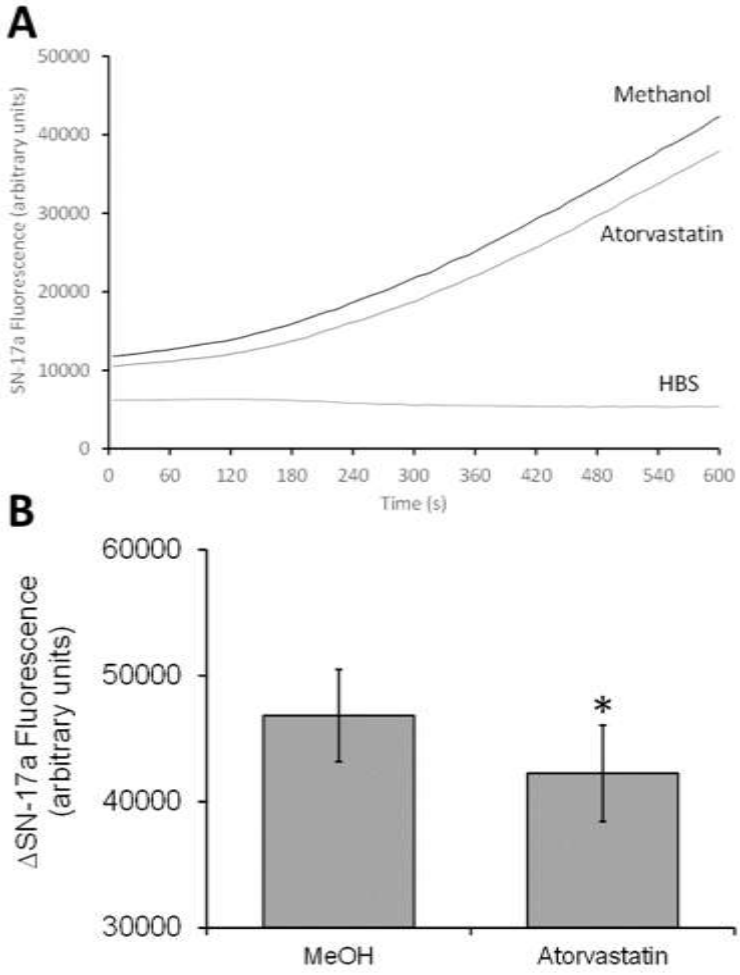

Figure 4.12 Atorvastatin decreases the tissue factor content of conditioned media extracted from the 3D neointimal constructs. 3D neointimal culture models were produced with THP-derived foam cells which were either treated with methanol (MeOH) or 20 µM atorvastatin at the same time as the oxLDL. At the end of the culture period, conditioned media was collected, and mixed with a $CaCl_2$-containing HBS, inactive Factor VII and SN-17a. (A) Fluorescence increases were then recorded for 15 minutes in a BioTek 2 Synergy microplate reader. (B) A bar chart summarising the mean increase in SN-17a fluorescence observed in methanol- and atorvastatin-treated constructs. * = $P < 0.05$ when compared to methanol treated control samples using a student's T-test. Values shown are Mean ± SEM of 6 experiments.

assess both the uptake of lipids into the foam cells, as well as the concentration of oxLDL remaining in the conditioned media after the incubation period with atorvastatin or methanol. As shown in Figure 4.13A, measurements of residual oxLDL remaining within the culture media at the end of the 72h culture period. An ELISA analysis of oxLDL within the culture media was then conducted and compared to the initial loading concentration to allow for a calculation of the residual oxLDL present. Although the proportion of the originally added oxLDL remaining in the sample was higher in atorvastatin-treated samples (5.6 ± 1.0%) than in methanol-treated samples (4.6 ± 0.4%; n = 6; P = 0.23) there was no significant difference in the residual oxLDL remaining within the sample. This may indicate that either there is no impact on cellular uptake of the oxLDL between atorvastatin-treated and control samples, or that there are other metabolic processes that may mask this difference through reduction or breakdown of the oxLDL during the prolonged loading period. To further clarify this, experiments were performed to directly assess the uptake of lipids into atorvastatin- and methanol-treated THP-1-derived foam cells. As can be seen in Figure 4.13B, an Oil Red O staining assay indicated that there is more lipid stored within the foam cells generated in methanol-treated conditions, than those neointimal cultures treated with atorvastatin. This data therefore is consistent with previous observations that statins block oxLDL uptake into macrophages and foam cells and indicates that oxLDL may be subject to other metabolic processes in the neointimal culture models other than scavenger receptor mediated uptake into the THP-1-derived foam cells.

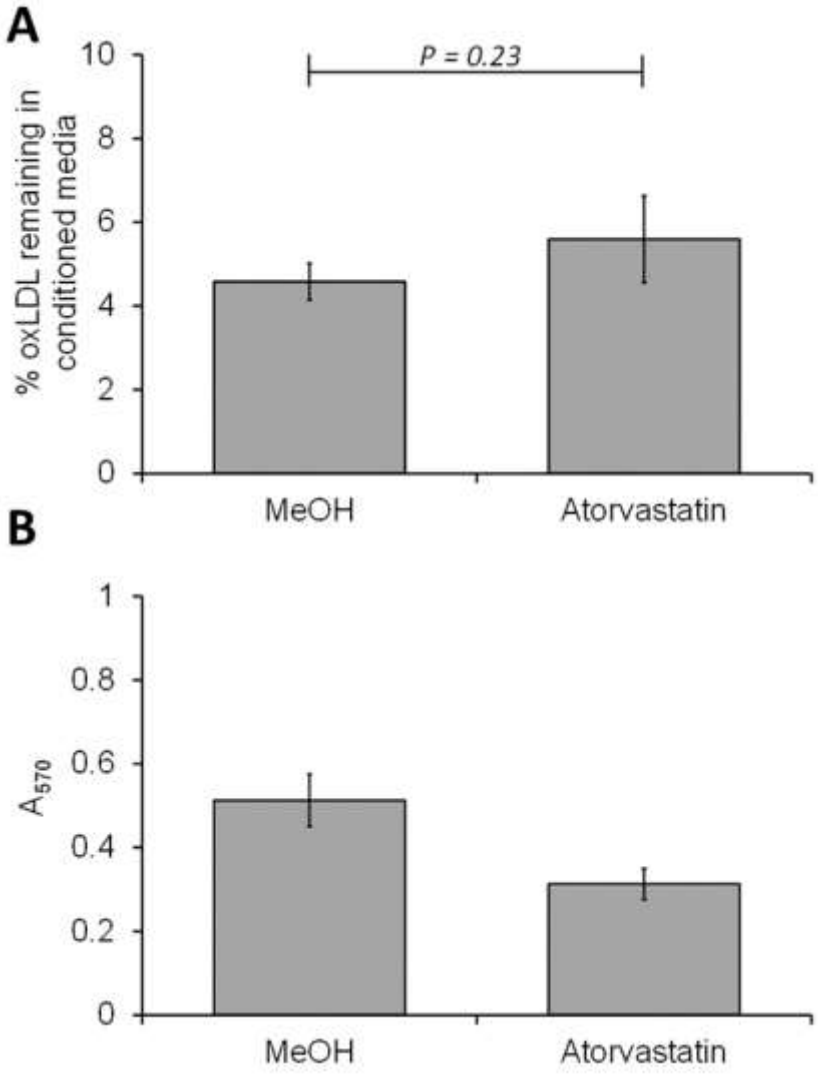

Figure 4.13. Atorvastatin treatment reduces lipid accumulation within THP-1-derived foam cells within the 3D neointimal co-culture model. (A) 3D neointimal culture models were produced with THP-derived foam cells which were either treated with methanol (MeOH) or 20 μM atorvastatin at the same time as the oxLDL. At the end of the culture period, conditioned media was collected and assayed for residual oxLDL using an ELISA assay kit performed according to the manufacturer's instructions. % Of residual was calculated against the initial concentration (33 μg/mL) added at the start of the experiment. (B) Washed human platelet suspensions resuspended in supplemented HBS containing 1 mM $CaCl_2$, were exposed to either an atorvastatin- or methanol (MeOH)-treated neointimal construct containing foam cells. The constructs were incubated for 10 minutes at 37°C under constant magnetic stirring. The gel was then removed and fixed with paraformaldehyde. The gels were then labelled with Oil Red O and washed three times to remove dye that remained unbound to intracellular lipids. After washing the remaining dye bound to intracellular lipids was leached out of the sample by incubation with isopropanol. The concentration of Oil Red O dye in the isopropanol sample was then measured by loading into a 96-well plate and using a BioTek 2 synergy microplate reader to assess sample absorbance at 570 nm. Values shown are Mean ± SEM of 6 experiments, * = $P < 0.05$ relative to the methanol-treated control using a students T-test.

4.2.9 Atorvastatin does not reduce IL-6 secretion from THP-1-derived foam cells cultured within the 3D neointimal culture model

In chapter 3 it was demonstrated that incubation with oxLDL induces an increased secretion of IL-6 into the culture media. Previous studies have demonstrated that atorvastatin can reduce the secretion of IL-6 from peripheral blood mononuclear cells (de Oliviera *et al*., 2020), and human platelets can be activated by IL-6 (Oleksowicz *et al*., 1994). Therefore, we hypothesised that the inhibitory effect of atorvastatin on platelet activation elicited by exposure to the 3D neointimal cultures may be due to reduced secretion of IL-6 from the 3D neointimal culture. However, no significant difference in IL-6 secretion could be observed in an assessment of IL-6 secretion into the conditioned media extracted from atorvastatin- and methanol-treated 3D neointimal cultures containing THP-1-derived foam cells (Figure 4.13). Therefore, atorvastatin does not function to reduce the prothrombotic effects of the neointimal culture model in this manner.

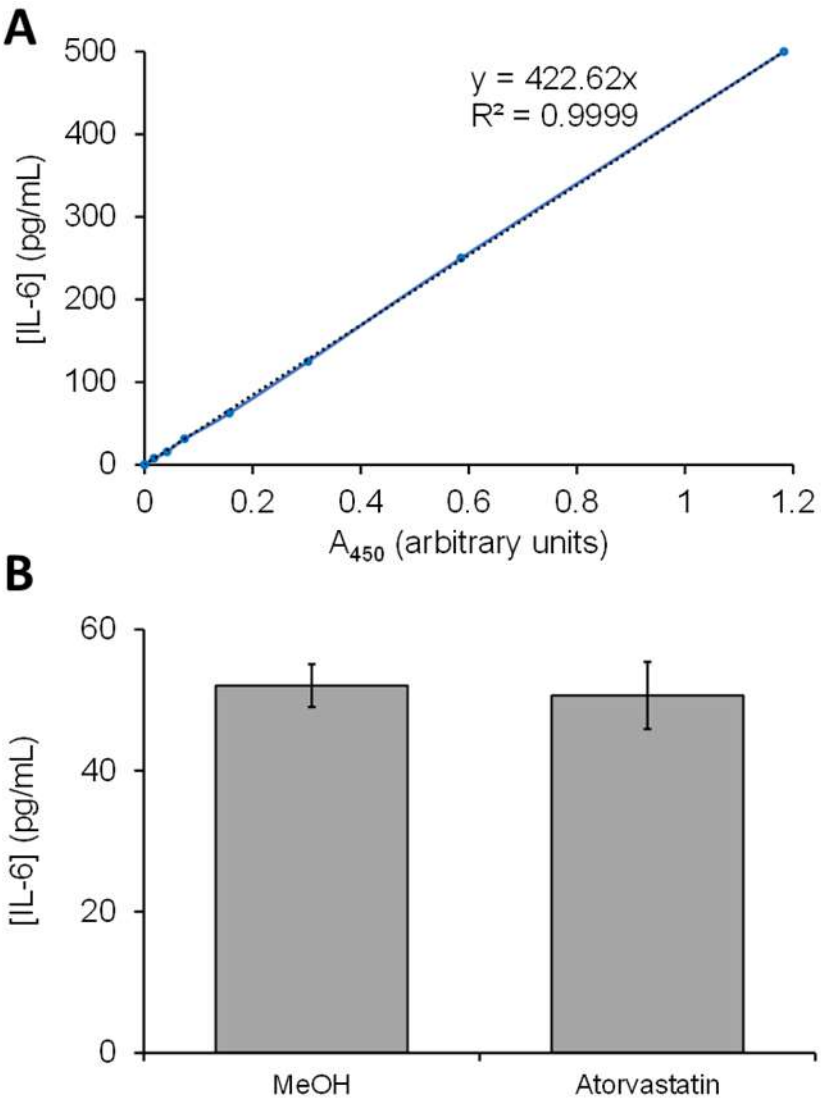

Figure 4.14. Atorvastatin does not reduce the IL-6 secretion of the THP-1-derved foam cell containing constructs. 3D neointimal culture models were produced with THP-derived foam cells which were either treated with methanol (MeOH) or 20 µM atorvastatin at the same time as the oxLDL. At the end of the culture period, conditioned media was collected and assayed using an IL-6 ELISA assay kit. (A) Calibration curve for the ELISA assay kit with using a student's T-test (B), n = 6.

4.3 Discussion

In this chapter, we have evaluated the potential prothrombotic effects of the 3D tissue engineered neointima containing THP-1-derived foam cells. The results demonstrate that the THP-1-derived foam cells within the gel provide a strong procoagulant activity as well as a weaker pro-aggregatory response to the construct. These data represent the first experimental evidence that a tissue-engineered model of a human atherosclerotic plaque can replicate the ability of an *in vivo* plaque to trigger the activation of the haemostatic system, and as such represents a viable method to study the atherothrombotic responses underlying myocardial infarction and stroke in an ex vivo environment.

4.3.1 THP-1-derived foam cells provide significant tissue factor activity to the 3D neointimal constructs

Many studies have reported the presence of significant tissue factor activity in *in vivo* atherosclerotic plaques (Wilcox *et al*., 1988; Annex *et al*., 1995; Marmur *et al*., 1996; Ardissino *et al*., 1997; Hatakeyama *et al*., 1997). This tissue factor activity has been shown to be associated both with foam cells and vascular smooth muscle cells, as well as microparticles created by apoptosis of foam cells within the plaque (Marmur *et al*., 1996; Kaikita *et al*., 1997; Landers and Gupta, 1994). Wilcox *et al.*, (1989) have reported that necrotic core of the atherosclerotic plaque is particularly rich with TF, which is the principal location of foam cells within the plaque. These data therefore suggest that a valid tissue-engineered model of the atherosclerotic plaque should possess significant tissue factor activity. As shown in Figure 4.3, the inclusion of THP-1-derived foam cells within the 3D neointimal cell culture model

provides a significant source of tissue factor activity within the construct, and this can trigger rapid activation of the coagulation cascade in PPP (Figure 4.1). These data therefore demonstrate that the model can effectively replicate the procoagulant properties of the atherosclerotic plaque. The data is consistent with previous findings that showed treatment with oxLDL is able to upregulate tissue factor activity of both THP-1 derived and SMCs-derived foam cells (Colli *et al*., 1999; Lesnik *et al*., 1992; Schwartz *et al*., 1981; Meisel, *et al*., 2011). This have been shown to occur through oxLDL-mediated activation of the NF-κβ tissue factor (nuclear factor -kappa B tissue factor) (Mackman *et al*., 1991; Sanguigni *et al*., 2005). Through augmenting this signalling pathway, it may be possible to further enhance the expression of tissue factor activity in these constructs. For example, previous studies have demonstrated that tissue factor activity can be augmented in THP-1 cell cultures through inclusion of Monocyte chemoattractant peptide-1 (Schechter *et al*., 1998). Thus, further optimisation of the culturing conditions may be able to further improve the thrombogenic properties of these constructs.

4.3.2 THP-1-derived foam cells activate human platelets exposed to the 3D neointimal constructs

As shown in Figures 4.5-4.9, the 3D tissue engineered can induce slow platelet activation and aggregation. This effect is mediated by the presence of M1- and THP-1 cells within the constructs, as the acellular collagen hydrogel was found not to possess this same activity. This is consistent with previous studies that have demonstrated that the soluble collagen hydrogel does not possess the requisite tertiary structure of collagen required to activate human platelets (Musa *et al*., 2016). These results therefore provide a first demonstration that foam

cells can elicit platelet activation. This work demonstrates one of the potential advantages of this layer-by-layer fabrication method as it allows us to identify novel intercellular interactions such as this, through allowing us to selectively alter the composition of the neointimal layer and examine how this modifies the responses of blood cells and cells of the vascular wall. The mechanism by which the THP-1 activity is elicited is unclear – this could be due to the release of a soluble platelet activator, the synthesis of an adhesive ligand on the surface of the 3D neointimal construct or directly providing a platelet-binding surface on the cell surface. The ability of M1 cells to inconsistently evoke this response, indicates that this stimulus is likely to be present in M1 cells but is upregulated by oxLDL treatment. Due to the slow and variable speed of the activation of the response it is unlikely that this is a strong platelet activator such as collagen or thrombin. The ELISA data presented here suggests that this is unlikely to be related to the release of IL-6, which is the cytokine that was observed to be released at greatest concentration from the neointimal cultures in chapter 3, as atorvastatin treatment does not impact on the release of this cytokine. However, other cytokines might also be involved. TNF-α production has also been shown to be enhanced by oxLDL production in our cultures, and therefore this might also represent another potential low-level activator of human platelets. Pignatelli and colleagues have documented a correlation between platelet activation and the plasma level of TNF- α among patients with heart failure in comparison with control group. In this *In vitro* study they have documented an upregulation for the platelets TNF-receptors expression. Furthermore, they have reported a statistically significant decrease in the platelet activation after they treated the plasma of the study group with TNF-antagonist and inhibitors of arachidonic acid. This indicates that the TNF- α may play an essential role in platelet activation in this situation through stimulation of arachidonic acid synthesis (Pignatelli *et al.*, 2005). This idea has been supported by another study has reported

that TNF- α stimulate platelet activation through upregulation of the platelet CD40L (which is a protein that has proinflammatory and procoagulant effects) among patients with heart failure in comparison with healthy control group. In this *in vitro* study they have documented that plasma TNF-α upregulated CD40L. Interestingly CD40 has been shown to be expressed in macrophages in atherosclerotic plaques (Häkkinen *et al*., 2000) – suggesting the possibility that TNF- α produced in the construct could initiate an expression of this cell surface ligand on the surface foam cells, which in turn could trigger platelet adhesion and activation on the surface of the construct. This would be consistent with the observation of binding of $CD41^{+}$, Hoechst- populations on the surface of the construct in close proximity to foam cells (Figure 4.9). Alternatively, the production of adhesive extracellular matrix molecules may play a key role in recruiting platelets to the surface of the construct. Generally, macrophages are considered principally to degrade the extracellular matrix through the production of matrix metalloproteinases, however, studies have demonstrated that they are able to synthesise collagen VI (Schnoor *et al*., 2008), which has been demonstrated to be able to trigger human platelet activation (Ross *et al*., 1995). However, it is unclear whether oxLDL application can upregulate collagen VI production in foam cells. Therefore, further experiments will be required to further assess this activating interaction between human platelets and THP-1-derived foam cells within the neointimal culture model.

4.3.3 Treatment with atorvastatin reduces the pro-aggregatory and pro-coagulant properties of the 3D neointimal constructs

Statins are known to decrease the morbidity and mortality of CVD (Davi and Patrono, 2007; Gallone *et al*.,2018) through a variety of different effects including counteracting dyslipidemia

(Cheng *et al*.,2009), decreasing platelets activation (Pignatelli *et al*.,2012), as well as their anti-inflammatory effects (Mobarrez *et al*., 2011). In this chapter, experiments have demonstrated that pre-treatment with atorvastatin significantly impacts on the thrombogenic properties of the 3D neointimal constructs through both reducing the proaggregatory and procoagulant properties of the construct. From the initial data seen here this does not appear to be a specific impact on IL-6 secretion as the rate of production of this cytokine appears not to be affected by atorvastatin treatment. However, we can see a significant reduction in the accumulation of lipids within the foam cells of our 3D neointimal constructs. This is consistent with previous studies that have reported that statin can decrease the intracellular lipid contents by stimulating the cholesterol efflux from foam cells (Chong *et al.*, 2020; Yu *et al.*, 2019.,Zheng *et al*.,2021). Pre-treatment with atorvastatin also induced a slight reduction in the % of residual oxLDL left over in the conditioned culture media at the end of the incubation period, however this was found not to be statistically significant. The lack of significant effect may be due to the prolonged incubation period masking a slowing of the loading of oxLDL into these samples, by allowing both samples to load to saturation. Alternatively, this experiment assumes that no other factors are involved either in modifying the oxidation state of the LDL or triggering their breakdown with the 3D culture environment during the course of the experiment – if other methods exist to remove oxLDL from the culture media these may also impact on our ability to detect a reduced lipid loading in this manner. Therefore, direct measurement of lipid loading within the foam cell is likely to represent a more accurate method for assessing the impact of statins here. As uptake of oxLDL has been shown to induce a number of changes in the cellular phenotype of foam cells (Bekkering *et al*., 2014), further assessment of the impact of atorvastatin on these genetic and epigenetic responses will be required to assess how atorvastatin has its impact on platelet

function. However, through replicating the anti-thrombotic properties elicited by atorvastatin treatment, these studies have demonstrated the potential of using the 3D neointimal culture model as a humanised model of atherosclerosis. This model could be used to screen the effects of drugs and drug combinations on preventing atherothrombotic events prior to clinical trials. This would provide a potential replacement to at least some of the *in vivo* models currently used in modelling human atherosclerosis.

4.4 Conclusion

In this chapter it has been demonstrated that the 3D neointimal model possesses the prothrombotic properties of the native plaque, through their ability to induce the activation of the blood coagulation cascade and weakly activate human platelet aggregation. This represents the first demonstration that a tissue-engineered atherosclerosis model can trigger significant thrombotic effects. Interestingly these pro-thrombotic effects were inhibited by pre-treatment of the 3D neointimal constructs with atorvastatin, consistent with the known ability of this statin to reduce the incidence of acute cardiovascular events in patients at risk of myocardial infarction. These studies therefore demonstrate the potential capability of the developed neointimal model as an *in vitro* humanised drug testing platform to assess the impact of novel drugs and drug combinations on atherothrombosis.

Chapter 5: Assessing the impact of the 3D neointimal cell culture model on the cellular phenotype of cocultured smooth muscle and endothelial cells

5.1 Introduction

Atherosclerosis is a complex pathology, with Its development and progression dependent upon two predominant factors - inflammation and lipid accumulation within the arterial wall. Several metabolic and genetic factors are involved in the pathogenesis of this disease (Libby *et al.*, 2019). The formation of an atherosclerotic plaque starts at a dysfunctional endothelial segment (Costa *et al*., 2016). Under normal conditions, endothelial cells create a tightly-meshed monolayer that covers the entire internal surface of the blood vessels (Qiu *et al.*, 2020; Qiu *et al*.,2021). Endothelial cells synthesize a range of molecules such as prostacyclin (PGI_2), NO, tissue factor pathway inhibitor and anti-thrombin III, to prevent platelet aggregation and activation of the blood coagulation cascade. Additionally, the healthy endothelial surface provides an anti-inflammatory lining to prevents leukocytes adherence and migration out of the blood vessel (Mitchell *et al*., 2008), and is characterized by high expression of CD31 (an endothelial cell marker) and minimal expression for ICAM1 (Granger and Senchenkova, 2010). When endothelial cells are exposed to toxic or inflammatory molecules, such as a high level of LDL molecules, this will lead to endothelial cell dysfunction (Qiu *et al*., 2020). Endothelial cells will start to produce adhesion molecules such as intercellular adhesion molecule-1 (ICAM-1), vascular cell adhesion molecule-1 (VCAM-1), ICAM2 and platelet endothelial cell adhesion molecule-1 (PECAM-1) as a response to the inflammation (Golia *et al*., 2014). These cell surface receptors will facilitate adhesion of leukocytes to the wall and facilitate their extravasation into the subendothelial space, where

they differentiate to macrophages. Additionally, inflammation will increase the permeability in the intercellular junctions, allowing plasma molecule such as LDL to enter the subendothelial space (Varghese *et al*., 2017). Here the LDL particles are subject to chemical modifications such as oxidation, acetylation, and desialylation, that facilitates their uptake by macrophages (Bobryshev *et al.*, 2016). The engulfment of the thrombogenic oxLDL triggers the formation of foam cells (Lillis *et al*., 2015). Further accumulation of foam cells will create fatty streaks, which is one of the earliest stages in atherosclerotic plaque development. After phagocytosis of oxLDL, the resultant foam cells increase their synthesis and secretion of cytokines and matrix metalloproteinase, that help to propagate the local inflammatory responses. These chemical signals include cytokines such as IL-1ß, IL-6, TNF-α, and platelet derived growth factor (PDGF; Biros, *et al*., 2021)

The inflammation in the affected vascular segment triggers the upregulation of pro-oxidative enzymes in macrophages, endothelial cells, and smooth muscle cells to trigger production of more oxLDL. These include enzymes such as myeloperoxidase, nitric oxide synthase, and 15-lipoxygenase (Bobryshev *et al.*, 2016) . Through reinforcing the inflammatory phenotype of the endothelial cells, the foam cell-produced cytokines trigger further recruitment of leukocytes, as well as increasing the endothelium's contribution to the oxidative modification of LDL in the subendothelial space (Westthorpe *et al*., 2012), thus favouring the expansion of the atherosclerotic plaque. Additionally, the pro-inflammatory cytokines and matrix metalloproteinases released by foam cells also contribute to alterations in the cellular phenotype and tissue remodelling that are required for the development of the atherosclerotic plaque to more advanced stages such as the fibroatheroma.

In the healthy blood vessel, the *tunica media* predominantly contains smooth muscle cells adopting a contractile phenotype that enables its effective participation in vasomotor responses of the artery. Contractile smooth muscle cells possess specific markers like smooth muscle cell actin, smooth muscle cell myosin heavy chain, and smoothelin (Bennett *et al*., 2016). Due to the inflammatory environment, smooth muscle cells within the tunica media switch from their normal contractile phenotype to a proliferative phenotype and begin to migrate to the intima. Once here they proliferate, assisting in the thickening of the neointima and the formation of the fibrous cap of the fibroatheroma. Additionally, proliferative smooth muscle cells also increase their deposition of extracellular matrix components, such as Type I collagen. This can play a significant role in mechanically strengthening the developing plaque and can help prevent against plaque rupture. The switch in smooth muscle cell phenotype occurs both through the loss of inhibitory signals (such as NO) from the dysfunctional endothelium and due to the localized release of cytokines such as IL-1β and platelet-derived growth factor (PDGF) from endothelial cells and macrophages (Sheikine and Hansson, 2006). Previously it has been suggested that it is difficult to assess vascular smooth muscle cell (VSMC) migration in human atherosclerotic plaque because the migrated cells do not have specific markers (Bennett *et al*., 2016). Therefore, a methodology which allows us to better assess VSMC migration could improve our ability to assess ways to slow the development of atherosclerotic plaque. Bennett *et al*., (2016) have also reported that matrix metalloproteinase, an enzyme secreted from neointimal macrophages and foam cells, promotes VSMCs phenotypic switching and enhances their proliferation and migration (Bennett *et al*.,2016). These phenotypically switched VSMCs play an essential role in the progression of the atherosclerotic plaque, as they will be the principal constituent of the fibrous cap. Some reports have thus considered a high density of VSMCs within the fibrous

cap as a protective step against plaque rupture (Xue *et al.*, 2020). Furthermore, it has been reported that most of these phenotypically switched VSMCs lack the expression of the common cell markers of the contractile VSMCs and instead start to express macrophage cell markers, like CD11b and CD68 (Feil *et al*., 2014). One study has documented that about 20% of CD68 cells in the advanced atherosclerotic plaque were VSMCs in origin (Gomez *et al*., 2013). Similarly, epigenetic research has reported that 38% of foam cells within late coronary atherosclerotic plaque were of VSMCs origin (Shankman *et al*., 2015). Allahverdian and colleagues have reported that SMCs can take up lipids in a similar manner to macrophages, and demonstrated that 50% of all foam cells in human atherosclerotic plaques are of smooth muscle origin(Wang *et al.*, 2019; Allahverdian *et al*., 2014), suggesting that these play a key role in maintaining the local inflammatory state and deciding the fate of the developed plaque.

Once SMC invades the neointimal space, they will begin to produce and release a range of extracellular matrix molecules such as collagen and proteoglycans, leading to creating a fibrous cap that lies between the endothelium and the collected foam cells. C-X-C motif chemokine 12 (CXCL12) is a protein responsible for regulating several biological processes. Overexpression of this protein was associated with a high rate of VSMCs proliferation and their transformation to foam cells. Antagonizing the effect of this chemokine may decrease the rate of VSMs derived foam cells formation, which could suppress the progression of atherosclerosis (Li *et al.*, 2020).

In addition to the cellular components, extracellular matrix proteins play a role in the pathogenesis of atherosclerosis. The essential interstitial substances in arteries are collagen and elastin. Type I and III collagen are the most common types that have been observed in

atherosclerotic plaque (Bentzon *et al.*, 2014), as well as providing mechanical strength to the wall, these collagens also contribute to the thrombogenic properties of the subendothelial matrix, playing a key role in atherothrombosis after plaque rupture (Clemetson and Clemetson, 2001). Matrix metalloproteinases released by macrophages also breakdown collagen and other extracellular matrix proteins, with the resultant products of this proteolysis enhancing VSMCs proliferation and migration (Fukumoto *et al*., 2004).

5.2 Aims and objectives

A valid *in vitro* model of the atherosclerotic plaque should be able to induce similar inflammatory changes in the phenotype of the blood vessel wall to that seen *in vivo* in the native plaque. In this chapter, the experiments aimed to establish coculture models incorporating the neointimal model and assess the impact of the 3D neointimal cell culture model on the phenotype of the cocultured smooth muscle and endothelial cells.

Objective 1: Establish the optimal parameters for creating neointimal co-cultures with endothelial and smooth muscle cells to facilitate the development of a full tissue-engineered atherosclerotic vessel that can undergo plaque rupture.

Objective 2: Investigate whether coculture of the neointimal model with human coronary artery smooth muscle cells (HCASMCs) can induce phenotype switching away from a contractile phenotype and towards a migratory, proliferative phenotype

Objective 3: Assessing the impact of co-culture of the neointimal model with human umbilical vein endothelial cells (HUVECs) on their anti-thrombotic and pro-inflammatory properties

5.3 Results

5.3.1 Optimizing media composition to allow optimal foam cell viability when cocultured with endothelial and smooth muscle cells

Previous work by Musa *et al*., (2016) and Njoroge *et al*., (2021) have utilized a layer-by-layer fabrication method to create tissue-engineered blood vessel constructs in which tissue-engineered intimal and medial layers were cultured separately prior to attachment using a collagen hydrogel adhesive, followed by a further period of coculture to allow full proliferation and maturation of cells. The intimal layer was created by culturing HUVECs on top of fibronectin-coated aligned PLA (Poly-L, D-lactic acid (96% l/4% d) nanofibers, whilst the medial layer was created by culturing HCASMCs within a non-compressed collagen hydrogel (Musa *et al.*, 2016).

In this project we aim to create a tissue-engineered blood vessel incorporating a neointimal layer between these constructs. To effectively coculture the foam cell constructs within HUVEC and HCASMCs, it is important to optimize a culture media that facilitates foam cell viability whilst allowing optimal development and proliferation of the cocultured cell. Experiments were conducted to assess the viability of foam cells when cultured in both Medium 200 and Medium 231. After culturing of THP-1-derived foam cells within the neointimal model for 10 days, the samples were transferred to either fresh RPMI (foam cell culture media), or complete Media 200 (endothelial cell culture media) or Media 231 (smooth muscle cell culture media). The cells were then incubated for a further 4 days and then cell viability of the THP-1-derived foam cells was assessed. As shown in Figure 5.1, foam cell viability was found to be largely unaffected by culturing within either the endothelial or smooth muscle cell media, with cell viability found to be comparable for cell cultured within

Media 200 (86.7 ± 1.6% of cells viable), Medium 231 (87.5 ± 0.9% of cells viable) and the base media for foam cells, RPMI (88.5 ± 1.6% of cells viable, n =18). These data therefore indicate that foam cells remain sufficiently viable when cultured within both the endothelial and smooth muscle cell culture media. Therefore, it was deemed viable to utilize the optimal conditions for endothelial and smooth muscle culture for the future coculture experiments.

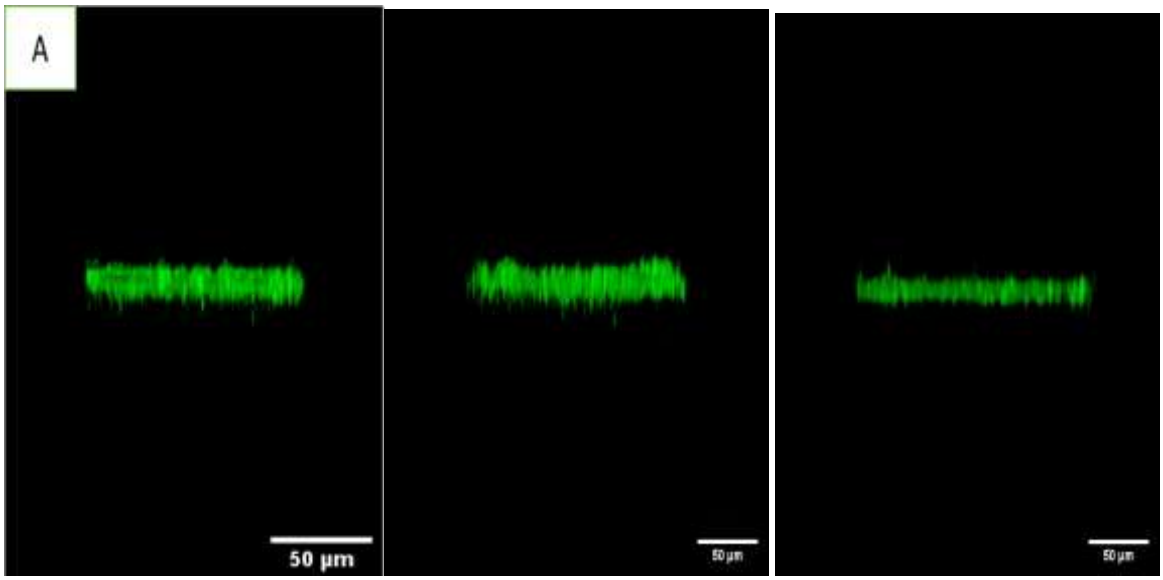

Figure 5.1 Cell viability of the compressed THP-1-derived foam cells within the neointimal model when cultured in different culture media. On the tenth day of the neointima experiment, the neointimal construct was placed into either (A) complete RPMI media (B) Complete Medium 200 or (C) Complete Media 231. The collagen hydrogels of the foam cells were then cultured for a further 4 days at 37°C, 5% CO_2 . After the culture period, the sample was stained with a Live/Dead Cell Staining Kit II and imaged using confocal microscopy. n=6

5.3.2 Creating a fibrin gel-based adhesive to create a reversible attachment of the neointimal culture to the tissue-engineered medial layer

The key clinical event in atherosclerotic plaque development is the process of plaque rupture or erosion that allows for the exposure of the thrombogenic contents of the neointimal layer to the flowing blood. To ensure that the developed tissue-engineered atherosclerotic arterial model can replicate this key event, a method will be required to facilitate reversible detachment of the tissue engineered neointimal layer from the underlying medial construct. Previously Musa *et al*., (2016) developed the use of freshly made collagen hydrogel to create effective attachment of the intima layer to the medial layer. Whilst this provide strong attachment of the constructs together it would be difficult to effectively detach these structures without disrupting the underlying tissue-engineered medial layers. Fibrin gels are widely used as a natural biodegradable scaffold for the construction in vascular tissue engineering (Shaikh *et al*., 2008; Li *et al*., 2015). They are made by mixing thrombin together with a calcified fibrinogen solution. The kinetics of fibrin formation and the density of fibrin fibres are dependent upon the concentration of calcium, thrombin, and fibrinogen, and so can be modified to provide different hydrogel properties dependent upon the use. A fibrin polymerization assay was performed to determine the thrombin required to initiate effective and reproducible fibrin gel formation. An ideal concentration would provide a high fibrin fibre density (high absorbance) but not start to polymerize for around 5 minutes after thrombin addition to provide time to pipette onto the construct and allow for appropriate alignment of the attached neointimal and medial constructs. As shown in Figure 5.2, a final concentration of 0.5 U/mL thrombin was found to reproducibly produce a dense fibrin gel, whilst not initiating fibrin production and polymerization too rapidly to ensure that it does not set

prematurely. This dose of thrombin was therefore used going forward in further experiments.

5.3.3 The use of fibrin gel followed by plasmin treatment permits reversible detachment of the tissue engineered constructs

Using the fibrin gel production method, we successfully attached together a compressed and non-compressed hydrogel to examine if we could attach the respective scaffolds of the 3D neointimal layer and the tissue-engineered medial layer using this fibrin adhesive solution. As can be seen in Figure 5.3A, B this permitted strong attachment of the constructs.

The breakdown of the fibrin scaffold holding together blood clots is mediated by plasmin *in vivo* (Chapin and Hajjar, 2015), as such this protease could be used to help selectively target the fibrin gel holding together the constructs and permit reversible detachment of the constructs. As shown in Figure 5.3C, these layers could be easily separated manually after treatment of the conjugated hydrogels using a PBS solution containing 30nM plasmin for one hour at room temperature. Following this treatment compressed collagen hydrogels were conjugated to a complete tissue engineered medial layer construct containing human

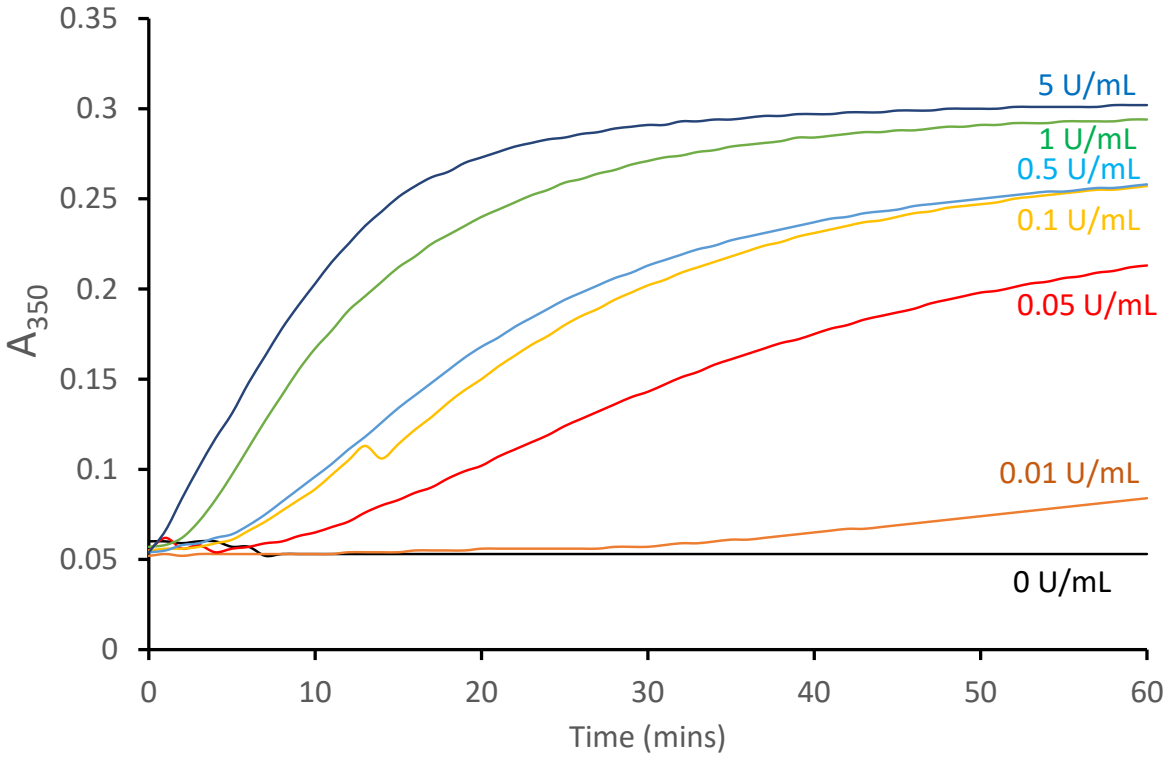

Figure 5.2. Fibrin gel polymerization assay. A 3 mg/mL fibrinogen solution made in HBS containing 5 mM $CaCl_2$ was mixed with a range of concentrations of thrombin, and the rate of absorbance was recorded at 350 nm by a microplate reader every minute for 1 hour. The results are representative of 4 independent experiments.

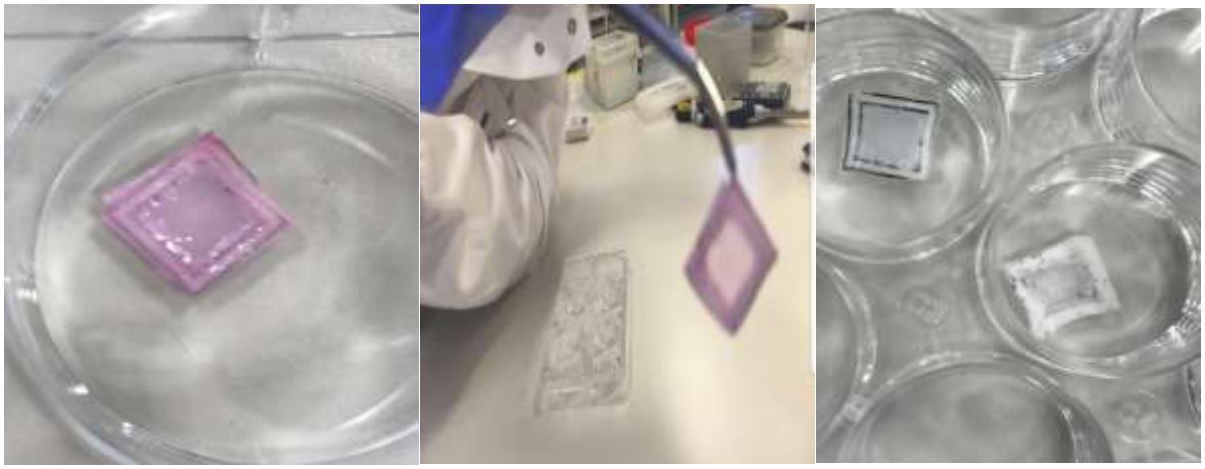

A B C

Figure 5.3 Plasmin-induced detachment of the neointimal-medial co-constructs produced using a fibrin attachment solution. The collagen hydrogels of the compressed neointima and the non-compressed medial layer were prepared using the same method. The two layers were attached together using a fibrin gel made by mixing a 3 mg/mL fibrinogen solution containing 5 mM $CaCl_2$ with 0.5 U/mL thrombin. Immediately after mixing, 20 -30 µL of the fibrinogen solution were distributed over the corners of the media layer then the collagen hydrogel of the neointima layer was put over it. The gel was left to set for 1 hour at room temperature prior to experiments. (A) A picture of the attached hydrogels. Note the two sets of filter paper frames that allow for independent handling of each construct. (B) A demonstration of the attachment, as the filter paper frame of one construct is held independently of the other gel. (C) The hydrogel conjugate was then treated for 1 h at room temperature with a 300 µL PBS solution containing 30nM Plasmin. Following this treatment, the gels were picked up by one of the filter paper frames of the conjugate to assess whether the attachment held. As shown, the gels could be separated easily whilst remaining intact. n=2

coronary artery smooth muscle cells using the fibrin attachment solution, and then detached using a plasmin detachment solution using the same methodology indicated above. Using this methodology, it was possible to successfully separate the cellular and acellular constructs. To assess whether the plasmin or the manual handling during this detachment impacted on cell viability, the detached TEML was subjected to live/dead cell staining. As shown in Figure 5.4, the tissue-engineered medial layer did not appear to be significantly impacted by the detachment process, with cell viability having been assessed as 91% ± 0.8% in the samples examined. These experiments demonstrate that using a fibrin-based attachment solution could provide a method to allow us to artificially trigger the rupture of the tissue-engineered neointimal model to assess the resultant thrombotic response.

5.3.4 Flow-mediated detachment of the fibrin-attached collagen hydrogel model

Plaque rupture is mediated by the mechanical weakening caused by thinning of the fibrous cap, in conjunction with the shear forces elicited by the flow of blood over the affected arterial segment. These shear forces can be particularly high in an artery subjected to significant stenosis by the thickening of the neointima, with previous studies suggesting shear stresses of between 500-3000 dynes/cm^2 (Strony *et al.*, 1993). These are significantly above the common ranges found in healthy large conduit arteries in which values range from 5-40 dynes/cm^2 (Cunningham and Gottlieb, 2005). These shear forces therefore play a significant role in dissociating the plaque from the surrounding vessel wall. Therefore, we investigated whether our plasmin-detached hydrogels could be dislodged from one another by laminar fluid flow over the top of the construct. Although it is possible to use gaskets to adapt the

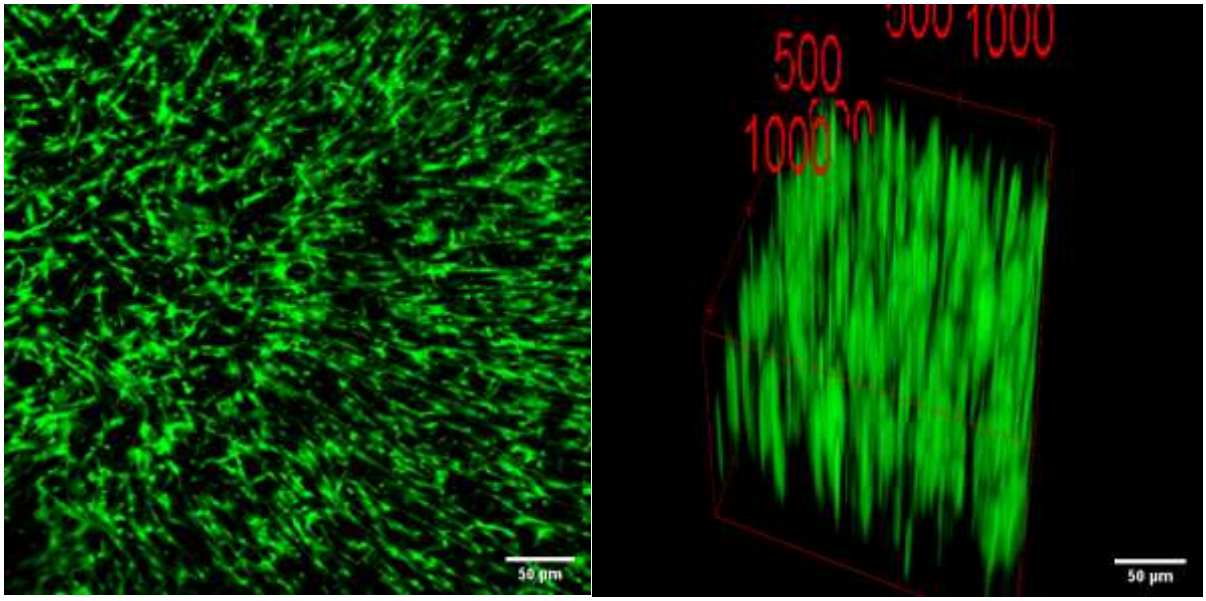

A B

Figure 5.4 Plasmin-induced detachment does not impact on the viability of human coronary artery smooth muscle cells within the tissue engineered medial layer. A compressed acellular collagen hydrogel was attached to a tissue-engineered medial layer containing human coronary artery using a fibrin attachment solution. Following setting the combined construct was incubated in a plasmin-containing PBS solution for 1h at room temperature. The TEML was then detached and stained using a live/dead cell staining kit II and imaged under a confocal microscope. (A) a slice showing the elongated morphology of HCASMCs within the hydrogel. (B) a 3D projection of the z-stack taken through the gel demonstrating that this treatment has no impact on cell viability, n=2.

hydrogel conjugates and tissue-engineered construct for use within commercially available flow chambers (Njoroge *et al*., 2021), the difficult in creating a limited flow space would significantly impede the development of any physiologically relevant shear stresses. Therefore, a custom-designed 3D-printed flow chamber was designed and produced in which to incorporate a smaller version of the hydrogel conjugates, as described in Section 2.2.2.6 These flow chambers provide a close fit with the hydrogels and permits greater control over the height and width of the flow chamber to ensure a better seal and to provide greater flexibility over the height of the flow channel over the construct.

A pilot experiment using the fibrin-attached hydrogel conjugates was performed to see whether it was possible to utilize shear forces initiated by fluid flow to initiate the detachment of Plasmin-treated hydrogels. To ensure maximal visibility of the construct during the experiment and to ensure steady pressure throughout, we performed the samples with HBS. Human plasma or whole blood was not used as any blood clotting would change flow resistance and could cause changes in the flow variables during the experiments. The flow elicited through the chamber at maximum pumping rate was 0.07 cm^3/s, corresponding to a shear stress of 4.7 dynes/cm^2 slightly below the range of shear stresses found in large conduit arteries. Following perfusion for 10 minutes, a notable deformation of the neointimal construct could be observed (Arrow; Figure 5.5B). These pilot experiments therefore demonstrate that use of the fibrin-plasmin attachment-detachment system provides a basis for creating an atherosclerotic plaque model that can be triggered to rupture upon plasmin treatment and exposure to physiologically relevant shear stresses. Further work using human blood samples and a syringe pump in this flow chamber systems will allow us to generate

higher shear rates that should facilitate better separation of the hydrogel-based constructs and assess the thrombotic responses to this plaque rupture model.

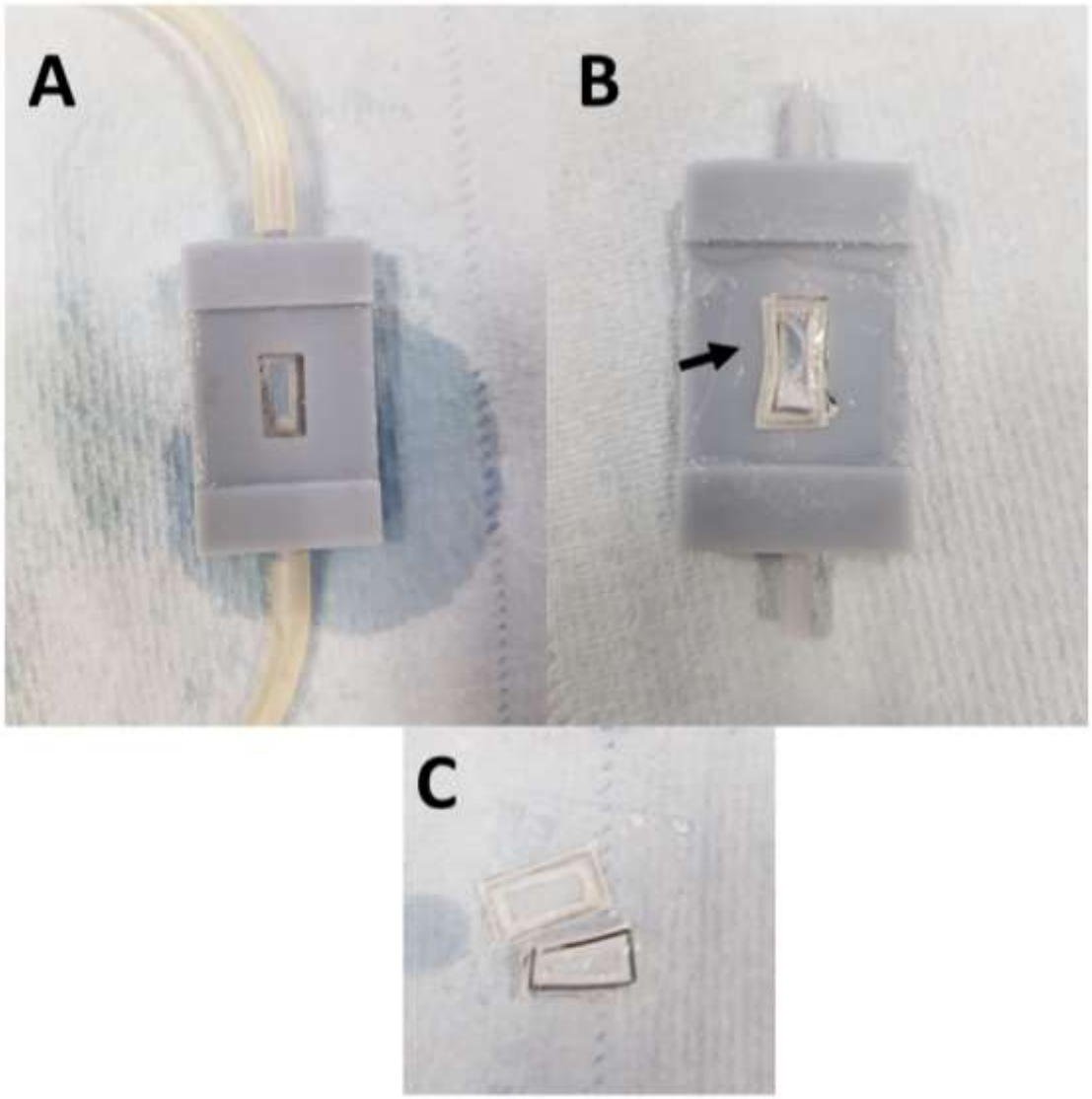

Figure 5.5 Perfusion of the Plasmin-detached hydrogel conjugate triggers hydrogel displacement. The compressed and non-compressed collagen hydrogel scaffold models of the neointimal and medial layers were attached using the fibrin-attachment solution as previously described. After setting the hydrogel conjugate was placed in a custom-made flow chamber (See Section 2.2.2.6 for full details; Huang *et al.*, 2020) and perfused with HBS at the maximal pumping rate of a Watson-Marlow 505 series peristaltic pump. This generated a shear stress of 4.7 dynes/cm^2. (A) The sample at the onset of perfusion. (B) The sample after 10 minutes of perfusion. The arrow indicates the separation of the neointimal and medial layers (C) Demonstration of sample detachment after the end of the experiment. n=3

5.3.5 The neointimal-medial layer co-construct containing THP-1-derived foam cells secretes higher levels of IL-6 and TNF-α

The macrophage-derived foam cells within the neointimal layer play a significant role in creating and maintaining the proinflammatory environment within the atherosclerotic plaque. They do this by synthesizing and secreting a range of cytokines, chemokines and matrix metalloproteinases into the local environment (Newby, 2016; Bekkering *et al*., 2014). To assess the pro-inflammatory environment that the THP-1-derived foam cells and HCASMCs are exposed, samples of conditioned culture media were collected at the end of the 14-day coculture and assayed for pro-inflammatory cytokines that have been shown to initiate changes in endothelial and vascular smooth muscle cell phenotypes. TNF-α, IL-1β and IL-6 have all been reported to be upregulated by oxLDL uptake by foam cells (Bekkering *et al*., 2014; Wang *et al.*, 2015; Liu *et al.*, 2014), whilst oxLDL has been reported to upregulate PDGF production by smooth muscle cells (Stiko-Rahm *et al*., 1992).

TNF-α has been shown to alter vascular smooth muscle cell behaviour by increasing proliferation, cell migration and extracellular matrix production, regulating apoptosis, and inducing phenotype switching towards a synthetic phenotype (Ali *et al.*, 2013; O'Blenes *et al*., 2001; Tang and Fang, 2017; Rastogi *et al*., 2012; Goetze *et al*., 1999). An ELISA assay demonstrated that significant TNF-α was produced by the neointimal-medial co-constructs produced with THP-1-derived foam cells, but not the M1 macrophage-containing or acellular constructs (Figure 5.6). These data are consistent with the results previously seen by others (Bekkering *et al*., 2014), as well as our previous studies in the neointimal constructs in isolation (Figure 3.21).

Previous studies have demonstrated the ability of IL-6 to induce vascular smooth muscle

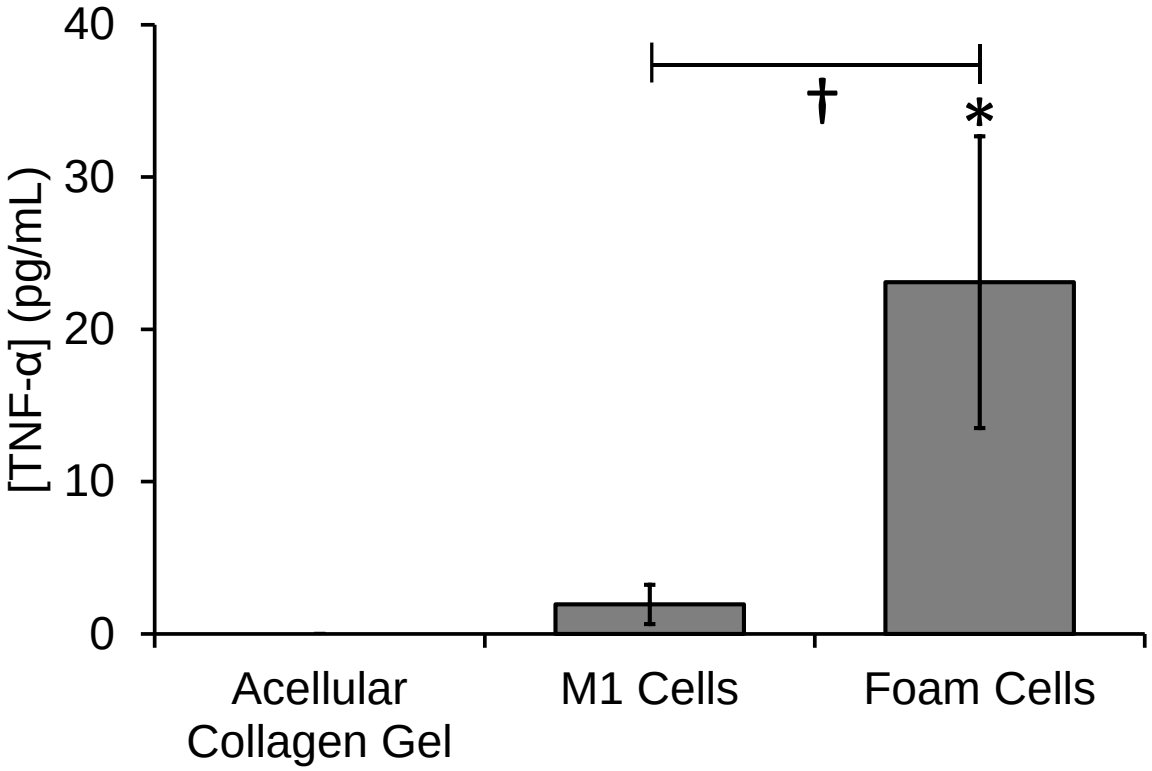

Figure 5.6. Inclusion of foam cells in the neointimal-medial co-construct enhances TNF-α secretion into the cell culture media. Neointimal constructs containing either no cells, M1 cells or foam cells were cultured until day 10, and a tissue engineered medial layer was cultured until day 6. On these days the neointimal model was attached on top of the medial layer construct using a fibrin attachment solution. After setting of the fibrin gels, the samples were cultured for a further 4 days at 37°C, 5% CO_2 in complete Medium 231. The cell culture media was then collected and assayed for TNF-α using an ELISA kit. * Indicates $P < 0.05$ relative to the acellular collagen gel. † Indicates $P < 0.05$ to the two indicates samples , one-way ANOVA with post hoc Tukey test was used as the statistical test of choice. n=6

migration in the vascular wall, increases cellular proliferation and MMP production, and induces phenotype switching towards the synthetic phenotype (Morimoto *et al*., 1991; Wang and Newman, 2003; Zhu *et al*., 2000; Ohkawa *et al.*, 1994). As shown in Figure 5.7, IL-6 can be found to be significantly raised above control levels in neointimal-media co-constructs containing THP-1-derived foam cells, but not M1 cells. These data are again consistent with the results obtained when the neointimal layer was cultured in isolation (Figure 3.21).

PDGF-BB has previously been shown to play a key role in endothelial cell control over vascular smooth muscle cell proliferation and phenotype, with endothelial-produced PDGF-BB favouring smooth muscle cells adopting a synthetic phenotype (Millette *et* al.,2004; Qi *et al*., 2011). Unlike our previous finding with the neointimal culture in isolation where we will unable to detect any PDGF-BB in any of the samples, we did detect low levels of PDGF-BB in the conditioned media taken from macrophage-containing samples (2/5 of the M1-containing cultures and 3/5 of the foam cell-containing cultures; Figure 5.8). However, the inconsistent findings meant that these were not statistically significant. These data therefore suggest that there might be low-level secretion of PDGF-BB from these cultures is around the threshold sensitivity limit for this ELISA assay (2.1 pg/mL).

IL-1β has also been reported to induce changes in the smooth muscle cell phenotype, increase cellular proliferation and elicit smooth muscle cell migration (Eun *et al.*, 2015; Alexander *et al*., 2012). The ELISA assay used to assess IL-1β secretion into the conditioned media sample provided absorbance readings in all samples that were consistently below the absorbance values provided by samples from the 0 mg/mL standard consisting solely of the sample diluent reagent (Figure 5.9). This was consistent with the previous findings in conditioned media samples cultured from the neointimal samples alone (Figure 3.22). These data indicate that

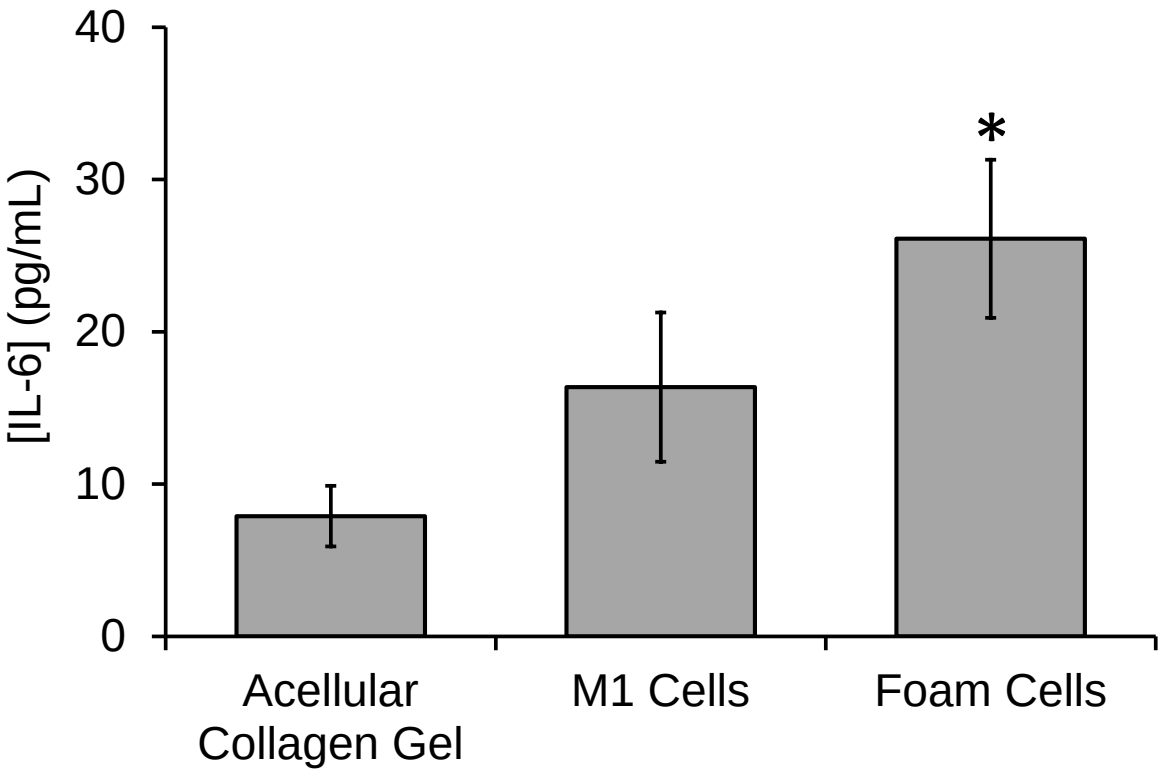

Figure 5.7. Inclusion of foam cells in the neointimal-medial co-construct enhances IL-6 secretion into the cell culture media. Neointimal constructs containing either no cells, M1 cells or foam cells were cultured until day 10, and a tissue engineered medial layer was cultured until day 6. On these days the neointimal model was attached on top of the medial layer construct using a fibrin attachment solution. After setting of the fibrin gels, the samples were cultured for a further 4 days at 37°C, 5% CO_2 in complete Medium 231. The cell culture media was then collected and assayed for IL-6 using an ELISA kit. * Indicates $P < 0.05$ relative to the acellular collagen gel using one way ANOVA with post hoc Tukey test, n=6

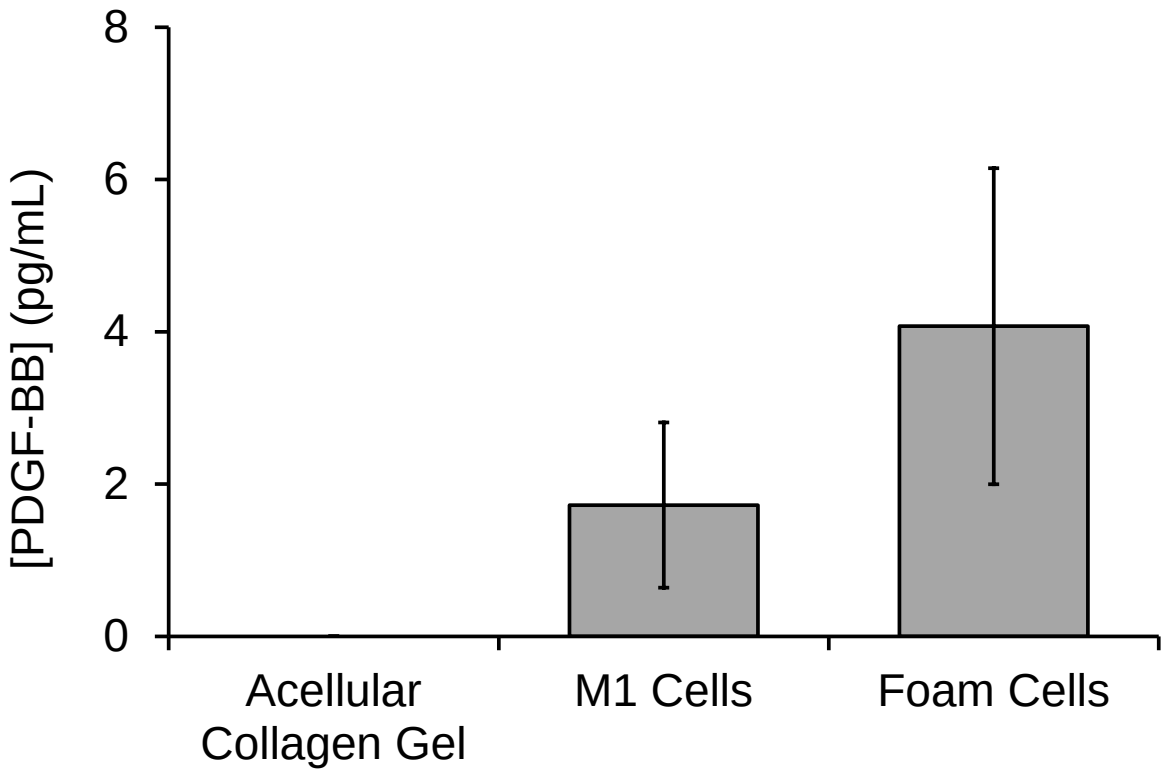

Figure 5.8. Inclusion of foam cells in the neointimal-medial co-construct inconsistently triggers detectable PDGF-BB secretion into the conditioned media. Neointimal constructs containing either no cells, M1 cells or foam cells were cultured until day 10, and a tissue engineered medial layer was cultured until day 6. On these days the neointimal model was attached on top of the medial layer construct using a fibrin attachment solution. After setting of the fibrin gels, the samples were cultured for a further 4 days at 37°C, 5% CO_2 in complete Medium 231. The cell culture media was then collected and assayed for PDGF-BB using an ELISA kit. * Indicates $P < 0.05$ relative to the acellular collagen gel using one way ANOVA with post hoc Tukey test. n=6

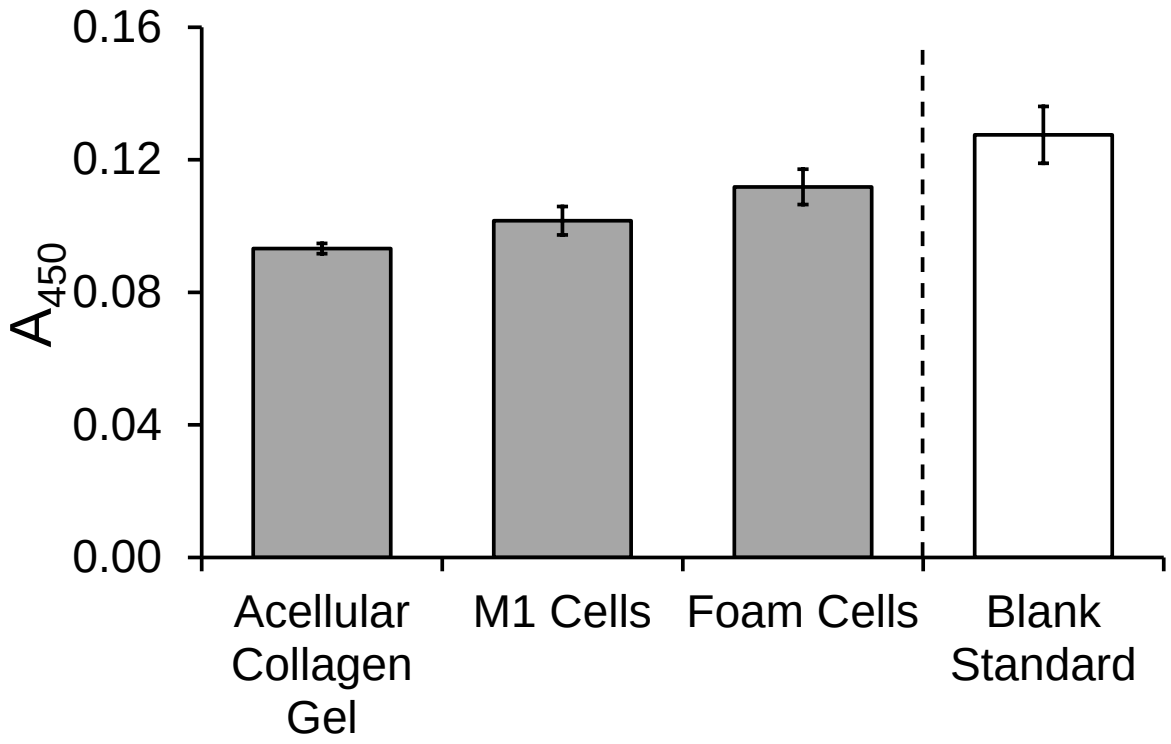

Figure 5.9. No IL-1β could be detected in the conditioned culture media of the neointimal-medial constructs. Neointimal constructs containing either no cells, M1 cells or foam cells were cultured until day 10, and a tissue engineered medial layer was cultured until day 6. On these days the neointimal model was attached on top of the medial layer construct using a fibrin attachment solution. After setting of the fibrin gels, the samples were cultured for a further 4 days at 37°C, 5% CO_2 in complete Medium 231. The cell culture media was then collected and assayed for IL-1β using an ELISA kit. The absorbance of the samples was recorded at 450 nm on a microplate reader and compared against a standard in which no IL-1β had been included in the sample dilution sample. * Indicates $P < 0.05$ relative to the blank standard using one way ANOVA with post hoc Tukey test which was used in the statistical analysis of these experiments, n=3.

is in insufficient IL-1β to be detected in this manner.

The ELISA assay demonstrates that the neointimal culture can replicate some, but not, all of the pro-inflammatory stimuli that are present within the atherosclerotic plaque. As TNF-α and IL-6 are both able to trigger vascular smooth muscle cell proliferation, migration and phenotype switching, it is possible they can replicate the changes in smooth muscle cell function that underlie the formation of the fibrous cap of the atherosclerotic plaque.

5.3.6 Assessment of smooth muscle cell localization within cryosections of the neointimal-medial co-constructs by light microscopy

Upon the establishment of the fatty streak, the inflammatory changes elicited by the foam cells elicit smooth muscle cell migration and proliferation from the medial layer of the artery. Here they lay down collagen and other extracellular matrix molecules creating the fibrous cap that helps strengthen the wall of the plaque and prevent contact with the blood of the prothrombotic contents of the neointima (Huang *et al.*, 2020). To assess whether similar changes can be elicited by the presence of foam cells within the neointimal-medial cocultures, samples from a coculture created with either no cells (acellular), M1 cells or foam cells within the neointimal constructs were produced and fixed with formaldehyde at the end of the 14-day coculture. Following this the samples were embedded within OCT (optimal cutting temperature) and cryosectioned to create 10 µm slices of the constructs to allow examination of the morphology and cellular properties at the end of the coculture period. As shown in Figure 5.10, the sectioning procedure caused dissociation of the compressed neointimal scaffold, and the non-compressed collagen hydrogel of the tissue engineered medial layer. These two constructs could be visually identified by the brighter eosin staining, greater

visibility, and presence of a striated internal structure of the compressed neointimal construct (Figure 5.10A). This allowed analysis of the structures within each of these constructs independently in M1- and foam cell-containing samples. In samples prepared with a compressed acellular collagen hydrogel, the compressed gel was consistently lost across all samples after dissolution of the OCT with PBS. This was likely due to the lack of cellular to bind to the poly-L-lysine surface such that the thin collagen hydrogel was unable to offer significant attachment to the slide and was lost through the washing process. Therefore, these were considered to contain negligible cellular content, and therefore have been subject to limited change during the culture period.

Initially, the cryosections were subject to haematoxylin and eosin staining, and examined by light microscopy (Figure 5.10). The eosin was seen to more effectively stain the compressed neointimal layer, indicating the higher collagen content of this hydrogel (Figure 5.10A). Additionally, whilst nuclear material could be identified in the medial layer through the dark staining of the haematoxylin, this was patchy in these non-compressed hydrogels, indicating a lower cell density in these layers (Figure 5.10B, C). Closer examination of the cellular morphology present within the individual gels found that the cells in the medial layer hydrogel showed an elongated shape that was consistent with the presence of smooth muscle cells in the layer in which they were introduced into the coculture (Figure 5.10B). Interestingly these elongated, spindle shaped could also be observed alongside smaller, irregularly shape cells in the neointimal layer of both the M1- and foam cell-containing sections. A small number of larger cells which were rounder and thicker were also observed at lower density, that may be indicative of either larger THP-1-derived macrophages or may be smooth muscle cells adopting a synthetic phenotype(Rensen, Doevendans and Van Eys, 2007). These observations

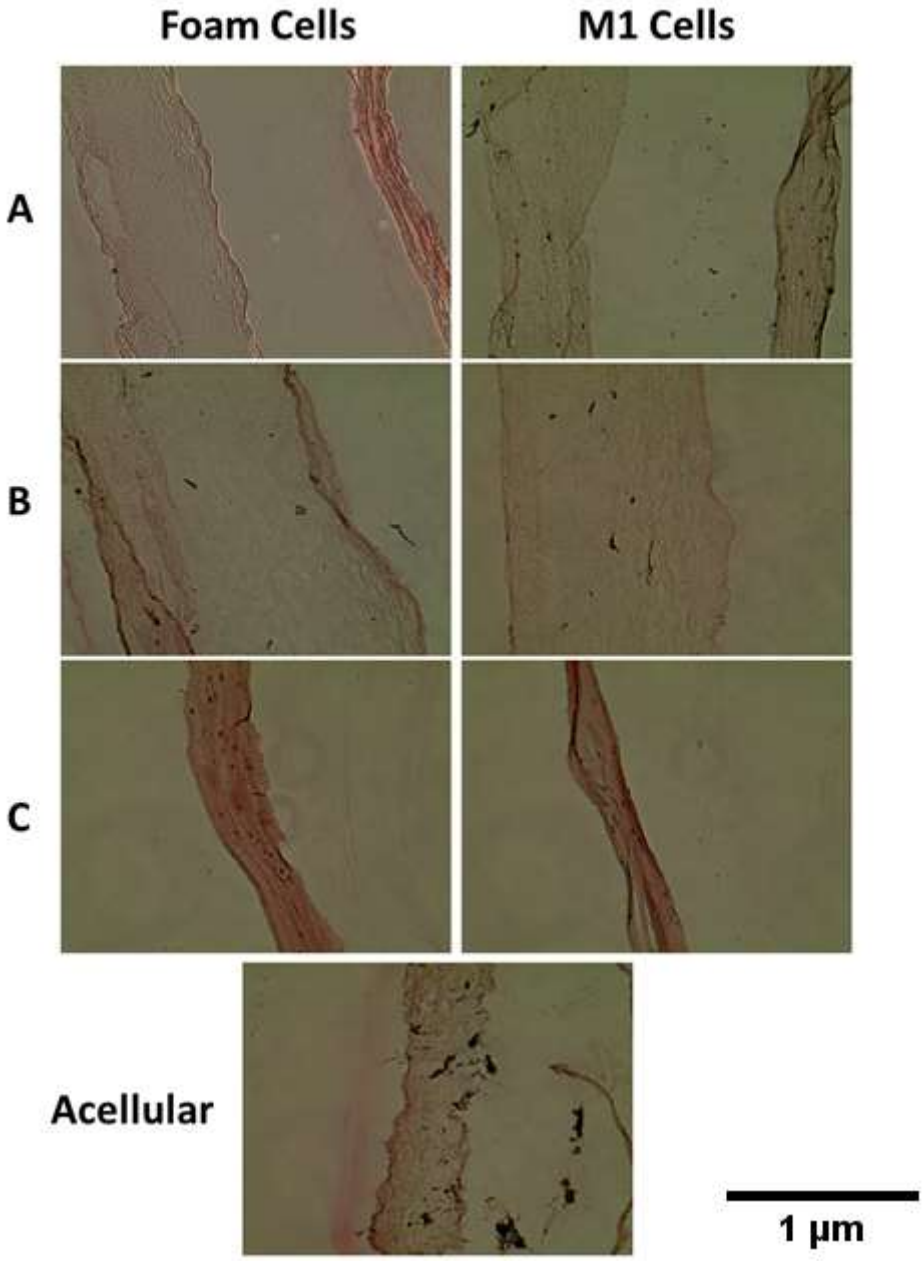

Figure 5.10. Smooth muscle cells could be detected within the compressed collagen hydrogel in cryosections of the neointimal-medial culture constructs. Neointimal constructs containing either no cells, M1 cells or foam cells were cultured until day 10, and a tissue engineered medial layer was cultured until day 6. On these days the neointimal model was attached on top of the medial layer construct using a fibrin attachment solution. After setting of the fibrin gels, the samples were cultured for a further 4 days at 37°C, 5% CO_2 in complete Medium 231. The samples were then cryosectioned and stained with H&E. (A) Picture taken with 10x objective showing both the compressed neointimal hydrogel model and non-compressed tissue engineered medial layer. (B, C) 20x objective pictures focussing on the tissue-engineered medial layer (B) and neointimal model (C). The bottom panel shows a section of the non-compressed gel from the acellular gels on the left-hand side, n=6.

indicated that contractile human coronary artery smooth muscle cells could be found in the neointimal layers of these samples and indicated the possibility that human coronary artery smooth muscle cells were migrating from the medial layer constructs into the neointimal models containing M1 macrophages and THP-1-derived foam cells. Further cellular characterization is needed to positively identify the smooth muscle cells within the neointimal layer and suggest their potential phenotype.

5.3.7 Immunofluorescent assessment of smooth muscle cell migration within cryosections of the neointimal-medial co-constructs

5.3.7.1 Nile Red staining

Initial studies attempted to validate the presence of foam cells within the construct by using the florescent lipid stain, Nile Red. This dye has no fluorescence in aqueous media but becomes fluorescent in hydrophobic environments. The spectral properties of the dye also change dependent upon the types of lipids present with the phospholipids of cellular membranes presenting with optimal excitation and emission at longer wavelengths compared to neutral lipids such as triacylglycerides and cholesterol esters, that cause a blue shift in the spectral properties of the dye (Greenspan and Fowler, 1985). The ability to specifically detect neutral lipid droplets within lipid-loaded macrophages was found to require excitation and of <570 nm, whilst Nile red loses its selectivity when fluorescence emissions are monitored at >590 nm (Greenspan *et al*., 1985). Therefore, the cryosections were stained with Nile Red and fluorescence emissions were examined using excitation wavelengths of 473 nm and 635 nm, and emissions were collected at 490-520 nm and 655-

755nm respectively to image fluorescence from intracellular neutral lipid droplet (pseudocoloured red in figures) and cellular membranes (pseudocoloured green).

Smooth muscle cells within the acellular constructs were found to stain with Nile red in both fluorescent excitations, demonstrating the lack of any significant presence of intracellular lipid droplets in these constructs (Figure 5.11). This is consistent with the lack of oxLDL used in these neointimal-medial cocultures. Similarly, in M1-cell containing cocultures the cells in the compressed neointimal layer predominantly showed weak staining of most of the cells, with a small minority of cells staining strongly for intracellular lipids, suggesting some limited droplets present within the M1 macrophages here (red). Similar findings were also observed for smooth muscle cells present within the medial layer. In contrast, in foam cell containing cultures, the cells within the compressed neointimal layers stained more strongly for intracellular lipid (as shown by orange-red staining cells in Figure 5.11C) indicating that foam cells can be detected in this layer. Interestingly this was observed for both irregularly shaped smaller cells as well as elongated contractile smooth muscle cells, indicating the possibility that the THP-1-derived foam cells release lipid during the coculture period which can be taken up by the nearby human coronary artery smooth muscle cells, as has previously been shown recently by other investigators (He *et al.*, 2020). Smooth muscle cells present within the medial layer constructs were found to stain weakly with Nile red indicating that they did not form foam cells (Figure 5.12). These data verify the differential lipid-loading present in these different constructs and indicate the possibility that vascular smooth muscle foam cells may develop in these cocultures.

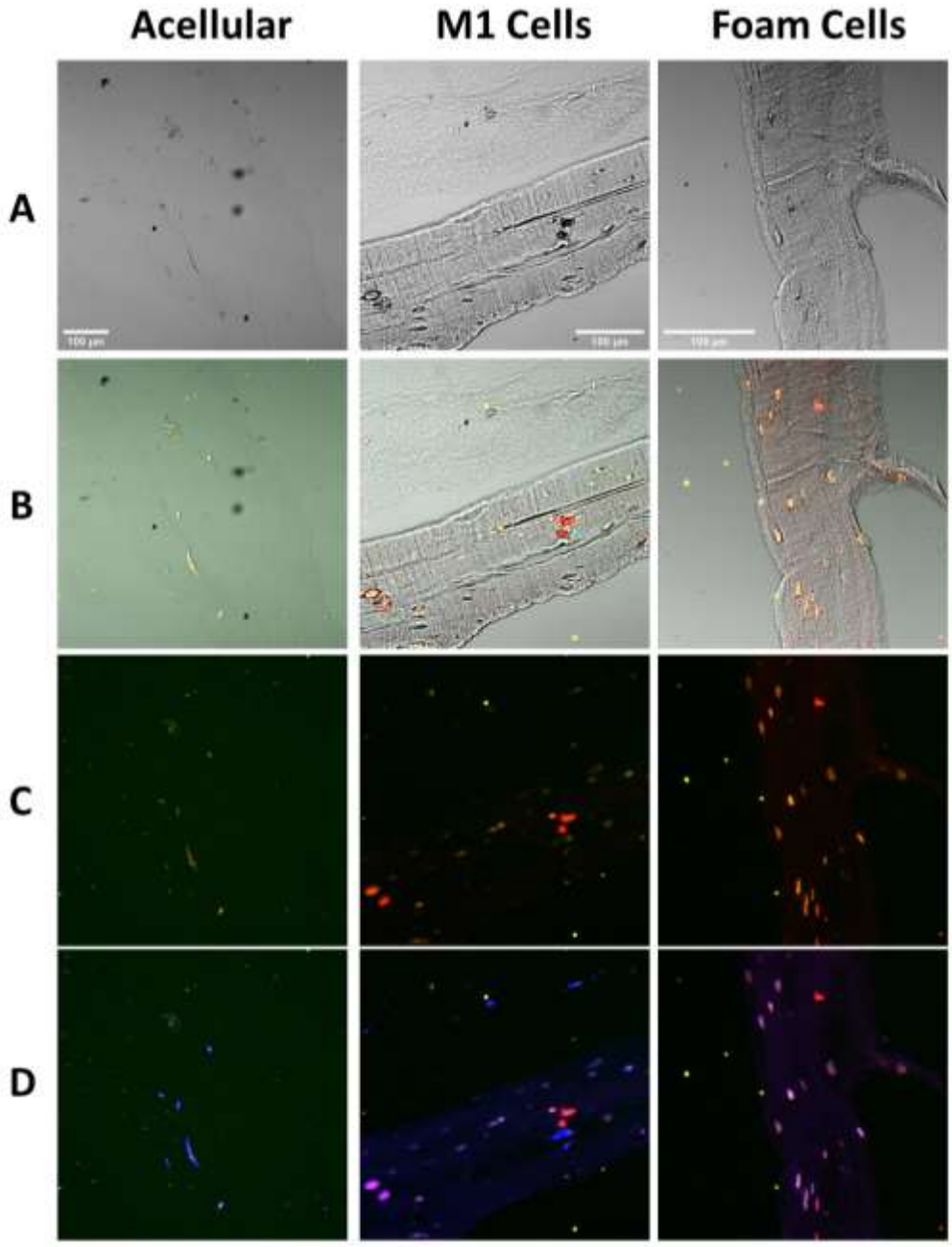

Figure 5.11. Nile red staining identifies intracellular lipid deposits in the compressed neointimal model of only the foam cell-containing cultures. Neointimal constructs containing either no cells, M1 cells or foam cells were cultured until day 10, and a tissue engineered medial layer was cultured until day 6. On these days the neointimal model was attached on top of the medial layer construct using a fibrin attachment solution. After setting of the fibrin gels, the samples were cultured for a further 4 days at 37°C, 5% CO_2 in complete Medium 231. The samples were then cryosectioned and stained with DAPI and Nile Red. A) Brightfield images of the remaining non-compressed medial layer of the acellular model, and compressed neointimal layer of the M1- and foam cell-containing models. Note the non-compressed hydrogel of the medial layer present in the upper half of the section containing M1 cells. (B, C) Overlay of emission recording using 473 nm (Red) and 635 nm (green) excitation wavelengths to differentiate between intracellular lipids (Red predominant) and cell membrane-based lipids (green predominant). (D) overlay of DAPI and Nile red fluorescence staining. Images taken at 20x objective on a confocal microscope, n=12.

During observations of the Nile red-stained cryosections containing THP-1-derived foam cells, one of the sections could be observed to contain a gel of a different density lying between the compressed neointimal model and the non-compressed medial layer (Figure 5.12). This layer is likely to be remnants of the fibrin gel used to attach the two samples together. These indicate that the fibrin hydrogel does not provide sufficient support to mechanical hold the two layers together under sectioning. Future studies may benefit from the use of a dense fibrin hydrogel made by increasing the basal fibrinogen concentration within the solution to help allow for cleaner sectioning.

Interestingly this layer could also be observed to contain a number of elongated, spindle shaped HCASMCs that were found on the surface adjacent to the neointimal layer (Figure 5.12). These cells were DAPI-stained but were weakly stained with Nile Red in both excitation wavelengths, consistent with other smooth muscle cells within the medial layer construct. These data therefore directly demonstrate an intermediate stage of the migration of smooth muscle cells out of the medial layer into the fibrin hydrogel, where they could then migrate into the neointimal model.

5.3.7.2 α-smooth muscle actin immunostaining

As the previous experiments had indicated the possibility of the migration of the HCASMCs from the medial layer into the neointimal model of co-constructs containing THP-1-derived cells, the cryosections were next stained for the key smooth muscle cell marker, α-smooth muscle actin (α-SMA;Owens, Kumar and Wamhoff, 2004). This marker is strongly expressed in contractile smooth muscle cells, and downregulated in vascular smooth muscle cells

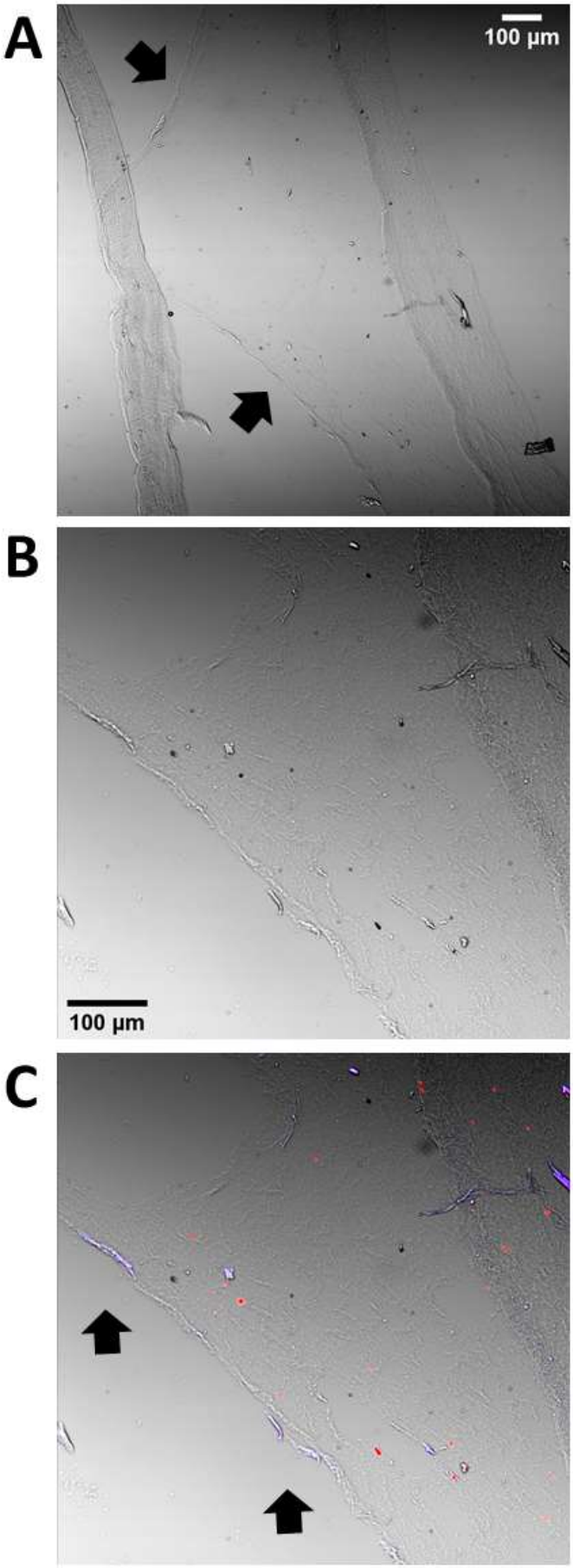

Figure 5.12 Smooth muscle cells appear to accumulate within fibrin hydrogel linking the neointimal model and the medial layer construct. Neointimal constructs containing either no cells, M1 cells or foam cells were cultured until day 10, and a tissue engineered medial layer was cultured until day 6. On these days the neointimal model was attached on top of the medial layer construct using a fibrin attachment solution. After setting of the fibrin gels, the samples were cultured for a further 4 days at 37°C, 5% CO_2 in complete Medium 231. The samples were then cryosectioned and stained with DAPI and Nile Red. (A) Brightfield image showing the fibrin gel linking the constructs (Black arrows) (B) Brightfield image showing close up of the fibrin gel. (C) Overlay with DAPI and Nile Red fluorescence (473 and 635nm). Note the DAPI-stained spindle-shaped HCASMCs present on the layer of the fibrin gel that would have been adjacent to the neointimal construct (Black arrows), n=3.

adopting a synthetic phenotype (Rensen *et al*., 2007) . As shown in Figure 5.13, cells staining strongly with α-SMA could be observed in the non-compressed medial layers from intimal-medial cocultures made using M1 macrophages, foam cells or no additional cells in the neointima (A, B1 and C1, Figure 5.13). This is consistent with the presence of contractile HCASMCs being present in these layers. Additionally, some smooth muscle cells could also be observed in the compressed neointimal layers of the M1- and foam cell-containing cocultures, however cells generally showing weaker staining than in the medial layer construct from that sample (B2 and C2, Figure 5.13). There did appear to be variance between cells with elongated, spindle-shaped cells generally showing brighter fluorescence than smaller more irregularly shaped cells, indicative of some cells switching phenotype towards a synthetic smooth muscle cell phenotype. To rule out non-specific binding, a primary-free antibody control was conducted on a section taken from a foam cell-containing coculture. As shown in Figure 5.14, no significant staining could be observed in any of the cells in this sample indicating that the fluorescence seen was not due to either non-specific binding of the secondary antibody to the sample nor due to autofluorescence of the sample at the fluorescent wavelengths used to identify the Alexa fluor488-labelled secondary antibody. These data provide further evidence that HCASMCs migrate during the coculture period, whether they appear to form subpopulations of synthetic and contractile smooth muscle cells.

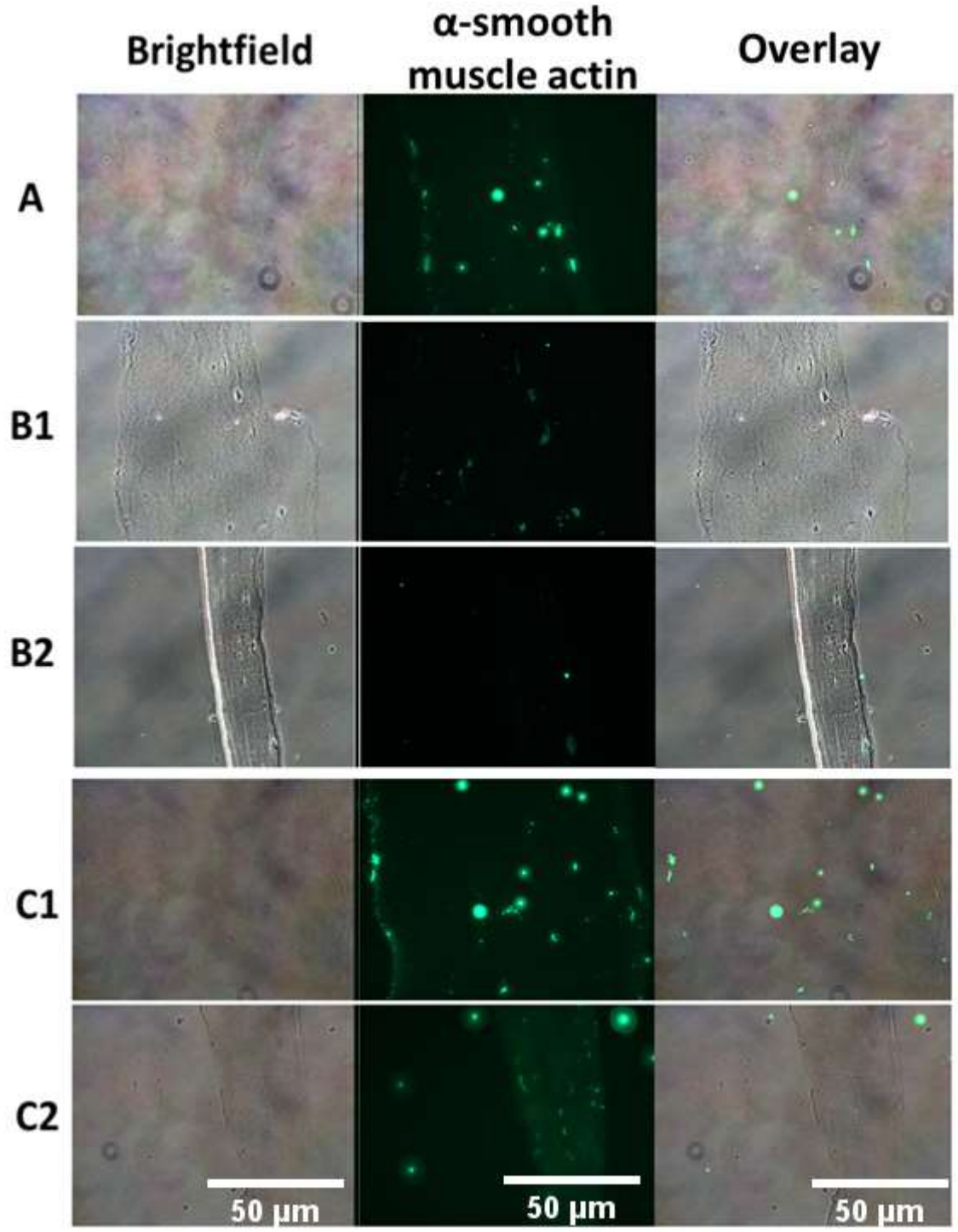

Figure 5.13. α-smooth muscle actin is present within both the medial and neointimal construct contain α-smooth muscle actin. Neointimal constructs containing either no cells, M1 cells or foam cells were cultured until day 10, and a tissue engineered medial layer was cultured until day 6. On these days the neointimal model was attached on top of the medial layer construct using a fibrin attachment solution. After setting of the fibrin gels, the samples were cultured for a further 4 days at 37°C, 5% CO_2 in complete Medium 231. The samples were then cryosectioned and labelled with a Mouse anti-α-smooth muscle actin antibody, followed by detection with an Alexa Fluor conjugated goat-anti mouse secondary antibody. Samples were imaged using a confocal microscope. A, B1 and

C1 are reprasanting the non-compressed medial layers of the acellular, M1 and foam cells neointima-medial construct. B2 and C2 are reprasanting the compressed neointima of the M1 and foam cells of the neointima-medial constructs,n=5.

Figure 5.14 Primary-free control for α-smooth muscle actin staining. A neointimal construct containing foam cells was cultured until day 10, and a tissue engineered medial layer was cultured until day 6. On these days the neointimal model was attached on top of the medial layer construct using a fibrin attachment solution. After setting of the fibrin gels, the samples were cultured for a further 4 days at 37°C, 5% CO_2 in complete Medium 231. The samples were then cryosectioned blocked and labelled overnight with a staining solution containing no primary antibody. This was followed by detection with an Alexa Fluor conjugated goat-anti rabbit secondary antibody. Samples were imaged using a confocal microscope, n=3.

5.3.7.3 Human type I collagen immunostaining

The reduction in α-SMA observed in some of the cells within the compressed neointimal construct indicated the potential presence of a subpopulation of the HCASMCs adopting a synthetic phenotype. Type I Collagen synthesis by synthetic human coronary artery smooth muscle cells has been used as a marker for detection of the presence of cells switching to this phenotype (Rensen *et al*., 2007). Previously Musa *et al*., (2016) have used an antibody specific to human type I collagen to specifically detect the production of neo-collagen within type I collagen hydrogels made using rat tail collagen (Musa *et al*., 2016). Cryosections from neointimal-medial construct containing either M1 macrophages, foam cells or an acellular neointimal model were stained using the same procedure utilized by Musa *et al*., (2016). As

shown in Figure 5.15, a low-level of type I collagen staining was observed in the non-compressed medial layers in acellular neointimal models, as well as those containing M1 macrophages and foam cells. In contrast, the compressed neointimal models containing both M1 macrophages and foam cells were seen to exhibit much greater immunofluorescent staining. Samples stained without the use of primary antibodies demonstrated minimal fluorescence in both the medial and neointimal layers of the coculture. A quantitative analysis found that fluorescent levels obtained in both the medial and neointimal layers of the primary-labelled samples were consistently higher than those from the equivalent primary-free control (Figure 5.16). This indicates that most of the fluorescent signal seen in the fully labelled samples was not due to either non-specific binding of the antibody or sample autofluorescence and was instead caused by specific binding of the antibody to type I human collagen within these constructs. As foam cells are not known to synthesis type I collagen (Schnoor *et al.*, 2021), these data indicate that synthetic smooth muscle cell subpopulations exist within both the medial and neointimal layers of the constructs imaged.

The quantitative analysis of the samples also demonstrated that the density of type I collagen present within the neointimal layer of the construct was found to be higher in cocultures in which foam cells were included. This is consistent with the finding that greater TNF-α and IL-6 is present within the culture media of these samples (Figures 5.6 and 5.7), as both of these cytokines have been demonstrated to initiate phenotype switching in vascular smooth muscle cells (Ali *et al.*, 2013; Ohkawa *et al.*, 1994; Owens *et al*., 2004). These data therefore indicate that smooth muscle cells migrate from the medial layer to the neointima of the coculture during the culture period. In the foam cell-containing cocultures the higher rate of secretion of pro-inflammatory cytokines from these cells elicits more of the smooth muscle cells to

adopt a synthetic phenotype facilitating the greater type I collagen deposition in these samples.

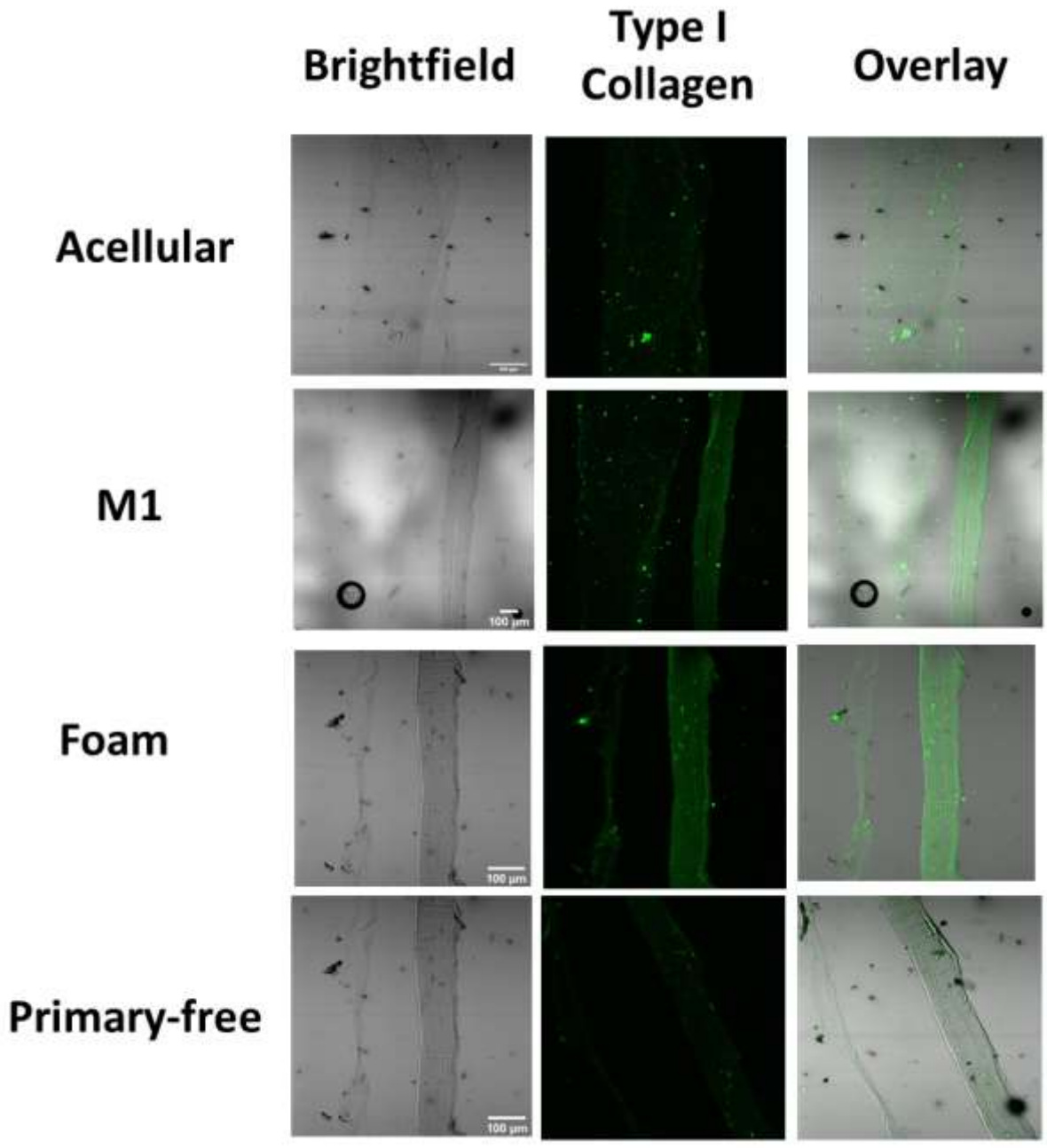

Figure 5.15 Human Type I collagen expression in the neointimal models. Neointimal constructs containing either no cells, M1 cells or foam cells were cultured until day 10, and a tissue engineered medial layer was cultured until day 6. On these days the neointimal model was attached on top of the medial layer construct using a fibrin attachment solution. After setting of the fibrin gels, the samples were cultured for a further 4 days at 37°C, 5% CO_2 in

complete Medium 231. The samples were then cryosectioned and labelled with a mouse anti-type I collagen antibody specific for human collagen, followed by detection with an Alexa Fluor conjugated goat-anti mouse secondary antibody. Samples were imaged using a confocal microscope, n=6.

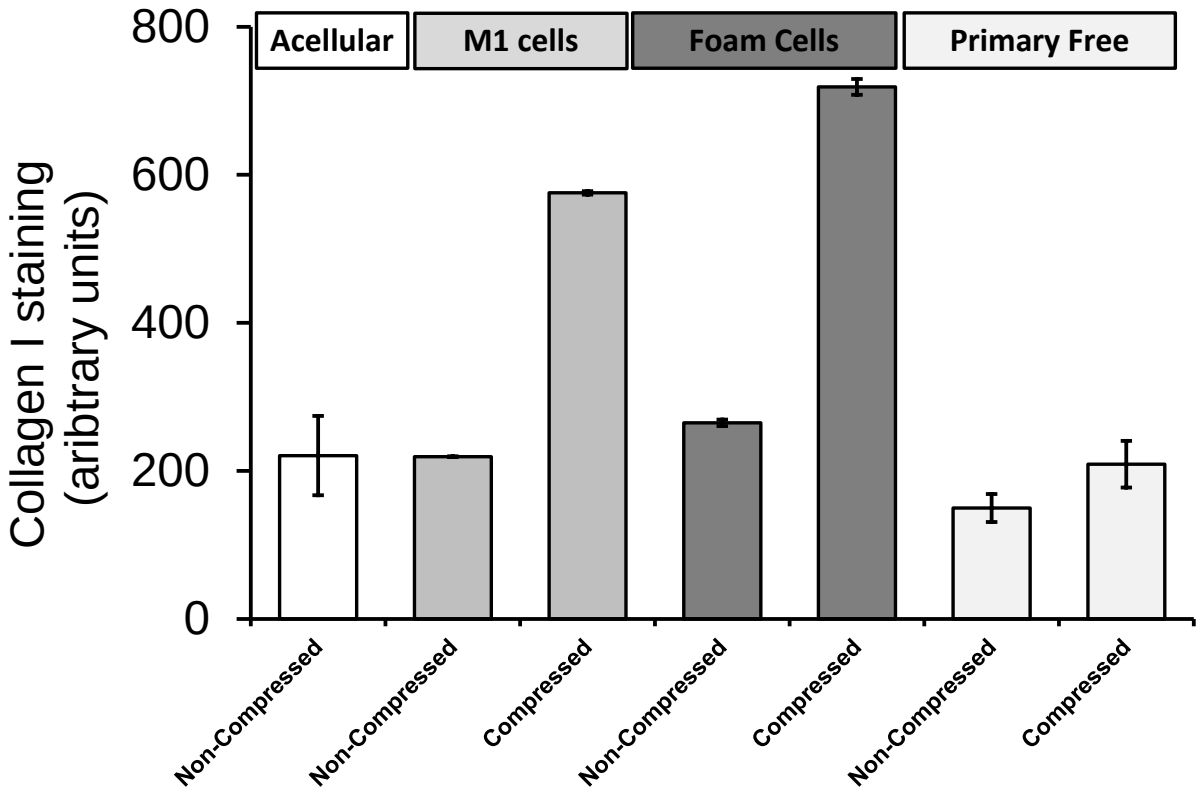

Figure 5.16: Initial quantification of the type I collagen immunofluorescence elicited from cryosections of the medial-neointimal cocultures. Image J was used to delineate the area occupied by the neointimal construct (compressed) and the medial layer construct (non-compressed) in the cryosection, or samples in which no primary antibody was included during the immunolabelling process. The mean pixel fluorescence from Type I Collagen immunostaining was measured for 2-3 slices of each gel type from a single neointimal-medial layer coculture. Data are shown as mean ± SEM of 6 experiments. * Indicates $P < 0.05$ with using of the one way ANOVA with post hoc Tukey test as a statistical test of choice, n=6 . n=6

5.3.7.4 Tissue Factor Immunostaining

In chapter 4, the neointimal constructs were demonstrated to possess measurable tissue factor activity that was able to elicit coagulation of platelet-poor plasma samples (Figures 4.2 and 4.3). Therefore, immunofluorescent staining for tissue factor was performed on sections from the neointimal-medial coculture to assess the presence of this key activator of the extrinsic coagulation pathway within the constructs. As shown in Figure 5.17, tissue factor activity was found associated with the cells in each of the constructs. This activity was found to be greatest in the compressed neointimal constructs due to their higher cell density than the non-compressed medial layer and the higher fluorescence coming from the small irregularly shaped foams cells in this culture. This is consistent with our previous findings in chapter 4, the neointimal layer containing foam cells was found to have a higher expression of tissue factor than those incorporating M1 cells or no cells within this structure. Crucially, minimal fluorescence was observed in medial and neo-intimal layers in which the sample was not treated with a primary antibody, thus demonstrating this effect is not due to non-specific binding of the antibody or autofluorescence of the sample. Therefore, these data would suggest that the medial-neointimal co-construct would also be able to trigger blood coagulation as we saw previously for the neointimal model in isolation.

5.8 Intimal-neointimal co-constructs show a variable aggregatory and secretory response

To create an intimal-neointimal construct, the neointimal model was cultured for 10 days and the uppermost surface was coated with fibronectin to enhance HUVEC cell attachment on the constructs. Following this HUVECs were seeded on the fibronectin-coated surface of the gel,

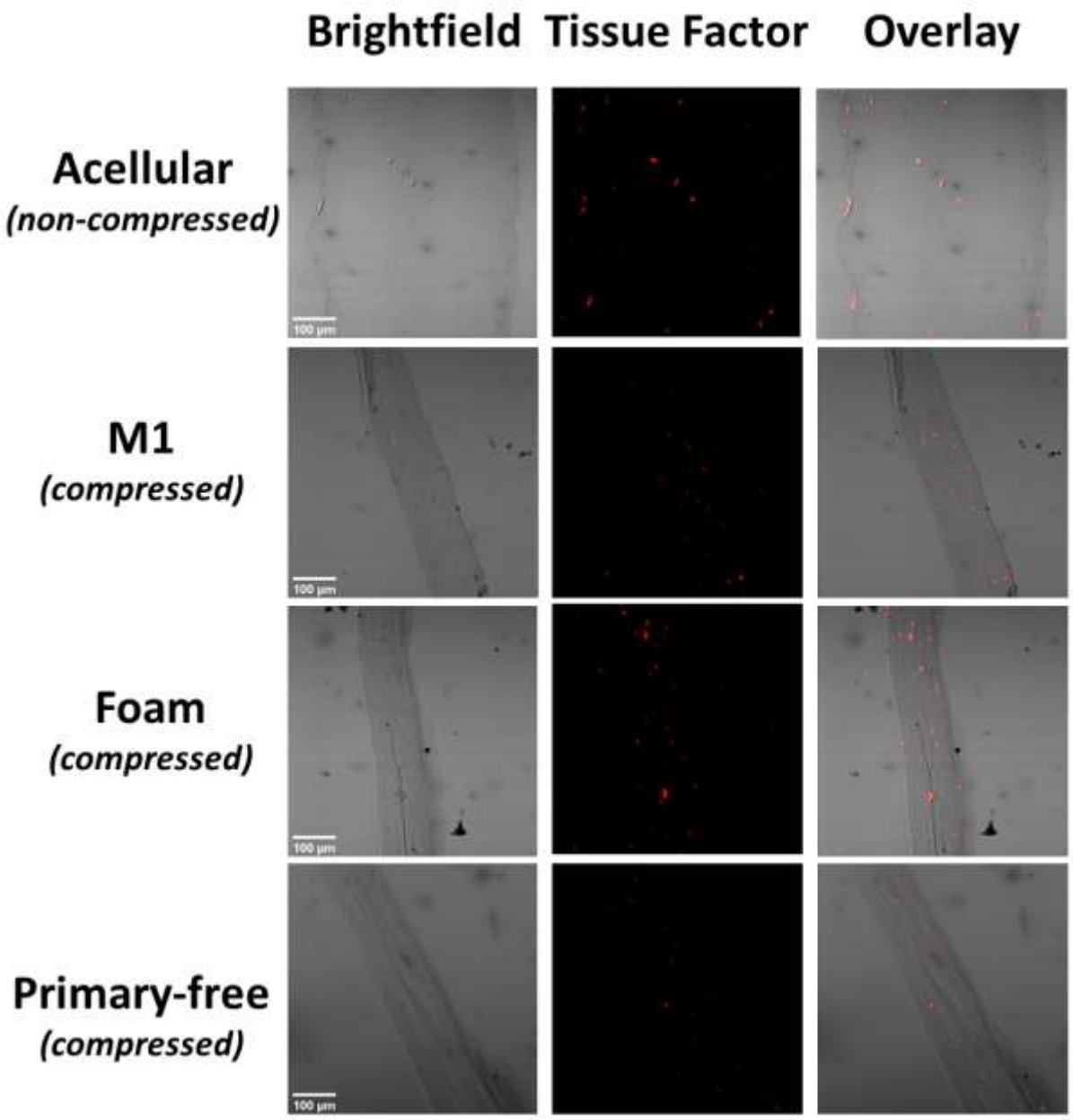

Figure 5.17 Tissue Factor expression in the neointimal-medial cocultures. Neointimal constructs containing either no cells, M1 cells or foam cells were cultured until day 10, and a tissue engineered medial layer was cultured until day 6. On these days the neointimal model was attached on top of the medial layer construct using a fibrin attachment solution. After setting of the fibrin gels, the samples were cultured for a further 4 days at 37°C, 5% CO_2 in complete Medium 231. The samples were then cryosectioned and labelled with a Rabbit anti-tissue factor antibody, followed by detection with an Alexa Fluor conjugated goat-anti rabbit secondary antibody. Samples were imaged using a confocal microscope,n=3.

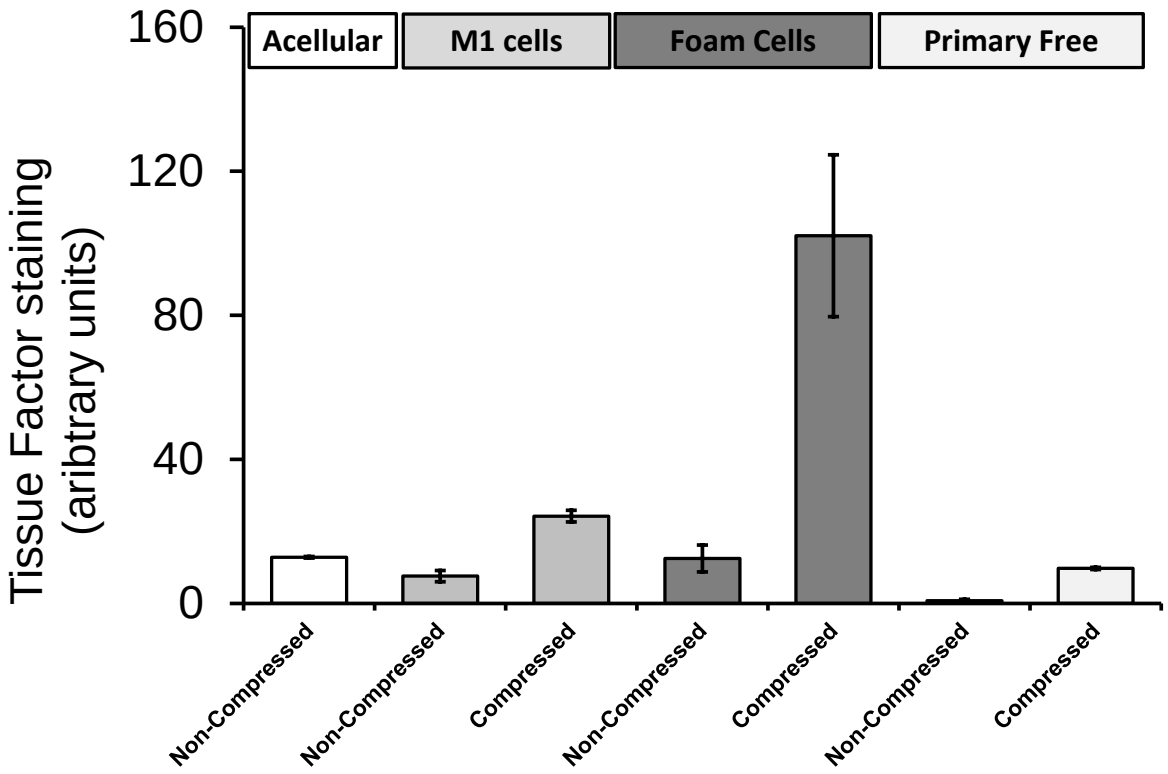

Figure 5.18: Initial quantification of the tissue factor immunofluorescence elicited from cryosections of the medial-neointimal co-cultures. Image J was used to delineate the area occupied by the neointimal construct (compressed) and the medial layer construct (non-compressed) in the cryosection, or samples in which no primary antibody was included during the immunolabelling process. The mean pixel fluorescence from tissue factor immunostaining was measured for 2-3 slices of each gel type from a single neointimal-medial layer coculture. Data are shown as mean ± SEM of 6 experiments. * Indicates $P < 0.05$ using one way ANOVA with post hoc Tukey test. n=6

allowed time to attach, and then placed in complete medium 200 and incubated at 37°C, 5% CO_2 for 4 days to allow time for the cells to proliferate across the surface of the construct.

As HUVECs synthesis and release a range of endogenous platelet inhibitors such as prostacyclin and NO, experiments were conducted to assess if this coating could inhibit the pro-aggregatory properties of the neointimal model. Samples were used intact or after treatment with ferric chloride ($FeCl_3$), which is widely used in *in vivo* thrombosis models to trigger thrombotic responses through redox-induced endothelial cell injury (Li *et al*., 2016), and thus allow us to identify if this endothelial response could be inhibited. $FeCl_3$ injury was applied through applying a thin 2 mm strip of $FeCl_3$-soaked filter paper to the centre of the neointimal surface of the 1 x 1 cm intimal-neointimal cocultures.

To assess endothelial-dependent inhibition of platelet responses, the intimal surface of the uninjured intimal-neointimal cocultures was held in contact with a human platelet suspension using sodium acetate frames in a spectrophotometer cuvette. A control sample in which the washed human platelet suspension was incubated without any hydrogel was used as a standard reference point for all platelet responses. The samples were then incubated for 10 minutes at 37°C under constant magnetic stirring. At the end of this period, the construct was removed and some of the platelet suspension was transferred to an aggregometer to read for 15 minutes, after this the suspension was activated with 0.05 U/mL thrombin to exogenously trigger platelet activation. At 10 minutes into the aggregometer recording, platelet suspension was also subject to a luciferin-luciferase-based assay of platelet dense granule secretion.

The dense granule secretion assay demonstrated that both the uninjured intimal-neointimal construct as well as the $FeCl_3$-treated construct on average had a higher basal secretory level

compared to the control sample not treated with a hydrogel-based construct (585 ± 310, 553 ± 274, arbitrary units for uninjured constructs, $FeCl_3$-treated constructs, and the platelet suspension respectively; n = 5; P > 0.05; Figure 5.19A). However, this was not found to be statistically significant despite consistently showing higher values than the control sample due to the significant variation in response observed in both the hydrogel construct. These data were consistent with the basal aggregometry readings taken from the samples which showed no significant change in the baseline reading (Figure 5.19B). These data therefore indicated that the degree of platelet activation triggered by either construct was weak or was insufficient to trigger platelet aggregation.

Following this and prior to thrombin addition, the aggregometer recordings were seen to demonstrate variable responses, with 1/5 of each of the platelet samples exposed to no gel, or the injured and uninjured constructs underwent full aggregation during this period. Additionally, 3/5 of the platelet samples exposed to the $FeCl_3$-injured cocultures underwent notable shape change, in contrast to 1/5 of the samples not exposed to a construct, and 1/5 of the platelet samples from the uninjured intimal-neointimal constructs. Thus 1/5 of the platelet samples exposed to the $FeCl_3$-treated cocultures remained quiescent through this incubation period, compared to 4/5 of the samples exposed to uninjured constructs, and 3/5 of the untreated platelet suspensions. These highly variable aggregatory and secretory responses contrast with the results observed in samples exposed to the neointimal construct in isolation which showed a consistent but slow pro-aggregatory and secretory response (Figures 4.7).

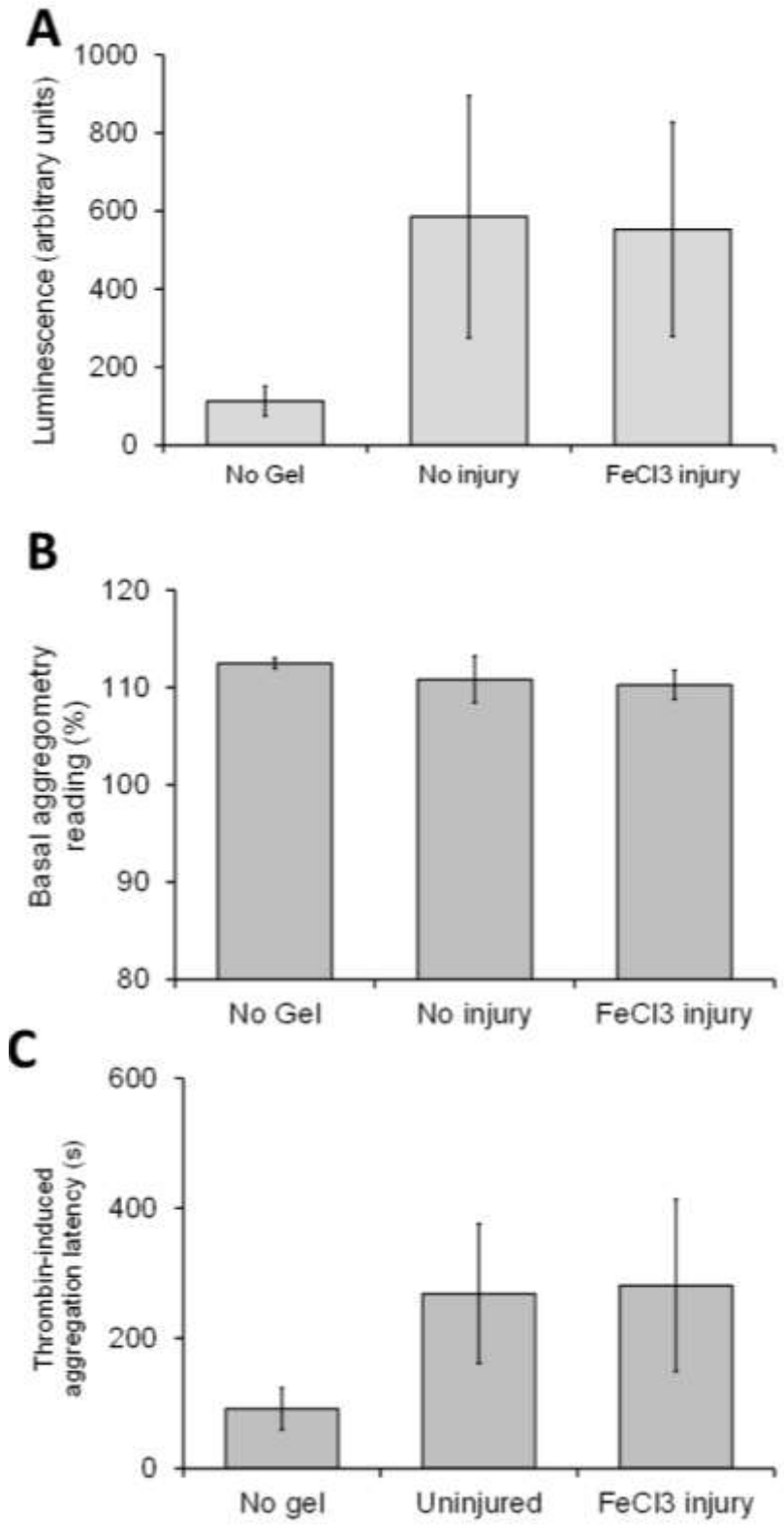

Figure 5.19. Intimal-neointimal co-cultures show a variable aggregatory and secretory response. HUVECs were seeded on top of Neointimal constructs for 4 days at 37°C. After the culturing period, samples were either subject to $FeCl_3$ injury or left intact, and then washed three times with HBS prior to use. The gels were then held in contact with a washed human platelet suspension for 10 minutes at 37°C under constant magnetic stirring. A gel-free platelet sample was used as a positive control sample. The construct was then removed, and the sample read on a light transmission aggregometer for 15 minutes, followed by treatment with 0.05 U/mL thrombin. A baseline (Luciferin-luciferase reading before thrombin addition (B) Basal aggregometry reading. (C) The time taken to transition from shape change into aggregation post thrombin. * Indicates $P < 0.05$ with using of the One-way ANOVA with post hoc Tukey test. Values shown are Mean ±SEM, n=12.

After the recording period, the platelet suspensions were then stimulated with 0.05 U/mL thrombin to assess if exposure to the constructs had sensitized or inhibited their responsiveness to platelet agonists. As shown in Figure 5.19C, the latency between the onset of thrombin addition and the onset of aggregatory responses (the time when the aggregometry trace transitions from shape change to aggregation at 0% on the calibrated traces), was shown to be consistently longer for platelet samples exposed to both uninjured and FeCl3-treated intimal-neointimal constructs. However again, the highly variable responses observed meant that these effects were not statistically significant. These data therefore indicate that the HUVEC lining is functional and able to inhibit platelet responsiveness to both the neointimal lining as well as exogenous thrombin, consistent with its role *in vivo*. The inability of the $FeCl_3$-treated constructs to trigger platelet activation or sensitize platelets to exogenous agonists may be due to the $FeCl_3$ injury only affecting a small central section of the construct.

5.9 Immunofluorescent staining of cryosections of intimal-neointimal co-constructs demonstrates inconsistent coverage of the intimal surface of the construct

The aggregometry and dense granule secretion assays demonstrate that the HUVEC lining is functional, but the variability of this effect suggest that the degree of coverage of the sample may not be optimal. To assess this further, a set of intimal-neointimal co-cultures were made in which the compressed neointimal gel contained either M1 macrophage, THP-1-derived foam cells or no cells (acellular). These were then cultured for 10 days, followed by fibronectin coating and seeding with HUVECs. These samples were then cultured for 4 days to match the process used in the previous experiments. At the end of this period, the samples were fixed

in formaldehyde, embedded in OCT and then 10 µm cryosections were made. These cryosections were labelled using antibodies targeted to the endothelial cell surface marker, CD31, and imaged using Alexa Fluor-labelled secondary antibodies.

As shown in Figure 5.20, CD31 staining was found to be specific for the surface of the construct in the acellular neointimal constructs, consistent with the seeding location of the endothelial cells. These data therefore indicate that endothelial cells remain on the surface of the constructs. The $CD31^{+}$ endothelial cells could be observed at low density on the surface of the acellular constructs leaving significant intercellular gaps and large sections of the construct surface uncoated. The HUVECs seen were relatively short and did not extend significantly over the surface of the construct. These data therefore suggest that the endothelial cells may have limited ability to adhere to the surface of the acellular neointimal constructs. This may provide an explanation as to why the constructs do not elongate over the surface of the construct and why there is limited surface coverage.

Cryosections on samples containing either M1 macrophages or THP-1-derived foam cells were found to show staining both of endothelial cells on the surface of the construct (yellow arrows) and the THP-1-derived cells seeded within the construct. As there was minimal fluorescence observed in primary-free control samples, this staining was unlikely to be due to non-specific binding of the secondary antibody to the THP-1-derived cells or autofluorescence of the samples. Instead, these data indicate that the CD31 antibody binds either specifically or non-specifically to the THP-1-derived cells. A literature search revealed that CD31 has previously been found to be expressed in macrophages and THP-1 cells (Virnon-Wilson, 2006; Liu and Shi, 2012), therefore indicating the likelihood that this binding is non-specific.

Therefore, future experiments will require the use of endothelial-specific markers not present in macrophages. However, examination of these samples indicated that the endothelial cells

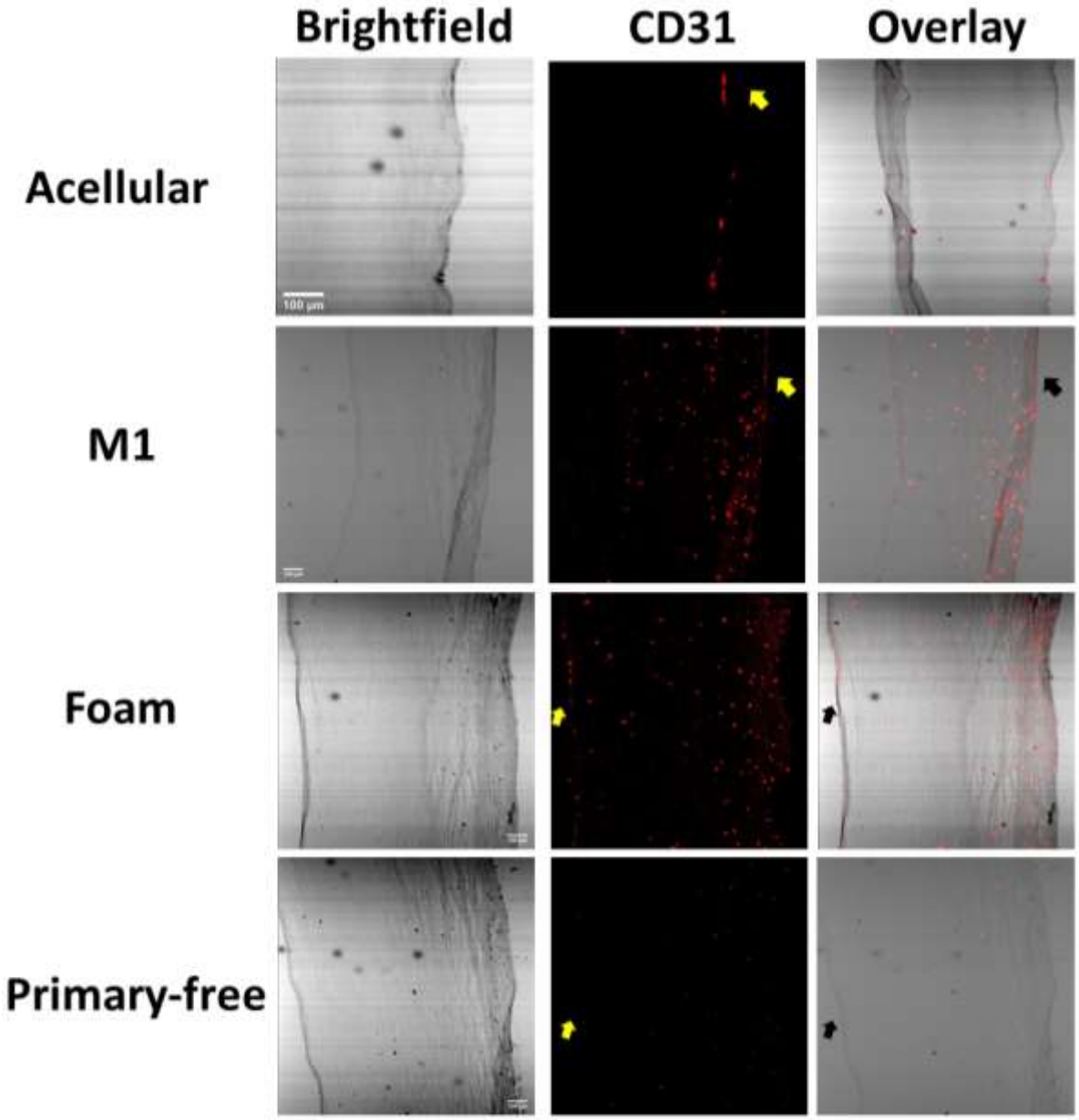

Figure 5.20 Endothelial cells only partially cover the surface of the intimal-neointimal constructs. HUVECs were seeded on top of neointimal constructs containing either M1 macrophage, foam cells or no additional cells (acellular) for 4 days at 37°C. Following this the samples were fixed with formaldehyde, embedded in OCT and subject to cryosectioning. The samples were then immunostained with a mouse anti-CD31 antibody and a goat anti-mouse secondary antibody labelled with Alexa Fluor633. Samples from each of the constructs were

also incubated without primary antibody to produce primary-free control samples. After labelling the samples were imaged using a confocal microscope. n=6

present on the surface of both the THP-1-derived cell-containing constructs appeared to be thinner and more elongated than those observed in the acellular constructs. This indicates the possibility that either cytokines secreted by these cells or the ability of these cells to produce extracellular matrix molecules within the coculture. Interestingly previous studies have demonstrated that human macrophages are able to produce fibronectin (Tsukamoto *et al*., 1981), suggesting that THP-1-cells might facilitate endothelial cell growth by facilitating greater endothelial cell attachment to allow their extension upon the surface.

Despite the improved phenotype surface coverage with endothelial cells was still poor with significant gaps between endothelial cells. This patchy growth upon the surface of the intimal-neointimal cocultures may explain the variable response of the washed platelet suspensions when exposed to these constructs, with different HUVEC cell densities on the surface of the construct altering the balance between the anti-platelet effects of the HUVECs and the pro-aggregatory properties of the neointimal model. This would also explain the lack of difference observed between intimal-neointimal cocultures that were untreated and those that had been subject to $FeCl_3$ injury. Due to the limited coverage the $FeCl_3$ injury does not significantly increase the surface area of the exposed construct and thus there is limited physical barrier to the interaction of the platelet suspension with the neointimal surface. Thus, triggering similar raised levels of basal platelet dense granule secretion. Interestingly, this data also indicates that low HUVEC coverage of the constructs can overcome the pro-aggregatory effects of the neointimal layer. To create a more realistic model in future, further

work will be required to enhance the confluency of HUVECs grown on top of the intimal-neointimal constructs.

5.4 Discussion

In this chapter, the aim was to establish coculture models incorporating our neointimal layer alongside endothelial and smooth muscle cells and examine whether it was possible for the neointimal model to trigger appropriate changes in the behaviour of these cells. This aim was partially met with initial data demonstrating that HCASMCs within the medial layer are triggered to migrate into the neointimal layer, mimicking the events that elicit the start of the transition of an initial fatty streak into a fibroatheroma – thus providing proof-of-concept that it is possible to develop advanced stages of atherosclerotic plaques within the context of an artificial vascular wall developed using tissue engineering techniques. In contrast, the attempt to establish a HUVEC monolayer on top of the neointimal model required modification, with the imaging studies demonstrating a low confluency of the HUVECs seeded on these constructs.

5.4.1 Development of a plaque rupture model through reversible attachment of the neointimal model to the medial layer

Before establishing our co-culture model, experiments were performed to assess whether it was possible to create a neointimal layer that can be artificially triggered to detach from the underlying medial layer to artificially replicate the process of atherosclerotic plaque rupture. Here we utilized a fibrin hydrogel coupled with subsequent plasmin treatment to selectively attach and then detach the layers of the coculture. This provides the opportunity to bathe the

construct in a plasmin-containing solution or inject a concentrated plasmin solution into the construct to trigger the breakdown of the construct. The initial studies have demonstrated that this has no adverse effect on the viability of HCASMCs within the construct, but further work will be required to ensure that the presence of this enzyme within the construct does not alter foam cells viability, or the thrombotic responses observed upon plaque detachment. The exposure of remnant fibrin on the exposed medial surface would provide a replica of the local activation of the blood coagulation system, and thus is unlikely to significantly alter the validity of the model. However, the potential presence of plasmin or fibrin-degradation products entering the blood flow over the surface of the construct could artificially slow platelet aggregation or the rate of fibrin formation by any formed thrombi (Larrieu *et al.*, 1975; Hoover-Plow, 2010) – thus future work will need to monitor exogenous plasmin or fibrin-degradation product entry from the rupture construct into the blood circulation and assess its impact on the thrombotic response seen. The presence of plasmin could be controlled through either washing of the constructs prior to incorporation in the flow chamber and/or the use of natural or artificial plasmin inhibitors following the incubation period. Alternatively a smart hydrogel could be used in place of the fibrin gel used here whose gelation can be triggered to reverse by a variety of external stimuli, such as in response to exposure to light, or changes in pH, temperature or ionic strength (Huang *et al.*, 2019; Kasiński *et al.*, 2020; Raman *et al.*, 2020). These would provide a more controlled dissociation of the gels but would need to be investigated for their biocompatibility with both the tissues within the gel and their effect on the haemostatic system prior to use.

The ability of shear stresses initiated by perfusion to trigger the separation of these layers in a hydrogel construct model demonstrates that this is a viable method. However, the shear

stress elicited in the flow chamber was marginally below the lowest end of the range found in arteries (Cunningham and Gotlieb, 2005). Modification of the methodology to use a syringe pump to increase the flow rate, and the use of whole human blood with its higher viscosity would increase the shear stresses and trigger greater separation of these layers. However further testing will be required to investigate whether this effect still occurs within a neointimal model that has been seeded with cells. As can be seen in Figure 5.15, these constructs will be stiffer due to the production of neo-collagen by HCASMCs, and so are likely to be harder to deform than the acellular compressed hydrogels used in these pilot studies. Therefore, whilst these pilot studies demonstrate the viability of this methodology, further studies will be required to demonstrate the validity of the flow-based system in mediating this dissociation.

Beyond the use in detachment of the neointimal-medial layer, the custom-made 3D printed flow chamber provides a prototype for the creation of a testing chamber for real-time imaging of the thrombotic response elicited upon exposure of the complete tissue-engineered atherosclerotic artery to platelet-rich plasma or whole human blood. This could create a humanized *ex vivo* plaque rupture model that could offer a viable alternative to current animal models. This would be beneficial in both improving the biological relevance of the model as well as reduce the costs of research due to the expensive nature of animal husbandry. The ability to independently culture each of the layers within the model also provides a route to selective alteration of specific proteins within the system to provide a targeted approach to the study of atherothrombosis.

5.4.2 Properties of the neointimal-medial co-cultures

The co-culture of a medial layer alongside the neointimal model did not significantly impact upon the inflammatory conditions present within the culture, with the relative amounts of IL-1β, IL-6, TNF-α and PDGF-BB release into the conditioned media of the coculture. The one difference found was the presence of threshold concentrations of PDGF-BB in the THP-1-derived cultures that were not observed in the neointimal construct alone. However, as this difference was not consistently observed in all samples this was not found to be statistically significant at this stage. These data therefore suggest that the use of complete Medium 231 or the presence of the smooth muscle cells in the coculture does not significantly alter the inflammatory responses of the THP-1-derived macrophages, and such they remain viable and functional within the coculture.

The co-culture imaging studies demonstrate the presence of human coronary artery smooth muscle within the neointimal construct at the end of the culture period. This is consistent with the behaviour of smooth muscle cells in the native artery when exposed to the pro-inflammatory conditions within the neointima (Biros *et al*., 2021). These data therefore indicate that the cells can migrate through the fibrin and collagen hydrogels to the compressed neointimal culture. The finding of smooth muscle cells within the linking fibrin hydrogels in the Nile red staining experiments (Figure 5.12) provides a demonstration of this intermediate step in the migration of the cells as well as the presence of elongated, spindle-shaped cells that are consistent with the presence of contractile smooth muscle cells within the neointimal layers. It is also possible to see significant presence of α-SMA positive cells and the deposition of type I collagen, which has previously been shown to be synthesized and secreted by the HCASMCs in collagen hydrogels (Musa *et al*., 2016). These data therefore

provide confidence that the medial-neointimal cocultures possess similar biological properties to the native artery. Importantly, this also provides us with a first demonstration that a tissue-engineered neointimal model can progress beyond a fatty streak and start to recruit the smooth muscle cells required to form the fibrous cap of the fibroatheroma. As can be seen in the immunostaining studies, it is already possible to observe uniform deposition of type I collagen across the construct, however further development will be required to attempt to direct this to coat the intimal surface of the construct to mimic the structure found *in vivo*.

To fully validate this work, several additional experiments will have to be performed. Firstly, a major limitation in the cryosectioning studies are they are based off of samples all taken from a single culture of the neointimal-medial constructs. To confirm that these initial findings are reproducible further work will be required to validate these in other samples. Secondly, the loss of the compressed collagen hydrogels from acellular samples limiting the ability to definitively conclude if this migration occurs in the absence of THP-1-derived cells, although given the limited ability of the construct to adhere to the slide it would seem unlikely that significant numbers of cells are moving. Approaches to solve this might be to enhance the attachment of the samples to the slide by producing paraformaldehyde-fixed samples and the use of egg whites to hold the samples more firmly in place. Further work will also be required to identify the stimulus triggering this migration. Previous studies have demonstrated that both TNF-α and IL-6 are both able to trigger smooth muscle cell migration (Goetze *et al*. 1999; Wang and Newman, 2003). Additionally, studies have also demonstrated that extracellular vesicles from macrophage-derived foam cells are also able to trigger this movement (Niu *et al.*, 2016). Therefore, many different macrophage-dependent stimuli could be initiating this biological response. Alternatively the response may be independent of the

THP-1 cells and triggered by non-cellular cues such as the gradient of hydrogel stiffness elicited by the compressed and non-compressed gels (Hartman *et al.*, 2016; Isenberg *et al*., 2015; Wong *et al*., 2003), or the presence of fibrin within the constructs (Naito *et al*., 1990). Therefore, additional studies will be required to assess the individual contribution of these such that we can maximize the smooth muscle migration to the neointimal layer.

5.4.3 Properties of the intimal-neointimal co-cultures

The intimal-neointimal co-cultures represented the initial attempt to develop an endothelial lining for the tissue-engineered atherosclerotic arterial model. The data shown in this chapter suggests that further modification of the scaffold supporting the attachment and proliferation of the endothelial cells will be required to create a confluent layer atop the neointimal model, as all constructs showed limited HUVEC coverage on the seeded surface. The morphology of HUVECs seeded upon acellular neointimal models indicated that there is insufficient density of matrix molecules to attach to as the HUVEC cells appear not to spread over the surface to the same extent seen in those containing either M1 macrophages or THP-1-derived foam cells. Previous work by Musa *et al*., (2016) found that HUVEC alter the adhesive properties of the rat tail collagen hydrogel through the production of type I and III human collagen during the culture period. Although macrophages are generally considered to principally remodel tissues through the release of matrix metalloproteinases, they have also been shown to synthesis their own extracellular matrix molecules such as fibronectin and type IV collagen (Tsukamoto *et al*., 1981; Schnoor *et al.*, 2021). Further work will be required to investigate if the THP-1-derived M1 macrophages and foam cells could be used to create a surface chemistry that would better support HUVEC attachment and proliferation across it. Alternatively, Musa *et al*., (2016) and Njoroge *et al*., (2021) have both utilized aligned

fibronectin-coated nanofibers to create an effective scaffold for the attachment and development of the intimal lining. This scaffold has previously been demonstrated to offer optimal properties for HUVEC attachment and development, with the aligned nanofibers helping to create an aligned endothelial cell monolayer through contact guidance (Musa *et al*., 2016). Future development of the intimal-neointimal model will utilize this methodology to produce an enhanced intimal layer for the coculture.

Despite the limited coverage of the neointima with HUVECs, this partial endothelial layer was still shown to possess significant anti-platelet activity inhibiting aggregation of washed platelet samples exposed to the intimal-neointimal constructs and slowing aggregatory responses to exogenous thrombin stimulation. These data therefore indicate that whilst a confluent monolayer was not produced in this study, the HUVECs were still functional within the system. Unexpectedly, the use of $FeCl_3$ injury was not sufficient to significantly inhibit this effect. This is likely due to the narrow region of the construct exposed to the $FeCl_3$-soaked filter paper. Use of a wider filter paper strip and prolonging the time for exposure to allow the $FeCl_3$ to diffuse further through the gel should improve this effect in future studies.

5.5 Conclusion`

In this chapter, a method has been developed for co-culturing the neointimal culture model with the previously devised tissue engineered medial layer. This co-culture still possessed the same pro-inflammatory properties of the neointimal model in isolation, as could be seen through the continued presence of TNF-α and IL-6 within the conditioned media. Through immunofluorescent and histological staining of cryosections of these co-cultures it was possible to demonstrate that smooth muscle cells from the medial layer could migrate through to the neointimal construct. This is the first demonstration of medial smooth muscle cell migration in any *in vitro* tissue engineered atherosclerosis model. This therefore demonstrates that this construct can be the earliest event in fibroatheroma formation. Through development of the construct, as well as utilising the prototype plaque rupture protocol and 3D printed flow chamber, this construct has the potential to be able to form a valid and accessible model of atherothrombosis.

Chapter 6: Discussion

This study aimed to develop and validate a simple 3D neointimal model that can be inserted into the previously developed human tissue-engineered arterial construct. This would provide the basis for creating a human *in vitro* tissue-engineered atherosclerotic plaque model for use as an alternative to current *in vivo* animal atherosclerosis studies and *ex vivo* studies on endarterectomy samples.

This thesis documents the successful development of a protocol for a novel neointimal culture model that, for the first time, demonstrates the effective culture of THP-1-derived foam cells within a compressed collagen hydrogel. The foam cells produced were found to retain good viability as well as an enhanced inflammatory phenotype initiated by oxidised LDL uptake, indicating that there is no significant loss of cell function from this culturing process. When exposed to other cells and blood plasma the construct could also be demonstrated to initiate appropriate changes in biological responses. This includes the activation of the blood coagulation cascade, as well as human coronary artery smooth muscle cell migration consistent with the known effects of these cells in elicit atherosclerotic plaque development and subsequent atherothrombotic responses upon its rupture. These data therefore provide an early confirmation that the neointimal model can replicate at least some of the biological properties of the native atherosclerotic plaque. However, a final validation will require direct comparison of the functional properties of the neointimal model when successfully integrated into the tissue-engineered arterial model, against endarterectomy samples taken from patients. Currently the neointimal model developed here is not an accurate replica of clinically relevant atherosclerotic plaques as the isolated model currently only replicates fatty streak formation, which is a clinically silent stage. When incorporated into co-cultures with smooth

muscle cells, the neointimal model demonstrates the initial stages of progression to the more advance fibroatheroma stage as medial smooth cells migrate into the neointima thus providing the potential for this model to develop into later stages of atherosclerosis.

6.1 Comparison to pre-existing tissue-engineered atherosclerosis models

Other groups have previously attempted to generate tissue-engineered models of human atherosclerosis. Prior to the beginning of this project, only two previous studies had been published by Robert *et al*., (2013) and Liu *et al*., (2017), with five other studies having been published subsequently (Figure 6.1). These studies utilised a range of different cells sources (e.g., induced pluripotent stem cells (iPSCs), primary cells extracted from umbilical tissues, cell lines) and scaffolds (e.g., collagen hydrogels, PGA (polyglycolic acid) meshes and cell-free cell culturing) for the development of their respective models. Whilst the use of THP-1 cells is a practical choice for model development, other groups have demonstrated it is feasible to use monocytes extracted from human blood (Robert *et al*., 2013; Zhang *et al*., 2020). Additionally, the recent pre-print report of using iPSCs provides a method to reduce the variability elicited by using primary cells from different donors or batches, however these cells still retain the foetal phenotype of this cell type that may impact upon their biological functionality (Mallone *et al*., 2020). These different reports demonstrate that there are likely to be multiple different methods to successfully develop models of atherosclerosis, with different groups employing different strategies (Figure 6.1). These can be evaluated by considering the biological relevance of the cells and scaffold used, the ability to effectively replicate the chemical and physical environment the cells develop in, as well as potential capacity to develop to advanced stages of atherosclerotic plaque formation.

The most used strategy is to utilise a replica of a model tissue engineered artery and use THP-1 or monocytic cells to induce monocytic migration and differentiation to foam

First Author (Year)	Cells	Scaffold	Strategy
Robert (2013)	SMC, EC, Monocytes	Artificial (PGA meshes)	Induce atherosclerosis in healthy tissue engineered artery using atherogenic stimuli
Liu (2017)	SMC, EC, THP1	Collagen	Induce atherosclerosis in healthy tissue engineered artery using atherogenic stimuli
Mallone (2018)	Myeloid cells and myofibroblasts	Endogenous (hanging drop)	Coating a spheroid model of cytokine-treated myeloid cells coated with myofibrasts. Independent of artery.
Gu (2019)	SMC, EC, THP1	Collagen	Induce atherosclerosis in healthy tissue engineered artery using atherogenic stimuli
Zhang (2020)	SMC, EC, Monocytes	Collagen (compressed)	Induce atherosclerosis in healthy tissue engineered artery using atherogenic stimuli
Garcia-Sabaté (2020)	THP1	Collagen	3D collagen hydrogels containing THP-1-derived foam cells
Mallone (2021)	iPSC-derived EC/SMC/ Macrophage), AF	Artificial (PGA meshes)	Induce atherosclerosis in healthy tissue engineered artery using atherogenic stimuli
Echrish (2021)	SMC, EC, THP1	Collagen (compressed)	Insert neointimal layer that is cultured independently of the layers of the healthy tissue engineered artery

Figure 6.1. A table comparing the methods used in published atherosclerosis models to the model developed in this study. AF = arterial fibroblasts, EC = Endothelial Cells, SMC = Smooth Muscle Cells, THP1 = THP-1 cells,

cells within the construct (Robert *et al*., 2013 ; Liu *et al*., 2017 ; Gu *et al*., 2019 ; Zhang *et al*., 2020 ; Mallone *et al*., 2021). Whilst these mimic the biological events underlying the onset of atherosclerosis, no-one of these groups have managed to document events involved in the formation of the advanced fibroatheroma stage of plaque development (Figure 6.2). The major limitation for this will be the culture length required to allow these models to begin to show the extensive cellular recruitment and tissue remodelling needed to induce these structures. Thus, whilst an attractive model for studying preventing early stages of atherosclerosis it does not look like a practical method for developing later stage atherosclerotic models – as this is a clinically-silent stage that naturally occurs in children it is unlikely to have an impact on patient treatment.

Other methods involve the generation of the models of the atherosclerotic plaque outside the confines of the artery (Mallone *et al*., 2018; Garcia-Sabaté *et al*., 2020). The spheroid fibroatheroma model developed by Mallone in which myeloid cells were encapsulated in a fibrous cap made from human umbilical vein myofibroblasts, replicates the most advanced stage model created currently. With the fibrous cap and an ability to recreate all of the major cell populations found within the human atherosclerotic plaque, this represents a highly impressive model. However, as it is produced in isolation from the arterial wall, it is not possible to use it to study endothelial dysfunction or plaque rupture – limiting its usefulness in studies of atherothrombosis. However, is conceivable that this model could be introduced artificially into a blood vessel model – although the spheroid generated by the hanging drop culture would make this more difficult than a layered model. The strategy developed in this thesis is a refinement of this strategy in which we aim to develop an advanced stage

atherosclerotic lesion outside of the artery, but in a format that is accessible for easy incorporation into a tissue-engineered arterial model. This is the strength of the layer-by-

First Author (Year)	Within arterial construct	Flow	Endothelial dysfunction	Monocyte infiltration	Foam Cell Formation	Smooth Muscle Cell Migration	Necrotic Core	Plaque Rupture	Thrombus Formation
Robert (2013)	Yes	Yes	Yes	Yes	No	No	No	No	No
Liu (2017)	Yes	No	Yes	Yes	Yes	No	No	No	No
Mallone (2018)	No	No	N/A	Yes	Yes	Fibrous Cap formed with myofibroblasts	No	N/A	No
Gu (2019)	Yes	Microfluidic	Yes	Yes	Yes	No	No	No	No
Zhang (2020)	Yes	Vascular	Yes	Yes	Yes	No	No	No	No
Garcia-Sabaté (2020)	No	No	N/A	Yes	Yes	N/A	No	N/A	No
Mallone (2021)	Yes	Yes	Yes	Yes	No	No	No	No	No
Echrish (2021)	Partial co-culture	Flow chamber developed	No	Yes	Yes	Yes	No	Model developed	Yes

Figure 6.2 A comparison of the stages of atherosclerotic plaque development achieved in this study to previously published tissue-engineered atherosclerosis models. N/A = not possible within this model.

layer fabrication methodology developed previously by Musa *et al*., (2016), as it provides the flexibility to introduce or remove individual biochemical and cellular elements from the construct and observe the effect on the biological activity. Through utilising this strategy, it should be possible to independently develop the culture of the neointimal layer construct to represent more advanced lesions more easily than if contained within the arterial construct. However, the demonstration that the neointimal layer can successfully trigger migration of HCASMCs from the medial layer does also provide the possibility of using cells within the construct to endogenously produce some of the maturation effects, rather than developing them exogenously. Therefore, there remains a number of possible routes to develop advanced stage atherosclerotic lesions from these constructs and demonstrates the great potential of this development strategy to successfully create a valid model of the atherosclerotic human artery.

As can be seen in Figure 6.2, the demonstration that our construct can trigger smooth muscle cell migration and trigger key events in thrombus formation, means the neointimal construct has demonstrated that it can replicate both fatty streak formation as well as some of the earliest events in fibroatheroma formation. These have not been previously demonstrated for tissue-engineered atherosclerotic plaques, and therefore represent a key advance in the process of replicating atherothrombotic events *ex vivo*. The finding that THP-1-derived foam cells within the neointimal model can generate tissue factor has been previously demonstrated (Owens *et al*., 2012), and thus the finding that the construct can trigger the coagulation of PPP is not unexpected. However, the demonstration that the THP-1-derived foam cells can weakly elicit platelet aggregation is a novel and unexpected finding. Future studies will examine if conditioned media taken from the foam cell-containing neointimal constructs is able to elicit activation of washed human platelets samples to examine if this is

a result of the production of a soluble agonist such as the cytokines that these cells have been demonstrated to produce, or because of deposition of an adhesive ligand on the surface of the construct. This adhesive surface could be extracellular matrix molecules, or it could be the surface of the THP-1-derived foam cells themselves. Interestingly the initial imaging data seemed to suggest the presence of an adhesive ligand as platelet could be observed to bind on or around the cell (Figure 4.9), indicating that the cell might be either producing a pericellular extracellular matrix or acting as binding surface for the platelets. This possibility could be tested by immunostaining the gels for extracellular matrix molecules or through blocking common platelet and macrophage surface receptors to see if they prevent this accumulation. Whilst the aggregation seen in these experiments is weak in these experiments, it will be interesting to also examine if the pro-aggregatory responsiveness is upregulated with inclusion of vascular smooth muscle-derived foam cells. Previously Musa *et al*., (2016) demonstrated that HCASMCs within the tissue engineered medial layer construct elicited a robust pro-aggregatory effect through the deposition of type I and III neocollagen within the collagen hydrogel scaffold. Therefore, the production of a fibrous cap may significantly enhance this pro-aggregatory effect. These interactions may also provide novel leads into identifying potential targets that can specifically inhibit platelet aggregation in response to plaque rupture but not vascular injury.

6.2 Comparison to *in vivo* animal atherosclerosis models

The ultimate aim of this work is to produce a model of the atherosclerotic human artery to use as a replacement for *in vivo* animal models used for drug testing and basic research. Therefore, it is important to also consider how the neointimal model compares to animal models. Currently, *in vivo* models remain superior to the model developed in this thesis due

to the ability to generated advanced atherosclerotic plaques within the artery, and the presence of physiological blood flow through the affected arteries. Our lab has previously demonstrated the ability to perfuse the tissue-engineered arterial construct with human blood products as a method for bridging the gap between current *in vivo* and *in vitro* thrombosis models (Njoroge *et al*., 2021). This expertise led to us developing a prototype 3D printed flow chamber to incorporate the neointimal construct. This was initially used to demonstrate the ability to use fluid perfusion to separate the plasmin-treated hydrogel conjugates (Figure 5.5). These pilot experiments demonstrated that the flow chamber is function and should permit us to examine the thrombotic responses elicited by the neointimal construct when perfusion with whole human blood under arterial shear stresses. Therefore, provided these are successful, it should be possible to bring the neointimal construct one step closer to being a novel model system for monitoring atherothrombotic responses *ex vivo*.

One of the major disadvantages of most *in vivo* animal models is that the elicited atherosclerotic lesions do not spontaneously rupture, and therefore these models are able not to reliably replicate the key clinical event that causes myocardial infarction or stroke. In this study, the development of the neointimal-medial constructs considered how to produce a model in which the neointimal model can be reversibly detached under flow conditions using a simple fibrin-plasmin interaction (Figure 5.5). Through this model we have been able to create a model that can be triggered to rupture after application of plasmin. This novel adaptation of our *in vitro* atherosclerosis model should therefore allow us to generate a model that can be triggered to rupture without requiring dietary, mechanical, or genetic interventions like some current animal models (Rosenfeld *et al*., 2002; Hartwig *et al*., 2015; van der Heiden *et al*., 2016). However, this approach does risk introducing artefactual changes in the atherothrombotic response elicited by the exogenous plasmin artificially

triggering fibrinolysis or through the presence of the resultant fibrin-degradation products. Therefore, whilst these experiments provide an initial proof-of-concept further refinement of the model could introduce other methods for eliciting the same effects. One potentially attractive model is the use of smart hydrogels that breakdown under light exposure (Ji *et al*., 2020) – this would allow the user to trigger a loss of gelation of the linking hydrogel after setting up the construct on an imaging platform, thus potential providing specific temporal and spatial control of these responses. However, this study still provides a first demonstration on how *in vitro* atherosclerotic models could generate this critical event in plaque development.

6.3 Future development of the atherosclerotic plaque model

As seen in Figure 6.2 and discussed above, whilst the neointimal model developed in this thesis is an exciting prototype that can be used to generate an *in vitro* model of the human atherosclerotic artery, there is still a need for further development, optimisation and refinement of the techniques showcased here.

Whilst it has been possible to meet most of the objectives for the project, one of the main limitations of the model was the inability to produce a confluent HUVEC lining upon the surface of the neointimal construct. From assessing the cryosections of the intimal-neointimal constructs, this appeared to be due to the limited ability of the HUVECs to bind to the surface of the hydrogel, with the acellular constructs demonstrating limited coverage and lacking the elongated morphology expected of these cells (Figure 5.20). These data therefore suggest the need to provide a more appropriate scaffold on which to grow the endothelial lining. Previously Musa *et al*., (2016) and Njoroge *et al*., (2021) have utilised aligned, fibronectin-coated PLA nanofibers to successfully create an endothelial monolayer to

represent the intimal lining of the tissue-engineered arterial construct. This methodology should be easily adaptable to the neointimal construct. As a verified method for producing the layer this does not appear to be a significant barrier to successfully generating the final tissue-engineered atherosclerotic artery. However, one disadvantage of this approach is the difficulty in other groups being able to generate these nanofiber scaffolds, as electrospinning is a specialist technique not widely used amongst biologists. Therefore, this technique may provide a significant barrier for other groups adopting this method as an alternative to current *in vivo* models of atherosclerosis. Another alternative would be to investigate the use of 3D bioprinting to generate a monolayer on the surface of the neointimal layer. As the techniques become more widely available due to the availability of custom made bioinks and protocols for the printing of endothelial cells, this may provide another method that is more easily accessible to researchers in future.

Once the intimal-neointimal layer has been generated and validated another key milestone in the development of this *in vitro* atherosclerosis model would be the development of a method to create an intimal-neointimal-medial layer co-construct. This would involve spending time assessing whether this model can remain viable and functional when cultured in these conditions. Previous studies have demonstrated that through using carefully optimised blends of the different culture media to maintenance each of the component cell type in culture, it is possible to maintain tissue-engineered arteries in culture effectively for a prolonged culture period to facilitate the onset of atherosclerotic events (Robert *et al.*, 2013; Mallone *et al*., 2021). Therefore, studies will need to optimise the culture conditions. Due to the presence of the foam cells, the pro-inflammatory environment will likely elicit significant changes in the biological properties of both the smooth muscle cells (as seen in this project), as well as the endothelial cells. Carefully controlled experiments will be required to ensure

that any changes are indicative of this co-culture and not artefactual events elicited by the inappropriate maintenance of the cells within the culture environment.

Following the full development and validation of the initial multi-layered atherosclerosis model, the next step in improving the current model would be to develop the neointimal plaque further to better resemble more advanced stages of atherosclerosis. In particular, the work would need to focus on the production of a necrotic core, creation of the fibrin cap, and replication of the biochemical and mechanical changes of plaque rupture. This will likely include the incorporation of other key cells and using bioengineering techniques to selectively trigger changes in their phenotype. For instance, in this thesis experiments have demonstrated the ability to culture vascular smooth muscle cell-derived foam cells within the collagen hydrogels used as a basis for these models. These cells are known to have differences in lipid metabolism compared to the macrophage-derived foam cells (Miller & Zhang, 2021). Therefore, inclusion of these cell may play a key role in modulating the development of a necrotic core due to the differential sequestration of LDL particles in these cell type. Therefore, assessing the impact of varying the ratio of macrophage-derived and smooth muscle cell-derived foam cells may provide a method for facilitating the development of optimal conditions to trigger an increased plaque development *in vitro*.

This progressive development of the neointimal layer has the additional benefit of also allowing us to examine how plaque development might impact on the atherothrombotic responses, and so may provide new insight into key targets for providing prophylactic treatment for patients at high risk of experiencing acute cardiovascular events. The developed mode would also provide a platform for pre-clinical testing of novel drugs aimed at targeting these responses. Through the layer-by-layer fabrication strategy it is possible to create both healthy and atherosclerotic arteries thus providing a basis for assessing the differential impact

of drugs on atherothrombotic and normal haemostatic responses, which in turn may help us develop anti-atherothrombotic drugs with less bleeding side effects.

6.4 Conclusion

This project has utilised a layer-by-layer fabrication method to develop a 3D human neointimal model that replicates the formation of the fatty streak, and the earliest events in fibroatheroma formation through eliciting smooth muscle cell migration from a co-culture medial layer. This ability to replicate both early and more advanced stage events in plaque development highlight the potential for this construct to be further developed into an effective model of atherosclerotic plaque rupture. This 3D neointimal culture model was also demonstrated to elicit a pro-thrombotic response when exposed to washed human platelets and platelet-poor plasma. Through further development of the construct and the prototype flow chamber document here, it will be possible to create a viable *in vitro* drug testing platform to assess the efficacy of new drugs at preventing atherothrombotic events.

7. Bibliography

Abela, O. G. *et al*. (2016) 'Plaque Rupture and Thrombosis: the Value of the Atherosclerotic Rabbit Model in Defining the Mechanism', Current Atherosclerosis Reports. Current Atherosclerosis Reports, 18(6). doi: 10.1007/s11883-016-0587-0.

Aikawa, M. *et al*. (1998) 'Muscle Cells Expressing Smooth Muscle Myosin Heavy', Circulation research, 83, pp. 1015–1026.

Aird, W. C. (2005) 'Spatial and temporal dynamics of the endothelium', Journal of Thrombosis and Haemostasis, 3(7), pp. 1392–1406. doi: 10.1111/j.1538-7836.2005.01328.x.

Aird, W. C. (2007) 'Phenotypic heterogeneity of the endothelium: I. Structure, function, and mechanisms', Circulation Research, 100(2), pp. 158–173. doi: 10.1161/01.RES.0000255691.76142.4a.

Aldo, P. B. *et al*. (2013) 'Effect of culture conditions on the phenotype of THP-1 monocyte cell line', American Journal of Reproductive Immunology, 70(1), pp. 80–86. doi: 10.1111/aji.12129.

Ali, M. S. *et al*. (2013) 'TNF induces phenotypic modulation in cerebral vascular smooth muscle cells: Implications for cerebral aneurysm pathology', Journal of Cerebral Blood Flow and Metabolism, 33(10), pp. 1564–1573. doi: 10.1038/jcbfm.2013.109.

Anitschkow, V.N., 1913. Uber die Veranderungen der Kannichenaorta bei experimentaeller Cholesterinsteatose. Beitrz Path Anatalllg Pathol, 56, pp.379-404.

Arbustini, E., Grasso, M., Diegoli, M., Pucci, A., Bramerio, M., Ardissino, D., Angoli, L., de Servi, S., Bramucci, E., Mussini, A. and Minzioni, G., 1991. Coronary atherosclerotic plaques with and without thrombus in ischemic heart syndromes: a morphologic, immunohistochemical, and biochemical study. The American journal of cardiology, 68(7), pp.B36-B50.

Asada, Y. *et al*. (2020a) 'Pathophysiology of atherothrombosis: Mechanisms of thrombus formation on disrupted atherosclerotic plaques', Pathology International. John Wiley & Sons, Ltd, 70(6), pp. 309–322. doi: 10.1111/pin.12921.

Asada, Y. *et al*. (2020b) 'Pathophysiology of atherothrombosis: Mechanisms of thrombus formation on disrupted atherosclerotic plaques', Pathology International, 70(6), pp. 309–322. doi: 10.1111/pin.12921.

Badimon, L. and Vilahur, G. (2014) 'Thrombosis formation on atherosclerotic lesions and plaque rupture', Journal of Internal Medicine, 276(6), pp. 618–632. doi: 10.1111/joim.12296.

Bennett, M.R., Sinha, S. and Owens, G.K., 2016. Vascular smooth muscle cells in atherosclerosis. Circulation research, 118(4), pp.692-702.

Bentzon, J. F. *et al*. (2014) 'Mechanisms of plaque formation and rupture', Circulation Research, 114(12), pp. 1852–1866. doi: 10.1161/CIRCRESAHA.114.302721.

Biros, E., Reznik, J. E. and Moran, C. S. (2021) 'Role of inflammatory cytokines in genesis and treatment of atherosclerosis', Trends in Cardiovascular Medicine. Elsevier Inc., (xxxx). doi: 10.1016/j.tcm.2021.02.001.

Bobryshev, Y. V. *et al*. (2016) 'Macrophages and Their Role in Atherosclerosis: Pathophysiology and Transcriptome Analysis', BioMed Research International, 2016(Figure 1). doi: 10.1155/2016/9582430.

Braunwald, E. *et al*. (2002) 'ACC/AHA guideline update for the management of patients with unstable angina and non-ST-segment elevation myocardial infarction - 2002: Summary article: A report of the American College of Cardiology/American Heart Association Task Force on Practice Guide', Circulation, 106(14), pp. 1893–1900. doi: 10.1161/01.CIR.0000037106.76139.53.

Brown, R.A., Wiseman, M., Chuo, C.B., Cheema, U. and Nazhat, S.N., 2005. Ultrarapid engineering of biomimetic materials and tissues: Fabrication of nano-and microstructures by plastic compression. Advanced functional materials, 15(11), pp.1762-1770.

Brown, T. M. and Bittner, V. (2009) 'Biomarkers of atherosclerosis: Clinical applications', Current Cardiovascular Risk Reports, 3(1), pp. 23–30. doi: 10.1007/s12170-009-0005-z.

Bruni, F. *et al*. (2003) 'Different effect induced by treatment with several statins on monocyte tissue factor expression in hypercholesterolemic subjects', Clinical and Experimental Medicine, 3(1), pp. 45–53. doi: 10.1007/s102380300015.

Cai, W., Sam Gambhir, S. and Chen, X., 2005. Multimodality tumor imaging targeting integrin αvβ3. Biotechniques, 39(6), pp.S14-S25.

Caligiuri, G., Nicoletti, A., Poirier, B. and Hansson, G.K., 2002. Protective immunity against atherosclerosis carried by B cells of hypercholesterolemic mice. The Journal of clinical investigation, 109(6), pp.745-753

Cavallari, I. *et al*. (2018) 'Metabolic syndrome and the risk of adverse cardiovascular events after an acute coronary syndrome', European Journal of Preventive Cardiology, 25(8), pp. 830–838. doi: 10.1177/2047487318763897.

Charo, I.F. and Taub, R., 2011. Anti-inflammatory therapeutics for the treatment of atherosclerosis. Nature reviews Drug discovery, 10(5), pp.365-376.

Cheema, U. and Brown, R. A. (2013) ' Rapid Fabrication of Living Tissue Models by Collagen Plastic Compression: Understanding Three-Dimensional Cell Matrix Repair In Vitro ', Advances in Wound Care, 2(4), pp. 176–184. doi: 10.1089/wound.2012.0392.

Chinetti-Gbaguidi, G. *et al*. (2011) 'Human atherosclerotic plaque alternative macrophages display low cholesterol handling but high phagocytosis because of distinct activities of the

PPARγ and LXRα pathways', Circulation Research, 108(8), pp. 985–995. doi: 10.1161/CIRCRESAHA.110.233775.

Cho, J. and Mosher, D. F. (2006) 'Role of fibronectin assembly in platelet thrombus formation', Journal of Thrombosis and Haemostasis, 4(7), pp. 1461–1469. doi: 10.1111/j.1538-7836.2006.01943.x.

Chong, H. *et al*. (2020) 'The PGC-1α/NRF1/miR-378a axis protects vascular smooth muscle cells from FFA-induced proliferation, migration and inflammation in atherosclerosis', Atherosclerosis. Elsevier, 297(April 2019), pp. 136–145. doi: 10.1016/j.atherosclerosis.2020.02.001.

Chung, C.P., Oeser, A., Solus, J.F., Avalos, I., Gebretsadik, T., Shintani, A., Raggi, P., Sokka, T., Pincus, T. and Stein, C.M., 2008. Prevalence of the metabolic syndrome is increased in rheumatoid arthritis and is associated with coronary atherosclerosis. Atherosclerosis, 196(2), pp.756-763.

Clarke, M. C. H. and Bennett, M. R. (2009) 'Cause or consequence: What does macrophage apoptosis do in atherosclerosis?', Arteriosclerosis, Thrombosis, and Vascular Biology, 29(2), pp. 153–155. doi: 10.1161/ATVBAHA.108.179903.

Copes, F. *et al*. (2019) 'Collagen-based tissue engineering strategies for vascular medicine', Frontiers in Bioengineering and Biotechnology, 7(JUL), pp. 1–15. doi: 10.3389/fbioe.2019.00166.

Costa, S. *et al*. (2016) 'Statins and oxidative stress in chronic heart failure', Revista Portuguesa de Cardiologia (English Edition). Sociedade Portuguesa de Cardiologia, 35(1), pp. 41–57.

Cunningham, K. S. and Gotlieb, A. I. (2005) 'The role of shear stress in the pathogenesis of atherosclerosis', Laboratory Investigation, 85(1), pp. 9–23. doi: 10.1038/labinvest.3700215.

Cyr, A.R., Huckaby, L.V., Shiva, S.S. and Zuckerbraun, B.S., 2020. Nitric oxide and endothelial dysfunction. Critical care clinics, 36(2), pp.307-321.

Daigneault, M. *et al*. (2010) 'The identification of markers of macrophage differentiation in PMA-stimulated THP-1 cells and monocyte-derived macrophages', PLoS ONE, 5(1). doi: 10.1371/journal.pone.0008668.

Dartsch, P.C., Bauriedel, G., Schinko, I., Weiss, H.D., Höfling, B. and Betz, E., 1989. Cell constitution and characteristics of human atherosclerotic plaques selectively removed by percutaneous atherectomy. Atherosclerosis, 80(2), pp.149-157.

Davignon, J. (2004) 'Beneficial cardiovascular pleiotropic effects of statins', Circulation, 109(23 SUPPL.), pp. 39–43. doi: 10.1161/01.cir.0000131517.20177.5a.

Davies, M.J. and Thomas, T., 1981. The pathological basis and microanatomy of occlusive thrombus formation in human coronary arteries. Philosophical Transactions of the Royal Society of London. B, Biological Sciences, 294(1072), pp.225-229.

Davies, M.J. and Thomas, A.C., 1985. Plaque fissuring--the cause of acute myocardial infarction, sudden ischaemic death, and crescendo angina. British heart journal, 53(4), p.363.

Davis, B. T. *et al*. (2014) 'Targeted disruption of LDLR causes hypercholesterolemia and atherosclerosis in Yucatan miniature pigs', PLoS ONE, 9(4), pp. 1–11. doi: 10.1371/journal.pone.0093457.

Davies, J.E., Lopresto, D., Apta, B.H., Lin, Z., Ma, W. and Harper, M.T., 2019. Using Yoda-1 to mimic laminar flow in vitro: A tool to simplify drug testing. Biochemical pharmacology, 168, pp.473-480.

Tentolouris, C., Tousoulis, D., Goumas, G., Stefanadis, C., Davies, G. and Toutouzas, P., 2000. L-Arginine in coronary atherosclerosis. International journal of cardiology, 75(2-3), pp.123-128.

Dejana, E., Orsenigo, F. and Lampugnani, M. G. (2008) 'The role of adherens junctions and VE-cadherin in the control of vascular permeability', Journal of Cell Science, 121(13), pp. 2115–2122. doi: 10.1242/jcs.017897.

De Groot, E., Van Leuven, S.I., Duivenvoorden, R., Meuwese, M.C., Akdim, F., Bots, M.L. and Kastelein, J.J., 2008. Measurement of carotid intima–media thickness to assess progression and regression of atherosclerosis. Nature clinical practice Cardiovascular medicine, 5(5), pp.280-288.

Van Der Donckt, C. *et al*. (2015) 'Elastin fragmentation in atherosclerotic mice leads to intraplaque neovascularization, plaque rupture, myocardial infarction, stroke, and sudden death', European Heart Journal, 36(17), pp. 1049–1058. doi: 10.1093/eurheartj/ehu041.

Dobos, A., Van Hoorick, J., Steiger, W., Gruber, P., Markovic, M., Andriotis, O.G., Rohatschek, A., Dubruel, P., Thurner, P.J., Van Vlierberghe, S. and Baudis, S., 2020. Thiol–gelatin–norbornene bioink for laser-based high-definition bioprinting. Advanced healthcare materials, 9(15), p.1900752.

Emini Veseli, B. *et al*. (2017) 'Animal models of atherosclerosis', European Journal of Pharmacology. Elsevier B.V., 816(May), pp. 3–13. doi: 10.1016/j.ejphar.2017.05.010.

Eto, M. *et al*. (2002) 'Statin prevents tissue factor expression in human endothelial cells: Role of Rho/Rho-kinase and Akt pathways', Circulation, 105(15), pp. 1756–1759. doi: 10.1161/01.CIR.0000015465.73933.3B.

Eun, S. Y. *et al*. (2015) 'IL-1β enhances vascular smooth muscle cell proliferation and migration via P2Y2 receptor-mediated RAGE expression and HMGB1 release', Vascular Pharmacology. Elsevier Inc., 72, pp. 108–117. doi: 10.1016/j.vph.2015.04.013.

Fan, J., Wang, J., Bensadoun, A., Lauer, S.J., Dang, Q., Mahley, R.W. and Taylor, J.M., 1994. Overexpression of hepatic lipase in transgenic rabbits leads to a marked reduction of plasma high density lipoproteins and intermediate density lipoproteins. Proceedings of the National Academy of Sciences, 91, pp.8724-8728.

Fan, J. *et al*. (2001) 'Overexpression of Lipoprotein Lipase in Transgenic Rabbits Inhibits Diet-induced Hypercholesterolemia and Atherosclerosis', Journal of Biological Chemistry, 276(43), pp. 40071–40079. doi: 10.1074/jbc.M105456200.

Feil, S., Fehrenbacher, B., Lukowski, R., Essmann, F., Schulze-Osthoff, K., Schaller, M. and Feil, R., 2014. Transdifferentiation of vascular smooth muscle cells to macrophage-like cells during atherogenesis. Circulation research, 115(7), pp.662-667.

Feintuch, A., Ruengsakulrach, P., Lin, A., Zhang, J., Zhou, Y.Q., Bishop, J., Davidson, L., Courtman, D., Foster, F.S., Steinman, D.A. and Henkelman, R.M., 2007. Hemodynamics in the mouse aortic arch as assessed by MRI, ultrasound, and numerical modeling. American Journal of Physiology-Heart and Circulatory Physiology, 292(2), pp.H884-H892.

Fruchart, J. C. *et al*. (2004) 'New risk factors for atherosclerosis and patient risk assessment', Circulation, 109(23 SUPPL.), pp. 15–19. doi: 10.1161/01.cir.0000131513.33892.5b.

Fukuhara, M., Matsumura, K., Ansai, T., Takata, Y., Sonoki, K., Akifusa, S., Wakisaka, M., Hamasaki, T., Fujisawa, K., Yoshida, A. and Fujii, K., 2006. Prediction of cognitive function by arterial stiffness in the very elderly. Circulation Journal, 70(6), pp.756-761.

Fukumoto, Y., Deguchi, J.O., Libby, P., Rabkin-Aikawa, E., Sakata, Y., Chin, M.T., Hill, C.C., Lawler, P.R., Varo, N., Schoen, F.J. and Krane, S.M., 2004. Genetically determined resistance to collagenase action augments interstitial collagen accumulation in atherosclerotic plaques. Circulation, 110(14),

Gal, D., Rongione, A.J., Slovenkai, G.A., DeJesus, S.T., Lucas, A., Fields, C.D. and Isner, J.M., 1990. Atherosclerotic Yucatan microswine: An animalmodel with high-grade, fibrocalcific, nonfatty lesions suitable for testing catheter-based interventions. American heart journal, 119(2), pp.291-300.

Gallo, D. *et al*. (2018) 'Segment-specific associations between local haemodynamic and imaging markers of early atherosclerosis at the carotid artery: An *in vivo* human study', Journal of the Royal Society Interface, 15(147). doi: 10.1098/rsif.2018.0352.

Gąsecka, A. *et al*. (2021) 'LDL-cholesterol and platelets: Insights into their interactions in atherosclerosis', Life, 11(1), pp. 1–13. doi: 10.3390/life11010039.

Gawaz, M. *et al*. (2005) 'Platelets in inflammation and atherogenesis Find the latest version : Review series Platelets in inflammation and atherogenesis', J Clin Invest, 115(12), pp. 3378–3384. doi: 10.1172/JCI27196.3378.

Gencer, B. *et al*. (2021) 'Cardiovascular risk and testosterone – from subclinical atherosclerosis to lipoprotein function to heart failure', Reviews in Endocrine and Metabolic

Disorders. Reviews in Endocrine and Metabolic Disorders, 22(2), pp. 257–274. doi: 10.1007/s11154-021-09628-2.

Genin, M. *et al*. (2015) 'M1 and M2 macrophages derived from THP-1 cells differentially modulate the response of cancer cells to etoposide', BMC Cancer. BMC Cancer, 15(1), pp. 1–14. doi: 10.1186/s12885-015-1546-9.

Getz, G. S. and Reardon, C. A. (2012) 'Animal models of Atherosclerosis', Arteriosclerosis, Thrombosis, and Vascular Biology, 32(5), pp. 1104–1115. doi: 10.1161/ATVBAHA.111.237693.

Golia, E. *et al*. (2014) 'Inflammation and cardiovascular disease: From pathogenesis to therapeutic target', Current Atherosclerosis Reports, 16(9). doi: 10.1007/s11883-014-0435-z.

Gomez, D., Kessler, K., Michel, J.B. and Vranckx, R., 2013. Modifications of chromatin dynamics control Smad2 pathway activation in aneurysmal smooth muscle cells. Circulation research, 113(7), pp.881-890.

Goodenough, D.A. and Paul, D.L., 2009. Gap junctions. Cold Spring Harbor perspectives in biology, 1(1), p.a002576.

Gough, P. J. *et al*. (2006) 'Macrophage expression of active MMP-9 induces acute plaque disruption in apoE-deficient mice', Journal of Clinical Investigation, 116(1), pp. 59–69. doi: 10.1172/JCI25074.

Granada, J. F. *et al*. (2009) 'Porcine models of coronary atherosclerosis and vulnerable plaque for imaging and interventional research', EuroIntervention, 5(1), pp. 140–148. doi: 10.4244/EIJV5I1A22.

Granger, D. N. and Senchenkova, E. (2010) Inflammation and the Microcirculation, Colloquium Series on Integrated Systems Physiology: From Molecule to Function. doi: 10.4199/c00013ed1v01y201006isp008.

Grant, E.G., Benson, C.B., Moneta, G.L., Alexandrov, A.V., Baker, J.D., Bluth, E.I., Carroll, B.A., Eliasziw, M., Gocke, J., Hertzberg, B.S. and Katanick, S., 2003. Carotid artery stenosis: gray-scale and Doppler US diagnosis—Society of Radiologists in Ultrasound Consensus Conference. Radiology, 229(2), pp.340-346.

Gross, S. *et al*. (2007) 'Vascular wall-produced prostaglandin E2 exacerbates arterial thrombosis and atherothrombosis through platelet EP3 receptors', Journal of Experimental Medicine, 204(2), pp. 311–320. doi: 10.1084/jem.20061617.

Grover, S. P. and Mackman, N. (2020) 'Tissue factor in atherosclerosis and atherothrombosis', Atherosclerosis. Elsevier, 307(June), pp. 80–86. doi: 10.1016/j.atherosclerosis.2020.06.003.

Gualtero, D. F., Lafaurie, G. I. and Fontanilla, M. R. (2018) 'Two-dimensional and three-dimensional models for studying atherosclerosis pathogenesis induced by

periodontopathogenic microorganisms', Molecular Oral Microbiology, 33(1), pp. 29–37. doi: 10.1111/omi.12201.

Guha, M. *et al*. (2001) 'Lipopolysaccharide activation of the MEK-ERK1/2 pathway in human monocytic cells mediates tissue factor and tumor necrosis factor α expression by inducing Elk-1 phosphorylation and Egr-1 expression', Blood, 98(5), pp. 1429–1439. doi: 10.1182/blood.V98.5.1429.

de Haan, W. *et al*. (2008) 'Atorvastatin increases HDL cholesterol by reducing CETP expression in cholesterol-fed APOE*3-Leiden.CETP mice', Atherosclerosis, 197(1), pp. 57–63. doi: 10.1016/j.atherosclerosis.2007.08.001.

Hansson, G. K., Holm, J. and Jonasson, L. (1989) 'Detection of activated T lymphocytes in the human atherosclerotic plaque', American Journal of Pathology, 135(1), pp. 169–175.

Hansson, G. K. and Jonasson, L. (2009) 'The discovery of cellular immunity in the atherosclerotic plaque', Arteriosclerosis, Thrombosis, and Vascular Biology, 29(11), pp. 1714–1717. doi: 10.1161/ATVBAHA.108.179713.

Hartman, C. D. *et al*. (2016) 'Vascular smooth muscle cell durotaxis depends on extracellular matrix composition', Proceedings of the National Academy of Sciences of the United States of America, 113(40), pp. 11190–11195. doi: 10.1073/pnas.1611324113.

Hartwig, H. *et al*. (2015) 'Atherosclerotic plaque destabilization in Mice: A comparative study', PLoS ONE, 10(10), pp. 1–14. doi: 10.1371/journal.pone.0141019.

He, C. *et al*. (2020) 'Cultured macrophages transfer surplus cholesterol into adjacent cells in the absence of serum or high-density lipoproteins', Proceedings of the National Academy of Sciences of the United States of America, 117(19), pp. 10476–10483. doi: 10.1073/pnas.1922879117.

Van Herck, J. L. *et al*. (2009) 'Impaired fibrillin-1 function promotes features of plaque instability in apolipoprotein E-deficient mice', Circulation, 120(24), pp. 2478–2487. doi: 10.1161/CIRCULATIONAHA.109.872663.

Herman, M. P. *et al*. (2001) 'Expression of Neutrophil Collagenase (Matrix Metalloproteinase-8) in Human Atheroma', Circulation, 104(16), pp. 1899–1904. doi: 10.1161/hc4101.097419.

Higuma, T. *et al*. (2015) 'A Combined Optical Coherence Tomography and Intravascular Ultrasound Study on Plaque Rupture, Plaque Erosion, and Calcified Nodule in Patients with ST-Segment Elevation Myocardial Infarction Incidence, Morphologic Characteristics, and Outcomes after Percu', JACC: Cardiovascular Interventions. Elsevier, 8(9), pp. 1166–1176. doi: 10.1016/j.jcin.2015.02.026.

Hoffman, M. (2003) 'A cell-based coagulation factor Vlla and the role of', Blood Reviews, 17, pp. S1–S5.

Hoshiba, Y. *et al*. (2006) 'Co-localization of von Willebrand factor with platelet thrombi, tissue factor and platelets with fibrin, and consistent presence of inflammatory cells in coronary thrombi obtained by an aspiration device from patients with acute myocardial infarction', Journal of Thrombosis and Haemostasis, 4(1), pp. 114–120. doi: 10.1111/j.1538-7836.2005.01701.x.

Hosseini, V. *et al*. (2021) ' Healthy and diseased in vitro models of vascular systems ', Lab on a Chip. doi: 10.1039/d0lc00464b.

Huang, H. *et al*. (2019) 'Thermo-sensitive hydrogels for delivering biotherapeutic molecules: A review', Saudi Pharmaceutical Journal. King Saud University, 27(7), pp. 990–999. doi: 10.1016/j.jsps.2019.08.001.

Huang, R. *et al*. (2020) 'Ursodeoxycholic acid inhibits intimal hyperplasia, vascular smooth muscle cell excessive proliferation, migration via blocking miR-21/PTEN/AKT/mTOR signaling pathway', Cell Cycle, 19(8). doi: 10.1080/15384101.2020.1732514.

Huo, Y., Schober, A., Forlow, S.B., Smith, D.F., Hyman, M.C., Jung, S., Littman, D.R., Weber, C. and Ley, K., 2003. Circulating activated platelets exacerbate atherosclerosis in mice deficient in apolipoprotein E. Nature medicine, 9(1), pp.61-67.

Ignatowski, A.C., 1908. Influence of animal food on the organsim of rabbits. Izvest Imper Voennomed Akad St Petersburg, 16, pp.154-173

Islam, K. *et al*. (2016) 'Co-culture Methods Used to Model Atherosclerosis In Vitro Using Endothelial, Smooth Muscle and Monocyte Cells', SM Journal of Biomedical Engineering, 2(1), p. 1008.

Ishibashi, S. *et al*. (1993) 'Hypercholesterolemia in low density lipoprotein receptor knockout mice and its reversal by adenovirus-mediated gene delivery', Journal of Clinical Investigation, 92(2), pp. 883–893. doi: 10.1172/JCI116663.

Jensen, T. O. *et al*. (2009) 'Macrophage markers in serum and tumor have prognostic impact in American joint committee on cancer stage I/II melanoma', Journal of Clinical Oncology, 27(20), pp. 3330–3337. doi: 10.1200/JCO.2008.19.9919.

Jia, H. *et al*. (2013) '*In vivo* diagnosis of plaque erosion and calcified nodule in patients with acute coronary syndrome by intravascular optical coherence tomography', Journal of the American College of Cardiology, 62(19), pp. 1748–1758. doi: 10.1016/j.jacc.2013.05.071.

Kaplan, Z.S. and Jackson, S.P., 2011. The role of platelets in atherothrombosis. Hematology 2010, the American Society of Hematology Education Program Book, 2011(1), pp.51-61.

Kasiński, A. *et al*. (2020) 'Smart hydrogels – synthetic stimuli-responsive antitumor drug release systems', International Journal of Nanomedicine, 15, pp. 4541–4572. doi: 10.2147/IJN.S248987.

Jaberi, N., Soleimani, A., Pashirzad, M., Abdeahad, H., Mohammadi, F., Khoshakhlagh, M., Khazaei, M., Ferns, G.A., Avan, A. and Hassanian, S.M., 2019. Role of thrombin in the pathogenesis of atherosclerosis. Journal of cellular biochemistry, 120(4), pp.4757-4765.

Jackson, I.L., Gurung, G., Poirier, Y., Gopalakrishnan, M., Cohen, E.P., Donohue, T.S., Newman, D. and Vujaskovic, Z., 2020. A New Zealand white rabbit model of thrombocytopenia and coagulopathy following total body irradiation across the dose range to induce the hematopoietic-subsyndrome of acute radiation syndrome. International journal of radiation biology, pp.1-13.

Jonasson, L., Holm, J., Skalli, O., Gabbiani, G. and Hansson, G.K., 1985. Expression of class II transplantation antigen on vascular smooth muscle cells in human atherosclerosis. The Journal of clinical investigation, 76(1), pp.125-131

Katsuda, S., Boyd, H.C., Fligner, C., Ross, R. and Gown, A.M., 1992. Human atherosclerosis. III. Immunocytochemical analysis of the cell composition of lesions of young adults. The American journal of pathology, 140(4), p.907.

Khandkar, C. *et al*. (2021) 'Atherothrombosis in Acute Coronary Syndromes-From Mechanistic Insights to Targeted Therapies', Cells, 10(4). doi: 10.3390/cells10040865.

Kolodgie, F. D. *et al*. (1996) 'Hypercholesterolemia in the Rabbit Induced by Feeding Graded Amounts of Low-Level Cholesterol: Methodological Considerations Regarding Individual Variability in Response to Dietary Cholesterol and Development of Lesion Type', Arteriosclerosis, Thrombosis, and Vascular Biology, 16(12), pp. 1454–1464. doi: 10.1161/01.ATV.16.12.1454.

Kidd, S.K., Bonaca, M.P., Braunwald, E., De Ferrari, G.M., Lewis, B.S., Merlini, P.A., Murphy, S.A., Scirica, B.M., White, H.D. and Morrow, D.A., 2016. Universal Classification System Type of Incident Myocardial Infarction in Patients With Stable Atherosclerosis: Observations From Thrombin Receptor Antagonist in Secondary Prevention of Atherothrombotic Ischemic Events (TRA 2° P)-TIMI 50. Journal of the American Heart Association, 5(7), p.e003237.

Kingwell, B.A., Waddell, T.K., Medley, T.L., Cameron, J.D. and Dart, A.M., 2002. Large artery stiffness predicts ischemic threshold in patients with coronary artery disease. Journal of the American College of Cardiology, 40(4), pp.773-779.

Lee, R. T. *et al*. (1991) 'Structure-dependent dynamic mechanical behavior of fibrous caps from human atherosclerotic plaques', Circulation, 83(5), pp. 1764–1770. doi: 10.1161/01.CIR.83.5.1764.

Li, L. *et al*. (2020) 'Foam cells promote atherosclerosis progression by releasing CXCL12', Bioscience reports, 40(1), pp. 1–12. doi: 10.1042/BSR20193267.

Libby, P. *et al*. (2019) 'Reassessing the Mechanisms of Acute Coronary Syndromes: The "vulnerable Plaque" and Superficial Erosion', Circulation Research, 124(1), pp. 150–160. doi: 10.1161/CIRCRESAHA.118.311098.

Lillis, A. P. *et al*. (2015) 'LDL receptor-related protein-1 (LRP1) regulates cholesterol accumulation in macrophages', PLoS ONE. Public Library of Science, 10(6). doi: 10.1371/journal.pone.0128903.

Lindmark, H. *et al*. (2004) 'Gene expression profiling shows that macrophages derived from mouse embryonic stem cells is an improved in vitro model for studies of vascular disease', Experimental Cell Research, 300(2), pp. 335–344. doi: 10.1016/j.yexcr.2004.06.025.

Liu, L. and Shi, G. P. (2012) 'CD31: Beyond a marker for endothelial cells', Cardiovascular Research, 94(1), pp. 3–5. doi: 10.1093/cvr/cvs108.

Liu, M., Karagiannis, A., Sis, M., Rask, E., Kidambi, S. and Chatzizisis, Y., 2017. THree-dimensional co-cultures of human coronary artery endothelial and smooth muscle cells: A novel in-vitro experimental model of atherosclerosis. Atherosclerosis, 263, pp.e77-e78.

Lordan, R., Tsoupras, A. and Zabetakis, I. (2021) 'Platelet activation and prothrombotic mediators at the nexus of inflammation and atherosclerosis: Potential role of antiplatelet agents', Blood Reviews. Elsevier Ltd, 45(April 2020). doi: 10.1016/j.blre.2020.100694.

Lund, M. E. *et al*. (2016) 'The choice of phorbol 12-myristate 13-acetate differentiation protocol influences the response of THP-1 macrophages to a pro-inflammatory stimulus', Journal of Immunological Methods. Elsevier B.V., 430, pp. 64–70. doi: 10.1016/j.jim.2016.01.012.

Madhvi, A., Mishra, H., Leisching, G.R., Mahlobo, P.Z. and Baker, B., 2019. Comparison of human monocyte derived macrophages and THP1-like macrophages as in vitro models for M. tuberculosis infection. Comparative immunology, microbiology and infectious diseases, 67, p.101355.

Mallavia, B., Oguiza, A., Lopez-Franco, O., Recio, C., Ortiz-Muñoz, G., Lazaro, I., Lopez-Parra, V., Egido, J. and Gomez-Guerrero, C., 2013. Gene deficiency in activating Fcγ receptors influences the macrophage phenotypic balance and reduces atherosclerosis in mice. PLoS One, 8(6), p.e66754.

Mallone, A. *et al*. (2018) 'Biofabricating atherosclerotic plaques: In vitro engineering of a three-dimensional human fibroatheroma model', Biomaterials. Elsevier Ltd, 150, pp. 49–59. doi: 10.1016/j.biomaterials.2017.09.034.

Mallone, A. *et al*. (2020) 'Curcumin affects ox-LDL-induced IL-6, TNF-α, MCP-1 secretion and cholesterol efflux in THP-1 cells by suppressing the TLR4/NF-κB/miR33a signaling pathway', Experimental and Therapeutic Medicine. BMC Cardiovascular Disorders, 146(1), pp. 1–11. doi: 10.1038/s41467-020-19197-8.

Massberg, S. *et al*. (2002) 'A critical role of platelet adhesion in the initiation of atherosclerotic lesion formation', Journal of Experimental Medicine, 196(7), pp. 887–896. doi: 10.1084/jem.20012044.

Mason, S.S., 2013. Exploring tissue engineering: vitamin d3 influences on the proliferation and differentiation of an engineered osteoblast precursor cell line during early bone tissue development.

Mast, A. E. (2016) 'Tissue Factor Pathway Inhibitor: Multiple Anticoagulant Activities for a Single Protein', Arteriosclerosis, Thrombosis, and Vascular Biology, 36(1), pp. 9–14. doi: 10.1161/ATVBAHA.115.305996.

Mastenbroek, T. G. *et al*. (2015) 'Acute and persistent platelet and coagulant activities in atherothrombosis', Journal of Thrombosis and Haemostasis, 13(S1), pp. S272–S280. doi: 10.1111/jth.12972.

Mazzolai, L., Duchosal, M.A., Korber, M., Bouzourene, K., Aubert, J.F., Hao, H., Vallet, V., Brunner, H.R., Nussberger, J., Gabbiani, G. and Hayoz, D., 2004. Endogenous angiotensin II induces atherosclerotic plaque vulnerability and elicits a Th1 response in ApoE−/− mice. Hypertension, 44(3), pp.277-282.

McDaniel, J.S., Antebi, B., Pilia, M., Hurtgen, B.J., Belenkiy, S., Necsoiu, C., Cancio, L.C., Rathbone, C.R. and Batchinsky, A.I., 2017. Quantitative assessment of optimal bone marrow site for the isolation of porcine mesenchymal stem cells. Stem cells international, 2017.

Mihaylov, D., van Luyn, M.J. and Rakhorst, G., 2000. Development of an animal model of selective coronary atherosclerosis. Coronary artery disease, 11(2), pp.145-149.

Miller, C. L. and Zhang, H. (2021) 'Clarifying the Distinct Roles of Smooth Muscle Cell–Derived Versus Macrophage Foam Cells and the Implications in Atherosclerosis', Arteriosclerosis, Thrombosis, and Vascular Biology, 41(6), pp. 2035–2037. doi: 10.1161/atvbaha.121.316287.

Mitchell, P.L. and McLeod, R.S., 2008. Conjugated linoleic acid and atherosclerosis: studies in animal models. Biochemistry and Cell Biology, 86(4), pp.293-301.

Monaco, C. *et al*. (2004) 'Canonical pathway of nuclear factor κB activation selectively regulates proinflammatory and prothrombotic responses in human atherosclerosis', Proceedings of the National Academy of Sciences of the United States of America, 101(15), pp. 5634–5639. doi: 10.1073/pnas.0401060101.

Murray, P. J. *et al*. (2014) 'Macrophage Activation and Polarization: Nomenclature and Experimental Guidelines', Immunity. Elsevier, 41(1), pp. 14–20. doi: 10.1016/j.immuni.2014.06.008.

Musa, F. I., Harper, A. G. S. and Yang, Y. (2016) 'A Real-Time Monitoring System to Assess the Platelet Aggregatory Capacity of Components of a Tissue-Engineered Blood Vessel Wall', Tissue Engineering - Part C: Methods, 22(7), pp. 691–699. doi: 10.1089/ten.tec.2015.0582.

Nakashima, Y. *et al*. (1994) 'the Arterial Tree', pp. 133–140.

National Institute for Health and Care Excellence (NICE) (2016) 'Cardiovascular disease: risk assessment and reduction, including lipid modification', National Institute for Health Care Excellence, CG181(July), pp. 1–38. Available at: https://www.nice.org.uk/guidance/cg181.

Navab, M. *et al*. (1988) 'Monocyte migration into the subendothelial space of a coculture of adult human aortic endothelial and smooth muscle cells', Journal of Clinical Investigation, 82(6), pp. 1853–1863. doi: 10.1172/JCI113802.

Newby, A. C. (2016) 'Metalloproteinase production from macrophages – a perfect storm leading to atherosclerotic plaque rupture and myocardial infarction', Experimental Physiology, 101(11), pp. 1327–1337. doi: 10.1113/EP085567.

Niessner, A., Goronzy, J.J. and Weyand, C.M., 2007. Immune-mediated mechanisms in atherosclerosis: prevention and treatment of clinical manifestations. Current pharmaceutical design, 13(36), pp.3701-3710

Nezu, T. *et al*. (2016) 'Carotid Intima-media thickness for atherosclerosis', Journal of Atherosclerosis and Thrombosis, 23(1), pp. 18–31. doi: 10.5551/jat.31989.

Niu, C. *et al*. (2016) 'Macrophage foam cell-derived extracellular vesicles promote vascular smooth muscle cell migration and adhesion', Journal of the American Heart Association, 5(10). doi: 10.1161/JAHA.116.004099.

Noonan, J., Grassia, G., MacRitchie, N., Garside, P., Guzik, T.J., Bradshaw, A.C. and Maffia, P., 2019. A novel triple-cell two-dimensional model to study immune-vascular interplay in atherosclerosis. Frontiers in immunology, 10, p.849.

de Oliveira, P. S. S. *et al*. (2020) 'Atorvastatin inhibits IL-17A, TNF, IL-6, and IL-10 in PBMC cultures from patients with severe rheumatoid arthritis', Immunobiology. Elsevier, 225(3), p. 151908. doi: 10.1016/j.imbio.2020.151908.

Okuyama, H., Langsjoen, P.H., Hamazaki, T., Ogushi, Y., Hama, R., Kobayashi, T. and Uchino, H., 2015. Statins stimulate atherosclerosis and heart failure: pharmacological mechanisms. Expert review of clinical pharmacology, 8(2), pp.189-199.

Otsuka, F. *et al*. (2016) 'Pathology of coronary atherosclerosis and thrombosis', Cardiovascular Diagnosis and Therapy, 6(4), pp. 396–408. doi: 10.21037/cdt.2016.06.01.

Ovsianikov, A., Khademhosseini, A. and Mironov, V. (2018) 'The Synergy of Scaffold-Based and Scaffold-Free Tissue Engineering Strategies', Trends in Biotechnology. Elsevier Ltd, 36(4), pp. 348–357. doi: 10.1016/j.tibtech.2018.01.005.

Owens, A. P. *et al*. (2012) 'Monocyte tissue factor - Dependent activation of coagulation in hypercholesterolemic mice and monkeys is inhibited by simvastatin', Journal of Clinical Investigation, 122(2), pp. 558–568. doi: 10.1172/JCI58969.

Owens, A. P. and MacKman, N. (2012) 'Sources of tissue factor that contribute to thrombosis after rupture of an atherosclerotic plaque', Thrombosis Research, 129(SUPPL. 2). doi: 10.1016/j.thromres.2012.02.026.

Owens, G. K., Kumar, M. S. and Wamhoff, B. R. (2004) 'Molecular regulation of vascular smooth muscle cell differentiation in development and disease', Physiological Reviews, 84(3), pp. 767–801. doi: 10.1152/physrev.00041.2003.

Paez-Mayorga J, Hernández-Vargas G, Ruiz-Esparza GU, Iqbal HM, Wang X, Zhang YS, Parra-Saldivar R, Khademhosseini A. Bioreactors for cardiac tissue engineering. Advanced healthcare materials. 2019 Apr;8(7):1701504.

Pignatelli, P. *et al*. (2005) 'Tumor necrosis factor-α as trigger of platelet activation in patients with heart failure', Blood, 106(6), pp. 1992–1994. doi: 10.1182/blood-2005-03-1247.

Poznyak, A. V. *et al*. (2020) 'Animal models of human atherosclerosis: Current progress', Brazilian Journal of Medical and Biological Research, 53(6), pp. 1–8. doi: 10.1590/1414-431x20209557.

Poznyak, Anastasia V. *et al*. (2020) 'Signaling Pathways and Key Genes Involved in Regulation of foam Cell Formation in Atherosclerosis', Cells, 9(3), p. 584. doi: 10.3390/cells9030584.

Qiu, F. *et al*. (2021) 'Amentoflavone inhibits M1 polarization of THP-1-derived foam cells by activating PPAR-α/γ', Nan fang yi ke da xue xue bao = Journal of Southern Medical University, 41(3), pp. 344–351. doi: 10.12122/j.issn.1673-4254.2021.03.05.

Qiu, L. *et al*. (2020) 'Activation of CXCR7 promotes endothelial repair and reduces the carotid atherosclerotic lesions through inhibition of pyroptosis signaling pathways', Aging Cell, 19(9), pp. 1–13. doi: 10.1111/acel.13205.

Raman, R. *et al*. (2020) 'Light-degradable hydrogels as dynamic triggers for gastrointestinal applications', Science Advances, 6(3), pp. 1–11. doi: 10.1126/sciadv.aay0065.

Reininger, A. J. *et al*. (2010) 'A 2-Step Mechanism of Arterial Thrombus Formation Induced by Human Atherosclerotic Plaques', Journal of the American College of Cardiology, 55(11), pp. 1147–1158. doi: 10.1016/j.jacc.2009.11.051.

Rensen, S. S. M., Doevendans, P. A. F. M. and Van Eys, G. J. J. M. (2007) 'Regulation and characteristics of vascular smooth muscle cell phenotypic diversity', Netherlands Heart Journal, 15(3), pp. 100–108. doi: 10.1007/BF03085963.

Plump, A.S., Smith, J.D., Hayek, T., Aalto-Setälä, K., Walsh, A., Verstuyft, J.G., Rubin, E.M. and Breslow, J.L., 1992. Severe hypercholesterolemia and atherosclerosis in apolipoprotein E-deficient mice created by homologous recombination in ES cells. Cell, 71(2), pp.343-353.

Robert, J. *et al*. (2013) 'A three-dimensional engineered artery model for in vitro atherosclerosis research', PLoS ONE, 8(11). doi: 10.1371/journal.pone.0079821.

Sato, Y. et al. (2005) 'Proportion of fibrin and platelets differs in thrombi on ruptured and eroded coronary atherosclerotic plaques in humans', Heart, 91(4), pp. 526–530. doi: 10.1136/hrt.2004.034058.

Schnoor, M. *et al*. (2021) 'Production of Type VI Collagen by Human Macrophages : A New Dimension in Macrophage Functional Heterogeneity 1 , 2'. doi: 10.4049/jimmunol.180.8.5707.

Seimon, T. and Tabas, I. (2009) 'Mechanisms and consequences of macrophage apoptosis in atherosclerosis', Journal of Lipid Research, 50(SUPPL.). doi: 10.1194/jlr.R800032-JLR200.

De Servi, S. *et al*. (1990) 'Granulocyte activation after coronary angioplasty in humans', Circulation, 82(1), pp. 140–146. doi: 10.1161/01.CIR.82.1.140.

Shahar, E. *et al*. (2003) 'Plasma lipid profile and incident ischemic stroke: The Atherosclerosis Risk in Communities (ARIC) Study', Stroke, 34(3), pp. 623–631. doi: 10.1161/01.STR.0000057812.51734.FF.

Shankman, L.S., Gomez, D., Cherepanova, O.A., Salmon, M., Alencar, G.F., Haskins, R.M., Swiatlowska, P., Newman, A.A., Greene, E.S., Straub, A.C. and Isakson, B., 2015. KLF4-dependent phenotypic modulation of smooth muscle cells has a key role in atherosclerotic plaque pathogenesis. Nature medicine, 21(6), pp.628-637.

Sheikine, Y.A. and Hansson, G.K., 2006. Chemokines as potential therapeutic targets in atherosclerosis. Current drug targets, 7(1), pp.13-27.

Siess, W. *et al*. (1999) 'Lysophosphatidic acid mediates the rapid activation of platelets and endothelial cells by mildly oxidized low density lipoprotein and accumulates in human atherosclerotic lesions', Proceedings of the National Academy of Sciences of the United States of America, 96(12), pp. 6931–6936. doi: 10.1073/pnas.96.12.6931.

Tang, M. and Fang, J. (2017) 'TNF-α regulates apoptosis of human vascular smooth muscle cells through gap junctions', Molecular Medicine Reports, 15(3), pp. 1407–1411. doi: 10.3892/mmr.2017.6106.

Territo, M., Berliner, J. A. and Fogelman, A. M. (1984) 'Effect of monocyte migration on low density lipoprotein transport across aortic endothelial cell monolayers', Journal of Clinical Investigation, 74(6), pp. 2279–2284. doi: 10.1172/JCI111655.

Timmis, A. *et al*. (2018) 'European Society of Cardiology: Cardiovascular disease statistics 2017', European Heart Journal, 39(7), pp. 508–577. doi: 10.1093/eurheartj/ehx628.

Timraz, S. B. H. *et al*. (2015) 'Stiffness of extracellular matrix components modulates the phenotype of human smooth muscle cells in vitro and allows for the control of properties of engineered tissues', Procedia Engineering. Elsevier B.V., 110, pp. 29–36. doi: 10.1016/j.proeng.2015.07.006.

Truskey, G. A. (2011) 'Endotheliar cell vascular smooth muscel co-culture assay for high throughput screening assays', International journal high throughput screen, 2010(1), pp171 181. doi: 10.2147/IJHTS.S13459.Endothelial.

Taylor, F., Huffman, M.D., Macedo, A.F., Moore, T.H., Burke, M., Smith, G.D., Ward, K. and Ebrahim, S., 2013. Statins for the primary prevention of cardiovascular disease. Cochrane database of systematic reviews, (1).

Valgimigli, M. and Biscaglia, S. (2014) 'Stable angina pectoris', Current Atherosclerosis Reports, 16(7). doi: 10.1007/s11883-014-0422-4.

Vasileiou, P.V., Xanthos, T., Barouxis, D., Pantazopoulos, C., Papalois, A.E., Lelovas, P., Kotsilianou, O., Pliatsika, P., Kouskouni, E. and Iacovidou, N., 2014. Erythropoietin administration facilitates return of spontaneous circulation and improves survival in a pig model of cardiac arrest. The American journal of emergency medicine, 32(8), pp.871-877.

Virmani, R. *et al*. (2000) 'Lessons From Sudden Coronary Death', Arteriosclerosis, Thrombosis, and Vascular Biology, 20(5), pp. 1262–1275. doi: 10.1161/01.atv.20.5.1262.

Virmani, R. *et al*. (2003) 'Pathology of the thin-cap fibroatheroma: A type of vulnerable plaque', Journal of Interventional Cardiology, 16(3), pp. 267–272. doi: 10.1034/j.1600-0854.2003.8042.x.

Van Der Wal, A. C. *et al*. (1994) 'Site of intimal rupture or erosion of thrombosed coronary atherosclerotic plaques is characterized by an inflammatory process irrespective of the dominant plaque morphology', Circulation, 89(1), pp. 36–44. doi: 10.1161/01.CIR.89.1.36.

Varghese, J. F., Patel, R. and Yadav, U. C. S. (2017) 'Novel Insights in the Metabolic

249

Syndrome-induced Oxidative Stress and Inflammation-mediated Atherosclerosis', Current Cardiology Reviews, 14(1), pp. 4–14. doi: 10.2174/1573403x13666171009112250.

Tedesco, S., De Majo, F., Kim, J., Trenti, A., Trevisi, L., Fadini, G.P., Bolego, C., Zandstra, P.W., Cignarella, A. and Vitiello, L., 2018. Convenience versus biological significance: are PMA-differentiated THP-1 cells a reliable substitute for blood-derived macrophages when studying in vitro polarization?. Frontiers in pharmacology, 9, p.71.

Urbina, E.M., Williams, R.V., Alpert, B.S., Collins, R.T., Daniels, S.R., Hayman, L., Jacobson, M., Mahoney, L., Mietus-Snyder, M., Rocchini, A. and Steinberger, J., 2009. Noninvasive assessment of subclinical atherosclerosis in children and adolescents: recommendations for standard assessment for clinical research: a scientific statement from the American Heart Association. Hypertension, 54(5), pp.919-950.

Wang, J. *et al*. (2017) 'Novel biomarkers for cardiovascular risk prediction', Journal of Geriatric Cardiology, 14(2), pp. 135–150. doi: 10.11909/j.issn.1671-5411.2017.02.008.

Wang, Y. *et al*. (2019a) 'Smooth Muscle Cells Contribute the Majority of Foam Cells in ApoE (Apolipoprotein E)-Deficient Mouse Atherosclerosis', Arteriosclerosis, Thrombosis, and Vascular Biology, 39(5), pp. 876–887. doi: 10.1161/ATVBAHA.119.312434.

Wang, Y. *et al*. (2019b) 'Smooth Muscle Cells Contribute the Majority of Foam Cells in ApoE (Apolipoprotein E)-Deficient Mouse Atherosclerosis', Arteriosclerosis, Thrombosis, and Vascular Biology, 39(5), pp. 876–887. doi: 10.1161/ATVBAHA.119.312434.

Wang, Y. C. *et al*. (2015) 'Ox-LDL Upregulates IL-6 Expression by Enhancing NF-κB in an IGF2-Dependent Manner in THP-1 Macrophages', Inflammation, 38(6), pp. 2116–2123. doi: 10.1007/s10753-015-0194-1.

Watanabe, Y., 1980. Serial inbreeding of rabbits with hereditary hyperlipidemia (WHHL-rabbit): incidence and development of atherosclerosis and xanthoma. Atherosclerosis, 36, pp.261-268.

Westhorpe, C.L., Dufour, E.M., Maisa, A., Jaworowski, A., Crowe, S.M. and Muller, W.A., 2012. Endothelial cell activation promotes foam cell formation by monocytes following transendothelial migration in an in vitro model. Experimental and molecular pathology, 93(2), pp.220-226.

White, F.C., Carroll, S.M., Magnet, A. and Bloor, C.M., 1992. Coronary collateral development in swine after coronary artery occlusion. Circulation Research, 71(6), pp.1490-1500.

White, F.C., Carroll, S.M., Magnet, A. and Bloor, C.M., 1992. Coronary collateral development in swine after coronary artery occlusion. Circulation Research, 71(6), pp.1490-1500.

Worthley, S.G., Helft, G., Fuster, V., Zaman, A.G., Fayad, Z.A., Fallon, J.T. and Badimon, J.J., 2000. Serial *in vivo* MRI documents arterial remodelling in experimental atherosclerosis. Circulation, 101, pp.586-589.

Van de Werf, F. *et al*. (2003) 'Management of acute myocardial infarction in patients presenting with ST-segment elevation', European Heart Journal, 24(1), pp. 28–66. doi: 10.1016/S0195-668X(02)00618-8.

Wilcox, J. N. *et al*. (1989) 'tissue factor', 86(April), pp. 2839–2843.

Wolf, D. and Ley, K., 2019. Immunity and inflammation in atherosclerosis. Circulation research, 124(2), pp.315-327

Wraith, K. S. et al. (2013) 'Oxidized low-density lipoproteins induce rapid platelet activation and shape change through tyrosine kinase and Rho kinase–signaling pathways', Blood, 122(4), pp. 580–589. doi: 10.1182/blood-2013-04-491688.

Wu, M., Yang, S., Wang, S., Cao, Y., Zhao, R., Li, X., Xing, Y. and Liu, L., 2020. Effect of berberine on atherosclerosis and gut microbiota modulation and their correlation in high-fat diet-fed ApoE−/− mice. Frontiers in pharmacology, 11, p.223.

Xue, Q. *et al*. (2020) 'CEMIP regulates the proliferation and migration of vascular smooth muscle cells in atherosclerosis through the WNT–beta-catenin signaling pathway', Biochemistry and Cell Biology, 98(2), pp. 1–9. doi: 10.1139/bcb-2019-0249.

Yang, Y., Li, G.P., Cheng, G.M., Li, Y.L. and Yang, K., 2009. Multiple deformation mechanisms of Ti–22.4 Nb–0.73 Ta–2.0 Zr–1.34 O alloy. Applied Physics Letters, 94(6), p.061901.

Yang, G. and Chen, L. (2016) 'An Update of Microsomal Prostaglandin e Synthase-1 and PGE2 Receptors in Cardiovascular Health and Diseases', Oxidative Medicine and Cellular Longevity, 2016. doi: 10.1155/2016/5249086.

Yang, S. *et al*. (2020) 'Macrophage polarization in atherosclerosis', Clinica Chimica Acta. Elsevier, 501(October 2019), pp. 142–146. doi: 10.1016/j.cca.2019.10.034.

Yonetsu, T. and Jang, I. K. (2018) 'Advances in intravascular imaging: New insights into the vulnerable plaque from imaging studies', Korean Circulation Journal, 48(1), pp. 1–15. doi: 10.4070/kcj.2017.0182.

Yurdagul Jr, A., Finney, A.C., Woolard, M.D. and Orr, A.W., 2016. The arterial microenvironment: the where and why of atherosclerosis. Biochemical Journal, 473(10), pp.1281-1295.

Yu, T. *et al*. (2019) 'Modulation of M2 macrophage polarization by the crosstalk between Stat6 and Trim24', Nature Communications, 10(1). doi: 10.1038/s41467-019-12384-2.

Zaidi, A. and Green, L. (2019) 'Physiology of haemostasis', Anaesthesia and Intensive Care Medicine. Elsevier Ltd, 20(3), pp. 152–158. doi: 10.1016/j.mpaic.2019.01.005.

Zhdanov, V. S. and Sternby, N. H. (2004) 'Monitoring of atherosclerosis', International Journal of Cardiology, 95(1), pp. 39–42. doi: 10.1016/j.ijcard.2003.03.018.

Zhang, J., Chen, H., Zhao, M., Liu, G. and Wu, J., 2020. 2D nanomaterials for tissue engineering application. Nano Research, 13(8), pp.2019-2034.

Zheng, S., Du, Y., Ye, Q., Zha, K. and Feng, J., 2021. Atorvastatin Enhances Foam Cell Lipophagy and Promotes Cholesterol Efflux Through the AMP-Activated Protein Kinase/Mammalian Target of Rapamycin Pathway. Journal of Cardiovascular Pharmacology, 77(4), pp.508-518.

Zuchi, C., Tritto, I., Carluccio, E., Mattei, C., Cattadori, G. and Ambrosio, G., 2020. Role of endothelial dysfunction in heart failure. Heart failure reviews, 25(1), pp.21-30.

Annex 1: Evidence of ethical approval from Keele University Research Ethics Committee

Keele UNIVERSITY

01/05/2018

Dear Alan

PI: Alan Harper
Title: Developing a 3D tissue-engineered model to study the biology and treatment of atherosclerosis
Ref: ERP3146

Thank you for submitting your application for review. The proposal was reviewed by the Panel Chair. I am pleased to inform you that your application has been approved by the Ethics Review Panel.

If the fieldwork goes beyond the date stated in your application, or there are any amendments to your study you must submit an 'application to amend study' form to the ERP administrator at research.governance@keele.ac.uk. This form is available via http://www.keele.ac.uk/researchsupport/researchethics/

If you have any queries please do not hesitate to contact me, in writing, via the ERP administrator, at research.governance@keele.ac.uk stating **ERP3146** in the subject line of the e-mail.

Yours sincerely
PP.

Dr Valerie Ball
Chair – Ethical Review Panel